JOURNAL OF THE
AEROSPACE SCIENCES

VOLUME 28 JANUARY, 1961 NUMBER 1

PURDUE UNIVERSITY
JAN 9 1961
LIBRARY

CONTENTS

Viscous Flow Past a Quarter-Infinite Plate ..... K. STEWARTSON 1

Steady Creep Bending of a Nonhomogeneous Beam ..... JEROME L. SACKMAN 11

Stability of Partially Controlled Motions of an Aircraft ..... T. HACKER 15

Inviscid-Incompressible-Flow Theory of Static Peripheral Jets in Proximity to the Ground ..... T. STRAND 27

A Stiffness Matrix for the Analysis of Thin Plates in Bending .... ROBERT J. MELOSH 34

On the Approach to Chemical and Vibrational Equilibrium Behind a Strong Normal Shock Wave ..... WILLIAM H. DORRANCE 43

Experimental Investigation of the Downstream Influence of Stagnation-Point Mass Transfer ..... PAUL A. LIBBY AND ROBERT J. CRESCI 51

Readers' Forum 65

MECHANICAL ENGINEERING
JAN 10 1961
LIBRARY

Published by
INSTITUTE OF THE AEROSPACE SCIENCES, INC.

JOURNAL OF THE AEROSPACE SCIENCES

Editor: W. R. SEARS
Director, Graduate School of Aeronautical Engineering, Cornell University

Associate Editor: ROBERT R. DEXTER *Managing Editor:* RITA J. TURINO

Editorial Assistant: CHARLOTTE C. ROBB

IAS Aerospace Technology Panels

Paul J. Burr, Technical Services Director, Coordinator

The members of the IAS Aerospace Technology Panels shown here are to be available, collectively or as individuals, to assist and advise IAS committees, Sections, and staff members as to currently interesting and important technical topics related to their specialties and as to people most qualified to speak or write on such topics. The panels will also stimulate thought and scientific papers of potential value for the future, and they should be sensitive to technical activity of other professional groups, seeking through joint action the enlightenment of all having professional aerospace interests. Panel chairmen are indicated with an asterisk (*).

Aerodynamics and Fluid Mechanics

Lester Lees*
Dean R. Chapman
Antonio Ferri
Paul Germain
Wayland C. Griffith
Hans W. Liepmann
C. C. Lin
W. R. Sears
John R. Sellars
R. T. Whitcomb
Hideo Yoshihara

Aeroelasticity

R. L. Bisplinghoff*
Y. C. Fung
I. E. Garrick
Martin Goland
Kurt H. Hohenemser
J. C. Houbolt
W. P. Jones
W. J. Mykytow
Robert F. Speaker

Biomedical Sciences

Brig. Gen. D. Flickinger, USAF*
W. Ross Adey
Capt. Wm. Augerson, USA
Hilding Bjurstedt
Stuart Bondurant
A. Scott Crossfield
Cdr. J. H. Ebersole, USN
W. R. Lovelace, II
Capt. Bruce Pinc, USAF
Stanley Roscoe

Communication

P. C. Sandretto*
James M. Bridges
Leonard Jaffe
David S. Little
Cdr. D. O. Mann, USN
William Sen
Arnold Shostack
Teck A. Wilson

Control, Guidance, and Navigation

C. S. Draper*
R. C. Berendsen
B. Paul Blasingame
Robert N. Brown
S. F. Eyestone
Percy Halpert
B. J. O'Connor
S. F. Schmidt
O. Hugo Schuck
H. Philip Whitaker

Energy Conversion

David Altman*
Robert Bromberg
M. U. Clauser
J. Preston Layton
Frank Marble
G. H. Markstein
A. M. Rothrock
Milton M. Slawsky
Martin Summerfield
T. Y. Toong

Flight Mechanics

H. J. Kelley*
Malcolm J. Abzug
H. Julian Allen
A. E. Bryson, Jr.
T. N. Edelbaum
William C. House
Angelo Miele
John D. Nicolaides
Charles B. Westbrook

Instrumentation

R. H. Tripp*
Paul F. Bechberger
J. M. Hungerford
Mac Lowy
Walter McKay
M. David Prince
Charles P. Sonett
George I. Toumanoff
William A. Wildhack

Meteorology

Thomas F. Malone*
Edgar M. Cortright
Robert D. Fletcher
Henry T. Harrison
Joseph Kaplan
D. S. Perkins
Herbert Riehl
Harry Wexler

Nuclear Applications

J. Donald Rauth*
Jack L. Armstrong
Robert W. Bussard
H. M. Dieckamp
Capt. R. L. Duncan, USN
Harold B. Finger
Donald J. Keirn
Frank E. Rom
Raymer E. Schreiber
D. Roy Shoults
T. B. Taylor

Operations

Benjamin S. Kelsey*
Maj. Gen. Otis Benson, USAF (MC)
Ernest A. Cutrell
Capt. E. E. Fawkes, USN
Melvin N. Gough
Franklin W. Kolk
Col. J. L. Marinelli, USA
Richard V. Rhode
W. E. Rhodes
M. B. Spaulding, Jr.
Ernest G. Stout
Maj. Gen. D. Yates, USAF

Propulsion Systems

Bruce T. Lundin*
Robert H. Boden
George W. Brady
David Cochran
Elliot Mitchell
Perry W. Pratt
C. C. Ross
John G. Wilder, Jr.
Maurice J. Zucrow

Space Physics

H. G. Stever*
John C. Evvard
Herbert Friedmann
Leo Goldberg
C. F. Hansen
Arthur Kantrowitz
Bruno Rossi
S. F. Singer
Leo Steg
Fred L. Whipple

Structures and Materials

Nicholas J. Hoff*
Samuel B. Batdorf
Bruno A. Boley
Pol Duwez
R. R. Heldenfels
Samuel Levy
George N. Mangurian
S. S. Manson
Nathan E. Promisel
Ernest E. Sechler

Vehicle Design

C. E. Pappas*
Ralph Alex
C. H. Christenson
A. J. Eggers, Jr.
E. V. Marshall
Rene H. Miller
John R. Ragazzini
George S. Trimble, Jr

SUBSCRIPTION RATES

JOURNAL OF THE AEROSPACE SCIENCES, Published Monthly. United States and Possessions: 1 Year, $15.00; Single Copies, $1.50. Foreign Countries Including Canada (American Currency Rates): 1 Year, $16.00; Single Copies, $1.50.

AEROSPACE ENGINEERING, Published Monthly. United States and Possessions: 1 Year, $5.00; Single Copies, $0.50. Foreign Countries Including Canada (American Currency Rates): 1 Year, $6.00; Single Copies, $0.50.

Notices of change of address, which should be sent at least 30 days prior to actual change of address, and correspondence regarding subscriptions should be sent to the Circulation Department, JOURNAL OF THE AEROSPACE SCIENCES, 2 East 64th Street, New York 21, N.Y.

Manuscripts for publication, proofs, and all correspondence should be addressed to the Editorial Office of the JOURNAL.

© Copyright, 1960, by the Institute of the Aerospace Sciences, Inc.

Publication Office, 20th and Northampton Sts., Easton, Pa. Second-Class Mail Privileges Authorized at Easton, Pa. Acceptance for mailing at a special rate of postage provided for in Section 1103, Act of October 3, 1917, authorized April 29, 1937.

JOURNAL OF THE AEROSPACE SCIENCES

VOLUME 28 JANUARY, 1961 NUMBER 1

Viscous Flow Past a Quarter-Infinite Plate

K. STEWARTSON*

The University of Durham, England

Summary

A study is made of the motion of an incompressible viscous fluid past a quarter-infinite plate, whose leading edge is perpendicular to and whose side edge is parallel to the undisturbed direction of the stream. It is assumed that the kinematic viscosity ν is small. The first approximation is taken to be the undisturbed motion, and successive approximations are obtained by iteration. The second approximation is the Blasius shear layer necessary to satisfy the boundary conditions on the plate. In turn, this layer leads to a velocity component normal to the plate which needs a potential solution, in which the velocities are $O(\nu^{1/2})$, to match with the conditions at infinity. Further, the match at the edge of the Blasius shear layer must be completed to $O(\nu^{1/2})$ by introducing a secondary shear layer. The regions near the leading and side edges are considered separately; in particular, the neighborhood of the side edge needs special care, because the determination of the chief terms is complicated by the presence of powers of $\log \nu^{-1}$. In particular it is shown that the effect of the edge is to change the skin-friction coefficient by a factor

$$O(\nu^{1/2} \log \nu^{-1})$$

(1) Introduction

THE VISCOUS FLOW past a semi-infinite flat plate placed edgewise in a uniform stream is the classical problem of boundary-layer theory. The asymptotic form was found by Blasius, and, as a result of papers by Carrier and Lin[1] and by Kaplun,[2] the solution is known everywhere except in the immediate vicinity of the leading edge when ν the kinematic viscosity is small. Moore[3] has shown that the Blasius solution is capable of generalization to a flat plate with a curved leading edge provided that the leading edge has no discontinuities of slope. It is, in fact, sufficient to say that the flow in any plane parallel to the direction of the incident stream and containing a normal to the plate is identical with that given by the Blasius solution.

This generalization breaks down when a discontinuity of slope occurs in the leading edge, for then the solution would imply discontinuities in velocity derivatives; indeed, in the extreme case which forms the subject of this paper, that of a quarter-infinite plate with its leading edge normal to and its side edge parallel to the incident stream, velocity components themselves are discontinuous. Although little has been published on this problem, it has created a good deal of interest, indeed, more than the problem would at first sight appear to warrant. This is because it raises problems of fundamental importance in the interplay between boundary layer and external flow and contributes to our knowledge of the role played by boundary-layer theory in obtaining solutions of the full equations of flow. One remark about the novelty of the problem is sufficient to convey the importance of it in boundary-layer theory. Calculations of the effect of the edge in increasing the skin-frictional force on the plate are, as has been shown for the model equations of Oseen by Howarth and myself[4] and will be shown below for the full Navier-Stokes equations, quite incomplete until one includes the effect of the boundary layer on the potential flow outside. Indeed, in practically every paper on edge effects which I have seen the author has failed to realize this crucial aspect of the problem.

When Professor Howarth and I began to think about the mathematical difficulties of this problem we soon decided that the danger of missing vital points in the argument because of the great complexity of the three-dimensional form of the Navier-Stokes equations was sufficient to make it worthwhile carrying out a preliminary investigation, using Oseen's model set, which has the merit of being linear while at the same time retaining many important features of the full equations of motion. The results of this work have been published elsewhere.[4] Unfortunately, for various reasons it was not possible to continue our collaboration after that part of the investigation was completed, and it was decided that I should attempt the extension of the ideas evolved to the case of the Navier-Stokes equations.

Although the essential ideas underlying the solution, so far as it has been obtained, are simple, some of the

Presented at the International Papers on Fluid Dynamics Session, IAS 28th Annual Meeting, N.Y., January 25–27, 1960.

* Professor of Applied Mathematics.

details are complicated, more so even than in the model set of Oseen. All I will attempt here is to obtain the next approximation after the Blasius, over as extensive a part of the field of flow as possible, to the full solution when ν is small. For the Oseen equations the whole field of flow outside the immediate vicinity of the tip could be found correct to order $\nu^{1/2}$. For the Navier-Stokes equations so much is not possible, but we can determine a good deal of the solution to that order. The exceptions are the immediate neighborhoods of the tip, the leading edge, and the side edge. The tip region is intractable. In the neighborhood of the leading edge even the two-dimensional problem has not been solved; we show that once that solution has been found ours is comparatively simple. In the neighborhood of the side edge the presence of certain logarithmic terms in the boundary conditions means that similarity arguments are inadequate and the solution to $O(\nu^{1/2})$ must involve an infinite series in inverse powers of $\log(\nu^{-1})$ and possibly of $\log\log(\nu^{-1})$ as well. The leading term of this series can be shown to satisfy a set of equations of boundary-layer type but of a particularly difficult variety. Some of the properties of the leading term are found, among them, the fact that the effect of the side edge on the skin friction is to add to it a term

$$O(\nu^{1/2} \log \nu^{-1})$$

So far as possible I shall follow the scheme of reference 4 in this paper; the interested reader may find it useful to compare the properties of the two solutions at each stage of the argument.

(2) The Blasius Problem

Some of the ideas for the present solution are contained in the two-dimensional problem of the flow past a semi-infinite plate, and, as I shall require to make use of the solution of this problem anyway, some discussion of it is a useful introduction. The exact solution of the Oseen equations is known; of the Navier-Stokes equations the solution is known except near the leading edge—for small ν it comprises a potential flow together with a conventional boundary layer. With U as the speed of the incident stream, the origin at the leading edge, the x axis parallel to the incident stream, and the y axis normal to the plate, the Navier-Stokes equations take on the form

$$u\frac{\partial u}{\partial x} + v\frac{\partial u}{\partial y} = -\frac{1}{\rho}\frac{\partial p}{\partial x} + \nu\left(\frac{\partial^2 u}{\partial x^2} + \frac{\partial^2 u}{\partial y^2}\right) \tag{2.1}$$

$$u\frac{\partial v}{\partial x} + v\frac{\partial v}{\partial y} = -\frac{1}{\rho}\frac{\partial p}{\partial y} + \nu\left(\frac{\partial^2 v}{\partial x^2} + \frac{\partial^2 v}{\partial y^2}\right) \tag{2.2}$$

$$(\partial u/\partial x) + (\partial v/\partial y) = 0 \tag{2.3}$$

where (u, v) are the components of the fluid velocity. At infinity we must have $u \to U$, $v \to 0$ and at the plate $u = v = 0$.

A useful way of looking at these equations when ν is small is to say that a first approximation to the solution is

$$u = U, \qquad v = 0 \tag{2.4}$$

The solution satisfies the equations of motion and all the boundary conditions except that $u \neq 0$ on the plate. We can expect, therefore, that when ν is small this solution is valid except in the immediate vicinity of the plate where there must be a shear layer to enable the condition at the plate to be satisfied. Inside the shear layer $\partial/\partial y \gg \partial/\partial x$ since it is thin, and so we are led to the well known boundary-layer equations

$$\left.\begin{aligned} u\frac{\partial u}{\partial x} + v\frac{\partial u}{\partial y} &= -\frac{1}{\rho}\frac{\partial p}{\partial y} + \nu\frac{\partial^2 u}{\partial y^2} \\ \frac{\partial u}{\partial x} + \frac{\partial v}{\partial y} &= 0, \quad \frac{\partial p}{\partial y} = 0 \end{aligned}\right\} \tag{2.5}$$

with boundary conditions

$u = v = 0$ on the plate
$u \to U$ outside the boundary layer

The solution of these equations is classical and confirms our implicit assumption that the shear layer is thin. In fact, if $x > 0$, $y \gtrless 0$,

$$\left.\begin{aligned} &u = UF'(\eta) \text{ where } \quad \eta = u(U/2\nu x)^{1/2} \\ &\text{and } F''' + F F'' = 0 \end{aligned}\right\} \tag{2.6}$$

with $F = F' = 0$ at $y = 0$, $F' \to 1$ as $y \to \infty$, while if $x < 0$, $u = U$.

The skin friction at the plate is

$$0.332\ \rho U^2(\nu/xU)^{1/2} \tag{2.7}$$

where ρ is the density of the fluid and, on emerging from the shear layer, v is not zero but

$$v = 0.860\ U(\nu/xU)^{1/2} \quad \text{if } x > 0 \tag{2.8}$$

and $v = 0$ otherwise.

This solution is valid except in the immediate vicinity of the leading edge, where nothing short of the full equations is useful, but it does not satisfy the boundary condition at infinity on v. Hence, even apart from the neighborhood of the boundary edge, about which I have nothing new to say, it is necessary to add to Eqs. (2.4) and (2.6) other terms which serve to adjust v to satisfy the required condition. These terms can be found by assuming that in the region of adjustment $\partial/\partial x$ and $\partial/\partial y$ are both of order unity. It is easy to see that any other assumption fails. In this case the new terms correspond to an inviscid flow, which from the known properties of such flows must be irrotational.

Therefore, for the next approximation to the field of flow outside the shear layer we write

$$u = U + (\partial\phi/\partial x), \quad v = \partial\phi/\partial y \tag{2.9}$$

The function ϕ is harmonic and determined by the requirement that the values of v from (2.9) and (2.5) must be equal at the edge of the shear layer. Accordingly, when ν is very small

$$\begin{aligned} \partial\phi/\partial y &= 0.860U(\nu/xU)^{1/2} \quad y = 0+, \quad x > 0 \\ &= 0 \qquad\qquad\qquad\quad y = 0+, \quad x < 0 \end{aligned} \tag{2.10}$$

and hence is easily found. For a complete match the

two formulas for u must also match at the edge of the shear layer. This cannot be achieved by making any further restriction $O(\nu^{1/2})$ on ϕ which is completely determined by Eq. (2.10) and its harmonic property. It may be achieved by assuming that the shear layer is controlled by a main stream

$$\left(U + \frac{\partial \phi}{\partial x}\right)\Big|_{y=0+}$$

instead of by U, since to $O(\nu^{1/2})$ the value of v at the edge of the shear layer is still given by Eq. (2.8). However, in the two-dimensional problem $\partial\phi/\partial x = 0$ at $x > 0$, $y = 0$ so that the shear layer and potential layer are completely matched by Eqs. (2.6) and (2.9).

(3) The Quarter Plate Problem: Potential Solution

With origin at the corner, the x axis parallel to the stream, the z axis along the leading edge, and the y axis perpendicular to the plate, the Navier-Stokes equations are

$$\frac{D\mathbf{v}}{Dt} = -\frac{1}{\rho}\operatorname{grad} p + \nu\nabla^2\mathbf{v} \tag{3.1}$$

$$\operatorname{div}\mathbf{v} = 0 \tag{3.2}$$

where $\mathbf{v} = (u, v, w)$ is the fluid velocity. The boundary conditions are that

$$\mathbf{v} = 0 \quad \text{when } x \geqslant 0,\ y = 0,\ z \geqslant 0 \tag{3.3}$$

and $\mathbf{v} \to U\mathbf{i}$ at infinity, where $\mathbf{i}$ is a unit vector parallel to the x direction.

As in the Blasius problem, we can expect that if ν is small the flow is almost undisturbed except in the vicinity of the plate. Near the plate there will be a shear layer of the conventional type in which $\partial/\partial y \gg \partial/\partial x$, $\partial/\partial z$ except for special regions in the neighborhood of the leading edge $x = 0$ and the side edge $z = 0$.

Thus, we start by taking

$$\mathbf{v} = U\mathbf{i} \tag{3.4}$$

as our first approximation and then removing the tangential slip by means of a shear layer which is identical with that in the Blasius problem. In the vicinity of $y = 0$

$$u = UF'(\eta), \quad w = 0 \tag{3.5}$$

if $x > 0$, $z > 0$ and

$$u = U, \quad w = 0 \tag{3.6}$$

otherwise. The equation of continuity now determines v.

The shear layer of course only covers the plate, and, on emerging from it,

$$\begin{aligned} v &= 0.860\ U(\nu/xU)^{1/2} \operatorname{sgn} y \qquad x > 0,\ z > 0 \\ &= 0 \qquad\qquad\qquad\qquad \text{otherwise} \end{aligned} \tag{3.7}$$

except in the immediate vicinity of the leading and trailing edges. Accordingly, Eqs. (3.4) and (3.5) together do not satisfy the boundary conditions at infinity and to these must therefore be added another, potential, solution to cancel Eq. (3.7). This means that outside the shear layer

$$\mathbf{v} = U\mathbf{i} + \operatorname{grad}\Phi \tag{3.8}$$

where Φ is harmonic, grad $\Phi \to 0$ at infinity, and

$$\begin{aligned} \frac{\partial\Phi}{\partial y}\Big|_{y=0+} &= 0.860U(\nu/xU)^{1/2} \operatorname{sgn} y \\ &\qquad\qquad x > 0,\ z > 0 \\ &= 0 \qquad\qquad \text{elsewhere} \end{aligned} \tag{3.9}$$

The determination of Φ subject to these conditions is straightforward and has, apart from the multiplicative factor, already been found in reference 4. There is no need to repeat the calculation here; it is sufficient to remark that when $y = 0$, $x > 0$, $z > 0$,

$$\partial\Phi/\partial x = 0.860\ U(\nu/xU)^{1/2}U_1(\xi) \tag{3.10}$$

$$\partial\Phi/\partial z = 0.860\ U(\nu/xU)^{1/2}W_1(\xi) \tag{3.11}$$

where $\xi = z/x$, and U_1, W_1, are known and have the following properties:

(1) If ξ is large,

$$U_1 \sim +\frac{0.848}{\pi\xi^{1/2}}, \quad W_1 \sim -\frac{1.854}{\pi\xi^{1/2}} \tag{3.12}$$

(2) If ξ is small,

$$\begin{aligned} U_1 &\sim -\frac{\xi}{2}\left(\log\frac{\xi}{8} + 1\right), \\ W_1 &= \frac{1}{\pi}\log\frac{\xi}{8} + O(\xi\log\xi) \end{aligned} \tag{3.13}$$

Further, if $y \neq 0$, $z \neq 0$ but $y^2 + z^2 \ll x^2$,

$$\frac{\partial\Phi}{\partial z} \sim \frac{0.860}{2\pi}\ U\left(\frac{\nu}{xU}\right)^{1/2} \log\frac{y^2 + z^2}{64x^2} \tag{3.14}$$

If instead of considering the quarter-infinite plane $x > 0$, $y = 0$, $z > 0$ we had supposed that the leading edge was a curve of arbitrary shape but that the side edge was unaltered, the value of v at the outer edge of the shear layer would be altered and so therefore would the potential problem corresponding to Eq. (3.9). In fact, the logarithmic singularity in W_1 shown by Eqs. (3.13) would be unchanged, but it would be necessary to add to W_1 a term $c(x)\ x^{1/2}$ where $c(x)$ depends on the shape of the leading edge. A corresponding addition would be necessary for U_1. In particular, if the plate is the semi-infinite strip $y = 0$, $x > 0$, $R > z > 0$ where R is large, then

$$c(x) = -\frac{1.854}{\pi R^{1/2}}$$

In the Blasius problem the determination of the potential flow completed the solution except in the vicinity of the leading edge; this was because matching $\partial\phi/\partial y$ with the out flow from the boundary layer also matched the x component of velocity. Here, however, the x, z components of grad Φ are not zero on the plate and hence the match is not complete. It may, however, be completed to $O(\nu^{1/2})$ if we use the values of

u, w on the plate calculated from Eq. (3.8) to set up a secondary shear layer. To this order the terms normally neglected in boundary-layer theory are still negligible and the pressure charge across it zero, so that the usual theory may be applied. The match now achieved is not perfect, for in the secondary shear layer there is an induced v which is not matched to $\partial\Phi/\partial y|_{y=0}$; however it is $O(\nu)$ and beyond the scope of the present theory.

(4) The Secondary Shear Layer

In this section we investigate the perturbation to the Blasius solution which is necessary if the values of u, w on emerging from the shear layer are to match with those of the potential solution outside to order $\nu^{1/2}$. The values of v to this order have already been matched.

Write

$$u = u_0 + u^*, \quad v = v_0 + v^*, \quad w = w_0 + w^* \tag{4.1}$$

where the suffix 0 refers to the Blasius solution and the asterisk to the perturbation. Then

$$u_0 = UF'(\eta), \quad v_0 = U\left(\frac{\nu}{2Ux}\right)^{1/2}[\eta F' - F], \qquad w_0 = 0 \tag{4.2}$$

and the starred quantities satisfy

$$u^*\frac{\partial u_0}{\partial x} + v^*\frac{\partial u_0}{\partial y} + u_0\frac{\partial u^*}{\partial x} + v_0\frac{\partial u^*}{\partial y} = -\frac{1}{\rho}\frac{\partial p}{\partial x} + \nu\frac{\partial^2 u^*}{\partial y^2} \tag{4.3}$$

$$u_0\frac{\partial w^*}{\partial x} + v_0\frac{\partial w^*}{\partial y} = -\frac{1}{\rho}\frac{\partial p}{\partial z} + \nu\frac{\partial^2 w^*}{\partial y^2} \tag{4.4}$$

$$\frac{\partial p}{\partial y} = 0, \quad \frac{\partial u^*}{\partial x} + \frac{\partial w^*}{\partial y} + \frac{\partial w^*}{\partial z} = 0 \tag{4.5}$$

with boundary conditions

$$\left.\begin{aligned} &u^* = v^* = w^* = 0 \quad \text{on the plate,}\\ &u^* \to 0.860\ U(\nu/xU)^{1/2}\quad U_1(\xi, 0)\\ &w^* \to 0.860\ U(\nu/xU)^{1/2}\quad W_1(\xi, 0)\end{aligned}\right\} \tag{4.6}$$

as $\eta \to \infty$, where $\xi = z/x$ from Eq. (3.10) and (3.11), and $u^* = w^* = 0$ if $z < 0$ or $x < 0$.

It is noted that in the equations of motion, differentiation with respect to z only occurs in the equation of continuity; since w^* is completely determined by Eq. (4.4) it follows that z may be treated as a parameter in the secondary layer. Further, since the pressure p is independent of η in the shear layer it may be calculated from the boundary conditions at $\eta = \infty$. In fact,

$$p = \text{const.} - \rho U(\partial/\partial x)\Phi(x, 0, z) \tag{4.7}$$

in the shear layer.

Consider first the equation for w^*. Substituting for u_0, v_0 in terms of F and writing

$$w^* = 0.860\ U(\nu/xU)^{1/2}(\partial/\partial\eta)H(\xi, \eta) \tag{4.8}$$

we find that

$$\frac{\partial^3 H}{\partial\eta^3} + F\frac{\partial^2 H}{\partial\eta^2} + \frac{\partial F}{\partial\eta}\frac{\partial H}{\partial\eta} + 2\xi\frac{\partial F}{\partial\eta}\frac{\partial^2 H}{\partial\eta\partial\xi} = W_1 + 2\xi\frac{dW_1}{d\xi} \tag{4.9}$$

where

$$\partial H/\partial\eta = 0 \quad \text{at } \eta = 0, \quad \partial H/\partial\eta \to W_1 \quad \text{as } \eta \to \infty$$

and

$$\partial H/\partial\eta \to 0 \quad \text{as} \quad \xi \to \infty$$

A complete specification of $\partial H/\partial\eta$ requires extensive numerical calculation, but in order to form a picture of the flow it is sufficient to calculate it when ξ is large and when ξ is small.

If ξ is large,

$$W_1 = -(1.854/\pi)\xi^{-1/2}$$

and so

$$\partial H/\partial\eta = -(1.854/\pi)\xi^{-1/2}K(\eta) \tag{4.10}$$

where

$$K'' + FK' = 0$$

with boundary conditions $K(0) = 0$, $K(\infty) = 1$. Accordingly,

$$K(\eta) = F'(\eta) \tag{4.11}$$

so that, in particular,

$$\left.\frac{\partial w^*}{\partial y}\right|_{y=0+} = \frac{0.336\ U}{(xz)^{1/2}} \tag{4.12}$$

If ξ is small

$$W_1 = \frac{1}{\pi}\log\frac{\xi}{8} + O(\xi\log\xi)$$

and so we write

$$\frac{\partial H}{\partial\eta} = \frac{1}{\pi}\log\frac{\xi}{8}L(\eta) + \frac{1}{\pi}M(\eta) \tag{4.13}$$

whence

$$L''' + FL'' + F'L' = 1 \tag{4.14}$$

$$M''' + FM'' + F'M' = 2 - 2F'L' \tag{4.15}$$

with boundary conditions

$$L'(0) = M'(0) = 0, \quad L'(\infty) = 1, \quad M'(\infty) = 0$$

The solution of Eq. (4.14) is

$$L'(\eta) = F''(\eta)\int_0^\eta \frac{\eta_1 - \beta}{F''(\eta_1)}\,d\eta$$

where

$$\beta = \lim_{\eta\to\infty}(\eta - F) = 1.217$$

In particular,

$$L''(0) = -\beta = -1.217 \tag{4.16}$$

A graph of $L'(\eta)$ is given in Fig. 1(a). The solution of Eq. (4.15) is

$$M'(\eta) = -2F''(\eta)\int_0^\eta \frac{d\eta_1}{F''(\eta_1)}\left\{\int_{\eta_1}^\infty (1 - F'L')d\eta_2\right\}$$

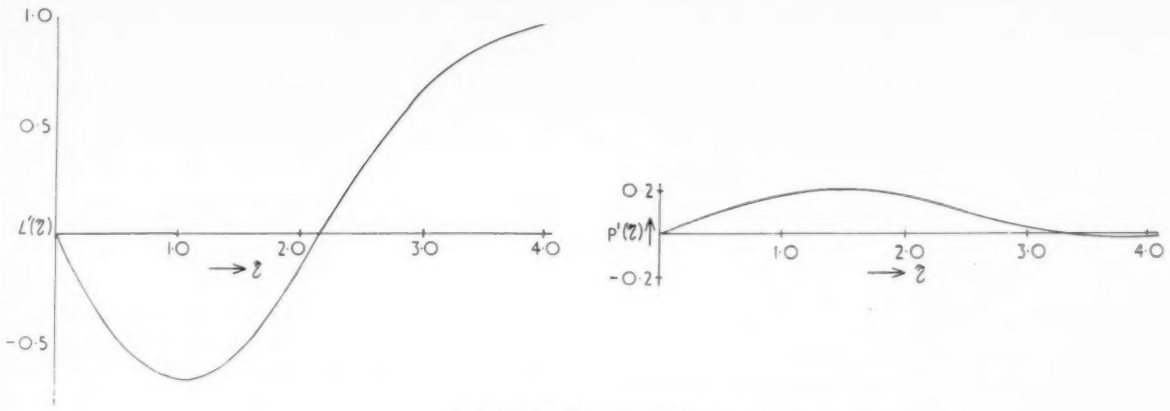

Graphs of $L'(\eta)$ and $P'(\eta)$.

In particular,

$$M''(0) = -2\int_0^\infty (1 - F'L')d\eta = -6.64$$

Thus, when ξ is small,

$$\left.\frac{\partial w^*}{\partial y}\right|_{y=0+} = -\frac{U}{x}\left(0.236 \log \frac{\xi}{8} + 1.286\right) \quad (4.17)$$

It is worth noticing that if z/x is small the component of the skin friction in the direction of z increasing is positive although the corresponding component of the velocity just outside the shear layer is negative. Further, the sideways force from the part of the plate defined by $0 < x < x_1$, $z_1 < z < z_2$, $z_1 \gg x_1$ is

$$1.34\,\mu U[x_1(z_2 - z_1)]^{1/2} \quad (4.18)$$

where μ is the coefficient of viscosity, and tends to infinity with z_2. The edge contributes an infinite sideways force in the strip $0 < x < x_1$.

Consider now the equation for u^*. Writing

$$u^* = 0.860\ U(\nu/xU)^{1/2}(\partial/\partial\eta)G(\eta, \xi) \quad (4.19)$$

we have from the equation of continuity

$$v^* = \frac{0.608\nu}{x}\left[\eta\frac{\partial G}{\partial \eta} + 2\xi\frac{\partial G}{\partial \xi} - 2\frac{\partial H}{\partial \xi}\right] \quad (4.20)$$

and depends not only on G but also on H. From the boundary condition $v^* = 0$ on the plate it follows that

$$H(\xi, 0) = 0 \quad (4.21)$$

The differential equation satisfied by G is

$$\frac{\partial^3 G}{\partial \eta^3} + F\frac{\partial^2 G}{\partial \eta^2} + \frac{\partial F}{\partial \eta}\frac{\partial G}{\partial \eta} - 2\xi\left[\frac{\partial G}{\partial \xi}\frac{\partial^2 F}{\partial \eta^2} - \frac{\partial F}{\partial \eta}\frac{\partial^2 G}{\partial \eta \partial \xi}\right] = U_1 + 2\xi\frac{dU_1}{d\xi} - 2\frac{\partial^2 F}{\partial \eta^2}\frac{\partial H}{\partial \xi} \quad (4.22)$$

with boundary conditions

$$G = \partial G/\partial \eta = 0 \quad \text{at} \quad \eta = 0$$
$$\partial G/\partial \eta \to U_1 \quad \text{as} \quad \eta \to \infty$$
$$\partial G/\partial \eta \to 0 \quad \text{as} \quad \xi \to \infty \quad (4.23)$$

Again it is only necessary to consider the behavior of G when ξ is large and when ξ is small to form a picture of the shear layer. When ξ is large

$$U_1 = +(0.848/\pi\xi^{1/2}), \quad H = -(1.854/\pi)\xi^{-1/2}F(\eta)$$

from Eqs. (3.12), (4.11), and (4.21) and using an argument similar to that used in deriving Eq. (4.11)

$$G = -(0.848/\pi\xi^{1/2})(\eta F' + F) \quad (4.24)$$

when ξ is large. Thus,

$$\left.\frac{\partial u_0^*}{\partial y}\right|_{y=0+} = -0.231\frac{U}{(xz)^{1/2}} \quad (4.25)$$

When ξ is small

$$U_1 = -\frac{\xi}{2\pi}\left(\log\frac{\xi}{8} + 1\right),$$

$$H = \frac{1}{\pi}\log\frac{\xi}{8}L(\eta) + \frac{1}{\pi}M(\eta)$$

and referring to Eq. (4.22) we see that the most important contribution to u^* when ξ is small comes from H; to find it write

$$G = (2/\pi\xi)P(\eta) \quad (4.26)\dagger$$

when

$$P''' + FP'' - FP' + 2PF'' = -F''L \quad (4.27)$$

with $P(0) = P'(0) = P'(\infty) = 0$.

It is found by numerical integration that

$$P''(0) = -0.198 \qquad P(\infty) = -0.383$$

A graph of $P'(\eta)$ is given in Fig. 1(b). The component (in the direction of the main stream) of the skin friction due to the secondary shear layer is

$$\mu\left.\frac{\partial u^*}{\partial y}\right|_{y=0+} = -0.077\frac{\mu U}{z} \quad (4.28)$$

Just as with the sideways component of the skin

†It is noted that the corresponding result (5.7) in reference 4 is incorrect due to the omission of the effect of the overall velocity distribution outside the shear layer on the flow near $\xi = 0$. The correct result is

$$u_2' = (3.708\eta/\pi^2 x^{1/2})\,(U\nu\xi)^{1/2}e^{-\eta^2} \quad \text{when } \xi \text{ is small}$$

friction, the behavior of $\partial u^*/\partial y|_{y=0+}$ when ξ is large means that the defect in the skin-friction component in the main stream direction, due to the secondary shear layer, in the strip

$$0 < x < x_1, \quad z_1 < z < z_2, \quad z_1 \ll x_1$$

is

$$0.924\ \mu U[x_1(z_2 - z_1)]^{1/2} \tag{4.29}$$

and tends to infinity with z_2. Both (4.18) and (4.29) are substantially in agreement with the results of reference 4 using the model Oseen equations. The divergence between the characters of the two secondary shear layers starts when ξ is no longer large, because when the full Navier-Stokes equations are used there is a coupling between (4.3) and (4.4) via the equation of continuity. In the Oseen form no coupling occurred. This coupling gets progressively stronger as ξ decreases until, when ξ is very small and we are approaching the neighborhood of the side edge, the behavior of w^* controls the behavior of u^* (but not vice versa). In addition the skin-friction component given by Eq. (4.28) is not integrable with respect to z at $z = 0$. This does not mean that the force is infinite, but that the additional force due to the secondary shear layer is of lower order than would otherwise be expected. If the secondary shear layer extends from $z = \delta > 0$ to $z = \infty$ where δ is a function of x to be determined, $0 < z < \delta$ being a region where the approximations of this layer do not apply, the contribution to the skin friction from

$$0 < x < x_1, \quad \delta < z < z_2$$

is

$$0.077\ \mu U x_1 \log \delta + O(\mu U\{x_1 z_2\}^{1/2}) \tag{4.30}$$

As we shall see below and as may be anticipated from the solution of Oseen's equations

$$\delta = O_l(\nu^{1/2}) \tag{4.31}$$

where the subscript l means that there is an unspecified power of $\log \nu$ multiplying $\nu^{1/2}$. Substituting in (4.30) it follows that the contribution to the skin friction is

$$-0.077\ \mu U x_1 \log (Ux/\nu)[1 + o(1)] \tag{4.32}$$

from the secondary shear layer.

(5) The Flow Near the Leading Edge Excluding the Corner Region

The two-dimensional flow near the leading edge of a flat plate has to date proved too difficult to solve even numerically, and so we can have no hope of solving the problem with the added complication of a corner. Our sole purpose here is to show that in fact the flow near the leading edge of a quarter-infinite plate is related in a simple manner to the flow near the leading edge of a semi-infinite plate.

Near the leading edge it is no longer permissible to neglect $\partial/\partial x$ in comparison with $\partial/\partial y$. However, since we exclude the corner region, $\partial/\partial z$ is smaller than either of these operators and is in fact $O(1)$. Accordingly, the term $\partial w/\partial z$ drops out of the equation of continuity and also all explicit dependence on z in the equations for u, v. The governing equations for u, v are then identical with Eqs. (2.1)–(2.3). The boundary conditions are slightly different, however, in that the fluid velocity just outside the leading region and the shear layer has a component in the x direction equal to

$$U\{1 + 0.232(\nu/Uz)^{1/2}\} \tag{5.1}$$

instead of U in the strict two-dimensional case. However, z may be taken as a parameter in Eqs. (2.1)–(2.3) so that the change expressed by (5.1) is only one of scale. Having obtained u and v, w may be found by solving

$$u\frac{\partial w}{\partial x} + v\frac{\partial w}{\partial y} = -\frac{1}{\rho}\frac{\partial p}{\partial z} + \nu\left(\frac{\partial^2 w}{\partial x^2} + \frac{\partial^2 w}{\partial y^2}\right) \tag{5.2}$$

where p is found with u, v, subject to the boundary conditions $w = 0$ on the plate and

$$w \to 0.507U\left(\frac{\nu}{xU}\right)^{1/2} \tag{5.3}$$

as $y \to \infty$.

(6) The Flow Near the Side Edge, Excluding the Corner Region

Near the side edge ($z = 0$) but away from the corner ($x = z = 0$) the governing equations are necessarily very complicated, for in addition to rapid changes taking place in the y direction they must also take place in the z direction. Were it not for the presence of the logarithmic terms it would be possible to assert, in a similar manner to the argument employed near the leading edge, that $\partial/\partial z$ and $\partial/\partial y$ were both of the same order and large compared with $\partial/\partial x$. In that case the Navier-Stokes equations would be reduced to three—namely, the equation of continuity and the x components of the equations of momentum and vorticity (the last two of these equations would be a little simplified). Further, a similarity solution could be found in which all dependent variables were effectively functions of

$$\eta = y\left(\frac{U}{2\nu x}\right)^{1/2}, \quad \theta = z\left(\frac{U}{2\nu x}\right)^{1/2} \tag{6.1}$$

only.

However, the presence of the logarithmic terms in the potential and secondary shear layer solutions rules out such a symmetrical and comparatively simple approach and makes the complete determination of the flow pattern to $O_l(\nu^{1/2})$ in w into a formidable program. Nevertheless, it is possible to write down equations of a boundary-layer type which describe the leading term of the flow pattern near the side edge.

First let us examine how the flow properties behave outside the neighborhood of the side edge as $y^2 + z^2 \to 0$. In this investigation, which stems from the work in

Sections (2), (3), and (4), we are assuming that $z/x = O(1)$ and then proceeding to the limit $z = 0$.

Outside the secondary shear layer the flow is dominated by the undisturbed flow together with the potential solution found in Section (3).

Hence, as $z \to 0$,

$$u \to U, \quad w \sim \frac{0.860}{2\pi}\left(\frac{\nu U}{x}\right)^{1/2} \log \frac{y^2+z^2}{64x^2} \tag{6.2}$$

and

$$v \sim \frac{0.860}{2\pi}\left(\frac{\nu U}{x}\right)^{1/2} \left\{\tan^{-1}\frac{z}{y} + \frac{\pi}{2}\right\} \tag{6.3}$$

In the shear layer; i.e., as $z \to 0$ from above with $\eta = O(1)$,

$$u \to UF'(\eta) + (\nu x/U)^{1/2}(U/z)P'(\eta) \tag{6.4}$$

$$w \to U(\nu/xU)^{1/2} \log\,(z/8x)\; L'(\eta) \tag{6.5}$$

where $P'(\eta)$, $L/(\eta)$ are defined in Eqs. (4.27), (4.14), respectively. In Eqs. (6.2)–(6.5) all leading terms up to and including those $O(\nu^{1/2})$ are given.

Whatever the solution in the neighborhood of the side edge is, as we leave it the values of (u, v, w) to $O(\nu^{1/2})$ must match up with Eqs. (6.2)–(6.5). In virtue of both (6.4) and (6.5) it follows that the length scale in the x direction is $O(1)$, ν being small, of course. The length scale in the z direction is a little harder to fix. It cannot be $O(\nu^{1/2})$, for that would mean w is $O(\nu^{1/2} \log \nu)$ from (6.5); hence, from the equation of continuity,

$$\partial w/\partial z = 0$$

which leads to a contradiction.

Accordingly, let us assume that the length scale in the z direction is δ and, further, that

$$\nu^{1/2}/\delta \to 0$$

as $\nu \to 0$. In order to get a reasonable solution it is essential that all three terms in the equation of continuity be of the same order and hence that

$$w = O(\delta) \tag{6.6}$$

In the x, z components of the equation of momentum the only viscous term which survives is

$$\nu(\partial^2/\partial y^2)\mathbf{v} \tag{6.7}$$

although all the inertia terms survive. The y component of the equation of momentum reduces to

$$\partial p/\partial y = O(\nu^{1/2}) \tag{6.8}$$

so that we finally get, for the equations governing the dominant flow in the neighborhood of the side edge,

$$u\frac{\partial u}{\partial x} + v\frac{\partial u}{\partial y} + w\frac{\partial u}{\partial z} = -\frac{1}{\rho}\frac{\partial p}{\partial x} + \nu\frac{\partial^2 u}{\partial y^2} \tag{6.9}$$

$$O(\nu^{1/2}) = -\frac{1}{\rho}\frac{\partial p}{\partial y} \tag{6.10}$$

$$u\frac{\partial w}{\partial x} + v\frac{\partial w}{\partial y} + w\frac{\partial w}{\partial z} = -\frac{1}{\rho}\frac{\partial p}{\partial z} + \nu\frac{\partial^2 w}{\partial y^2} \tag{6.11}$$

$$\frac{\partial u}{\partial x} + \frac{\partial v}{\partial y} + \frac{\partial w}{\partial z} = 0 \tag{6.12}$$

These equations also govern the flow in a general three-dimensional boundary layer on a flat plate. The boundary conditions which we can specify are

$$u = v = 0 \quad \text{when} \quad x > 0, \quad y = 0, \quad z > 0$$

$$\partial u/\partial y = v = \partial w/\partial y = 0$$
$$\text{when } x > 0, \quad y = 0, \quad z < 0$$

Eq. (6.2) is satisfied as $y \to \infty$ for fixed z, x, and as $z \to -\infty$ for fixed y, x; (6.4), (6.5) is satisfied as $z \to \infty$ for fixed y, x. It must be remembered that the length scale in the z direction is very small so that z can be large on it but yet small on the length scale of the flow outside the neighborhood of the side edge. Setting $z/\delta = z'$ and supposing that z' is of order one in the neighborhood of the side edge, it follows from (6.2), (6.5) that

$$w = O(\nu^{1/2} \log \delta) \tag{6.13}$$

in the side edge region. Hence, from Eq. (6.6),

$$\delta = A\nu^{1/2} \log \delta^{-1}$$

where A is independent of ν, whence

$$\delta = (1/2)A\nu^{1/2} \log \nu^{-1} + A\nu^{1/2} \log\log \nu^{-1} + \ldots$$

Thus, as a first approximation,

$$\delta = O(\nu^{1/2} \log \nu^{-1}) \tag{6.14}$$

and the terms neglected are of order $\nu^{1/2} \log\log \nu^{-1}$.

Accordingly, as a first step let us eliminate the logarithm from the equations of motion and the boundary conditions by writing

$$w = \nu^{1/2}w' \log\,(Ux/\nu), \quad z = \nu^{1/2}z' \log\,(Ux/\nu) \tag{6.15}$$

and throughout the new equations neglect all differentiations of $\log\,(Ux/\nu)$ with respect to x. Then Eqs. (6.9)–(6.12) are unaltered except that w, z are replaced by w', z' and the pressure term in Eq. (6.11) becomes

$$-\frac{1}{\rho}\frac{\partial p}{\partial z'}\frac{1}{\nu\{\log\,(Ux/\nu)\}^2} \tag{6.16}$$

The boundary conditions on u are unaltered; on w' they are as on w except that, when y is large on the scale of the side edge region,

$$w' \approx \frac{0.860}{2\pi}\left(\frac{U}{x}\right)^{1/2}\frac{1}{\log\,(Ux/\nu)} \times \log\frac{y^2 + \nu z'^2\{\log\,(Ux/\nu)\}^2}{64x^2}$$

so that in the limit $\nu \to 0$

$$w' = -\frac{0.860}{2\pi}\left(\frac{U}{x}\right)^{1/2} \quad \text{when } y \text{ is large}$$

In other words, the leading term in the expansion of

the z component of the velocity in terms of ν must satisfy

$$w' \to -\frac{0.860}{2\pi}\left(\frac{U}{x}\right)^{1/2} \quad \text{as } y \to \infty \tag{6.17}$$

With this boundary condition the way is clear to write a similarity form for u, w to satisfy the boundary conditions and (6.9)–(6.11).

Write

$$\zeta = \frac{0.860}{2\pi}\left(\frac{U}{\nu x}\right)^{1/2}\frac{z}{\log\,(Ux/\nu)} \tag{6.18}$$

$$u = U\frac{\partial X}{\partial \eta}, \quad w = -\frac{0.860U}{2\pi}\left(\frac{\nu}{Ux}\right)^{1/2}\times \left(\log\frac{Ux}{\nu}\right)\frac{\partial Z}{\partial \eta} \tag{6.19}$$

where X, Z are functions of η, ζ only. Then

$$v = U\left\{\eta\frac{\partial X}{\partial \eta} - X + \zeta\frac{\partial X}{\partial \zeta} + 2\frac{\partial Z}{\partial \zeta}\right\}\left(\frac{\nu}{2Ux}\right)^{1/2} \tag{6.20}$$

neglecting terms of order $\{\log\,(Ux/\nu)\}^{-1}$.

Substituting into Eqs. (6.9)–(6.11) and neglecting all terms of higher order, by inverse powers of $\log\,(Ux/\nu)$, than the leading term, we obtain

$$\frac{\partial^3 X}{\partial \eta^3} + \frac{\partial^2 X}{\partial \eta^2}\left\{X - \zeta\frac{\partial X}{\partial \zeta} - 2\frac{\partial Z}{\partial \zeta}\right\} + \frac{\partial^2 X}{\partial \eta \partial \zeta}\left\{\zeta\frac{\partial X}{\partial \eta} + 2\frac{\partial Z}{\partial \eta}\right\} = 0 \tag{6.21}$$

$$\frac{\partial^3 Z}{\partial \eta^3} + \frac{\partial^2 Z}{\partial \eta^2}\left\{X - \zeta\frac{\partial X}{\partial \zeta} - 2\frac{\partial Z}{\partial \zeta}\right\} + \frac{\partial^2 Z}{\partial \eta \partial \zeta}\left\{\zeta\frac{\partial X}{\partial \eta} + 2\frac{\partial Z}{\partial \eta}\right\} = 1 - \frac{\partial X}{\partial \eta}\frac{\partial Z}{\partial \eta} \tag{6.22}$$

where the pressure terms have been written down using the properties of X, Z when η is large and the fact that the pressure change across the boundary layer is smaller by an inverse power of $\log\,(Ux/\nu)$ than the pressure change along it. The boundary conditions on X, Z reduce to

$$\text{(i)}\quad Z = X = \frac{\partial X}{\partial \eta} = \frac{\partial Z}{\partial \eta} = 0 \qquad \text{when } \eta = 0,\ \zeta > 0 \tag{6.23}$$

since the fluid on the plate is at rest;

$$\text{(ii)}\quad Z = X = \frac{\partial^2 X}{\partial \eta^2} = \frac{\partial^2 Z}{\partial \eta^2} = 0 \qquad \text{when } \eta = 0,\ \zeta < 0 \tag{6.24}$$

since on the plane $y = 0$ but off the plate the flow is symmetrical with respect to y and free from singularities;

$$\text{(iii)}\qquad \frac{\partial X}{\partial \eta} \to 1, \quad \frac{\partial Z}{\partial \eta} \to 1 \tag{6.25}$$

as $\zeta \to -\infty$ for fixed η and as $\eta \to +\infty$ for fixed ζ since away from the plate the flow must match up with the potential solution as we leave the neighbourhood of the side edge:

$$\text{(iv)}\qquad \frac{\partial X}{\partial \eta} \to \frac{\partial F}{\partial \eta}, \quad \frac{\partial Z}{\partial \eta} \to \frac{\partial L}{\partial \eta} \tag{6.26}$$

as $\zeta \to +\infty$ for fixed η to match up with the flow in the secondary shear layer.

It is noted that no attempt has been made to match the values of v determined from (6.20) with the values of v determined from the potential flow, as has been done with u, w. Such a match cannot be effected at this stage because of the parabolic nature of the equation governing the dominant flow in the side-edge region. Presumably when the complete solution for w is found in the side edge region the matching of v will follow automatically.

Even though the equations satisfied by X, Z are formally much simpler than those which would have governed the flow near the side edge had *w not* included a logarithmic term, they are still too hard to solve by techniques known at present to the author. This is principally because they allow, over a certain range of values of ζ, small disturbances to propagate both in the direction of ζ *increasing* and in the direction of ζ *decreasing*. The pressure of boundary conditions at $\zeta = +\infty$ and at $\zeta = -\infty$ independent of each other suggests such a property and it may be seen from (6.21) when written in the form

$$\frac{\partial^3 X}{\partial \eta^3} + \frac{\partial^2 X}{\partial \eta \partial \zeta}\left\{\zeta\frac{\partial X}{\partial \eta} + 2\frac{\partial Z}{\partial \eta}\right\} = \frac{\partial^2 X}{\partial \eta^2}\left(2\frac{\partial Z}{\partial \zeta} + \zeta\frac{\partial X}{\partial \zeta} - X\right) \tag{6.27}$$

As written the dominant terms are on the left; terms on the right may be regarded merely as forcing terms. Eq. (6.27) is a parabolic equation for $\partial X/\partial \eta$, in which small disturbances diffuse in the η direction and propagate in the ζ direction with a sense of direction given by the sign of

$$\kappa = -\left(\zeta\frac{\partial X}{\partial \eta} + 2\frac{\partial Z}{\partial \eta}\right) \tag{6.28}$$

which may therefore be regarded as a sort of "coefficient of heat conduction." If $\kappa > 0$ a small disturbance propagates in the direction of ζ increasing, and vice versa. If, however, at a particular value of ζ, κ changes from 0 to ∞, propagation occurs in both senses of direction.

The study of parabolic equations in which the sign of the highest order derivative may change is very much in its infancy at present. I know of no existence or uniqueness theorems for even the simplest example of the type. There are, however, several examples of such equations in boundary-layer theory, among them being the boundary-layer equations in a region of a reversed flow, the boundary-layer equations associated with the unsteady motion of bodies with sharp leading edges, and the boundary-layer equations associated with the motion of a gas in a shock tube after a dia-

phragm separating two regions at different pressures has been ruptured. All that has been done in these flow problems is to recognize the inherent difficulties of obtaining solutions and in some cases to attempt to show how the solution could be continued from the boundaries. Even this modest effort has not always been successful and there is no doubt that much remains to be done from a purely mathematical aspect before it will be possible to proceed with confidence in any of the boundary-layer problems so far encountered.

In the present problem all we shall do is indicate certain of the properties of X, Z which might be expected to hold from our knowledge of parabolic equations in which the sign of the highest order derivative is constant. When ζ is large and negative,

$$X = Z = \eta$$

$\kappa = -(\zeta + 2)$, and so propagation is in the direction of ζ increasing. Accordingly, the velocity in the fluid at a large negative value of ζ depends only on the boundary conditions at $\eta = 0$, $\eta = \infty$ and at $\zeta = -\infty$. We infer that for these values of ζ

$$X = Z = \eta \tag{6.29}$$

and, continuing the argument as far as we can, Eq. (6.29) is the correct solution if

$$\zeta < -2 \tag{6.30}$$

If $\zeta > -2$, to a first approximation $\kappa > 0$, whence X, Z depend on boundary condition to the right of $\zeta = -2$; i.e., are independent of those at $\zeta = -2$. This does not seem very likely; it is more likely that, in a range of ζ satisfying $\zeta > -2$, X, Z depend on conditions both to the right and to the left. Let us investigate the behavior of X, Z if $\zeta + 2$ is small and positive, assuming that (6.29) is the correct first approximation. To find the second write

$$X = \eta + X^* \qquad Z = \eta + Z^* \tag{6.31}$$

Neglecting squares and products of X^*, Z^* we have

$$\frac{\partial^3 X^*}{\partial \eta^3} + \frac{\partial^2 X^*}{\partial \eta \partial \zeta}(\zeta + 2) + \eta \frac{\partial^2 X^*}{\partial \eta^2} = 0 \tag{6.32}$$

with solution

$$\frac{\partial X^*}{\partial \eta} = \sum_{n=0}^{\infty} A_n (\zeta + 2)^{2n+1} \frac{d^{2n}}{d\eta^{2n}} e^{-\eta^2/2} \tag{6.33}$$

where A_n is an arbitrary function of n only. Further,

$$\frac{\partial^3 Z^*}{\partial \eta^3} + \frac{\partial^2 Z^*}{\partial \eta \partial \zeta}(\zeta + 2) + \eta \frac{\partial^2 Z^*}{\partial \eta^2} + \frac{\partial Z^*}{\partial \eta} + \frac{\partial X^*}{\partial \eta} = 0 \tag{6.34}$$

with solution

$$\frac{\partial Z^*}{\partial \eta} = \sum_{0}^{\infty} B_n (\zeta + 2)^{2n} \frac{d^{2n}}{d\eta^{2n}} e^{-\eta^2/2} - \frac{\partial X^*}{\partial \eta} \tag{6.35}$$

where B_n is an arbitrary function of n. These two sets of constants are quite indeterminate without making use of the boundary conditions at $\zeta = +\infty$. Assuming that velocity components are continuous at $\zeta = -2$, when ζ is just greater than -2,

$$\kappa = -(\zeta + 2) + A_1(\zeta + 2)e^{-\eta^2/2} + \ldots$$

and so if $A_1 > 1$ propagation ζ-wise takes place in the direction ζ increasing near $\eta = 0$ and in the direction ζ decreasing when η is large. At the same time there is diffusion in the η direction so that, in fact, propagation occurs both ways.

The point $\zeta = 0$, $\eta = 0$ being the edge of the plate is of some interest. In virtue of the parabolic form of the equation we may expect there to be a singularity at this point but we cannot be sure about its form. If $\kappa > 0$ at $\zeta = 0$, propagation would be to the right, X_η and Z_η would be smooth in $\zeta < 0$, and $X_{\eta\eta}$, $Z_{\eta\eta}$ would have algebraic singularities with exponent $-(1/2)$ at $\zeta = 0+$, $\eta = 0$. Similarly, if $\kappa < 0$ at $\zeta = 0$, $X_{\eta\eta}$, $Z_{\eta\eta}$ would be smooth in $\zeta > 0$ while X_η, Z_η would have algebraic singularities with exponent $+(1/2)$ at $\zeta = 0-$, $\eta = 0$. However, it is more than likely that κ will change sign for some η at $\zeta = 0$ in which case little is known about the behavior of X, Z near $\eta = \zeta = 0$. Possibly singularities occur at $\zeta = 0\pm$.

Now consider the behavior of X_η, Z_η if ζ is large and positive when κ is certainly negative. Accordingly, disturbances propagate ζ-wise in the direction of ζ decreasing only and we infer that so long as $\kappa < 0$

$$X = F, \quad Z = L \tag{6.36}$$

This state of affairs persists until

$$-\zeta(\partial F/\partial \eta) - 2(\partial L/\partial \eta) = 0 \qquad \text{for some } \eta$$

and from the properties of L' in (4.14), (4.16), and its graph (Fig 1) this first occurs at

$$\eta = 0, \quad \zeta = 5.02 = \zeta_0$$

The properties of X, Z as of functions of ζ, η for $\zeta < \zeta_0$ may now be examined on the same terms as when $\zeta = -2+$. Indeed the form of the equation is closely similar to one occurring in the theory of the unsteady motion of a semi-infinite flat plate in a viscous fluid[6] and it is possible that the variable ζ enters here via an essential singularity {the perturbation term being $\sim \exp + [A/(\zeta - \zeta_0)^2]$} just as with the corresponding variable in that problem. However, the presence of the term

$$\frac{\partial^2 X}{\partial \eta^2}\left(X - \zeta \frac{\partial X}{\partial \zeta} - 2\frac{\partial Z}{\partial \zeta}\right) \tag{6.37}$$

in Eq. (6.18) together with a corresponding term in Eq. (6.20) adds greatly to the complication, and, in view of the admittedly speculative nature of the whole discussion of the equations, it may be wiser not to pursue the matter further in this paper.

To sum up, the most important contribution to the flow from the neighborhood of the side edge manifests itself in a flow of the shear layer type controlled by the usual conditions on the plate and a main stream in which

$$u = U, \quad w = -\frac{0.860}{2\pi} U \left(\frac{\nu}{xU}\right)^{1/2} \log \frac{Ux}{\nu}$$

It is confined to the range of values of z

$$-2 \leqslant \frac{0.860}{2\pi} \left(\frac{U}{\nu x}\right)^{1/2} \frac{z}{\log (Ux/\nu)} \leqslant 5.02 \quad (6.38)$$

Outside this region the dominant terms of the flow are given by the potential flow described in Section (3), if z is negative or if η is large, and by the shear layer solutions of Sections (2) and (4) if z is positive and η is finite.

In this region the governing equations are of the heat conduction type in which the coefficient of conductivity changes sign. The components of skin friction are

$$O\left\{\rho U^2 \left(\frac{\nu}{Ux}\right)^{1/2}\right\}, \quad O\left\{\rho U^2 \left(\frac{\nu}{Ux}\right) \log \frac{Ux}{\nu}\right\}$$

in the x, z directions so that the contribution to the x component of the drag on the plate is

$$O\left(\rho U^2 \frac{\nu}{Ux} \log \frac{Ux}{\nu}\right) \quad (6.39)$$

and of the same order as that from the secondary shear layer. On the other hand, the contribution to the sideways force on the plate from the neighborhood of the side edge is negligible in comparison with that from the secondary shear layer.

It is noted again that in the neighborhood of the side edge only the dominant terms have been discussed. This is in contrast to the corresponding discussion of the Oseen equation[4] in which a full solution to order $\nu^{1/2}$ was found. In that discussion it was pointed out that the description of the flow to order $\nu^{1/2}$ cannot be made using local considerations only; it is necessary first to look at the large scale properties of the flow outside the shear layer. However, the leading term of the expansion of w in terms of ν near the side edge is

$$O(\nu^{1/2} \log \nu^{-1})$$

and depends on local conditions only. The same conclusions can be drawn about the flow near the side edge using the full Navier-Stokes equations. Again it depends on the large scale properties of the flow and further since the velocity components are now fully interdependent even the determination of u to $O_l(1)$ can only be made once these are known. However, in the present paper, owing to the difficulties of obtaining the solution we are only able to write down the leading terms, which, as in the case of the Oseen equations, are dependent only on local considerations. It can be expected that the next term of $O_l(1)$ in u and of $O_l(\nu^{1/2})$ in w will depend on the large scale properties of the flow.

References

[1] Carrier, S. F., and Lin, C. C., *On the Nature of the Boundary Layer Near the Leading Edge of a Flat Plate*, Quart. Appl. Math., Vol. 6, pp. 63–68, 1948.

[2] Kaplun, S., *The Role of Coordinate Systems in Boundary-Layer Theory*, ZAMP, Vol. 5, pp. 111–135, 1954.

[3] Moore, F. K., Article on *Three-Dimensional Boundary Layer Theory*, Advances in Applied Mechanics, Vol. 4, pp. 159–228, 1956.

[4] Howarth, L., and Stewartson, K., *On the Flow Past a Quarter-Infinite Plate Using Oseen's Equations*, J. Fluid Mech., Vol. 7, Part 1, pp. 1–21, January, 1960.

[5] Stewartson, K., *On the Impulsive Motion of a Flat Plate in a Viscous Fluid*, Quart. Appl. Math. & Mech., Vol. 4, pp. 182–198, 1951.

Change of Address

Since the Post Office Department does not as a rule forward magazines to forwarding addresses, it is important that the Institute be notified of changes in address 30 days in advance of publishing date to ensure receipt of every issue of the JOURNAL and AEROSPACE ENGINEERING. Notices should be printed legibly and sent to:

Circulation Department
Institute of the Aerospace Sciences, Inc.
2 East 64th Street, New York 21, N.Y.

An Authorized Binding for
Journal of the Aerospace Sciences

Arrangements have been made by the Institute of the Aerospace Sciences for members and subscribers to have their Journals bound carefully and economically. Simply write for details to:

Publisher's Authorized Bindery Service, 5809 West Division St., Chicago 51, Ill.

Steady Creep Bending of a Nonhomogeneous Beam†

JEROME L. SACKMAN*

Institute of Flight Structures, Columbia University

Summary

The bending stress in a steadily creeping, linearly viscous beam (with a viscosity coefficient varying exponentially through the beam depth) is obtained by the use of the theory of generalized plane stress and compared to the solution based on elementary flexure theory. It is found that the smoother the bending moment distribution, or the shallower the beam, the better does the elementary solution approximate the generalized plane stress solution. Furthermore, the depth-to-span ratio below which the elementary theory is a good approximation depends not only on the parameter describing viscosity variation, but also on the face of the beam to which the load is applied. A useful and simple parameter gauging the range of validity of elementary flexure theory is seen to be the ratio of the applied transverse load stress to the resulting longitudinal bending stress (based on elmentary theory) at the loaded face of the beam.

Symbols

c	= half-thickness of beam
h	= depth of beam
L	= half-wavelength of sinusoidally distributed transverse load
N	= dimensionless parameter of viscosity variation
u, v	= velocities in the x and y directions
w	= maximum intensity of sinusoidally distributed transverse load stress
x, y, z	= Cartesian coordinates
ϵ_x, ϵ_y	= strain rate components in the x and y directions
γ_{xy}	= shearing strain rate component
σ_x, σ_y	= normal components of stress parallel to x and y axes
τ_{xy}	= shearing stress component
$\sigma_y^{(E)}$	= bending stress from elementary theory, Eq. (17)
β	= nondimensional beam depth; $\beta = h/L$
γ	= nondimensional beam depth, reciprocal of nondimensional wavelength of sinusoidally distributed load; $\gamma = \pi h/\sqrt{2}L$
η	= coefficient of viscosity
ϕ, ϕ_0	= fluidity; fluidity at $x = 0$; $\phi = 1/\eta$
ξ	= nondimensional span coordinate; $\xi = y/L$
ζ	= nondimensional depth coordinate; $\zeta = x/h$
Ψ	= Airy stress function
M	= bending moment

Introduction

THE BENDING STRESS distribution in a nonhomogeneous beam undergoing steady creep has been investigated in references 2 and 3 on the basis of elementary (Bernoulli-Euler) flexure theory. It is the purpose of this paper to investigate the limitations of this elementary solution for the case of a linearly viscous material having the same variation of the viscosity coefficient as considered in references 2 and 3. Such a viscosity variation (exponential in the depth coordinate of the beam) could be caused by a linear temperature distribution across the beam depth.

In this paper the theory of generalized plane stress is utilized to obtain the bending stress distribution in an infinitely long, thin, rectangular, transversely loaded beam (Figs. 1a, b). This solution is then compared to the elementary solution. The transverse load is taken to be sinusoidally distributed along the length of the beam, and can be considered as a typical harmonic of a more generally distributed load. If desired, the generalized plane stress solution for a finite beam under general shear forces and bending moments at the ends and under a general distributed transverse load, can be constructed by summing the solutions of the infinite beam for suitably selected harmonics together with the (generalized plane stress) solutions for pure bending and for the cantilever under end load. The generalized plane stress solutions for the latter two cases are easily obtained, and coincide with the elementary solutions. The present analysis shows that for smoothly varying bending moments, or for shallow beams, the elementary solution is adequate. Further, because of the asymmetry of the viscous properties about the mid-depth of the beam, the range in which the elementary solution becomes invalid depends not only on the parameter describing the viscosity variation, but also on whether the load is acting on the top or bottom face of the beam. A simple means for determining whether elementary flexure theory is applicable in any particular case is afforded by considering the ratio of the applied transverse load stress to the resulting (longitudinal) bending stress (based on elementary theory) at the loaded face of the beam. Whenever this ratio is much less than unity, the elementary solution is reliable.

Solution

Consider a beam, as shown in Figs. 1a,b, with a thickness $2c$ which is small compared to the beam dimensions in the xy plane. The equations governing the theory of generalized plane stress for such a steadily creeping, incompressible, linearly viscous body are the equilibrium equations

$$\left.\begin{aligned} \sigma_{x,x} + \tau_{xy,y} &= 0 \\ \tau_{xy,y} + \sigma_{y,y} &= 0 \end{aligned}\right\} \qquad (1)$$

Received December 9, 1959.

† This paper is derived from a portion of the author's Eng. Sc.D. thesis at Columbia University.

This investigation was sponsored by the Office of Naval Research under Contract Nonr 266(34) (reference 1).

* Assistant Professor of Civil Engineering.

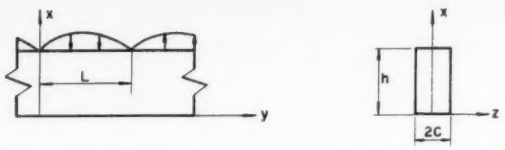

$\Psi_{,yy} = \sigma_x = 0, \quad -W\sin\pi y/L, \quad$ ON $x = 0, h$

$-\Psi_{,xy} = \tau_{xy} = 0, \quad$ ON $x = 0, h$

FIG. 1a. Sinusoidal load on soft face.

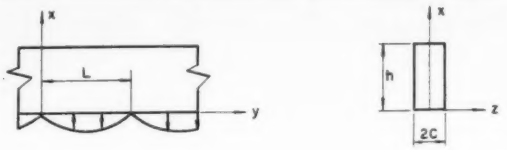

$\Psi_{,yy} = \sigma_x = -W\sin\pi y/L, 0, \quad$ ON $x = 0, h$

$-\Psi_{,xy} = \tau_{xy} = 0, \quad$ ON $x = 0, h$

FIG. 1b. Sinusoidal load on stiff face.

the strain rate-velocity relations

$$\left.\begin{aligned} \epsilon_x &= u_{,x} \qquad \epsilon_y = v_{,y} \\ \gamma_{xy} &= u_{,y} + v_{,x} \end{aligned}\right\} \tag{2}$$

and the (incompressible) strain rate-stress relations

$$\left.\begin{aligned} \epsilon_x &= (1/6\eta)(2\sigma_x - \sigma_y) \\ \epsilon_y &= (1/6\eta)(2\sigma_y - \sigma_x) \\ \gamma_{xy} &= (1/\eta)\tau_{xy} \end{aligned}\right\} \tag{3}$$

where η is the (variable) viscosity coefficient. The comma notation denotes partial differentiation with respect to the variable indicated. Here $\sigma_x, \ldots, \epsilon_x, \ldots, u, v$ represent the stress, strain rate and velocity components averaged over the thickness coordinate (z) of the beam, under the assumption that the normal stress component in the z direction vanishes throughout the beam. (See reference 4, section 2.23, for a derivation of the basic equations of generalized plane stress.) From Eqs. (2) the compatibility equation may be derived:

$$\epsilon_{x,yy} + \epsilon_{y,xx} - \gamma_{xy,xy} = 0 \tag{4}$$

Eqs. (1) imply the existence of the Airy stress function, Ψ, such that

$$\sigma_x = \Psi_{,yy} \quad \sigma_y = \Psi_{,xx} \quad \tau_{xy} = -\Psi_{,xy} \tag{5}$$

By substituting Eqs. (5) into Eqs. (3), and then this result into Eq. (4), the governing differential equation is obtained as:

$$\nabla_1^2(\phi\nabla_1^2\Psi) - (3/2)[(\phi\Psi_{,yy})_{,xx} - 2(\phi\Psi_{,xy})_{,xy} + (\phi\Psi_{,xx})_{,yy}] = 0 \tag{6}$$

where $\phi = 1/\eta$ is the fluidity, and $\nabla_1^2\Psi = \Psi_{,xx} + \Psi_{,yy}$. (This equation has the same form as the homogeneous equation governing the bending of a plate of variable thickness; see reference 5, p. 195.) Choosing the same fluidity distribution as in references 2 and 3,

$$\phi = \phi_0 \exp(Nx/h) \tag{7}$$

Eq. (6) reduces to

$$\nabla_1^4\Psi + 2(N/h)\nabla_1^2\Psi_{,x} + (N^2/h^2)[\Psi_{,xx} - (1/2)\Psi_{,yy}] = 0 \tag{8}$$

where $\nabla_1^4\Psi = \nabla_1^2(\nabla_1^2\Psi)$, ϕ_0 is the (constant) fluidity at $x = 0$, x is the depth coordinate of the beam (Figs. 1a, b), h is the total depth of the beam, and N is the parameter which describes the fluidity variation through the depth of the beam. As x increases, the fluidity increases (for $N > 0$), so that the bottom portion of the beam is more rigid than the portion at the top.

The beam is subjected to a transverse load varying sinusoidally along the span, as shown in Figs. 1a, b (where the boundary conditions are also given). For such a loading the stress function may be taken in the form

$$\Psi(x, y) = f(x) \sin \pi y/L \tag{9}$$

where L is the half-wavelength of the sinusoidally distributed load. Eq. (8) then becomes (in nondimensional coordinates):

$$D^4f + 2ND^3f + (N^2 - 4\gamma^2)D^2f - 4N\gamma^2Df + (N^2\gamma^2 + 4\gamma^4)f = 0 \tag{10}$$

where D is the operator $d/d\zeta$, $\zeta = x/h$, and $\gamma = \pi h/\sqrt{2}L$. The general solution of Eq. (10) is

$$f(\zeta) = \sum_{j=1}^{4} A_j e^{m_j\zeta} \tag{11}$$

where the m_j are the roots of the characteristic equation

$$m^4 + 2Nm^3 + (N^2 - 4\gamma^2)m^2 - 4N\gamma^2m + (N^2\gamma^2 + 4\gamma^4) = 0 \tag{12}$$

The substitution $m = n - N/2$ yields a biquadratic equation in n, and the four roots of Eq. (12) are then simply obtained:

$$m_{1,2,3,4} = -(N/2)(1 \pm a \pm ib) \tag{13a}$$

where $i = \sqrt{-1}$ and

$$\left.\begin{aligned} a &= [(1/2)(r + s)]^{1/2} \qquad b = [(1/2)(r - s)]^{1/2} \\ r &= [1 + 32(\gamma^2/N^2) + 64(\gamma^4/N^4)] \qquad s = 1 + 8(\gamma^2/N^2) \end{aligned}\right\} \tag{13b}$$

Given particular values of γ and N, the roots are computed from Eqs. (13a, b), and the constants A_j ($j = 1, 2, 3, 4$) are computed from the traction boundary conditions at $\zeta = 0, 1$. The stress function is then known and the stress components are computed from Eqs. (5). This has been done for the case of a transverse load on the "soft" face ($\zeta = 1$), and on the "stiff" face ($\zeta = 0$), as depicted in Figs. 1a and 1b, respectively. The bending stress (σ_y) at the stiff face is shown in Fig. 2 for two values of N and a wide range of γ.

General expressions for the stress components when $0 \leq \zeta \leq 1$ are more easily obtained if restrictions are made to cases where $(N/\gamma) \gg 1$. The roots simplify:

$$m_{1,2} \doteq -N[1 \pm (\gamma/N)i] \qquad m_{3,4} \doteq \gamma[(3\gamma/N) \pm i] \tag{14}$$

If γ is further restricted such that $\exp(3\gamma^2/N) \doteq 1$, the expressions for the stress components simplify further. For example, when the load is on the stiff face, the bending stress becomes

$$\sigma_y \doteq -\frac{M(y)N^2}{2ch^2\Delta'}\left\{\Delta'\left[\cos\gamma\zeta - \frac{N}{\gamma}\sin\gamma\zeta\right]e^{-N\zeta} - e^{-N}\left[7\frac{\gamma}{N}\sin\gamma\cos\gamma\,(\sin\gamma\zeta + \cos\gamma\zeta) + \frac{\gamma^2}{N^2}\cos\gamma\zeta + \sin\gamma\sin(\gamma - \gamma\zeta)\right] + e^{-N(1+\zeta)}\left[\left(\frac{N^2}{\gamma^2}\sin^2\gamma + 1\right)\left(\cos\gamma\zeta - \frac{N}{\gamma}\sin\gamma\zeta\right) - \frac{N}{2\gamma}\sin 2\gamma\cos\gamma\zeta\right] + \frac{\gamma^2}{N^2}e^{-2N}\left[\cos\gamma\zeta - \frac{3\gamma}{N}\sin\gamma\zeta\right] - e^{-N(2+\zeta)}\left[\cos\gamma\zeta - \frac{N}{\gamma}\sin\gamma\zeta\right]\right\} \tag{15}$$

where $\Delta' = 1 - e^{-N}[2 + (N^2/\gamma^2)\sin^2\gamma] + e^{-2N}$ and $M(y) = (wh^2c/\gamma^2)\sin\sqrt{2}\,\gamma y/h$ is the bending moment. When the load is on the soft face,

$$\sigma_y \doteq -\frac{MN^2}{2ch^2\Delta'}\left\{\left[\cos\gamma\zeta - \frac{N}{\gamma}\sin\gamma\zeta\right]e^{-N\zeta}\cos\gamma + \frac{\gamma^2}{N^2}\left[\frac{3\gamma}{N}\sin(\gamma - \gamma\zeta) - \cos(\gamma - \gamma\zeta)\right] - e^{-N\zeta}\left[4\sin\gamma\zeta - \frac{5\gamma}{N}\cos\gamma\zeta\right]\sin\gamma + e^{-N}\left[\sin\gamma\sin\gamma\zeta - \frac{\gamma}{N}\times\left(7\sin\gamma - \frac{\gamma}{N}\cos\gamma\right)\cos\gamma\zeta\right] - e^{-N(1+\zeta)}\left[\frac{N}{\gamma}\sin(\gamma - \gamma\zeta) + \cos(\gamma - \gamma\zeta)\right]\right\} \tag{16}$$

where $M = -(wh^2c/\gamma^2)\sin\sqrt{2}\,\gamma y/h$. These approximations (evaluated at $x = 0$) are also shown in Fig. 2 (for $N = 20$), where it is seen that they yield good results within the restricted ranges of N and γ stated above. As $\gamma \to 0$ (keeping M finite), both Eqs. (15 and 16) approach the elementary solution

$$\sigma_y^{(E)} = -MN^2[1 - N\zeta - (1 + N - N\zeta)e^{-N\zeta}]e^{-N\zeta} \div 2ch^2\Delta \tag{17}$$

where $\Delta = 1 - (2 + N^2)e^{-N} + e^{-2N}$. The elementary solution predicts for the maximum bending stress (at $x = 0$)

$$\sigma_y^{(E)}]_{x=0} = -MN^2[1 - (1 + N)e^{-N}]/2ch^2\Delta \tag{18}$$

Because of the very simple analogy which exists between nonhomogeneous viscous and elastic materials (reference 1, p. 10), the stress distribution obtained here is identical to that occurring in an (incompressible) elastic beam having a modulus of rigidity varying exponentially through the beam depth.

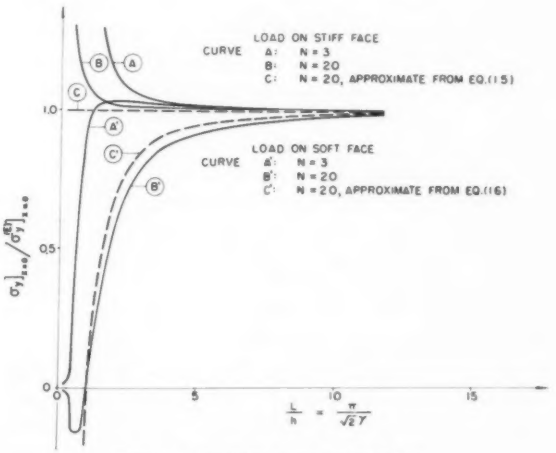

FIG. 2. Bending stress at stiff face.

Discussion

In Fig. 2 the elementary result, Eq. (18), is compared to the results from two-dimensional theory. It is seen that the smaller γ is (i.e., the "shallower" the beam, or the "smoother" the bending moment) the better is the elementary solution. This same general result was obtained in investigations of the limitations of the elementary theory for elastic beams with homogeneous material properties.[6] (Bear in mind that the approach of σ_y to $\sigma_y^{(E)}$ as L/h becomes large does not mean that the bending stress becomes linear through the beam depth, since the elementary solution, Eq. (17), is not linear through the beam depth.)

From Fig. 2 it is seen that for loads on the stiff face, the larger N is, the larger γ may be (i.e., the deeper the beam may be) before the elementary solution becomes invalid. This might have been predicted on the basis of a "strength boundary layer" at the cold face introduced in reference 3. It was stated there that as N increases, the strength of the beam becomes concentrated in a thinner layer at the stiff side. [This is seen from the elementary solution, Eq. (17).] Thus there is effectively a homogeneous beam, shallower than the actual one, the material outside of the "strength boundary layer" developing negligible stresses. As is already known from investigations of homogeneous materials,[6] for a given loading, the shallower the beam the better the elementary solution is expected to be. Hence (for a given loading), as N increases the shallower the beam effectively becomes, and thus the better is the elementary solution. Therefore the larger N is, the larger γ may be before the elementary solution breaks down. This is true as long as the load is applied directly to the "strength boundary layer" (i.e., to the stiff face).

When the load is applied to the soft face it is seen that

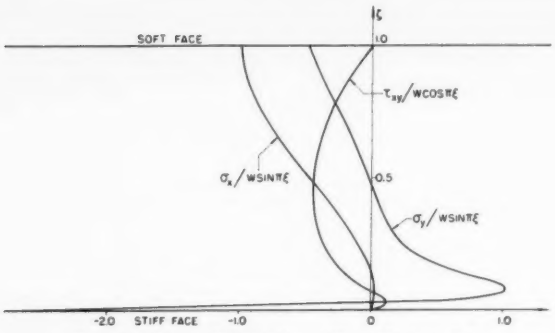

FIG. 3. Stress distribution; $N = 20$, $\gamma = 2.5$.

as N increases the smaller γ must be (i.e., the shallower the beam must be) in order that the elementary solution be valid. This too has a simple physical explanation. In elementary theory it is assumed that the state of stress is effectively uniaxial (and in the spanwise direction). When conditions are such that this assumption is no longer valid, then the elementary theory can be expected to fail. This will be the case when the direct stress (σ_x) becomes of the same order of magnitude as the bending stress (σ_y) in the region under the transverse load. Therefore the larger the ratio σ_x/σ_y (in the region under the transverse load) the poorer the elementary solution is expected to be. From Eq. (17) it is seen that for a given loading on a given beam, the larger N becomes, the smaller σ_y becomes at the soft face while the larger it becomes at the stiff face. Thus for a given transverse load on the soft face, the ratio σ_x/σ_y (under the load) increases with N, and hence the elementary solution becomes poorer. Therefore as N increases, γ is required to decrease in order that the elementary solution be applicable.

It may be noted that the ratio σ_x/σ_y (under the load) decreases with increasing N when the load is on the stiff face. Thus for loads on the stiff face, it can be predicted that the larger N, the better the elementary solution will be. This is consistent with the results discussed in a preceding paragraph.

The ratio σ_x/σ_y is a simple means for measuring the validity of elementary flexure theory. It may be evaluated (under the transverse load) by the elementary formulas, and whenever it is of the order of magnitude of unity, the elementary solution can be expected to be in error. This ratio can also be expected to be a good measure of the limitation of elementary flexure theory even when nonlinear steady creep laws are utilized.

A further comment is required with regard to Fig. 2. It is noted that for $N = 20$, with the load on the soft face, the bending stress at $x = 0$ has the expected sign for small values of γ, but changes sign for large values of γ. Such a reversal in sign never occurs for the homogeneous material ($N = 0$). This peculiar phenomenon could have been predicted on a purely mathematical basis from an inspection of the roots, Eqs. (13a, b), which are seen to have an imaginary part, $Nb/2$. When this quantity is large, the solution can be expected to be highly oscillatory in ζ. When $N = 0$, $Nb/2 = 0$, and thus for the homogeneous material there is no oscillatory solution and therefore no "peculiar" stress distributions are obtained. $Nb/2$ will be large if both N and γ are large, and for this range of parameters stress distributions which oscillate through the thickness may be expected.

In Fig. 3 such a stress distribution is shown for $N = 20$ and $\gamma = 2.5$. Consider the portion of the beam between $y = 0$ and $y = L$. From Fig. 3 it is seen that the beam appears to divide itself into two parts. The upper portion of the beam has a stress distribution expected of a beam being bent downwards under a compressive load at $\zeta = 1$, while the very lowest portion has a stress distribution expected of a beam being bent upwards under a tensile load at $\zeta = 0.08$. When the velocities are computed it is found that the top portion of the beam is moving downward under the compressive load at $\zeta = 1$, while the bottom portion of the beam is moving upward (but at a velocity which is much less than the downward velocity at $\zeta = 1$). It is further found that the horizontal component of the velocity, v, in the upper portion of the beam is such that the material is flowing outward under the compressive load. (That is, in the upper portion of the beam $v \leq 0$ for $0 \leq y \leq L/2$ and $v \geq 0$ for $L/2 \leq y \leq L$.) Thus it appears that the softer material at the top of the beam, in flowing outward from under the load, drags the stiffer material at the very bottom of the beam upwards, thereby giving rise to the peculiar stress distribution of Fig. 3.

A two-dimensional investigation could also have been undertaken by applying the method of reference 6 to Eq. (8). In such a case the solution for the bending stress takes the form

$$\sigma_y = M(\xi)f_0(\zeta) + \beta^2(d^2M/d\xi^2)f_2(\zeta) + \beta^4(d^4M/d\xi^4)f_4(\zeta) + \ldots \quad (19)$$

where $\beta = h/L$ and $\xi = y/L$. The first term in the series (Mf_0) represents the elementary solution, and the higher-order terms may be regarded as corrections to the elementary theory. This form of the solution allows one to draw some of the conclusions already stated. It is seen that the shallower the beam or the smoother the bending moment, the better is the elementary solution. The ratio of the elementary solution to the first correction term is proportional to the ratio $\sigma_y^{(E)}/\sigma_x$, and therefore this quantity is again seen to serve as a parameter for gauging the range of validity of the elementary solution.

The heterogeneity of the viscosity coefficient [as given by Eq. (7)] upsets the symmetry of material properties about the midheight of the beam. Therefore the solution depends on whether the load is placed on the top or bottom face of the beam. The elementary term (Mf_0) is the only term in the series (19) which is independent of the face to which the load is applied. In order to study any interesting effects arising from this unsymmetrical situation (or to study the range in which the elementary solution is poor), it would be

(Continued on page 33)

Stability of Partially Controlled Motions of an Aircraft

T. HACKER*

Institute of Applied Mechanics of the Academy of the Rumanian People's Republic

Summary

Based on the actual situation that the aircraft and the pilot form a single dynamic system, which as a whole must be stable (while the machine alone may be an unstable component of the flying system[14]), this paper presents a method for approaching the problems of the stability of the partially controlled motions of an aircraft. The forces and moments brought into play by the pilot's continuous intervention appear as random and unknown, but are nevertheless susceptible of approximate evaluation. The assumption is made that their order of magnitude is determined by the bounds within which the pilot is able to restrain the deviations he counteracts. Hence these forces and moments are small, provided that the above-mentioned bounds are sufficiently small.

The problem is solved in principle, on the basis of stability under continuously acting disturbances. Then the theory is applied to a few particular cases of longitudinal and lateral stability of aircraft.

As regards the longitudinal disturbed motion, it is shown that by simultaneous control of the pitch angle and the flight velocity, or even by adequate control of the pitch angle alone, the longitudinal stability is ensured for a wide range of flight regimes; on the other hand, constraining only the flight velocity is not sufficient to ensure stability in climb or even in level flight. For ensuring lateral stability when the basic motion is unstable in free flight, the present theory indicates the necessity of controlling the aircraft motion about its longitudinal axis.

Examples of calculations are included.

In Appendix I a relation is deduced for determining how small the constrained variables should be as a consequence of the pilot's intervention, in order that the free variables not exceed certain given bounds.

In Appendix II certain ideas are presented for estimating the controllability of various kinematic parameters according to the nature and rapidity of their variation.

Symbols

t	= aerodynamic time, dimensionless—independent variable in motion equations
V	= $\hat{V}V_{max}$ = velocity of aircraft in undisturbed flight, m./sec.
M	= Mach number
ρ	= air density, kg.-sec.^{2}/m.^{4}
α	= angle of incidence in undisturbed flight, rad.
γ	= upward inclination of flight path to the horizontal in undisturbed flight, rad.
θ	= angular pitch, rad.
$\Delta\hat{V}$	= $\Delta V/V$ or $\Delta\hat{V} = \Delta V/V_{max}$; deviation of velocity in disturbed flight, dimensionless
$\Delta\alpha$, $\Delta\theta$, $\Delta\beta$, $\Delta\phi$	= deviations of angles of incidence, pitch, sideslip and roll, respectively, in disturbed flight, rad.
$\Delta\hat{p}$, $\Delta\hat{q}$, $\Delta\hat{r}$	= deviations of rates of roll, pitch and yaw, respectively, in disturbed flight, dimensionless
C_W	= nondimensional flight speed-dependent coefficient of aircraft weight, equal to $W(^1/_2\rho V^2S)^{-1}$
$\bar{q}$	= $(k_y/V)q$ or $\bar{q} = (k_y/V_{max})q$; argument for partial derivative $\partial C_m/\partial\bar{q}$
$\dot{\bar{\alpha}}$	= $\frac{k_y}{V}\frac{d\alpha}{dt_{\text{dim.}}}$ or $\dot{\bar{\alpha}} = \frac{k_y}{V_{max}}\frac{d\alpha}{dt_{\text{dim.}}}$; argument for partial derivative $\partial C_m/\partial\dot{\bar{\alpha}}$ ($t_{\text{dim.}}$ = time, sec.)
C_L	= lift coefficient
C_D	= drag coefficient
C_M	= pitching-moment coefficient
C_T	= nondimensional coefficient of thrust, $C_T = T(^1/_2\rho V^2S)^{-1}$
C_{TV}	= nondimensional form of derivative $\partial T/\partial V$ $(C_{TV} = (\partial T/\partial V)(\rho VS)^{-1}$
$C_{y\beta}$	= rate of change of lateral force coefficient with sideslip angle
C_{lp}, C_{lr}, $C_{l\beta}$	= rates of change of rolling-moment coefficient with angular velocity of roll, angular velocity of yaw and angle of sideslip, respectively, dimensionless
C_{np}, C_{nr}, $C_{n\beta}$	= idem for coefficient of yawing moment
W	= weight of aircraft, kg.
S	= total wing area, sq. m.
$\hat{S}_t$	= S_t/S = tailplane area, dimensionless
b	= wing span, m.
c	= mean wing chord, m.
l_t	= tail arm, m.
z_T	= distance between c.g. and thrust vector situated above the c.g., m.
T	= thrust, kg.
$\hat{z}_T$	= z_T/k_y or $\hat{z}_T = z_T/c$; nondimensional form of thrust-vector arm
m	= total mass of aircraft, kg.-sec.^{2}/m.
μ	= relative density of aircraft, dimensionless
k_y	= radius of gyration of aircraft about lateral axis, m.
i_x, i_y, i_z	= nondimensional moments of inertia in roll, pitch and yaw, respectively
i_{xz}	= nondimensional product of inertia about axes OZ and OX of the reference system of body axes through the c.g.

Received October 20, 1959. Revised and received April 14, 1960.

* Head, Laboratory of Flight Dynamics, Aeromechanics Division.

The author acknowledges his indebtedness to A. Halanay of the Institute of Mathematics of the Academy of the Rumanian People's Republic, whose collaboration led to the conception of the mathematical scheme and methods employed in the present paper.

Thanks are also due to S. Moşoiu for his kind help with the language. Together with him, the author expresses apologies for unavoidable imperfections in English style and diction.

The author also wishes to acknowledge with thanks the suggestions and comments of the referee.

(1) Introduction

THE DEFINITION GENERALLY ADOPTED for the dynamic stability of aircraft does not take into account the pilot's intervention to stabilize the flight. In other

words, the uncontrolled aircraft is the dynamic system whose stability is discussed. In compliance with such a definition, the stability criteria applied to the set of equations for the induced motion, e.g., the Routh-Hurwitz criteria, will indicate only a requirement of complete inherent stability* which, one may say, was given up from the very beginning of aircraft construction.

Generally, it is not necessary that all the components of the solution of the disturbed motion equations be stable, i.e., that the aircraft be stable with respect to all kinematic parameters characterizing the flight. In order to find criteria which would indicate stability with respect to only certain dynamic variables, it is necessary either to solve the stability problem separately for each disturbance element, or to abandon the conventional definition of aircraft stability and to include the stabilizing effect of controls within the dynamic system considered.

The first possibility led to the study of some simplified equations. This simplification consisted, on the one hand, of proceeding from only a few mathematical considerations and, on the other hand, of excluding in one way or in another those variables which it was thought a priori must behave in a certain manner. In this way, the longitudinal stability could be dealt with independently of the lateral stability, and within the longitudinal induced motion, the rapid incidence adjustment and the slow mode were discussed separately. Thus a considerable simplification in the analysis of various factors was obtained. The differentiated treatment of various disturbance elements through certain qualitative methods also proved to be possible in the following two cases: (1) in the case of a stable solution when certain allowable bounds are sought on the values of both the initial and the continuously acting disturbances (reference 2), and (2) in the case of an actual partial instability (reference 3).

The second case leads along less trodden ways but is nevertheless sufficiently promising.

As is known, the problem of the stability of an aircraft equipped with an automatic pilot led to the consideration of the machine *cum* monitoring device as a single dynamic system. It is to be noticed that since on one hand the aircraft *cum* automatic pilot system must *stricto sensu* be stable and since on the other hand the operation of a device lends itself more readily to mathematical description than does the human being's reactions, the stability problem is not to be solved through a separate investigation of the behavior of a part of the disturbance elements, but on the contrary through inclusion of the equations of the automatic device in the set of motion equations. In consequence, the mathematical problem as well as the calculus operations become more cumbersome, owing to the occurrence of an additional number of degrees of freedom.

When the stabilizing effect of the human pilot's intervention is taken into account, such a treatment is not to be recommended. As response characteristics vary not only from pilot to pilot, but also in the same pilot according to his degree of fatigue, the inclusion of equations representing mean human reaction characteristics in the system would not lead to satisfactory results. It is desirable that in considering the stabilizing intervention of the pilot, an accurate mathematical description not be necessary.

S. Neumark suggested quite an ingenious procedure which avoids the above difficulty: he assumed that the pilot operates one of the controls "so as to keep one of the usual variables, or a linear combination of them, equal to zero (or constant), while other elements of the disturbances are still free to vary according to the (suitably modified) system of dynamic equations" (reference 4, p. 21). For such an approach to lead to a simplification of the equation set, Neumark also assumed that the gearing of the control affects but one equation of the system—i.e., as the system is a linearized one, in all equations except one the terms due to the pilot's intervention are quantities of at least the second order of smallness in comparison with the deviation magnitude. Thus the order of the system drops by at least one and furthermore the remaining equations become simpler.

The new concept of "stability under constraint" introduced by Neumark is of particular interest from the theoretical and practical point of view; but the simplifying assumptions made in view of a practical calculus procedure and which are not inherent to the concept itself diminish the probability of realizing in flight the ideal schemes constructed on such a basis. These assumptions are the following: (1) one of the variables is always kept constant or equal to zero; (2) to achieve this, only one simple control is used (e.g., elevator or throttle); and (3) the operation of this control affects but one of the linearized equations of the induced motion.

The above assumptions are expected to be completely acceptable in some particular, simple cases. For such cases, the theory put forth by Neumark provides a convenient way for estimating the dynamic stability characteristics of an aircraft.

In the following, a procedure will be presented which, by keeping the idea of considering the stability of partially controlled motions, will use as few assumptions as possible which are not directly derived from the actual phenomena investigated. It is obvious that thus the theory will become more complicated in some ways, but it will nevertheless provide a general method for approaching the problem of stability of partially controlled motions of an aircraft, and some practical applications of great simplicity will result.

(2) Some Remarks and Definitions

Before discussing the main subject, it seems necessary to point out the sense in which the concept of stability

* "If the solution of these linear equations of disturbances contains *no unstable component*, the system under investigation is said to be stable for small disturbances." [The italics are ours (T. H.); quoted from reference 1, p. 113.]

will be used in this paper. If the concept consecrated in the aeronautical literature is used, the mathematical statement of the problem is unavoidably restricted. Indeed, the stability concept accepted in this literature may be seen from the following quotation.

"A given state of equilibrium at rest or in steady motion of a dynamical system is said to be stable when the influence of an imposed disturbing impulse, or force acting throughout a finite interval of time, ultimately becomes vanishingly small. Thus, stability is an attribute of the free motion which follows a disturbance . . . . Usually we are concerned with disturbances which are so small that the equations governing the motions of disturbances are linear. . . . . It must also be emphasized that the concept of stability only applies to systems in equilibrium, at rest or in some regular motion, either free or with prescribed forces." (reference 1, page 113.)

Accordingly, (1) the stability of only steady motions is considered; (2) the induced motion is examined only from the instant the disturbing random force ceases to act, the case of a disturbing random force acting throughout the induced motion being excluded; and (3) the disturbances are assumed to be sufficiently small that the small-deviation method may be applied and the linearized equation set may be considered.

From these three particularizations it follows that if the motion discussed is stable, it represents either a pure subsidence or a purely damped oscillation, i.e., it behaves asymptotically. In other words, an amplification of the deviation at any stage of the induced motion is not to be expected. The above facts are due, to quote A. R. Collar, "to a fortuitous but fortunate property of linear equations with constant coefficients."[5]

Nevertheless, as will be shown subsequently, the problem of stability of the partially controlled motions requires the presence, in the disturbed motion equations, of some unknown variable terms representing random forces which are due to pilot's intervention. Such terms will play the part of continuously acting disturbing forces. In addition, the theory presented in this paper applies to the general case of any steady or unsteady basic motion. For this reason, it is necessary to point out the sense in which we will use various notions related to the concept of the stability of a given motion or of a given particular solution of the motion equations. These mathematical concepts will have the meaning given by A. M. Liapounoff and his followers.*

We present here a few mathematical definitions.
Let

$$dx_s/dt = X_s(t; x_1, \ldots, x_n) \qquad (s = 1, \ldots, n) \qquad \text{(a)}$$

be the system of the equations for the deviations induced by an initial disturbance, with $X_s(t; 0, \ldots, 0) \equiv 0$. The solution $x_1 = x_2 = \ldots = x_n = 0$ corresponds to the basic (undisturbed) motion. Let $x_s = x_s(t; t_0, x_{10}, \ldots, x_{n0})$, $s = 1, \ldots, n$, be the components of any solution of the system (a).

(1) The basic motion is said to be *stable* if for each $\epsilon_s > 0$ and $t_0 \geq 0$, there is a set of numbers $\eta_s(\epsilon_1, \ldots, \epsilon_n, t_0)$ such that inequalities $|x_{s0}| < \eta_s$ imply $x_s(t; t_0, x_{10}, \ldots, x_{n0}) < \epsilon_s$ for $t \geq t_0$.

(2) The *stability* is said to be uniform if the numbers η_s do not depend upon t_0.

(3) If the basic motion is stable and if, in addition, for sufficiently small initial conditions

$$\lim_{t \to \infty} x_s(t; t_0, x_{10}, \ldots, x_{n0}) = 0,$$

then it is said to be *asymptotically stable*.

(4) The basic motion is said to be *uniformly-asymptotically stable* if it is uniformly stable and if there is a set of numbers δ_s and a function $T(\epsilon_s, \ldots, \epsilon_n)$ such that

$$|x_{s0}| < \delta_s, \quad t_0 \geq 0, \quad t \geq t_0 + T(\epsilon_1, \ldots, \epsilon_n)$$

imply $|x_s(t; t_0, x_{10}, \ldots, x_{n0}) < \epsilon_s$.

Now, in addition to Eqs. (a), the system

$$dx_s/dt = X_s(t; x_1, \ldots, x_n) + R_s(t; x_1, \ldots, x_n) \qquad \text{(b)}$$

is considered, where the terms R_s characterize the continuously acting disturbing factors. These generally unknown functions will be assumed to be sufficiently small in the sense required by the following definition.

(5) The basic motion is said to be stable under continuously acting disturbances if there exist two sets of functions, $\rho_s(\epsilon_1, \ldots, \epsilon_n)$ and $\eta_s(\epsilon_1, \ldots, \epsilon_n)$, such that for any $R_s(t; x_1, \ldots, x_n)$ provided that $|R_s| < \rho_s$ and for any initial conditions x_{s0} if $|x_{s0}| < \eta_s$, the solution $\bar{x}_s(t; t_0, x_{10}, \ldots, x_{n0})$ of system (b) satisfies the inequality

$$|\bar{x}_s(t; t_0, x_{10}, \ldots, x_{n0})| < \epsilon_s \quad \text{for } t > t_0$$

(6) The function $V(x_1, \ldots, x_n)$ is said to be *positive definite* if it is positive for any x_s and vanishes only when $x_1 = x_2 = \ldots = x_n = 0$. (A similar definition applies to negative definite functions.)

(7) The function $W(t; x_1, \ldots, x_n)$ is *positive definite* if there is a positive definite $V(x_1, \ldots, x_n)$ such that $W(t; x_1, \ldots, x_n) \geq V(x, \ldots x_n)$, and is *negative definite* if $W(t; x_1, \ldots, x_n) \leq -V(x_1, \ldots, x_n)$ in the range of definition.

(8) The total derivative of a function $W(t; x_1, \ldots, x_n)$ for the set (a) is defined as

$$\frac{dW}{dt} = \frac{\partial W}{\partial t} + \sum_{s=1}^{n} \frac{\partial W}{\partial x_s} X_s(t; x_1, \ldots, x_n)$$

A theorem concerning the stability under continuously acting disturbances will be used in the following section. This theorem, stated by I. G. Malkin,[9] is given here without proof:

Theorem. If the solution $x_1 = x_2 = \ldots = x_n = 0$ of system (a) is uniformly-asymptotically stable, it will be stable under continuously acting disturbances [see system (b)].

In view of the important positive and especially the negative high accelerations that have lately come into use in flight techniques for aircraft, missiles and so on, several studies have been carried out with the aim of establishing the effect of motion unsteadiness upon the dynamic stability characteristics. Accordingly, the conventional definition of aircraft stability (see above), which includes only the case of steady basic motion, was to be extended. Such an extension of the concept of stick-fixed dynamic stability was stated in reference 10

* See reference 6 and also references 7 (pp. 11–12, 16–17) and 8 (pp. 187–188, 204).

Readers may omit the following paragraphs (1)–(8) and the theorem; these have been included only for the benefit of those to whom the various mathematical notions employed in the present paper are unfamiliar.

and is reproduced as follows in a more general form*:

When the basic motion is variable (unsteady), a scheme similar to that of the stick-fixed condition can be used. For this reason, the variation of the basic motion is considered as given a priori in the form of a flight program which the aircraft must observe. Thus by implication the law of the time variation of the positions (settings) of different controls is determined. It is assumed that this law of variation is maintained even during the disturbed motion—i.e., that the pilot does not try, after a disturbance, to restore the aircraft to the motion prescribed by the program.

3. Theoretical Solution of the Problem

As mentioned earlier, the aircraft need not be stable in the generally accepted sense, i.e., as regards all kinematic parameters in uncontrolled flight. The pilot, the stabilizer or the automatic pilot are continuously actuating the controls so as to ensure the flight stabilization. Thus the human pilot continually intervenes, even during flight through a generally still atmosphere, countering by very slight reflex movements the small accidental disturbances due to various factors (e.g., the slightly asymmetric working of the engines, mass displacements within the machine, gusts of small intensity or slight piloting errors). For this reason, the pilot is usually unaware of the existence of the slight instability of the free motion, e.g., a slight longitudinal oscillatory instability in the phugoid phase or a slight lateral spiral instability in the uncontrolled flight.

Now it is obvious that, as the aircraft is stable as regards some of the motion parameters, the pilot does not have to counteract all the disturbance elements. Some of these simply could not be countered by the pilot, while the elimination of others would be an excessively fatiguing task. It is a question of the character and rapidity of the variation of the respective disturbance element. Thus, some kinematic parameters acted on by the disturbing phenomenon present variations whose nature (high-frequency oscillations) or rapidity make it impossible for the pilot to restore the flight of the aircraft to its undisturbed values. With regard to these kinematic parameters the aircraft must definitely be stable during the induced motion—that is, without the pilot's intervention (1) the respective deviations should ultimately decay and (2) they should not exceed, at any stage of the disturbed motion, certain values imposed by safety requirements.

Accordingly, in investigating the stability of a piloted aircraft (or eventually, that of one equipped with an automatic stabilizer) under actual flight conditions, the first problem is to find those kinematic parameters with regard to which the aircraft must definitely be stable in uncontrolled flight, and those which may be controlled comfortably by the pilot.

* The extension given in reference 10 concerns only certain longitudinal motions (reference 10, page 24) for the respective objects of study.

Throughout this paper, the deviations of the latter parameters will be denoted by x_i and those of the former by y_j. Together the deviations x_i and y_j constitute the dynamic variables of the induced motion equations obtained as variation equations from the general equations of motion of the aircraft.

For the present, it is assumed that in one way or another the variables x_i and y_j could be identified. Of the number n of dynamic variables, let k be the number of variables x_i ($i = 1, \ldots, k$) and m the number of variables y_j ($j = 1, \ldots, m$). As is known, the equations of the free, induced motion may be written in the form

$$\left.\begin{aligned} dx_i/dt &= \\ &X_i(t; x_1, \ldots, x_k, y_1, \ldots, y_m) \quad i = 1, \ldots, k \\ dy_j/dt &= \\ &Y_j(t; x_1, \ldots, x_k, y_1, \ldots, y_m) \quad j = 1, \ldots, m \end{aligned}\right\} \tag{3.1}$$

where in general the right-hand sides X_i and Y_j are functions of time and the dynamic variables, which are expansible into power series with respect to the dynamic variables or at least have continuous first and second partial derivatives with respect to these variables.† These functions represent deviations (or increments) of some generalized external forces of a well-known nature.‡

Further, it is assumed that the pilot by means of various controls acts upon the variables x_i and succeeds in keeping their values sufficiently small.** As a consequence of the pilot's intervention, let the variables x_i be bounded at any instant t by some constant quantities ξ_i, $|x_i(t)| \leq \xi_i$.

Through the pilot's intervention, the right-hand sides of all the equations (3.1) will be modified, generally speaking, and the set will thus become

$$dx_i/dt = X_i(t; x_1, \ldots, x_k, y_1, \ldots, y_m) + R_{x_i}(t; x_1, \ldots, x_k, y_1, \ldots, y_m) \tag{3.2a}$$

$$dy_j/dt = Y_j(t; x_1, \ldots, x_k, y_1, \ldots, y_m) + R_{y_j}(t; x_1, \ldots, x_k, y_1, \ldots, y_m) \tag{3.2b}$$

In putting the system in this form, no assumption is made concerning either the duration of the effect of pilot's intervention, or the instant at which he operates

† For the present, the general equations for any unsteady basic motion and nonlinearized induced motion are considered. In the case of a linearized system, the X_i and Y_j stand for linear homogeneous functions of the dynamic variables $x_1, \ldots, x_k$, $y_1, \ldots, y_m$ whose coefficients either depend on t or, in the particular case of a steady basic motion, are constant.

‡ Owing to the physical nature of these forces and in some cases to the fact that only small deviations are dealt with, the functions X_i and Y_j enjoy certain mathematical properties of regularity (i.e., continuity, differentiability, existence of a bound and of bounded partial derivatives, etc.), at least within the range and time interval considered. If these functions lacked such properties, some of the reasonings employed in this section would not be valid. In order to avoid, as far as possible, the use of mathematical notions, the enumeration of mathematical hypotheses will be omitted whenever such omission does not lead to confusion (e.g., in differentiating a function, it will be implicitly assumed that it is differentiable, etc.).

** Quantitative details are given in Appendix I.

the controls. The functions R_{xi} and R_{yj} represent generalized forces that are present following the gearing of controls. They are considered as unknown functions except that some assumptions are made that are compatible with the physical nature of the forces. Accordingly, it will be assumed that R_{xi} and R_{yj} enjoy certain mathematical properties of regularity similar to those of the functions X_i and Y_j, and that R_{xi} and R_{yj} vanish for any values of the variables t and y_j, if all of the variables x_i are equal to zero. In a few cases, this assumption corresponds only approximately to the actual situation, but in all practical cases the agreement is quite satisfactory. This hypothesis means, in fact, that the pilot, who intervenes immediately after a disturbance has modified a part or the whole of the parameters under his control, will cease to act at the exact instant when the respective parameters have returned to their undisturbed flight values. Since only deviations whose variations are either aperiodic or oscillatory of low frequency are taken as x_i variables, the agreement with actuality is good.

It is to be noted that, strictly speaking, the present theory does not require that the functions R_{xi} and R_{yj} vanish for $x_1 = x_2 = \ldots = x_k = 0$. It is enough that these functions are small for small values of the arguments x_i, e.g., that they satisfy a Lipschitz condition with respect to these arguments.

The assumption that $R_{yj}(t; x_1, \ldots, x_k, y_1, \ldots, y_m)$ is identically equal to zero when $x_1 = x_2 = \ldots = x_k = 0$, or that this function is small when $x_1, x_2, \ldots, x_k$ are small, might not be justified when there is a substantial lag in the operation of controls. Thus, for instance, in the case of thrust control of turbojet aircraft or aircraft with fixed-pitch propellers, the present method must be applied with caution.

Further, Eqs. (3.2b), may be written as follows:

$$dy_j/dt = Y_j(t; 0, \ldots, 0, y_1, \ldots, y_m) + [Y_j(t; x_1, \ldots, x_k, y_1, \ldots y_m) - Y_j(t; 0, \ldots, 0, y_1, \ldots y_m)] + R_{yj}(t; x_1, \ldots, x_k, y_1, \ldots, y_m) \quad (3.3)$$

or

$$dy_j/dt = Y_j(t; 0, \ldots, 0, y_1, \ldots, y_m) + \sum_{i=1}^{k} x_i \left\{ \frac{\partial}{\partial x_i} (Y_j + R_{yj}) \right\} \quad (3.4)$$

where the partial derivatives in the summation are taken for certain intermediate values of the variables x_i.

The sums on the right-hand side of Eqs. (3.4) appear as continuously acting disturbing forces. But it was shown* that the uniform asymptotic stability of the zero solution of the system, from which these terms were omitted, implies the stability of the solution when the system (3.4) is complete.

Let

$$Y_j(t; 0, \ldots, 0; y_1, \ldots, y_m) = \bar{Y}_j(t; y_1, \ldots, y_m)$$

and let the equations

$$dy_j/dt = \bar{Y}_j(t; y_1, \ldots, y_m) \qquad j = 1, 2, \ldots, m \quad (3.5)$$

be referred to as an auxiliary system.

Then, the first result may be stated as follows: If the zero solution of the auxiliary system (3.5) is uniformly-asymptotically stable, then the partially controlled basic motion of an aircraft is stable. Hence, the criteria for the uniform asymptotic stability of the imaginary basic motion described by the particular solution $y_1 = y_2 = \ldots = y_m = 0$ of the system (3.5) are at the same time stability criteria for the actual partially controlled motion of an aircraft, corresponding to the solution $x_1 = \ldots = x_k = y_1 = \ldots y_m = 0$ of the system (3.4). Thus the problem of finding stability criteria is solved by means of the auxiliary system, the order of which is k degrees smaller than that of system which describes the actual disturbed motion (where k represents the number of kinematic parameters controlled by the pilot). In most practical cases, the investigation of the solution of the auxiliary system may yield more than just the stability criteria. Indeed, in the case of a flight under conditions sufficiently quiet that not too severe interventions of the pilot are required, the auxiliary system may in many respects successfully replace the system (3.4) which governs the actual motion.

Thus the solution of the auxiliary system may furnish, to a very close approximation, indications of the velocity with which the disturbances decay, the oscillatory or nonoscillatory character of the deviation throughout the transitory motion induced by a disturbance, etc.

As shown above, a complementary condition is, however, required by the present method. This consists in the fact that the additional terms of the system (3.4) must be sufficiently small—i.e., the pilot must ensure sufficiently small values for the upper bounds ξ_i of the variables x_i.

(4) Aircraft Stability in Several Particular Cases of Partially Controlled Motions

In the following, a few practical applications will be presented to illustrate the manner in which the above method may be used. Naturally, the few cases discussed herein far from exhaust the range of applications.

Longitudinal Stability

Referring the aircraft motion to wind axes, the variation equations which describe the longitudinal disturbed motion will be, as is known, of the form†

* See the theorem stated in the previous section.

† See the list of symbols. For details concerning the reduction of the dynamic equations to nondimensional form, see references 10 and 11. In the numerical example given in this section, the reduction to nondimensional forms is carried out as in reference 12. The variation of lift and drag with angular velocities is disregarded.

$$\left.\begin{aligned} d\Delta\hat{V}/dt &= a_{11}(t)\Delta\hat{V} + a_{12}(t)\Delta\alpha + a_{13}(t)\Delta\theta + F_1(t;\ \Delta\hat{V},\ \Delta\alpha,\ \Delta\theta,\ \Delta\hat{q}) \\ d\Delta\alpha/dt &= a_{21}(t)\Delta\hat{V} + a_{22}(t)\Delta\alpha + a_{23}(t)\Delta\theta + \Delta\hat{q} + F_2(t;\ \Delta\hat{V},\ \Delta\alpha,\ \Delta\theta,\ \Delta\hat{q}) \\ d\Delta\theta/dt &= \Delta\hat{q} \\ d\Delta\hat{q}/dt &= a_{41}(t)\Delta\hat{V} + a_{42}(t)\Delta\alpha + a_{43}(t)\Delta\theta + a_{44}(t)\Delta\hat{q} + F_4(t;\ \Delta\hat{V},\ \Delta\alpha,\ \Delta\theta,\ \Delta\hat{q}) \end{aligned}\right\} \quad (4.1)$$

where

$$\begin{aligned} a_{11}(t) &= -\hat{V}[2C_D + M(\partial C_D/\partial M) + C_{T_V}\cos\alpha] \\ a_{12}(t) &= \hat{V}^2[(\partial C_D/\partial\alpha) + C_T\sin\alpha - C_W\cos\gamma] \\ a_{13}(t) &= -\hat{V}^2 C_W\cos\gamma \\ a_{21}(t) &= -[2C_L + M(\partial C_L/\partial M) - 1/\hat{V}(d\gamma/dt)] \\ a_{22}(t) &= -\hat{V}[(\partial C_L/\partial\alpha) - C_W\sin\gamma] \doteq -\hat{V}(\partial C_L/\partial\alpha) \\ a_{23}(t) &= -\hat{V}C_W\sin\gamma \\ a_{41}(t) &= \hat{V}\{\mu[2C_m + M(\partial C_m/\partial M) + \hat{Z}_t C_{T_V}] - \hat{V}(\partial C_m/\partial\dot{\bar{\alpha}})[2C_L + M(\partial C_L/\partial M) - 1/\hat{V}(d\gamma/dt)]\} \\ a_{42}(t) &= \hat{V}^2\{\mu(\partial C_m/\partial\alpha) - \hat{V}[(\partial C_L/\partial\alpha) + C_T\cos\alpha - C_W\sin\gamma]\} \doteq \hat{V}^2[\mu(\partial C_m/\partial\alpha) - \hat{V}(\partial C_L/\partial\alpha)] \\ a_{43}(t) &= -\hat{V}^3 C_W(\partial C_m/\partial\dot{\bar{\alpha}})\sin\gamma \\ a_{44}(t) &= \hat{V}^2[(\partial C_m/\partial\bar{q}) + (\partial C_m/\partial\dot{\bar{\alpha}})] \end{aligned}$$

In the right-hand sides of the system (4.1), the linear terms are written separately, so that the functions F_1, F_2, and F_4 represent the respective nonlinear terms. For certain reasons such an arrangement of the equations proves to be more convenient, since it makes it possible either to include the nonlinear terms in the additional terms R_s, or to disregard them completely, as is currently done in the theory of aircraft stability. In both cases, as the auxiliary system [see Eq. (3.5)] a linearized system of the following form may be used:

$$dy_j/dt = a_{j1}(t)y_1 + \ldots + a_{jm}(t)y_m \quad (4.2)$$

Case of Uniform Basic Motion

If the undisturbed motion is a steady one, the right-hand sides of the equations of induced motion will not depend explicitly upon t. In other words, F_1, F_2, and F_4 will be functions only of the dynamic variables $\Delta\hat{V}$, $\Delta\alpha$, $\Delta\theta$, and $\Delta\hat{q}$, and the coefficients a_{ij} of the linear terms will be constants.

As the variation of the deviations of the incidence angle and angular velocity of pitch is generally rapid, i.e., oscillatory of high frequency, these deviations are in practice out of the pilot's control. Accordingly, only three different cases will be considered here: (1) the pilot acts only upon the pitch angle; (2) the pilot keeps the flight speed within a sufficiently close neighborhood of its undisturbed value; and (3) the pilot gears the controls to act upon both the pitch angle and flight speed deviations.

(*a*) *Longitudinal Stability When the Pitch Angle Is Under the Pilot's Control*—Assume that the pilot must maintain a small pitch-angle deviation. In this case, the linearized auxiliary system that furnishes stability criteria for the partially controlled motion will be

$$\left.\begin{aligned} d\Delta\hat{V}/dt &= a_{11}\Delta\hat{V} + a_{12}\Delta\alpha \\ d\Delta\alpha/dt &= a_{21}\Delta\hat{V} + a_{22}\Delta\alpha + \Delta\hat{q} \\ d\Delta\hat{q}/dt &= a_{41}\Delta\hat{V} + a_{42}\Delta\alpha + a_{44}\Delta\hat{q} \end{aligned}\right\} \quad (4.3)$$

for which the characteristic equation is

$$\lambda^3 + b_1\lambda^2 + b_2\lambda + b_3 = 0 \quad (4.4)$$

with

$$\begin{aligned} b_1 &= -(a_{11} + a_{22} + a_{44}) \\ b_2 &= a_{22}a_{44} - a_{42} + a_{11}(a_{22} + a_{44}) - a_{12}a_{21} \\ b_3 &= -a_{11}(a_{22}a_{44} - a_{42}) + a_{12}(a_{21}a_{44} - a_{41}) \end{aligned}$$

On comparing Eq. (4.4) with the characteristic equation of the complete linearized system of the induced motion in uncontrolled flight, viz.,

$$\lambda^4 + a_1\lambda^3 + a_2\lambda^2 + a_3\lambda + a_4 = 0 \quad (4.5)$$

in which

$$a_1 = b_1,\quad a_2 = b_2,\quad a_3 = b_3 - a_{13}a_{22}a_{41}$$
$$a_4 = a_{13}(a_{21}a_{42} - a_{41}a_{22})$$

it is readily seen that the coefficients of the $(n-1)$ and $(n-2)$ powers (where n represents the degree of the respective equations) are identical, while the coefficients of λ^{n-3} differ very slightly for the two equations. Then, since a_3 is small in comparison with a_1, and a_2, b_3 will also be small compared with b_1 and b_2, the following conclusion may immediately be drawn:

It is known that the solution of Eq. (4.5) consists of a pair of roots numerically large in absolute value (corresponding to the rapid mode of the induced motion) and a pair of roots numerically small in absolute value (the phugoid roots). According to the comparison made above, the pair of large roots reappears almost identically when the angle of pitch is controlled by the pilot. Hence, the rapid incidence adjustment and the rapid decay of the rate of pitch deviation are ensured in this case of partially controlled motion.

The third root of Eq. (4.4) will generally assume a small absolute value. This root may be taken in a first approximation as equal to $-b_3/b_2$. As b_2 is positive in all cases of practical importance, the relation

$$b_3 \equiv -a_{11}(a_{22}a_{44} - a_{42}) + a_{12}(a_{21}a_{44} - a_{41}) > 0 \quad (4.6)$$

which in most cases may be replaced by

$$-a_{11} \equiv 2C_D + M(\partial C_D/\partial M) + C_{T_V}\cos\alpha > 0 \quad (4.7)$$

gives a first, approximate indication concerning the stability in this case of partially controlled motion.

It is readily seen that the inequality (4.7) is fulfilled when the drag coefficient is independent of, or increases with, the Mach number (since $C_{T_V}\cos\alpha$ is negligible). It is to be noticed that under the same conditions, the basic motion of the uncontrolled aircraft may be unstable, since the free term of Eq. (4.5) may be negative.

To illustrate the above conclusions, the following numerical example is considered.

A fighter aircraft with the characteristics*

* See reference 12, p. 391.

$W = 6{,}900$ kg. $\quad c = 1.95$ m. $\quad z_T = 0.25$ m.
$S = 21.7$ m.^{2} $\quad S_t = 3.8$ m.^{2} $\quad k_Y{}^2 = 3.48$ m.^{2}
$l_t = 6$ m.

flies on a straight level path at a speed of 248 m./sec. The following data correspond to this flight regime:

$$\begin{array}{llll} C_L & = 0.1 & \partial C_D/\partial\alpha & = 0.057 \\ C_D & = 0.02 & \partial C_D/\partial M & = 0.088 \\ T & = 1{,}360 \text{ kg.} & \partial C_D/\partial\bar{q} & = 0 \\ \mathrm{M} & = 0.74 & & \\ \alpha = \theta & = 0.0131 \text{ rad.} & \partial C_m/\partial\alpha & = -0.17 \\ \gamma & = 0 & & \\ \partial C_L/\partial\alpha & = 5.12 & & \\ \partial C_I/\partial M & = 0.5 & \partial C_m/\partial M & = -0.0615 \\ \partial C_L/\partial\bar{q} & = 0 & \partial C_m/\partial\bar{q} & = -5.9 \\ & & \partial C_m/\partial\dot{\bar{\alpha}} & = -2.95 \end{array}$$

$$(\partial/\partial M)(C_D - C_T) = 0.141$$
$$(\partial/\partial M)(C_m - \hat{Z}_T C_T) = 0.0055$$

Then the coefficients of the differential equation system of the longitudinal symmetric induced motion will be**

$$\left.\begin{array}{lll} a_{11} = -0.104 & a_{21} = -0.57 & a_{41} = -11.30 \\ a_{12} = 0.043 & a_{22} = -5.12 & a_{42} = -43.60 \\ a_{13} = -0.100 & a_{23} = 0 & a_{43} = 0 \\ & a_{24} = 1 & a_{44} = -9.68 \end{array}\right\} \quad (4.8)$$

and the roots of the characteristic equation

$$\lambda^4 + 14.90\lambda^3 + 94.66\lambda^2 + 9.29\lambda - 3.29 = 0$$

are:

$$\lambda_{1,2} = -7.38 \pm 6.19i \quad \lambda_3 = -0.267 \quad \lambda_4 = +0.161$$

Since one of the roots is positive (but small in value), the basic motion of the uncontrolled aircraft is slightly unstable.

Consider now that the pilot maintains the aircraft attitude near that of the undisturbed flight. In this case, the condition (4.7) is fulfilled ($a_{11} = -0.104$) and consequently the partially controlled motion is expected to be stable. Indeed, the characteristic equation of the auxiliary system (4.3) will be

$$\lambda^3 + 14.90\lambda^2 + 94.76\lambda + 10.42 = 0$$

and its roots:

$$\lambda_{1,2}' = -7.39 \pm 6.20i \quad \lambda_3' = -0.112$$

It is readily seen (1) that the pair of roots with large absolute values scarcely differs from that of the characteristic equation of the complete system, and thus the rapid incidence adjustment is ensured, and (2) that the partially controlled motion is stable, since the third root is negative. It is quite natural that the control of the pitch angle, which after the incidence adjustment results in the maintaining of a very nearly level path, excludes the phugoid oscillations thus causing the slow mode to degenerate in a pure subsidence.

** For expressions of the coefficients a_{ij} see reference 12, page 380, and for the reduction to nondimensional forms see *ibid.*, pages 376–379.

(*b*) *Longitudinal Stability When the Flight Velocity Is Under the Pilot's Control*—It is assumed that the pilot succeeds in maintaining at small values the flight velocity deviations induced by a disturbance. For this case the linearized auxiliary system will be

$$\left.\begin{array}{l} d\Delta\alpha/dt = a_{22}\Delta\alpha + a_{23}\Delta\theta + \Delta\hat{q} \\ d\Delta\theta/dt = \Delta\hat{q} \\ d\Delta\hat{q}/dt = a_{42}\Delta\alpha + a_{43}\Delta\theta + a_{41}\Delta\hat{q} \end{array}\right\} \quad (4.9)$$

with the characteristic equation

$$\lambda^3 + c_1\lambda^2 + c_2\lambda + c_3 = 0 \quad (4.10)$$

where

$$\begin{aligned} c_1 &= a_1 + a_{11} \\ c_2 &= a_2 + [a_{12}a_{22} - a_{11}(a_{22} + a_{44}) - a_{43}] \\ c_3 &= a_{22}a_{43} - a_{23}a_{42} \end{aligned}$$

It is readily seen that the values of the coefficients of λ^3 and λ^2 are close enough to those of λ^4 and λ^3, respectively, in the characteristic equation (4.5) of the complete system. Accordingly, Eq. (4.10) will yield for conventional flight regimes a complex pair of roots numerically large in absolute value, and thus the rapid incidence adjustment is ensured in this case also.

In certain cases, however, it is not sufficient to control only the flight speed, since the third root of the characteristic equation (4.10) may be positive. Indeed, for the incidence range below stalling, and for statically stable machines, the coefficients

$$a_{22} = -[(\partial C_L/\partial\alpha) + C_T\cos\alpha]$$

and

$$a_{42} = \mu(\partial C_m/\partial\alpha) - (\partial C_m/\partial\dot{\bar{\alpha}})\,[(\partial C_L/\partial\alpha) + C_T\cos\alpha]$$

are negative,* and hence the expressions

$$-a_{23}a_{42} = -a_{42}(C_D - C_T\cos\alpha)$$

and

$$a_{22}a_{43} = a_{22}(1/i_Y{}^2)(\partial C_m/\partial\dot{\bar{\alpha}})(C_D - C_T\cos\alpha)$$

are of the same sign, namely, the sign of $(C_D - C_T\cos\alpha)$. In compliance with one of the Routh-Hurwitz criteria for a negative third root, it is necessary that the free term of the characteristic equation be positive, that is,

$$C_D - C_T\cos\alpha > 0 \quad (4.11)$$

It is readily seen that condition (4.11) is not fulfilled when the aircraft is on a climbing path. For level flight, as the free term vanishes ($a_{23} = a_{43} = 0$) one of the roots of the characteristic equation (4.10) of the auxiliary system will be zero. Considering the unlinearized auxiliary system, it is readily seen that the zero root leads in this case to instability,† even if the

* For statically stable aircrafts the coefficient a_{42} is usually negative since the numerical value of μ is relatively large.

† Concerning the method of investigating the stability of stationary motions when the characteristic equation of the linearized equation admits one root equal to zero, see reference 6 and page 85 of reference 7.

continuously acting disturbing factor due to pilot's intervention is not taken into account.

Summing up, it can be said that for both climbing and level flights, stabilization through flight-speed control alone is insufficient.

(*c*) *Longitudinal Stability When Both Attitude and Flight Velocity Are Under the Pilot's Control*—In this case the linearized auxiliary system becomes the well-known set of equations for pure short-period oscillations.

$$\left.\begin{aligned} d\Delta\alpha/dt &= a_{22}\Delta\alpha + \Delta\hat{q} \\ d\Delta\hat{q}/dt &= a_{42}\Delta\alpha + a_{44}\Delta\hat{q} \end{aligned}\right\} \tag{4.12}$$

with the characteristic equation

$$\lambda^2 + d_1\lambda + d_2 = 0 \tag{4.13}$$

where

$$d_1 = a_1 + a_{11} \quad d_2 = a_2 + [-a_{11}(a_{22} + a_{44}) + a_{12}a_{22}]$$

It is known that for statically stable aircraft, Eq. (4.13) will have conjugate complex roots. Since their real parts are negative and large, rapid damping of the deviation of the incidence angle and of the rate of pitch is assured. These roots are generally slightly different from the numerically large pair of roots of Eq. (4.5). Resuming the above numerical example, the roots of Eq. (4.13), $\lambda_{1,2}'' = -7.40 \pm 6.20i$, are comparable with the numerically large roots of the characteristic equation for the system of disturbed motion in uncontrolled flight, $\lambda_{1,2} = -7.38 \pm 6.19i$.

Case of Nonuniform Basic Motion

We consider here only the case of straight, level basic motion in which the pilot controls both the attitude and the velocity.

In such a case, the linearized auxiliary system will be

$$\left.\begin{aligned} d\Delta\alpha/dt &= a_{22}(t)\Delta\alpha + \Delta\hat{q} \\ d\Delta\hat{q}/dt &= a_{42}(t)\Delta\alpha + a_{44}(t)\Delta\hat{q} \end{aligned}\right\} \tag{4.14}$$

It was shown[10] that if the aircraft is statically stable throughout the range of all regimes proper to the given machine, then the zero solution of the system (4.14) may be unstable only in decelerated flight. For such a case a stability criterion was deduced[10] in the form of two inequalities both of which must be satisfied at any instant:

$$a_{22}(t) < 0 \qquad a_{44}(t) - \tfrac{1}{2}(d/dt)\ln[-a_{42}(t)] < 0 \tag{4.15}$$

The inequalities (4.15) are fulfilled if the absolute value of the undisturbed acceleration does not exceed the magnitude ng, where g is the gravitational constant and*

$$n = \frac{\rho}{2}\frac{S}{W}V_{max}^2 \min\left\{\left[\hat{V}^2\left(\frac{\partial C_L}{\partial\alpha} + C_D\right)\right]; \left[-\hat{V}^3\left(\frac{\partial C_m}{\partial\bar{q}} + \frac{\partial C_m}{\partial\dot{\bar{\alpha}}}\right)\right]\right\}$$

* By "min" is meant the smallest of the two bracketed values.

Lateral Stability

As is known, the set of equations for lateral-antisymmetric motion (deduced as variation equations from the set of motion equations referred to the body axes) may be written in the form

$$\left.\begin{aligned} d\Delta\hat{p}/dt &= b_{11}(t)\Delta\hat{p} + b_{12}(t)\Delta\hat{r} + b_{13}(t)\Delta\beta \\ d\Delta\hat{r}/dt &= b_{21}(t)\Delta\hat{p} + b_{22}(t)\Delta\hat{r} + b_{23}(t)\Delta\beta \\ d\Delta\beta/dt &= b_{31}(t)\Delta\hat{p} + b_{32}(t)\Delta\hat{r} + \\ &\qquad b_{33}(t)\Delta\beta + b_{34}(t)\Delta\phi \\ d\Delta\phi/dt &= b_{41}(t)\Delta\hat{p} + b_{42}(t)\Delta\hat{r} \end{aligned}\right\} \tag{4.16}$$

where

$$b_{11} = K_0(\overline{C}_{l_p} + K_1\overline{C}_{n_p}) \qquad b_{12} = K_0(\overline{C}_{l_r} + K_1\overline{C}_{n_r})$$

$$b_{21} = K_0(\overline{C}_{n_p} + K_2\overline{C}_{l_p}) \qquad b_{22} = K_0(\overline{C}_{n_p} + K_2\overline{C}_{l_p})$$

$$b_{31} = \mu\alpha \qquad b_{32} = \mu$$

$$b_{41} = \mu \qquad b_{42} = -\mu\tan\theta\dagger$$

$$b_{13} = K_0(\overline{C}_{l_\beta} + K_1\overline{C}_{n_\beta})$$

$$b_{23} = K_0(\overline{C}_{n_\beta} + K_2\overline{C}_{l_\beta})$$

$$b_{33} = {}^1/_2C_{y_\beta} \qquad b_{34} = {}^1/_2C_L$$

with

$$K_0 = 1 - [(i_{zx})^2/i_xi_z] \simeq 1, \quad K_1 = i_{zx}/i_x, \quad K_2 = i_{zx}/i_z$$

$$\overline{C}_{l_p} = C_{l_p}/i_x, \quad \overline{C}_{l_r} = C_{l_r}/i_z, \quad \overline{C}_{l_\beta} = C_{l_\beta}/i_x$$

$$\overline{C}_{n_p} = C_{n_p}/i_z, \quad \overline{C}_{n_r} = C_{n_r}/i_z, \quad \overline{C}_{n_\beta} = C_{n_\beta}/i_z$$

With the possible exception of the controllability of the angular roll deviation, the lateral controllability for stabilizing the disturbed motion depends upon the imaginary part of the complex roots of the characteristic equation of the set governing the uncontrolled disturbed flight. Hence, the main parameter is the "weathercock stability" coefficient C_{n_β}. A large absolute value of this coefficient may lead to an excessively high oscillation frequency. (The existence of static weathercock stability corresponds to $C_{n_\beta} < 0$.)

Since in the variation of the roll-angle deviation aperiodic modes generally prevail, this deviation may be countered successfully by the pilot in all practical cases.

Case of Uniform Basic Motion

Several particular cases of partially controlled motion will be discussed.

(*a*) *Lateral Stability When the Angle of Sideslip Is Under the Pilot's Control*—The auxiliary system will be

$$\left.\begin{aligned} d\Delta\hat{p}/dt &= b_{11}\Delta\hat{p} + b_{12}\Delta\hat{r} \\ d\Delta\hat{r}/dt &= b_{21}\Delta\hat{p} + b_{22}\Delta\hat{r} \\ d\Delta\phi/dt &= b_{41}\Delta\hat{p} + b_{42}\Delta\hat{r} \end{aligned}\right\} \tag{4.17}$$

It is readily seen that the characteristic equation of the system yields a zero root. Consequently, the existence or nonexistence of stability will be indicated

† The value of the pitch angle θ taken here is that corresponding to the undisturbed flight regime.

by higher-order terms in $\Delta\hat{p}$, $\Delta\hat{r}$, and $\Delta\phi$, by all the terms in $\Delta\beta$, as well as by the terms representing the disturbing forces due to pilot's intervention. Owing to the random character of the last terms, instable situations are likely to develop. Consequently, when the pilot acts only upon the sideslip angle, the stabilization is not completely ensured.

(*b*) *Lateral Stability When the Angle of Roll Is Under the Pilot's Control*—As is readily seen, the characteristic equation of the auxiliary system for this case,

$$\left.\begin{aligned} d\Delta\hat{p}/dt &= b_{11}\Delta\hat{p} + b_{12}\Delta\hat{r} + b_{13}\Delta\beta \\ d\Delta\hat{r}/dt &= b_{21}\Delta\hat{p} + b_{22}\Delta\hat{r} + b_{23}\Delta\beta \\ d\Delta\beta/dt &= b_{31}\Delta\hat{p} + b_{32}\Delta\hat{r} + b_{33}\Delta\beta \end{aligned}\right\} \qquad (4.18)$$

is somehow comparable to that of the complete system (4.16). Indeed, this equation may be written in the form

$$-\lambda\mathbf{D}(\lambda) + b_{34}\mathbf{L}(\lambda) = 0 \qquad (4.19)$$

where $\mathbf{D}(\lambda) = 0$ represents the characteristic equation of the auxiliary system (4.18) and $\mathbf{L}(\lambda)$ stands for a binomial of the first degree in λ. On comparing the equation $\mathbf{D}(\lambda) = 0$ with Eq. (4.19), one may easily draw certain conclusions:

As the coefficients of the high powers of λ are identical for the two equations, the numerically large real root of Eq. (4.19) will reappear almost unchanged in the solution of the characteristic equation of the auxiliary system.

It should be noticed that the numerically small real root of Eq. (4.19), which may assume a positive value and thus lead to the instability of the uncontrolled aircraft, no longer appears. Thus the partially controlled motion is entirely stable.

(*c*) *Lateral Stability When Both Sideslip and Roll Angles Are Under the Pilot's Control*—Here the auxiliary system is of the second order:

$$\left.\begin{aligned} d\Delta\hat{p}/dt &= b_{11}\Delta\hat{p} + b_{12}\Delta\hat{r} \\ d\Delta\hat{r}/dt &= b_{21}\Delta\hat{p} + b_{22}\Delta\hat{r} \end{aligned}\right\} \qquad (4.20)$$

Since $b_{11} \doteq \overline{C}_{l_p}$ is large in comparison with $b_{12} \doteq \overline{C}_{l_r}$ and $b_{21} \doteq \overline{C}_{n_p}$, the characteristic equation of the system (4.20) will yield two real roots. In order that both of them be negative, it is required either that $b_{12}b_{21} < 0$ or, if $b_{12}b_{21} > 0$, that $b_{11}b_{22} > b_{12}b_{21}$.

(*d*) *Lateral Stability When the Sideslip Angle and the Rate of Yaw Are Under the Pilot's Control*—As is readily seen, the zero solution of the auxiliary system

$$\left.\begin{aligned} d\Delta\hat{p}/dt &= b_{11}\Delta\hat{p} \\ d\Delta\phi/dt &= b_{41}\Delta\hat{p} \end{aligned}\right\} \qquad (4.21)$$

cannot be uniformly-asymptotically stable but may enjoy simple stability. Consequently, it cannot provide valid conclusions as regards the actual partially controlled motion.

(*e*) *Lateral Stability When the Roll Angle and Its Time Rate of Change Are Under the Pilot's Control*—The characteristic equation of the auxiliary system

$$\left.\begin{aligned} d\Delta\hat{r}/dt &= b_{22}\Delta\hat{r} + b_{23}\Delta\beta \\ d\Delta\beta/dt &= b_{32}\Delta\hat{r} + b_{33}\Delta\beta \end{aligned}\right\} \qquad (4.22)$$

yields complex roots for conventional values of the "weathercock stability" coefficient. Since the real part is in all cases negative, the partially controlled motion is stable.

Numerical example: Consider a machine having the following characteristics:*

$$W = 5{,}000 \text{ kg.} \quad S = 20 \text{ m.}^2 \quad b = 10 \text{ m.}$$
$$i_x = 0.05 \qquad i_z = 0.2 \qquad i_{zx} = 0.001$$

The aircraft climbs on a straight path at about 5,000 m. with a constant speed of $V = 258$ m./sec. The following data correspond to this regime:**

α	$= 0.0525$	$\overline{C}_{l_p}$	$= -8.0$
$\tan\theta$	$= 0.08$	$\overline{C}_{l_r}$	$= -2.0$
C_L	$= 0.2$	$\overline{C}_{l_\beta}$	$= -0.6$
$\overline{C}_{n_p}$	$= -0.13$	K_0	$= 1$
$\overline{C}_{n_r}$	$= -0.75$	K_1	$= 0.02$
$\overline{C}_{n_\beta}$	$= -0.60$	K_2	$= 0.005$

Then the coefficients of system (4.16) will assume the values

$b_{11} = -8.00$	$b_{12} = -2.015$	$b_{13} = -0.612$
$b_{21} = -0.170$	$b_{22} = -0.760$	$b_{23} = -0.603$
$b_{31} = +3.57$	$b_{32} = +68.0$	$b_{33} = -0.15$
$b_{41} = +68.0$	$b_{42} = -5.44$	$b_{34} = +0.1$

and the roots of its characteristic equation

$$\lambda^4 + 8.91\lambda^3 + 50.30\lambda^2 + 323.00\lambda - 7.70 = 0$$

will take the values

$$\lambda_1 = -7.8 \qquad \lambda_2 = +0.0238 \qquad \lambda_{3,4} = -0.567 \pm 6.41i$$

Hence it is likely that in uncontrolled flight the aircraft will enjoy a slight amount of spiral instability.

When the angle ϕ is under the pilot's control, the characteristic equation

$$\mathbf{D}(\lambda) \equiv -\lambda^3 - 8.91\lambda^2 - 50.30\lambda - 319.10 = 0$$

of the auxiliary system (4.18) admits the following three roots (which were calculated with the same degree of approximation as the preceding ones):

$$\lambda_1' = -7.74 \qquad \lambda_{2,3}' = -0.585 \pm 6.39i$$

As was to be expected, the numerically large real negative root is reproduced almost identically, the pair of complex roots reappears with a slight improvement of the damping decrement (i.e., the real part), while the numerically small root, to which the instability is due, no longer appears. Thus the zero solution of the auxiliary system (4.18) is uniformly-asymptotically stable and, accordingly, the actual partially controlled

---

* See reference 12, page 466.

** For reducing the dynamic equations of the lateral-antisymmetric motion to nondimensional forms, the following units (scales) were used: force, $\frac{1}{2}\rho V^2 S$; moment, $\frac{1}{2}\rho V^2 Sb$; angular velocity, $2Vb^{-1}$; mass, $\frac{1}{2}\rho Sb$; and time, $m(\rho VS)^{-1}$.

motion, with the pilot acting upon the roll angle, is stable.

If the pilot holds under his control both the angle of roll and the angle of sideslip, the roots of the characteristic equation

$$\lambda^2 + 8.76\lambda + 5.74 = 0$$

of the auxiliary system are real and negative ($\lambda_1'' = -8.05$, $\lambda_2'' = -0.71$) and consequently the partially controlled motion is stable.

Lastly, when the roll angle and the angular velocity of roll are controlled by the pilot, the respective characteristic equation admits the following pair of complex roots: $\lambda_{1,2} = -0.455 \pm 6.35i$. This implies the stability of the actual partially controlled basic motion. Considering the solution of the auxiliary system, we would expect the actual disturbed motion to be a damped oscillation of high frequency.

Case of Nonuniform Basic Motion

Only the case in which the pilot controls both the angle of roll and the angle of sideslip will be considered.

A procedure similar to that given in reference 10 will be used. The linearized auxiliary system will be of the form

$$\left.\begin{aligned} d\Delta\hat{p}/dt &= b_{11}(t)\Delta\hat{p} + b_{12}(t)\Delta\hat{r} \\ d\Delta\hat{r}/dt &= b_{21}(t)\Delta\hat{p} + b_{22}(t)\Delta\hat{r} \end{aligned}\right\} \quad (4.23)$$

$$\text{Let} \quad \mathbf{W}(t;\ \Delta\hat{p},\ \Delta\hat{r}) \equiv A(t)\Delta\hat{p}^2 + B(t)\Delta\hat{r}^2 \quad (4.24)$$

be a positive definite quadratic form with the coefficients $A(t)$ and $B(t)$ bounded for any $t \geq t_0$. In such a case, in compliance with I. G. Malkin's theorem,* if the total derivative of the function $\mathbf{W}$ for the system (4.23) is negative definite, the zero solution is stable under continuously acting disturbances, i.e., the partially controlled basic motion is stable.

As is known, the quadratic form**

$$d\mathbf{W}/dt \equiv (\dot{A} + 2Ab_{11})\Delta\hat{p}^2 + 2(Ab_{12} + Bb_{21})\Delta\hat{p}\Delta\hat{r} + (\dot{B} + 2Bb_{22})\Delta\hat{r}^2 \quad (4.25)$$

is negative definite if and only if the two characteristic roots of its matrix are negative. Hence,

$$\left.\begin{aligned} \dot{A} + \dot{B} + 2(Ab_{11} + Bb_{22}) &< 0 \\ (Ab_{12} + Bb_{21})^2 &< (\dot{A} + 2Ab_{11})(\dot{B} + 2Bb_{22}) \end{aligned}\right\} \quad (4.26)$$

A sufficient stability condition may be obtained by setting $A = B = \text{const}$. Then, the inequalities (4.26) yield

$$\left.\begin{aligned} b_{11} + b_{22} &< 0 \\ (b_{12} + b_{21})^2 &< 4b_{11}b_{22} \end{aligned}\right\} \quad (4.27)$$

The relations (4.27) may be written approximately as follows:

$$\left.\begin{aligned} \overline{C}_{l_p} + \overline{C}_{n_r} &< 0 \\ (\overline{C}_{l_r} + \overline{C}_{n_p})^2 &< 4\overline{C}_{l_p}\overline{C}_{n_r} \end{aligned}\right\} \quad (4.28)$$

The first of the inequalities (4.28) is always fulfilled. If the second is also fulfilled at any instant $t > t_0$, then, in the case of an unsteady basic motion, the lateral stability of the partially controlled motion is ensured.

Appendix I

Limits of Applicability of the Theory

As shown above, the theorem of stability under continuously acting disturbances imposes a quantitative condition on these disturbances. Therefore one must determine whether the pilot can in practice ensure the fulfilment of this condition by gearing his controls. To this end, it is necessary to evaluate the functions $\rho_s(\epsilon_1, \ldots, \epsilon_n)$†, which may be done for instance through the use of reasoning similar to that employed by I. G. Malkin in demonstrating one of his theorems of stability under continuously acting disturbances.‡

Consider the system [cf. Eqs. (3.4) and (3.5)]

$$dy_j/dt = \bar{Y}_j(t;\ y_1, \ldots y_m) + R_j(t;\ x_1, \ldots x_k,\ y_1, \ldots, y_m) \quad (A1)$$
$$j = 1, 2, \ldots, m$$

where $\bar{Y}_j$ may be written in the first approximation as $\bar{Y}_j(t;\ y_1, \ldots, y_m) = \sum_{s=1}^{m} p_{js}(t)y_s$, and where R_j denotes the additional terms included in the right-hand sides of Eqs. (3.4):

$$R_j(t;\ x_1, \ldots, x_k,\ y_1, \ldots, y_m) = \sum_{s=1}^{k} x_s\{(\partial/\partial x_s)(Y_j + R_{y_j})\} \quad (A2)$$

The functions R_j satisfy for any $t > t_0$, certain inequalities of the form

$$|R_j(t;\ x_1, \ldots, x_k,\ y_1, \ldots, y_m)| < \rho_j = \text{const.} \quad (A3)$$

Now, let $\mathbf{W}(t;\ y_1, \ldots, y_m)$ be a positive definite function (e.g., a quadratic form)†† whose total time derivative for the system (3.5) is negative definite. Then, the evaluation of $\rho_s(\epsilon_1, \ldots, \epsilon_m)$ will result from the condition

---

* See reference 7, page 294.

** Dotted symbols denote derivatives with respect to t.

† See Section 2, Definition (5).

‡ See reference 7, 294, and also reference 2. Some allowable bounds for the values of the additional terms R_s may be determined also through another procedure. This procedure consists in evaluating the part contributed by these additional terms to the general solution of the equations of the induced motion, by means of the method of the variation of parameters (see, for instance, reference 13).

†† *Note.* In the case of steady basic motion, the coefficients of the quadratic form $\mathbf{W}(y_1, \ldots, y_m)$ are determined from the condition that the total time derivative of $\mathbf{W}$ for the system which describes to a first approximation the motion induced by an initial disturbance (the homogeneous linear system with constant coefficients) is identically equal to a given negative definite quadratic form $-V$ (e.g., $-V = -\sum_{s=1}^{m} y_s^2$). The function $\mathbf{W}$ is uniquely determined, and if we assume that all the roots of the characteristic equation of the homogeneous linear system have negative real parts, this function will be positive definite.

When the basic motion is unsteady, $\mathbf{W}$ functions will be employed, e.g., functions of the form of those indicated in Section 4 [see formula (4.24)] or in reference 10.

that at any point on the moving ellipsoid in the space of variables y_s: $\mathbf{W}(t; y_1, \ldots, y_m) = C^2$ where

$$C^2 < \underset{\substack{t > t_0 \\ |y_s| > \epsilon_s}}{\text{g.l.b.}} \mathbf{W}(t; y, \ldots, y_m)^{**},$$

and at any instant $t \geq t_0$, the inequalities

$$\left\{\frac{\partial \mathbf{W}}{\partial t} + \sum_{j=1}^{m} (\bar{Y}_j + \rho_j) \frac{\partial \mathbf{W}}{\partial y_j}\right\}_{\mathbf{W}=C^2} < 0 \qquad \text{(A4)}$$

are fulfilled, provided that the initial conditions satisfy the relation

$$\mathbf{W}(t_0; y_{10}, \ldots, y_{m0}) < C^2 \qquad \text{(A5)}$$

Let $\bar{\rho}(\epsilon_1, \ldots, \epsilon_m)$ be the limit value obtained in this way for ρ_j. Next, one may set [see Eq. (A2)]

$$|R_j(t; x_1, \ldots x_k, y_1, \ldots, y_m)| \leq$$

$$\sum_{s=1}^{k} \xi_s \underset{\substack{x_s \leq \xi_s \\ y_s \leq \epsilon_s \\ t > t_0}}{\text{l.u.b.}} \left| \frac{\partial}{\partial x_s} (Y_j + R_{yj}) \right| \qquad \text{(A6)}$$

where in the right-hand side, the maximum values or some other upper bounds of the partial derivatives in the respective range are taken. The values of such upper bounds, which deserve consideration only from the viewpoint of their orders of magnitude, may be estimated by analytical or experimental procedures. It is to be remembered that the constants ξ_s represent orders of magnitude of the bounds within which the pilot is able to maintain the values of the dynamical variables.

Considering now the linearized problem, as in the particular cases treated above the partial derivatives $\partial Y_j/\partial x_s$ reduce to the respective coefficients of the linear terms in x_s, i.e., $\partial Y_j/\partial x_s = p_{js}(t)$, and hence formula (A6) may also be written

$$|R_j| \leq \sum_{s=1}^{k} \xi_s \underset{\substack{x_s \leq \xi_s \\ y_s \leq \epsilon_s \\ t > t_0}}{\text{l.u.b.}} \left| p_{js} + \frac{\partial R_{js}}{\partial x_s} \right| \qquad \text{(A7)}$$

For the sake of simplicity, the linearized form is to be used.

Consequently, by acting on some of the kinematic parameters, the pilot can ensure the stability of the complete motion of the aircraft if, as regards the order of magnitude, the inequalities

$$\sum_{s=1}^{k} \xi_s \underset{\substack{x_s \leq \xi_s \\ y_s \leq \epsilon_s \\ t > t_0}}{\text{l.u.b.}} \left| p_{js} + \frac{\partial R_{js}}{\partial x_s} \right| \leq \bar{\rho}_j(\epsilon_1, \ldots, \epsilon_m) \qquad \text{(A8)}$$

$$j = 1, 2, \ldots, m$$

are satisfied.

The meaning of formula (A8) is as follows: Let the bounds $\epsilon_1, \epsilon_2, \ldots, \epsilon_m$, within which it is necessary to maintain the values of the free variables, be given on the basis of practical considerations (such as accuracy of flight evolution, safety, comfort, and so on). Then formula (A8) indicates the required smallness of the bounds ξ_s of the constrained variables due to the pilot's intervention. The constants p_{js} are given as functions of the aircraft construction and of the undisturbed motion parameters, $\partial R_{js}/\partial x_s$ is evaluated according to the nature of the respective control, and $\bar{\rho}_j$ is calculated as a function of $\epsilon_1, \epsilon_2, \ldots, \epsilon_m$ through the mathematical procedure indicated above or through one similar to it. Thus, if sufficiently small values of ξ_s cannot be ensured for given values of ϵ_i throughout the whole time interval of the disturbed motion, the existence of a solution that is mathematically stable does not imply a sufficient smallness of values of the uncontrolled variables.

Another important conclusion yielded by formula (A8) is that for a given aircraft and a given basic motion, the efficiency of the partial control depends not only upon the choice of the constrained variables but also upon the choice of the control. In other words, for the same basic motion, the same disturbance, and constraint of the same variables, a certain control may prove efficient while another one may not. This conclusion may readily be drawn from the fact that any control, in addition to affecting the variable for which it has been applied, unavoidably affects to a less or greater extent the other motion parameters also. If these secondary effects act in an unwanted sense and are too great, the condition (A8) may no longer be satisfied. Thus, for instance, the constraint of the pitch angle through thrust control may result in an undesirable deviation of the flight velocity as a secondary effect. In other cases, however, the secondary effects may act in the same sense as the principal effect, thus contributing to the motion stabilization. For example, consider the case of the pilot controlling the pitch angle by means of the elevator, in the phugoid phase of longitudinally disturbed motion. The effect of this control on the flight velocity deviation, as well as that on the pitch angle deviation, is a stabilizing one. It is in this sense that one may speak of constraining the flight velocity through elevator control. Obviously, for each case the pilot selects rapidly, by reflex, the control which ensures either favorable secondary effects or unfavorable ones with as low values as possible (e.g., such that the R_{yj}, in a linear approximation, are independent of the variables y_s).

An analysis of the operation of various controls and of the aircraft response with regard to both the fulfilment of the assumption that the $R_{yj}(t; x_1, \ldots, x_k, y_1, \ldots, y_m)$ are small for small values of $x_1, x_2, \ldots x_k$, and the satisfaction of the inequalities (A8), would be a useful extension of the present paper.

** Since a quadratic form is usually taken for the W function, in a sufficiently close neighborhood of the origin, in the space of y_s variables,

$$\text{g.l.b. } \mathbf{W}(t; y_1, \ldots, y_m) = \mathbf{W}(t; s_1, \ldots, s_m)$$

(The abbreviations g.l.b. and l.u.b. stand for the greatest lower bound and the least upper bound, respectively.)

Appendix II

Some Thoughts on Estimating the Character of the Variation of the Disturbance Elements

The criterion indicating the controllability of a disturbance element is undoubtedly related to the time rate of change of the disturbance element. More exactly, at a given instant t the pilot can counteract a given disturbance element if its time rate of change is sufficiently small and does not change in sign over a sufficiently large time interval.

Since the value of the respective rate of change is given by the right-hand side of one of the equations of the induced motion, it is readily seen that in a sufficiently close neighborhood of the origin (in the space of the dynamic variables) the first of the above conditions coincides with the requirement that the degree of instability be slight.* The second condition coincides in certain particular cases (e.g., in the case of a steady basic motion) with that imposed by a sufficiently small oscillation frequency.** Throughout this section, the dynamic variables are assumed to be sufficiently regular functions of time so that, in the general case of any (unsteady) basic motion, this last condition may be replaced by that according to which the minimum interval between two consecutive zeros of the respective variable is sufficiently large to ensure convenient piloting.

At present, the author's further investigations concern the problem of estimating the controllability of various kinematic parameters. Herewith is given the solution for a rather particular case, that in which the variables assumed to fall under the pilot's control are separated from the others, and their variation is governed by a second-order equation.

For definiteness, the behavior of variables $\Delta\hat{V}$ and $\Delta\theta$ during longitudinally symmetric motion will be considered. When the incidence adjustment has taken place, this motion, in the case of straight level basic motion, may be described approximately by the following system:†

$$\begin{aligned} d\Delta\hat{V}/dt &= p_{11}(t)\Delta\hat{V} + p_{12}(t)\Delta\theta \\ d\Delta\theta/dt &= p_{21}(t)\Delta\hat{V} \end{aligned} \qquad \text{(A9)}$$

where the coefficients p_{ij}, expressed as functions of the coefficients of the system (4.1), are

$$\begin{aligned} p_{11} &= a_{11} + a_{12}(a_{41} - a_{21}a_{44})/(a_{22}a_{44} - a_{42}) \doteq a_{11} \\ p_{12} &= a_{13} \\ p_{21} &= (a_{21}a_{42} - a_{22}a_{41})/(a_{22}a_{44} - a_{42}) \end{aligned}$$

Such a system is obtained by assuming that during the phugoid phase the angle of incidence varies much more slowly than the pitch angle, and that the angular pitching movement in its turn is sufficiently slow, that the second derivatives with respect to time may be neglected. In estimating the accuracy corresponding to these assumptions, the following should be noted. If Eq. (4.5) is the characteristic equation of the system that describes to a first approximation the complete longitudinal induced motion in the case of steady basic motion, then there is a linearized system corresponding to the above simplifying assumptions and having the following characteristic equation:

$$a_2\lambda^2 + a_3\lambda + a_4 = 0 \qquad \text{(A10)}$$

Hence, the accuracy is better the larger the discrepancy between the values of the two pairs of roots of Eq. (4.5).

For the very important case of steady basic motion, the interval τ between two consecutive zeros of any of the variables considered [when the roots of Eq. (A10) are complex‡] is constant and equal to the half period of oscillation

$$\tau = \frac{\pi}{\sqrt{[-p_{12}p_{21} - (p_{11}/2)^2]}} \qquad \text{(A11)}$$

For evaluating the minimum interval between two consecutive zeros of the variables $\Delta\hat{V}$ and $\Delta\theta$ in the general case of the unsteady basic motion, one may proceed as follows:

Perform the substitution

$$\Delta\hat{V} = \zeta\cos\psi \qquad \Delta\theta = \zeta\sin\psi \qquad \text{(A12)}$$

Then the system (A9) yields

$$\left.\begin{aligned} \dot{\psi} &= p_{21}\cos^2\psi - p_{11}\cos\psi\sin\psi - p_{12}\sin^2\psi \\ d\ln\zeta/dt &= p_{11}\cos^2\psi + (p_{12} + p_{21})\cos\psi\sin\psi \end{aligned}\right\} \qquad \text{(A13)}$$

It is readily seen that the time interval between two consecutive zeros of the deviations $\Delta\hat{V}$ and $\Delta\theta$ [see (A12)] will depend exclusively upon the function ψ.

Only the case in which, at any instant,

$$-p_{12}p_{21} - (p_{11}/2)^2 > 0$$

will be dealt with.†† Then, since $p_{12}(t) < 0$, the matrix of the quadratic form with respect to $\cos\psi$ and $\sin\psi$,

$$p_{21}\cos^2\psi - p_{11}\cos\psi\sin\psi - p_{12}\sin^2\psi \qquad \text{(A14)}$$

will admit only positive characteristic roots, and hence ψ will be an (strictly) increasing function of t. Accordingly, the interval between two consecutive zeros of the functions $\Delta\hat{V}$ and $\Delta\theta$ will be given at any moment t by the following equation in τ:

$$\psi(t + \tau) - \psi(t) = \pi \qquad \text{(A15)}$$

The lower bound of the interval $\tau(t)$ for $t > t_0$ can be evaluated as follows:

Let $\Lambda_M(t)$ and $\Lambda_m(t)$ be at any instant the numerically large and small characteristic roots, respectively, of the matrix of the quadratic form in $\cos\psi$ and $\sin$

* For quantitive details see reference 1, page 5.

** See reference 1.

† The assumption is made that for statically stable aircraft the two characteristic phases of the induced motion are present also when the basic motion is unsteady.

‡ In the case of nonoscillatory variation, which corresponds to real roots, the interval τ during which the respective deviations change monotonically is naturally infinite.

†† The fulfilment of this condition in the case of steady basic motion ensures complex roots for the characteristic equation.

(*Continued on page 50*)

Inviscid-Incompressible-Flow Theory of Static Peripheral Jets in Proximity to the Ground

T. STRAND*

Convair, A Division of General Dynamics Corporation

Summary

An "exact" flow theory of peripheral jets issuing symmetrically from a hovering aerial-ground vehicle is presented. The theory is exact insofar as no simplifying assumptions have been made in obtaining a solution of the governing inviscid, two-dimensional hydrodynamical flow equations. The results are valid for all jet thickness/vehicle height ratios. The limit of applicability of existing theories (very low thickness/height ratios) are defined. Jet reaction, lift, and power coefficients for static conditions are introduced and computed. Lift augmentation and lift/power ratios are also calculated.

Applications to three-dimensional vehicles with rotational symmetry are indicated.

(1) Introduction

THE PURPOSE of this article is to present an "exact" theory of static two-dimensional peripheral jets (Fig. 1) issuing symmetrically from a hovering aerial-ground vehicle. The theory is "exact" insofar as no simplifying assumptions of any kind have been made in the governing hydrodynamic equations. The theory is thus applicable to all jet thickness/vehicle height ratios. This is in contradistinction to the two theories presently available in this field, which are both limited to very low thickness/height ratios.[1–4]

The first elementary theory of two-dimensional peripheral jets issuing symmetrically from a hovering vehicle was apparently developed independently in references 1 and 2. The authors assumed that the lift augmentation obtainable close to the ground could be calculated with sufficient accuracy by considering the jets to be very thin. In fact the jet thickness is not a parameter in this analysis. Subsequent tests have substantiated this initial analysis remarkably well in that the measured augmentation is about 80 per cent of the predicted values in the region of validity of the theory. The three most important relations of the theory, obtained by writing the equilibrium equation across the jet between centrifugal and pressure forces, are as follows:

$$p_1 - p_0 = j(1 - \sin\gamma)/h \tag{1}$$

$$L = 2j\cos\gamma + (p_1 - p_0)l \tag{2}$$

$$A = \cos\gamma + (1 - \sin\gamma)/(2h/l) \tag{3}$$

where

- j = jet momentum, assumed constant along the jet
- p_0 = ambient pressure
- p_1 = base pressure
- h = vehicle height above the ground
- l = vehicle length (see Fig. 1)
- γ = jet exit angle, positive outboard from the vertical to the ground
- L = lift
- A = lift augmentation ($L/2j$)

It is worth noting that Eq. (1) indicates that the base pressure increases without bounds as the vehicle height above the ground is decreased. Thus the lift would approach infinity as the vehicle height is reduced to zero.

An improved theory which does consider the jet thickness and which correctly shows that the base pressure can never exceed the jet total head was subsequently developed in references 3 and 4. According to these authors the analysis is valid for jet exit thickness vehicle height ratios (t_e/h) less than unity. In fact, it will be shown here by the "exact" theory that their analysis is only valid for $t_e/h \leq 0.3$ approximately. This is, however, still within the range of application of most of the present day aerial-ground vehicles. Because of this and for completeness in presentation this theory will be reviewed below.

Consider the jet thickness (t_e) to be constant between the exit from the vehicle and the point where the jet first touches the ground. In other words, assume that all contraction of the jet takes place along the ground.

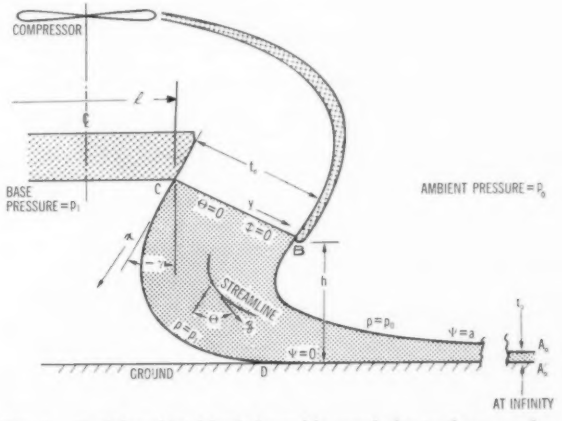

FIG. 1. Peripheral jet (shaded area) in proximity to the ground—two dimensions.

Received January 21, 1960.

* Formerly, Design Specialist, Convair—San Diego. Now, Director of Research, Vehicle Research Corporation.

The author is indebted to Dr. H. Yoshihara of Convair—San Diego, for several helpful discussions during this study and is also grateful to Mrs. Helen Grijalva for valuable computing help.

The simplified force balance equation in the radial direction in a polar coordinate system, with r as the radial distance, is then simply

$$dp/dr = \rho U^2/r$$

Here U is the velocity at the point in the jet where the pressure is p. The density (ρ) is assumed to be constant. Integration using the Bernoulli equation yields the velocity distribution across the jet:

$$\frac{U}{U_0} = \frac{1 - t_e/h}{1 - (t_e/h)\sin\gamma - (1 - \sin\gamma)(t_e/h)(y/t_e)} \quad (4)$$

where U_0 is the velocity corresponding to ambient pressure. The coordinate system employed is defined in Fig. 1. In this case however, y is also any radial coordinate with origin on the interior jet boundary since all radial velocity distributions are identical. When y is zero, $U = U_1$ (the jet velocity adjacent to the base region where the pressure is p_1), and we have

$$U_1/U_0 = (1 - t_e/h)/[1 - (t_e/h)\sin\gamma] \quad (5)$$

The base pressure can now be calculated by substituting Eq. (5) into the following relation derived from the Bernoulli equation:

$$(p_1 - p_0)/(H - p_0) = 1 - (U_1/U_0)^2 \quad (6)$$

where H is the jet total head.

Next we shall deviate from references 3 and 4 by defining a few new nondimensional coefficients to aid in the interpretation of the theory. These coefficients are based upon the jet "free-stream" dynamic pressure (at infinity downstream). The dynamic pressure is, of course, equal to the difference between the total head and the ambient pressure, and is thus easily available in experimental undertakings. The coefficients have been barred to make them more easily distinguishable from those based upon the dynamic pressure in forward flight. The jet reaction, lift, and power coefficients are defined, respectively, as follows:

$$\bar{C}_j \equiv j/[(1/2)\rho U_0^2 t_e] \quad (7)$$

$$\bar{C}_L \equiv L/[(1/2)\rho U_0^2 l] \quad (8)$$

$$\bar{C}_p \equiv P/[(1/2)\rho U_0^3 l] \quad (9)$$

Then with the jet reaction calculated from

$$j = \int_0^{t_e} (p - p_c + \rho U^2)dy \quad (10)$$

the lift from Eq. (2), and the power from

$$P = 2\int_0^{t_e} [p - p_0 + (1/2)\rho U^2]U\, dy \quad (11)$$

it is easy to show that

$$\bar{C}_j = [2h/l - (t_e/l)(1 + \sin\gamma)]/[h/l - (t_e/l)\sin\gamma] \quad (12)$$

$$\bar{C}_L = 2(t_e/l)\bar{C}_j \times \left\{\cos\gamma + \frac{(1 - \sin\gamma)[1 - 2(t_e/l)\cos\gamma]}{2[h/l - (t_e/l)\sin\gamma]}\right\} \quad (13)$$

$$\bar{C}_p = \frac{2(h/l - t_e/l)}{1 - \sin\gamma} \ln\left[\frac{h/l - (t_e/l)\sin\gamma}{h/l - t_e/l}\right] \quad (14)$$

Note that the power may also be set equal to the kinetic energy at infinity downstream ($\rho U_0^3 t_0$), where t_0 is the jet thickness at infinity. Hence, $t_0/l = \bar{C}_p/2$ and the jet contraction ratio becomes

$$t_0/t_e = \bar{C}_p/(2\, t_e/l) \quad (15)$$

Next let us consider the lift augmentation ratio. Some authors have defined this to be the ratio between the lift in the ground effect to the theoretical jet reaction out of the ground effect. This concept of the augmentation is, however, not too useful as the experimental and the theoretical jet reactions out of the ground effect are quite different due to a viscous interaction phenomenon which creates a low-pressure region between the two jets.

Other authors have defined the augmentation to be the ratio of lift in the ground effect to the jet reaction out of the ground effect with the same amount of mass flow in both cases and without interference. This is the definition we shall use here as the mass flow (m) is always directly measurable in experiments, and so is the total head from which

$$U_0 = \sqrt{(2/\rho)(H - p_0)}$$

Thus,

$$A \equiv \frac{L}{m\, U_0} = \frac{\bar{C}_L}{4(t_0/t_e)(t_e/l)} = \frac{\bar{C}_L}{2\bar{C}_p} \quad (16)$$

where $m = 2\,\rho\, U_0\, t_0$. Written this way it is seen that the lift augmentation is really not what the name indicates because the mass flow changes under the influence of the ground. Instead the augmentation is in fact half the free-stream velocity times the lift/power ratio—i.e.,

$$U_0 L/H.P. = 1{,}100\, A \quad (17)$$

This is very convenient because the lift/power ratio is of utmost importance for aerial-ground vehicles while the theoretical lift augmentation is of only secondary interest. Most of the above relations are shown dotted on the figures for comparison with the exact theory.

It may be noticed that all pertinent equations, except the lift expression, of this "thick" jet theory reduce to those of the simple "thin" jet theory of references 1 and 2 in the limit as t_e/h approaches zero. As mentioned previously, the "thick" jet theory exhibits some abnormalities, at the other end of the t_e/h scale. Thus the lift/power ratio approaches infinity as the vehicle height approaches the jet thickness. This would be just what everybody working in the ground effect field has been looking for—if it is true. The difficulty was realized in reference 3. The author, however, dismisses the point by suggesting that viscous effects will enter into the picture in such a manner that a purely nonviscous approach is no longer possible. This is not the case, as the following development will show. Rather the breakdown of the solution of the "thick" jet

theory as t_e/h approaches unity from below is a result of the original simplifying assumption of constant jet thickness along the initial portion of the path. This will be evident from the "exact" development presented in the following section.

(2) Exact Flow Solution

Consider one of the two symmetrical two-dimensional peripheral jets of constant total head issuing from a hovering vehicle. The flow within the jet is to be considered inviscid and incompressible. The problem under consideration is to determine the flow field—i.e., the magnitude and direction of the velocity vector at all points within the jet—when the vehicle height above the ground and the jet thickness at the exit are given. Specifically, we are interested in determining the velocity vectors along the interior boundary of the jet and across the jet exit, because, if these are known, the lift augmentation and the lift/horsepower ratio can be calculated. The problem will be formulated as a boundary value problem and will be solved through the use of a conformal mapping scheme. We must then initially specify one flow property along each boundary of the jet. This means that we cannot start out by specifying the height and the jet thickness, but must first select a base pressure and then calculate the corresponding thickness/height ratio.

Considering then the boundaries of the jet in Fig. 1, the pressures p_0 and p_1 are known along A_0 B and CD. The subscripts 0 and 1 will be used consistently to indicate conditions along the exterior and interior boundaries, respectively. Along the boundaries BC and DA_0' the flow angles (direction of the velocity vectors) are known. We shall require the flow angles along BC to be zero—i.e., the jet issues normal to the exit (if necessary this condition can be enforced by vanes placed across the exit). This implies that the velocity potential (ϕ) is constant along this boundary. Since a potential is only determined up to an arbitrary constant, we might as well select ϕ to be zero along BC. From Fig. 1 it is seen that the flow angle along DA_0' is $(\pi/2 - \gamma)$.

The stream function (ψ) has arbitrarily been assigned the value zero along the inner jet boundary CDA_0', and the constant value a along A_0B. The constant velocities U_1 and U_0 along CD and A_0B can be computed from the Bernoulli equation. If t_0 is the jet width (so far unknown) at infinity it is seen that $a = U_0 t_0$.

With the boundary conditions thus clearly defined we may then proceed with a simple conformal mapping scheme involving three planes (Fig. 2). First the w plane ($w = \phi + i\,\psi$) is mapped onto the first quadrant of the ζ plane through the following Schwartz-Christoffel transformation[5]

$$\zeta = \cosh\,(\pi w/2a) \tag{18}$$

Next, the hodograph plane defined by $Q = \ln\,(U_0/q) + i\theta$ is mapped on to the same quadrant in the ζ plane. Here (q, θ) is the velocity vector in polar coordinates at

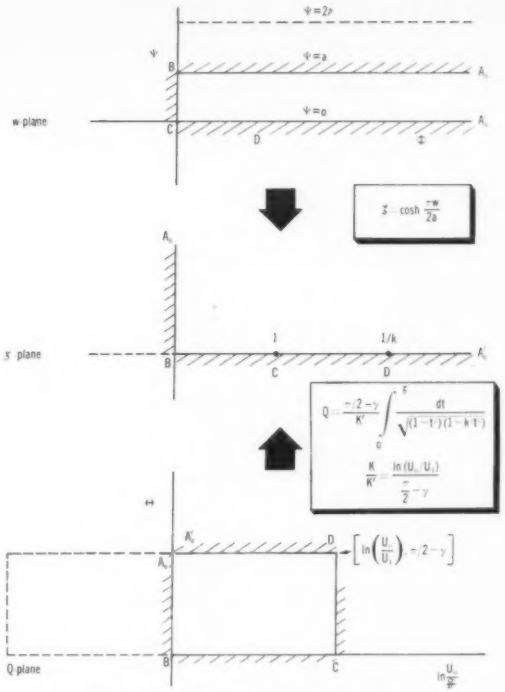

FIG. 2. Conformal mapping planes.

any point in the flow field. This transformation is accomplished by mapping the four corners of the large rectangle in Fig. 2, defined by the rectangle enclosing the flow field and its mirror image, on to the points ± 1 and $\pm\ 1/k$ on the real axis in the ζ plane by the following general Schwartz-Christoffel transformation:

$$Q = M \int_0^{\zeta} \frac{dt}{\sqrt{(1 - t^2)(1 - k^2t^2)}} + N \tag{19}$$

Here, M, N, and k are unknown constants that can be determined by the corner conditions of the transformation to be

$$M = (\pi/2 - \gamma)/K' \tag{20}$$

$$N = 0 \tag{21}$$

$$K/K' = \ln\,(U_0/U_1)/(\pi/2 - \gamma) \tag{22}$$

where

$K = K\,(k)$ = the complete elliptic integral of the first kind with modulus k where $0 \leq k \leq 1$

$K' = K(k')$ = the complete elliptic integral of the first kind with modulus k' where $k'^2 = 1 - k^2$

Note that k must first be determined from the last equation [Eq. (22)] above. The value of k so determined can then be substituted into the expression for M.

Eliminating ζ between Eqs. (18) and (19) we have

$$Q = \left[\frac{(\pi/2 - \gamma)}{K'}\right] \int_0^{\cosh\,(\pi w/2a)} \frac{dt}{\sqrt{(1 - t^2)(1 - k^2t^2)}} \tag{23}$$

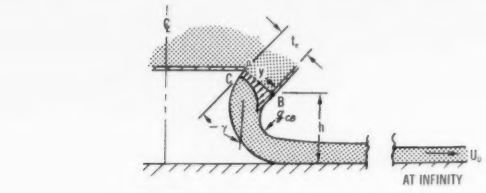

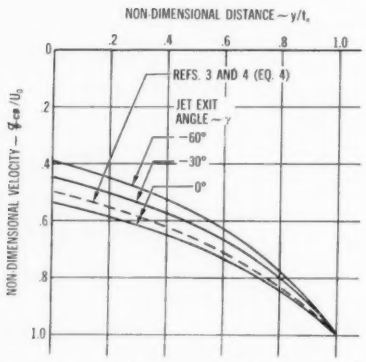

FIG. 3. Sample velocity distribution across jet exit; $t_e/h = 0.5$.

This relation then yields complete information about the jet velocity (magnitude and angle) as a function of the velocity potential and the stream function.

Next we shall establish the connection between the velocity potential and the stream function, and the x and y coordinates. The simplest way to do this is to use the chain rule to obtain expressions for the total derivatives of the velocity potential and the stream function, and subsequently solve for dx and dy. Then making the variables nondimensional by dividing by the volume flow a, and multiplying by U_0, we find

$$d(x/t_0) = (U_0/q)[\cos\theta \cdot d(\phi/a) - \sin\theta \cdot d(\psi/a)] \quad (24)$$

$$d(y/t_0) = (U_0/q)[\sin\theta \cdot d(\phi/a) + \cos\theta \cdot d(\psi/a)] \quad (25)$$

In the following development we shall restrict our attention to the flow field along the two lines BC and CD. It will be shown that by determining the flow variables along these two lines we can extract all information needed to calculate the lift of the vehicle and the power required to sustain the flow. Let us first consider the line BC. Along this line both the flow angle and the velocity potential are zero. Thus, by Eq. (23),

$$(\ln U_0/q_{CB}) = [(\pi/2 - \gamma)/K'] \times \int_0^{\cos(\pi\psi/2a)} \frac{dt}{\sqrt{(1-t^2)(1-k^2t^2)}} \quad (26)$$

which can be reduced to the following tabulated standard form:

$$q_{CB}/U_0 = \exp\{-(\pi/2 - \gamma)\, F[k, (\pi/2)(1 - \psi/a)]/K'\} \quad (27)$$

Here $F[k, (\pi/2)(1 - \psi/a)]$ indicates the incomplete elliptic integral of the first kind with modulus k and amplitude $(\pi/2)(1 - \psi/a)$. By substitution into Eq. (25) and integrating from 0 to ψ/a we obtain

$$y_{CB}/t_0 = \int_0^{\psi/a} \exp\{(\pi/2 - \gamma) \times F[k, (\pi/2)(1 - \psi/a)]/K'\} d(\psi/a) \quad (28)$$

The maximum value of ψ/a along BC is of course unity. Letting t_e be the length of BC, it is seen that when $\psi/a = 1$, $y = t_e$ and hence Eq. (28) becomes

$$t_e/t_0 = \int_0^1 \exp\{(\pi/2 - \gamma) \times F[k_2(\pi/2)(1 - \psi/a)]/K'\} d(\psi/a) \quad (29)$$

Dividing Eq. (28) by Eq. (29), t_0 is eliminated and we have

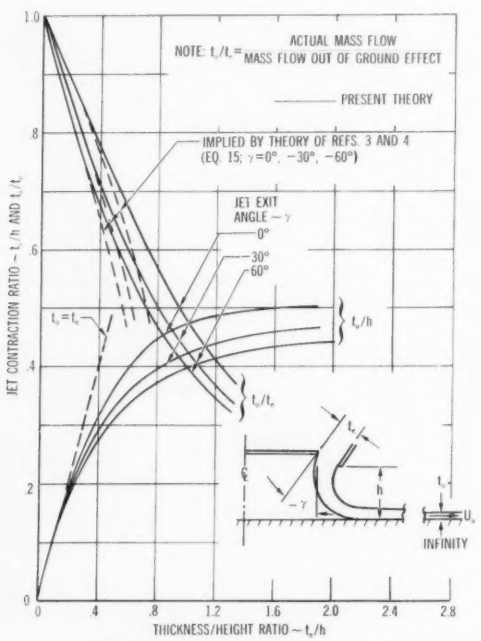

FIG. 4. Jet contraction ratios.

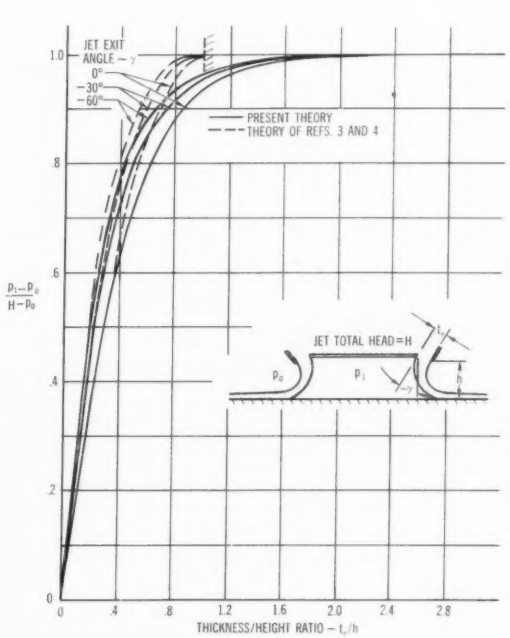

FIG. 5. Base pressure.

$$y_{CB}/t_e = \frac{\int_0^{\psi/a} \exp\left\{(\pi/2 - \gamma)F[k, (\pi/2)(1 - \psi/a)]/K'\right\} d(\psi/a)}{\int_0^1 \exp\left\{(\pi/2 - \gamma)F[k,(\pi/2)(1 - \psi/a)]/K'\right\} d(\psi/a)} \tag{30}$$

This is then the nondimensional distance along the jet exit from the origin of our coordinate system to the point where the nondimensional velocity is q_{CB}/U_0 [Eq. (27)]. A plot of the velocity distribution across the jet exit for three different jet exit angles—namely, $\gamma = 0°$, $-30°$, and $-60°$ for a constant value of the parameter $t_e/h = 0.5$ (the equation of which is determined below)—is presented in Fig. 3. It is seen that directing the jet inward while keeping the jet exit geometry and the vehicle height constant results in increased base pressure as evidenced by the decrease in the minimum value of q_{CB}/U_0. Notice that the mass flow is also decreased. At the same time the vertical component of the jet reaction is of course decreased.

The jet contraction ratio [Eq. (29)] is presented in Fig. 4 and compared with the simplified theory mentioned in the Introduction. The two theories are for practical purposes identical up through a t_e/h of 0.3.

Next, let us consider the boundary CD along which the velocity is U_1. Here the stream function is equal to zero. From the imaginary part of Eq. (23) we then have

$$\theta_{CD} = [(\pi/2 - \gamma)/K'] \times \int_1^{\cosh(\pi\phi/2a)} \frac{dt}{\sqrt{(t^2 - 1)(1 - k^2t^2)}} \tag{31}$$

A reduction to standard tabulated form yields

$$\theta_{CD} = (\pi/2 - \gamma) \times \left\{1 - F\left[k', \sin^{-1}\left(\frac{1}{k'}\sqrt{1 - k^2\cosh^2\left(\frac{\pi\phi}{2a}\right)}\right)\right]\Big/K'\right\} \tag{32}$$

where $0 \leq \phi/a \leq (2/\pi)\cosh^{-1}(1/k)$

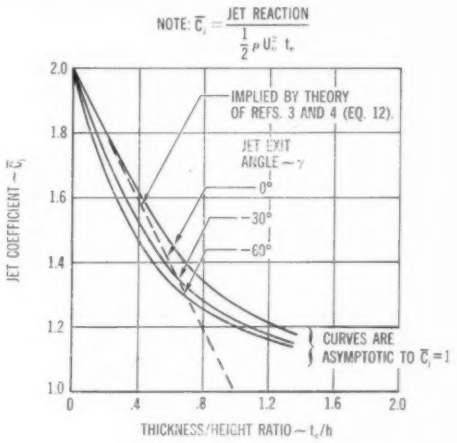

FIG. 6. Jet reaction.

The coordinates of the point in the flow field where the angle of the velocity vector is θ_{CD} can be obtained by integrating Eqs. (24) and (25). Thus,

$$x_{CD}/t_0 = (U_0/U_1)\int_0^{\phi/a} \cos\theta_{CD}\, d(\phi/a) \tag{33}$$

$$y_{CD}/t_0 = (U_0/U_1)\int_0^{\phi/a} \sin\theta_{CD}\, d(\phi/a) \tag{34}$$

The nominal nondimensional height of the vehicle above the ground (Fig. 1) is now

$$h/t_0 = (\cos\gamma)(x_{CD}/t_0)_{max} + (\sin\gamma)[t_e/t_0 - (y_{CD}/t_0)_{max}] \tag{35}$$

Note that the inverse of this relation may also be considered to be a jet contraction ratio (Fig. 4). Dividing through by t_e/t_0 we have

$$t_e/h = \left\{\sin\gamma + \frac{(\cos\gamma)(x_{CD}/t_0)_{max} - (\sin\gamma)(y_{CD}/t_0)_{max}}{t_e/t_0}\right\}^{-1} \tag{36}$$

Eq. (36) shows that there corresponds a certain equilibrium t_e/h to each velocity ratio across the jet because we started out by assuming the velocities U_0 and U_1 known, and with this information we have now calculated t_e/h. For calculation purposes it is convenient to select a k and compute t_e/h from Eq. (36) and find the corresponding U_1/U_0 from Eq. (27) with $\psi/a = 0$. Then using Eq. (6) the base pressure can be found (Fig. 5). It is seen that there is a very rapid rise in the base pressure with increasing thickness/height ratio, and that at a t_e/h of somewhat larger than unity the base pressure is for all practical purposes equal to the jet total head. The base pressure by the simplified theory is also shown for comparison.

Some results of the calculation of the jet reaction coefficient are presented in Fig. 6. Here the following equation for the jet coefficient [Eq. (7)] has been used:

$$\bar{C}_j = 1 + \frac{\int_0^1 \exp\left\{-(\pi/2 - \gamma)F[k, (\pi/2)(1 - \psi/a)]/K'\right\} d(\psi/a)}{\int_0^1 \exp\left\{+(\pi/2 - \gamma)F[k, (\pi/2)(1 - \psi/a)]/K'\right\} d(\psi/a)} \tag{37}$$

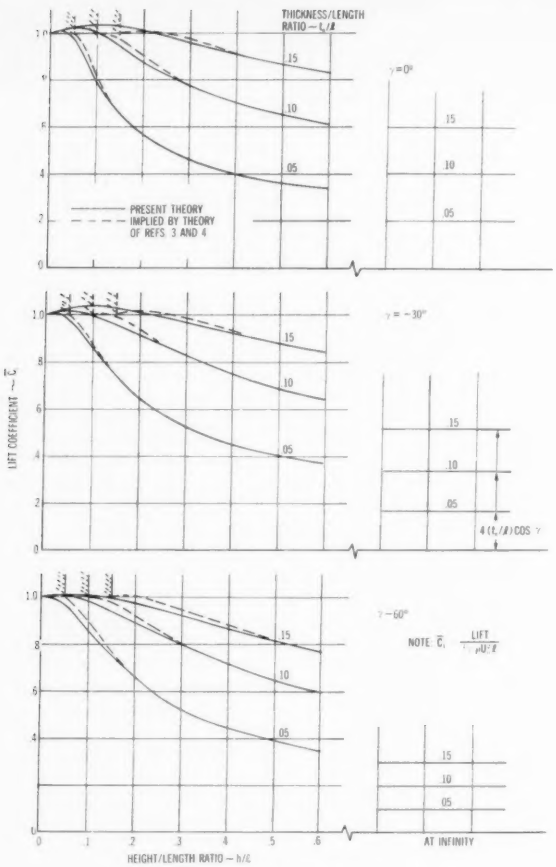

FIG. 7. Lift coefficient.

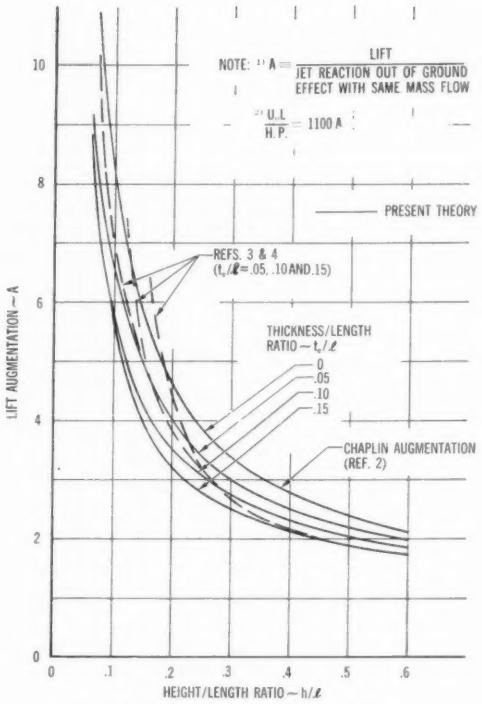
NOTE: [1] $A \equiv \frac{\text{LIFT}}{\text{JET REACTION OUT OF GROUND EFFECT WITH SAME MASS FLOW}}$
[2] $\frac{U_e L}{H.P.} = 1100\,A$
PRESENT THEORY
REFS. 3 & 4 (t_c/ℓ=.05, .10 AND .15)
THICKNESS/LENGTH RATIO — t_c/ℓ
0
.05
.10
.15
CHAPLIN AUGMENTATION (REF. 2)
LIFT AUGMENTATION — A
HEIGHT/LENGTH RATIO — h/ℓ

FIG. 8(a). Lift augmentation $\sim\gamma = 0°$.

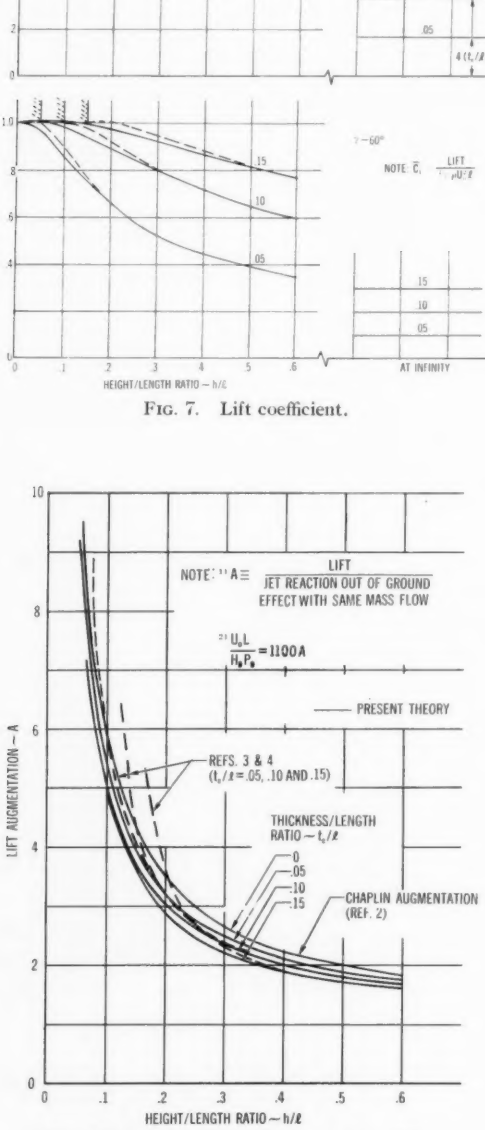
NOTE: [1] $A \equiv \frac{\text{LIFT}}{\text{JET REACTION OUT OF GROUND EFFECT WITH SAME MASS FLOW}}$
[2] $\frac{U_e L}{H_e P_e} = 1100\,A$
PRESENT THEORY
REFS. 3 & 4 (t_c/ℓ=.05, .10 AND .15)
THICKNESS/LENGTH RATIO — t_c/ℓ
0
.05
.10
.15
CHAPLIN AUGMENTATION (REF. 2)
LIFT AUGMENTATION — A
HEIGHT/LENGTH RATIO — h/ℓ

FIG. 8(b). Lift augmentation $\sim\gamma = -30°$.

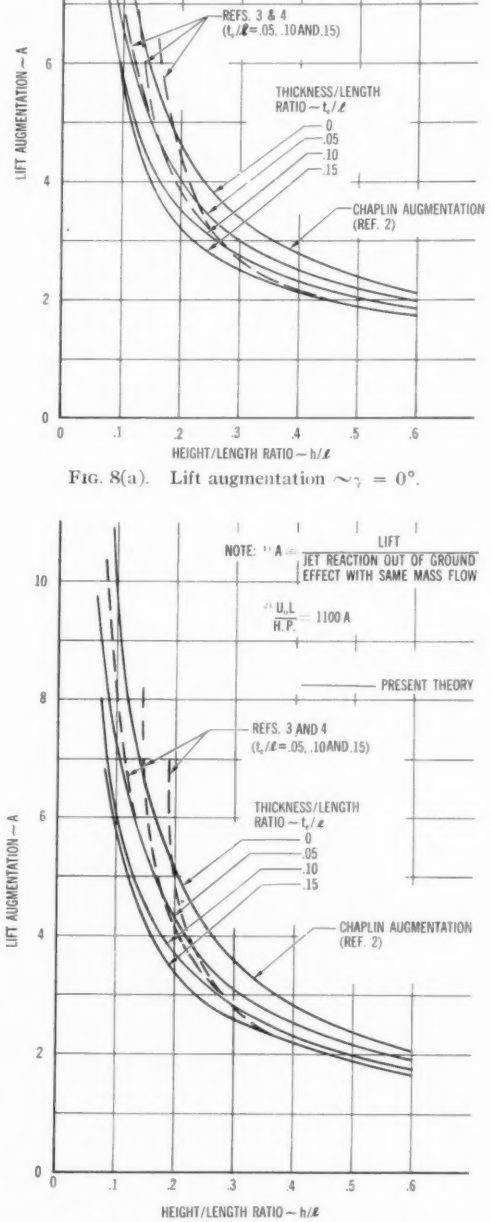
NOTE: [1] $A \equiv \frac{\text{LIFT}}{\text{JET REACTION OUT OF GROUND EFFECT WITH SAME MASS FLOW}}$
[2] $\frac{U_e L}{H.P.} = 1100\,A$
PRESENT THEORY
REFS. 3 AND 4 (t_c/ℓ=.05, .10 AND .15)
THICKNESS/LENGTH RATIO — t_c/ℓ
0
.05
.10
.15
CHAPLIN AUGMENTATION (REF. 2)
LIFT AUGMENTATION — A
HEIGHT/LENGTH RATIO — h/ℓ

FIG. 8(c). Lift augmentation $\sim\gamma = -60°$.

The lift coefficient may be found plotted in Fig. 7. It is seen that this coefficient never exceeds unity by very much. Hence the real lift augmentation—i.e., the ratio of the lift coefficient in the ground effect over that out of the ground effect (without viscous interference)—is never enormously large for reasonable t_e/l ratios.

The augmentation ratio as defined by Eq. (16), with $\bar{C}_p = 2(t_0/t_e)(t_e/l)$, and plotted in Figs. 8(a), 8(b), 8(c) does, however, approach infinity as the vehicle height is decreased to zero. This is as it should be since it was previously shown that this augmentation ratio is really a measure of the lift/power ratio and this ratio should approach infinity as h is decreased to zero. In the limit for a vehicle which touches the ground it is very possible to have lift; for instance, by pumping up the base region. The mass flow out of the vehicle is, however, in this case zero. Hence the power is zero, giving infinite lift/power ratio.

(3) Three Dimensions With Rotational Symmetry

The theory developed in the preceding section can be applied to vehicles with rotational symmetry (saucer-like vehicles) in the cases where the diameter (d) of the vehicle is much larger than both the jet thickness and the vehicle height above the ground. The flow field in the immediate neighborhood of the rim is then essentially two-dimensional and the results of our two-dimensional flow calculations apply. Outside this neighborhood the jet behaves differently. Thus the jet thickness far downstream is no longer a constant. From mass flow considerations (continuity) it is seen that we now must have $\rho\, 2\pi\, R\, t\, U_0 =$ constant. Here R is the radius from the center of the vehicle to a point far downstream where the jet thickness is t. Far downstream the pressure is once more p_0; hence, the velocity is constant and equal to U_0. It is concluded that the jet, while being two-dimensional in the neighborhood of the rim, will, far downstream, change its cross section to be inversely proportional to the distance from the vehicle, while maintaining a constant velocity.

Defining the jet reaction, lift, and power coefficients in three-dimensional flow as follows:

$$\bar{C}_j = j/[(1/2)\rho U_0^2 \pi (d + t_e) t_e] \tag{38}$$

$$\bar{C}_L = L/[(1/2)\rho U_0^2 \pi\, d^2/4] \tag{39}$$

$$\bar{C}_p = P/[(1/2)\rho\, U_0^3 \pi\, d^2/4] \tag{40}$$

it can easily be shown that these coefficients are identical in magnitude to those defined by Eqs. (7), (8), and (9) for two-dimensional flow if we associate l with $d/2$. This coincidence has previously been pointed out in reference 2. Hence, all graphs presented here are valid for three-dimensional flow for pertinent vehicles with rotational symmetry by replacing l by $d/2$.

References

[1] Boehler, G. D., *The Airborne Ground Vehicle. A New Device for Improving Tactical Mobility of Ground Based Military Units*, Proposal Submitted to the Army Ordnance Research Office, January 8, 1957.

[2] Chaplin, H. R., *Theory of the Annular Nozzle in Proximity to the Ground*, Aerodynamics Laboratory, David Taylor Model Basin, Navy Department, Aero Report 923, July, 1957.

[3] Pinnes, R. W., *A Power Plant Man's Look at the Ground Effect Machine*, Bureau of Aeronautics, Navy Department, Research Division Report No. DR-1958, April, 1959.

[4] Rethorst, S., and Royce, W. W., *Lifting Systems for VTOL Vehicles*, Paper presented at the National Summer Meeting, Institute of the Aeronautical Sciences, June 16–19, 1959.

[5] Milne-Thomson, L. M., *Theoretical Hydrodynamics*, MacMillan and Co., 1938.

✦ ✦ ✦

Steady Creep Bending (*Continued from page 14*)

necessary to investigate the higher-order terms in the series. These terms may be obtained in an elementary manner but the final expressions are extremely unwieldy. For this particular purpose the method utilized here appears to be more expedient.

References

[1] Sackman, J. L., *On the Use of Stress Functions for Heterogeneous Maxwell Bodies*, Contract Nonr 266(34), Tech. Rep. No. 6, Columbia University, September, 1958.

[2] Freudenthal, A. M., *Problems of Structural Design for Elevated Temperatures*, Trans. N.Y. Acad. Sci., Ser. II, Vol. 19, No. 4, pp. 328–342, February, 1957.

[3] Bleich, H. H., *On the Analysis of Nonlinear Viscoelastic Structures with Temperature Gradients*, Contract Nonr 266(34), Tech. Rep. No. 3, Columbia Univ., June, 1957.

[4] Coker, E. G., and Filon, L. N. G., *A Treatise on Photo-Elasticity*, 2nd Ed., Cambridge Univ. Press, Cambridge, 1957.

[5] Timoshenko, S., *Theory of Plates and Shells*, McGraw-Hill Book Co., Inc., N. Y., 1940.

[6] Boley, B. A. and Tolins, I. S., *On the Stresses and Deflections of Rectangular Beams*, J. Appl. Mech., Vol. 23, No. 3, pp. 339–342, 1956.

✦ ✦ ✦

A Stiffness Matrix for the Analysis of Thin Plates in Bending

ROBERT J. MELOSH*
Boeing Airplane Company

Summary

A stiffness matrix is developed for an isotropic rectangular plate panel of uniform thickness for application to the analysis of thin plates of variable thickness in bending. The convergence characteristics of this matrix are demonstrated on simple problems with known exact, analog, and experimental solutions. The usefulness of the matrix in the determination of the elastic characteristics of thin, low aspect-ratio wings is exhibited.

Symbols

a	= length of sides of rectangle parallel to x axis, in.
a_{ij}	= influence coefficients
A_i	= constants
b	= length of sides of rectangle parallel to y axis, in.
D	= flexural rigidity = $Eh^3/12(1-\nu^2)$, lb-in.
E	= Young's modulus, lbs./sq. in.
F_{zi}	= force in z direction at node i, lbs.
h	= plate thickness, in.
I	= bending moment of inertia, in.^{4}
k_{ij}	= stiffness coefficient, lbs.
$M_{\theta i}$	= bending moment in θ direction at node i, in.-lb.
n	= matrix order
N	= matrix condition number
U	= strain energy
w	= displacement in z direction, in.
w_{xx}, w_{yy}, w_{xy}	= $\partial^2 w/\partial x^2$, $\partial^2 w/\partial y^2$, $\partial^2 w/\partial x \partial y$, respectively
x, y, z	= coordinate axes
ν	= Poisson's ratio
λ	= eigenvalue of matrix
φ	= angular rotation about x axes
θ	= angular rotation about y axes
σ	= stress, psi

Introduction

THE SIMILARITY between the elastic characteristics of plates and of low aspect-ratio wings has increased the importance of being able to analyze thin plates of variable thickness in bending. Solutions of the plate equations have been attempted by imposing constraints on the streamwise deformations, by using Rayleigh-Ritz methods, and by directly attacking the differential equations by finite difference schemes.

Reissner and Stein[10] constrained deformations to linear expressions in the streamwise coordinate and recast the plate equations in the form of two ordinary differential equations for simultaneous solution. Later Stein and Sanders[11] extended this formulation to include parabolic deflections in the streamwise direction, organizing the solution in matrix form with the use of difference relations. These solutions have been applied primarily in the preliminary design area because of the unknown limitations imposed by the basic assumptions and the difficulties associated with applying these solutions to practical wings.

Employing Rayleigh-Ritz methods, Duffin, Gustafson, and Warner[3] obtained fair results in predicting the modes and frequencies of constant-thickness plates of various sweeps and aspect ratios. Extending these solutions by the use of up to 14 parameters, Lubkin and Luke[5] obtained good results for 45-degree right triangular plates despite problems occasioned by poorly conditioned matrices. The basic nature of the poor conditioning of matrices when a large number of power series terms are taken, and the difficulty of choosing suitable functions to match boundary conditions for boundaries of irregular shape, make the Rayleigh-Ritz solution in this form unattractive for the solution of practical problems.

Benscoter and MacNeal[1] presented the solution of the plate equations in the form of first-order difference relations which they used for the design of suitable analog circuits. Fung[4] broadened the difference attack by first casting the plate equations in the form of two stress functions which permitted inclusion of variable thickness and mixed boundary conditions, and yielded moments directly. Williams[15] suggested forming the stiffness matrix directly from finite difference equations of the fourth-order partial differential equation with variable coefficients, and considered the use of a digital computer. In general, these methods require special care in imposing boundary conditions correctly and are not directly addressed to the solution of practical problems, in that no cognizance is taken of local complexities in the distribution or discontinuity of elastic characteristics.

The direct formation of the stiffness matrix from component stiffness matrices[14] is a method suited to the irregular geometry and boundary conditions found in the practical structure. In this method the structure is regarded as an assemblage of parts. Each part is assigned a stiffness matrix relating forces and displacements at its terminals, which are called nodes. The stiffness matrix for the complete, connected structure is obtained by addition of the component stiffness matrices. A given column of the matrix consists of a list of the forces at each of the nodes for unit displacement of a given node in the direction of one of the coordinate axes. Where two or more members have a

Received April 13, 1959. Revised and received November 23, 1959.

* Research Engineer, Aerospace Division.

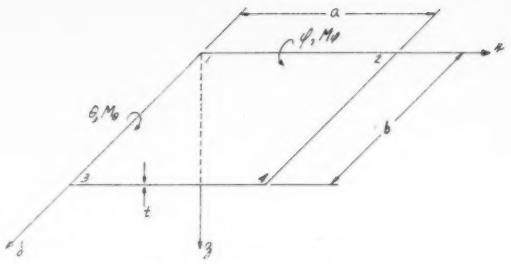

FIG. 1. Coordinate system.

common node, forces are simply added. Boundary conditions and loading are expressed in terms of node displacements and loads. The inverse of the stiffness matrix is the matrix of influence coefficients.

This paper will present a stiffness matrix for thin plates bending under lateral forces and edge couples, suitable for use in the analysis of the elastic characteristics of plates of variable thickness. Problems showing the accuracy of solutions obtained with the use of the matrix and relatively coarse nodal networks are included. The application to a typical wing problem is illustrated.

Development of the Stiffness Matrix for Plate Bending

Since a stiffness matrix involving both moments and forces is desired, the angles of rotation ϕ and θ about the x and y axes, respectively, and the lateral displacement at each node will be chosen as the coordinates. Thus, identifying the stiffness with a rectangular panel (Fig. 1), we see that a 12×12 matrix is required. This matrix will be developed by adding stiffness matrices corresponding to each term of the bending energy expression.

The expression of the bending strain energy for a plate of uniform flexural rigidity and isotropic material is

$$U = \frac{D}{2} \iint [w_{xx}^2 + w_{yy}^2 + 2\nu w_{xx} w_{yy} + 2(1 - \nu)\, w_{xy}^2]\, dA \quad (1)$$

where D is the flexural rigidity, ν is Poisson's ratio, the subscripts denote differentiation, i.e., $w_{xx} = \partial^2 w/\partial x^2$, and w is the displacement function.

The four terms of the energy expression (1) may be defined by analogy with an elementary beam as the x bending stiffness, the y bending stiffness, the bending coupling, and the torsional stiffness, respectively. If the x axis is along the chord and the y axis along the span, scalars may be applied to the first and second terms to approximate the effects on elastic response, of varying the amounts of chordwise and spanwise bending material. Similarly, wing cut-out effects can be approximated. Normally, when cutouts are made, additional bending material is placed in the spars and ribs to replace the lost normal stress-carrying capability of the skin. The loss of shear-carrying capability can be approximated by multiplying the torsional stiffness matrix by one half before combining it with the bending terms, since a shear flow analysis would attribute half of the rigidity to the spars and half to the skin panels.

The reader might suggest that stiffness matrices other than that presented here could be derived for the plate. A matrix giving exactly the results obtained by a finite difference representation of the fourth-order differential equation (with the use of the coordinates chosen here) has been derived. In addition, matrices based on the terms of a third-order polynomial in x and y describing the displacement over the panel have been derived. While any one of these matrices is as valid as another, the matrix chosen for use will be the one that demonstrates the best accuracy for a given network refinement. In all three problems used in this paper to compare these matrices (problems on three plates of uniform thickness) the matrix derived here gave the best results.

The reader might suggest also the virtues of a matrix associated with a triangular panel. Assaults on this problem utilizing the third-order polynomial have demonstrated that when four triangles are used to form a rectangular panel, the accuracy of the solution of the problem is much less than that obtained with the rectangular panel stiffness matrix developed in this paper. The results of making up a right-triangle stiffness matrix by eliminating the fourth node in a rectangle have been equally disappointing.

In deriving the plate stiffness matrix, the bending curvatures will be obtained by assuming the displacements along the edges of the panel as third-order polynomials. The bending coupling will be obtained by integrating the products of these cubics over a quadrant of the plate and the torsion term will be based on simple torsion of the rectangular cell. Thus the displacement along line 1-2 (Fig. 1) is written:

$$\left.\begin{aligned} w &= A_3x^3 + A_2x^2 + A_1x + A_0 \\ w_x &= \theta = 3A_3x^2 + 2A_2x + A_1 \\ w_{xx} &= 2(3A_3x + A_2) \end{aligned}\right\} \quad (2)$$

The four constants of the displacement expression, A_i, can be evaluated by requiring that this function give the displacements and slopes of nodes 1 and 2 at $x = 0$ and $x = a$. Then, in matrix form, the expression for the curvature becomes:

$$w_{xx} = \frac{2}{a}\left[\frac{3x}{a} - 2, \frac{6x}{a^2} - \frac{3}{a}, \frac{3x}{a} - 1, -\frac{6x}{a^2} + \frac{3}{a}\right]\begin{Bmatrix}\theta_1 \\ w_1 \\ \theta_2 \\ w_2\end{Bmatrix} \quad (3)$$

w_{xx}^2 can be obtained by multiplying (3) by its transpose. The total strain energy contributed by w_{xx}^2 can be found by integrating the result over x between zero and a and multiplying by $b/2$, assuming that the w_{xx}^2 term varies linearly with y. Then, invoking Castigliano's relation, $(\partial/\partial\delta)U = F_i$, differentiation yields:

$$\begin{Bmatrix} M_{\theta_1} \\ F_{z_1} \\ M_{\theta_2} \\ F_{z_2} \end{Bmatrix} = Db/a^2 \begin{bmatrix} 2a & & \text{Sym.} & \\ 3 & 6/a & & \\ a & 3 & 2a & \\ -3 & -6/a & -3 & 6/a \end{bmatrix} \begin{Bmatrix} \theta_1 \\ w_1 \\ \theta_2 \\ w_2 \end{Bmatrix} \quad (4)$$

It is of interest to note that (4) constitutes an elementary beam stiffness matrix, neglecting shear deformations, for a beam of width $b/2$, with $Db/2$ equal to EI. This is evident if Eq. (11a) of reference 14 (page 811) is transformed so that angular rotation and vertical displacement become the deformation parameters. This identity makes it convenient to approximate shear deformation effects in the plate analysis if they are desired.

A matrix similar to (4) can be written in terms of the angular rotations and vertical displacements of nodes 3 and 4, and by combining the two matrices one can get

$$\begin{Bmatrix} M_{\theta_1} \\ F_{z_1} \\ M_{\theta_2} \\ F_{z_2} \\ M_{\theta_3} \\ F_{z_3} \\ M_{\theta_4} \\ F_{z_4} \end{Bmatrix} = Db/a^2 \begin{bmatrix} 2a & & & & & & & \\ 3 & 6/a & & & & \text{Symmetric} & & \\ a & 3 & 2a & & & & & \\ -3 & -6/a & -3 & 6/a & & & & \\ 0 & 0 & 0 & 0 & 2a & & & \\ 0 & 0 & 0 & 0 & 3 & 6/a & & \\ 0 & 0 & 0 & 0 & a & 3 & 2a & \\ 0 & 0 & 0 & 0 & -3 & -6/a & -3 & 6/a \end{bmatrix} \begin{Bmatrix} \theta_1 \\ w_1 \\ \theta_2 \\ w_2 \\ \theta_3 \\ w_3 \\ \theta_4 \\ w_4 \end{Bmatrix} \quad (5)$$

If functions of the form of (2) are selected in the y direction as well, the y bending stiffness matrix can be written from (5) immediately from symmetry and takes the form:

$$\begin{Bmatrix} M_{\phi_1} \\ F_{z_1} \\ M_{\phi_2} \\ F_{z_2} \\ M_{\phi_3} \\ F_{z_3} \\ M_{\phi_4} \\ F_{z_4} \end{Bmatrix} = Da/b^2 \begin{bmatrix} 2b & & & & & & & \\ 3 & 6/b & & & & \text{Symmetric} & & \\ 0 & 0 & 2b & & & & & \\ 0 & 0 & 3 & 6/b & & & & \\ b & 3 & 0 & 0 & 2b & & & \\ -3 & -6/b & 0 & 0 & -3 & 6/b & & \\ 0 & 0 & b & 3 & 0 & 0 & 2b & \\ 0 & 0 & -3 & -6/b & 0 & 0 & -3 & 6/b \end{bmatrix} \begin{Bmatrix} \phi_1 \\ w_1 \\ \phi_2 \\ w_2 \\ \phi_3 \\ w_3 \\ \phi_4 \\ w_4 \end{Bmatrix} \quad (6)$$

To obtain the bending coupling energy, the transpose of w_{xx} is multiplied by w_{yy}, integrated, and differentiated as before. A product can be taken at each node, integration performed over a quadrant of the plate, and the sum of the four products used to represent the coupling energy. For example, choosing w_{xx} along 1-2 and w_{yy} along 1-3 gives

$$\frac{D}{2} w_{xx}' w_{yy} = \frac{2D}{ab} |\theta_1 \; w_1 \; \theta_2 \; w_2| \times$$

$$\begin{bmatrix} \left(\frac{9xy}{ab} - \frac{6x}{a} - \frac{6y}{b} + 4\right) & \left(\frac{18xy}{ab^2} - \frac{9x}{ab} - \frac{12y}{b^2} + \frac{6}{b}\right) & \left(\frac{9xy}{ab} - \frac{3x}{a} - \frac{6y}{b} + 2\right) & -\left(\frac{18xy}{ab^2} + \frac{9x}{ab} + \frac{12y}{b^2} - \frac{6}{b}\right) \\ \left(\frac{18xy}{a^2b} - \frac{12x}{a^2} - \frac{9y}{ab} + \frac{6}{a}\right) & \left(\frac{36xy}{a^2b^2} - \frac{18x}{a^2b} - \frac{18y}{ab^2} + \frac{9}{ab}\right) & \left(\frac{18xy}{a^2b} - \frac{6x}{a^2} - \frac{9y}{ab} + \frac{3}{a}\right) & \left(-\frac{36xy}{a^2b^2} + \frac{18x}{a^2b} + \frac{18y}{ab^2} - \frac{9}{ab}\right) \\ \left(\frac{9xy}{ab} - \frac{6x}{a} - \frac{3y}{b} + 2\right) & \left(\frac{18xy}{ab^2} - \frac{9x}{ab} - \frac{6y}{b^2} + \frac{3}{b}\right) & \left(\frac{9xy}{ab} - \frac{3x}{a} - \frac{3y}{b} + 1\right) & \left(-\frac{18xy}{ab^2} + \frac{9x}{ab} + \frac{6y}{b^2} - \frac{3}{b}\right) \\ \left(-\frac{18xy}{a^2b} + \frac{12x}{a^2} + \frac{9y}{ab} - \frac{6}{a}\right) & \left(-\frac{36xy}{a^2b^2} + \frac{18x}{a^2b} + \frac{18y}{ab^2} - \frac{9}{ab}\right) & \left(-\frac{18xy}{a^2b} + \frac{6x}{a^2} + \frac{9y}{ab} - \frac{3}{a}\right) & \left(\frac{36xy}{a^2b^2} - \frac{18x}{a^2b} - \frac{18y}{ab^2} + \frac{9}{ab}\right) \end{bmatrix} \begin{Bmatrix} \phi_1 \\ w_1 \\ \phi_3 \\ w_3 \end{Bmatrix} \quad (7)$$

Integrating (7) from $x = 0$ to $a/2$ and from $y = 0$ to $b/2$ yields

$$\frac{\nu D}{16} |\theta_1 \; w_1 \; \theta_2 \; w_2| \begin{bmatrix} 25 & 30/b & 5 & -30/b \\ 30/a & 36/ab & 6/a & -36/ab \\ 5 & 6/b & 1 & -6/b \\ -30/a & -36/ab & -6/a & 36/ab \end{bmatrix} \begin{Bmatrix} \phi_1 \\ w_1 \\ \phi_3 \\ w_3 \end{Bmatrix} \quad (8)$$

Then, differentiating (8) with respect to each of the displacement coordinates and equating the result to the differential of the potential energy gives

$$\begin{Bmatrix} M\theta_1 \\ M\phi_1 \\ F_{z1} \\ M\theta_2 \\ F_{z2} \\ M\phi_3 \\ F_{z3} \end{Bmatrix} = \nu D/16 \begin{bmatrix} 0 & & & & & & \\ 25 & 0 & & & \text{Symmetric} & & \\ 30/b & 30/a & 72/ab & & & & \\ 0 & 5 & 6/b & 0 & & & \\ 0 & -30/a & -36/ab & 0 & 0 & & \\ 5 & 0 & 6/a & 1 & -6/a & 0 & \\ -30/b & 0 & -36/ab & -6/b & 36/ab & 0 & 0 \end{bmatrix} \begin{Bmatrix} \theta_1 \\ \phi_1 \\ w_1 \\ \theta_2 \\ w_2 \\ \phi_3 \\ w_3 \end{Bmatrix} \tag{9}$$

Repeating these operations at the three other nodes and adding together the matrices of the form (9) results in a form of the bending coupling stiffness matrix:

$$\begin{Bmatrix} \\ M\theta_1 \\ M\phi_1 \\ F_{z1} \\ M\theta_2 \\ M\phi_2 \\ F_{z2} \\ M\theta_3 \\ M\phi_3 \\ F_{z3} \\ M\theta_4 \\ M\phi_4 \\ F_{z4} \end{Bmatrix} = \nu D/16 \begin{bmatrix} 0 & & & & & & & & & & & \\ 25 & 0 & & & & & \text{Symmetric} & & & & & \\ 30/b & 30/a & 72/ab & & & & & & & & & \\ 0 & 5 & 6/b & 0 & & & & & & & & \\ -5 & 0 & -30/a & -25 & 0 & & & & & & & \\ -6/b & -30/a & -72/ab & -30/b & 30/a & 72/ab & & & & & & \\ 0 & -5 & -30/b & 0 & 1 & 6/b & 0 & & & & & \\ 5 & 0 & 6/a & 1 & 0 & -6/a & -25 & 0 & & & & \\ -30/b & -6/a & -72/ab & -6/b & 6/a & 72/ab & 30/b & -30/a & 72/ab & & & \\ 0 & -1 & -6/b & 0 & 5 & 30/b & 0 & -5 & 6/b & 0 & & \\ -1 & 0 & -6/a & -5 & 0 & 6/a & 5 & 0 & 30/a & 25 & 0 & \\ 6/b & 6/a & 72/ab & 30/b & -6/a & -72/ab & -6/b & 30/a & -72/ab & -30/b & -30/a & 72/ab \end{bmatrix} \begin{Bmatrix} \theta_1 \\ \phi_1 \\ w_1 \\ \theta_2 \\ \phi_2 \\ w_2 \\ \theta_3 \\ \phi_3 \\ w_3 \\ \theta_4 \\ \phi_4 \\ w_4 \end{Bmatrix} \tag{10}$$

Considering the simple torsion of cell a-b, the curvature can be defined as:

$$w_{xy} = \frac{1}{ab}[1, -1, -1, 1] \begin{Bmatrix} w_1 \\ w_2 \\ w_3 \\ w_4 \end{Bmatrix} \tag{11}$$

By premultiplication, integration over ab, and differentiation, the stiffness form can be found as

$$\begin{Bmatrix} F_{z1} \\ F_{z2} \\ F_{z3} \\ F_{z4} \end{Bmatrix} = 2(1-\nu)D/ab \begin{bmatrix} 1 & & \text{Sym.} & \\ -1 & 1 & & \\ -1 & 1 & 1 & \\ 1 & -1 & -1 & 1 \end{bmatrix} \begin{Bmatrix} w_1 \\ w_2 \\ w_3 \\ w_4 \end{Bmatrix} \tag{12}$$

Expressions (5), (6), and (10) and (12) define all the components of the energy expression (1). Summing these relations one finds the stiffness matrix for a thin rectangular plate.

With the change of displacement coordinates and moment normalizing indicated in Eq. (13) (see page 38), the elements of the matrix become nondimensional quantities. The reader may also observe that a given column of the matrix defines a set of forces which satisfy the three equilibrium equations.

This stiffness matrix is closely related to the evaluation of stiffness by Levy's torque tube and beam analogy.[17] Here, however, the Poisson ratio coupling has been retained, and a single matrix includes both bending and torsion.

Convergence Criteria

When the exact solution to a problem is unknown, it is usually necessary to compare solutions based on different nodal refinements to evaluate the accuracy of the answers. Before applying Eq. (13) to some problems, convergence criteria will be considered.

Convergence could be evaluated by obtaining a statistical value of the percentage changes in elements of either the stiffness or influence matrices as the network is refined. Since the influence matrix is generally not very sensitive to changes in elements of the stiffness matrix and since the loads are usually the independent variables, the statistical percentage would logically be based on the influence matrix. If the influence matrix is to be calculated anyway, the N condition number introduced by Turing[13] can conveniently be found. This number is approximately proportional to the ratio of the maximum to minimum eigenvalues of the matrix. Not only is it a useful number for evaluating convergence, but it is a measure of the susceptibility of the matrix to round-off errors in inversion. The N condition number is defined as

$$N = \frac{1}{n}\sqrt{\sum_{i,j} a_{ij} \sum_{i,j} k_{ij}} \tag{14}$$

where the a_{ij} are elements of the influence matrix, the k_{ij} are elements of the stiffness matrix, and n is the matrix order. High N condition numbers are associated with poorly conditioned matrices. Matrices conditioned best have N numbers of 1.0. Turing indicates that typical values of N are of the order $n^{1/2}$, where n is the matrix order. To make valid comparisons of N condition numbers of solutions based on different nodal refinements, it is evident that matrices must be of the same order and must apply to the same nodes.

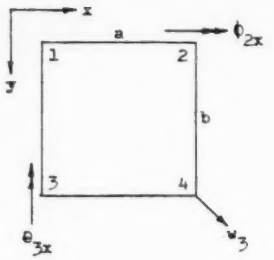

$$D = \frac{Eh^3}{12(1-\nu^2)} \qquad \nu = \text{Poisson's Ratio} \qquad Z = \text{Down}$$

$$\begin{Bmatrix} M\theta_1/b \\ M\phi_1/a \\ Z_1 \\ M\theta_2/b \\ M\phi_2/a \\ Z_2 \\ M\theta_3/b \\ M\phi_3/a \\ Z_3 \\ M\theta_4/b \\ M\phi_4/a \\ Z_4 \end{Bmatrix} = D/ab \begin{bmatrix} 2 & & & & & & & & & & & \\ 25\alpha & 2 & & & & & & & & & & \\ 3P^{-1}+30P\alpha & 3P+30P^{-1}\alpha & 6P^{-2}+6P^2+72\alpha+\beta & & & & & & & & & \\ 1 & 5\alpha & 3P^{-1}+6P\alpha & 2 & & & & & & & & \\ -5\alpha & 0 & -30P^{-1}\alpha & -25\alpha & 2 & & & & & & & \\ -3P^{-1}-6P\alpha & -30P^{-1}\alpha & -6P^{-2}-72\alpha-\beta & -3P^{-1}-30P\alpha & 3P+30P^{-1}\alpha & 6P^{-2}+6P^2+72\alpha+\beta & & & & & & \\ 0 & -5\alpha & -30P\alpha & 0 & \alpha & 6P\alpha & 2 & & & & & \\ 5\alpha & 1 & 3P+6P^{-1}\alpha & \alpha & 0 & -6P^{-1}\alpha & -25\alpha & 2 & & & & \\ -30P\alpha & -3P-6P^{-1}\alpha & -6P^2-72\alpha-\beta & -6P\alpha & 6P^{-1}\alpha & 72\alpha+\beta & 3P^{-1}+30P\alpha & -3P-30P^{-1}\alpha & 6P^2+6P^{-2}+72\alpha+\beta & & & \\ 0 & -\alpha & -6P\alpha & 0 & 5\alpha & 30P\alpha & 1 & -5\alpha & 3P^{-1}+6P\alpha & 2 & & \\ -\alpha & 0 & -6P^{-1}\alpha & -5\alpha & 1 & 3P+6P^{-1}\alpha & 5\alpha & 0 & 30P^{-1}\alpha & 25\alpha & 2 & \\ 6P\alpha & 6P^{-1}\alpha & 72\alpha+\beta & 30P\alpha & -3P+6P^{-1}\alpha & -6P^2-72\alpha-\beta & -3P^{-1}-6P\alpha & 30P^{-1}\alpha & -6P^{-2}-72\alpha-\beta & -3P^{-1}-30P\alpha & -3P-30P^{-1}\alpha & 6P^2+6P^{-2}+72\alpha+\beta \end{bmatrix} \begin{Bmatrix} \theta_1{}^b \\ \phi_1{}^a \\ w_1 \\ \theta_2{}^b \\ \phi_2{}^a \\ w_2 \\ \theta_3{}^b \\ \phi_3{}^a \\ w_3 \\ \theta_4{}^b \\ \phi_4{}^a \\ w_4 \end{Bmatrix} \tag{13}$$

SYMMETRIC

$\alpha = \nu/16$

$\beta = 2(1-\nu)$

$P = a/b$

Rectangular plates Bending K matrix

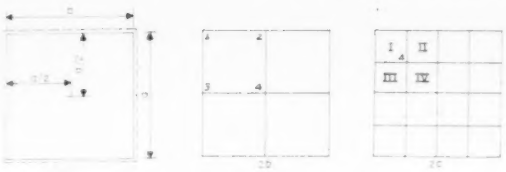

FIG. 2. Simple plate problem.

TABLE 1

Poisson's ratio	Coefficient of D/a^2F	Percentage error
0.0	0.01250	7.759
0.1	0.01237	6.629
0.2	0.01225	5.603
0.3	0.01213	4.578
0.4	0.01202	3.612
0.5	0.01191	2.698

Matrix Convergence Characteristics

Eq. (13) will yield the exact result only for a problem with a network that is sufficiently refined, and the measure of the usefulness of (13) is the refinement of the nodal network required to obtain a given degree of accuracy. To demonstrate these characteristics, three problems on plates of uniform flexural rigidity will be considered first; exact solutions are known for two of these, and for the third experimental and analog solutions are available.

As the first problem, consider the square plate of Fig. 2a. This plate is of uniform thickness and has continuous simple supports on all four edges and a single concentrated load at the center. Because of deformation symmetries, only one quadrant need be considered in the solution. For the choice of the network of Fig. 2b and the panel 1-2-3-4, the boundary conditions, loading conditions, and symmetry conditions are

$$\text{B.C.:}\quad \theta_1 = \phi_1 = w_1 = \theta_2 = \phi_3 = w_2 = w_3 = 0$$
$$\text{L.C.:}\quad M\theta_3 = M\theta_2 = 0$$
$$\text{S.C.:}\quad \theta_4 = \phi_4 = 0, \quad F_{z4} = F/4$$

The zero displacement conditions are imposed by deleting the corresponding columns of the stiffness matrix. Since the corresponding rows are expressions of the reactions in terms of the remaining three displacement coordinates and are not of interest in this problem, they will be discarded. Then, since b/a is equal to one, (14) becomes:

$$\begin{Bmatrix} \frac{M_{\phi 2}}{a} \\ \frac{M_{\theta 2}}{a} \\ F_{z4} \end{Bmatrix} = \begin{Bmatrix} 0 \\ 0 \\ F_4 \end{Bmatrix} = \frac{D}{16a^2} \begin{bmatrix} 3 & & \text{Sym.} \\ \nu & 32 & \\ (-48 - 6\nu) & (-48 - 6\nu) & (224 + 40\nu) \end{bmatrix} \begin{Bmatrix} \phi_2 a \\ \theta_2 a \\ w_4 \end{Bmatrix} \tag{15}$$

The solution of these equations for w gives:

$$w_4 = \frac{(32 + \nu)}{32(16 - \nu)(5 + \nu)} \frac{Fa^2}{D} \tag{16}$$

Of course, in a practical problem, the numerical value of Poisson's ratio will be known. The form (16) has been obtained to show the effect on the solution of varying Poisson's ratio. Timoshenko gives the exact solution of this problem (page 158, reference 12) as $0.01160(a^2/D)$. Thus it would be hoped that the choice of Poisson's ratio would have little effect on the stiffness solution other than its effect on D. Table 1 gives the variation of the solution of Eq. (16) with the choice of Poisson's ratio for this coarse network.

It can be seen that the error varies inversely with Poisson's ratio approximately linearly, over a narrow range. In forming the stiffness matrix for finer nodal networks, stiffnesses are added as indicated in the introduction. Thus for the breakdown shown in Fig. 2c, the force required at node 4 to obtain unit vertical deflection at 4 while no other nodes are permitted to rotate or deflect is an element of the overall stiffness matrix obtained by adding terms from the stiffness matrices for panels I, II, III, and IV. The repetitive use of these simple operations—row and column deletion, row and column reduction, and stiffness summation—make this method readily adaptable to automatic digital manipulation. Table 2 gives the solutions of this problem for successively finer networks, compared with the exact answers, the eigenvalue ratios, and the N condition numbers. In obtaining these results Poisson's ratio was taken as 1/3. Variations in Poisson's ratio were found to have negligible effect on the solution obtained by use of the finest network, as was expected. For simplicity, the condition numbers were identified with reduced matrices of order two.

As a second problem, consider a plate with the same geometry as that of the first problem but with fixed edges. Timoshenko provides the exact solution in reference 12, page 231: $0.00560(a^2/D)$. The solutions obtained with the stiffness matrix are shown in Table 3.

The reader can observe the large error resulting from the use of the 2×2 network. Even without the exact

TABLE 2

Network	Coefficient of D/a^2	Error	Percentage error	$\lambda_{max}/\lambda_{min}$	N condition no.
2×2	0.012093	0.000493	4.250	—	—
4×4	0.011881	0.000281	2.422	18.866	9.459
8×8	0.011703	0.000103	0.889	16.523	8.292
12×12	0.011654	0.000054	0.469	16.421	8.239

TABLE 3

Network	Coefficient of D/a^2	Error	Percentage error	$\lambda_{max}/\lambda_{min}$	N condition no.
2 × 2	0.004213	0.001387	−24.759	—	—
4 × 4	0.005738	0.000138	2.461	10.748	5.420
8 × 8	0.005687	0.000087	1.552	8.899	4.506
12 × 12	0.005655	0.000055	0.978	8.805	4.460

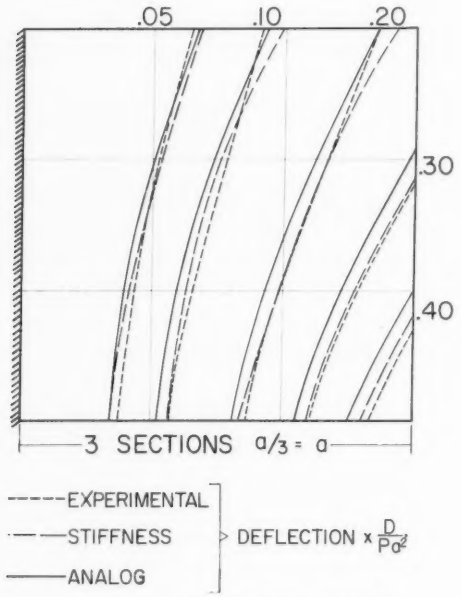

FIG. 3. Cantilevered plate problem.

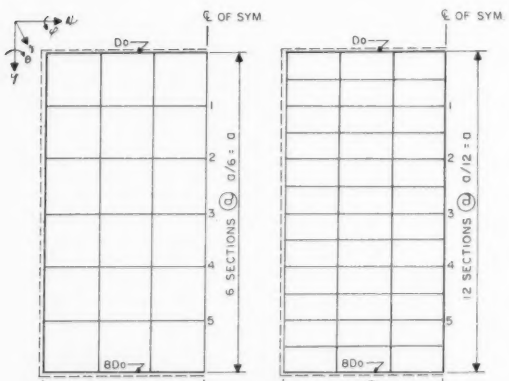

FIG. 4. Olsson's problem.

TABLE 4

Solution	First mode	Second mode
Experimental	0.547	1.359
Stiffness	0.526	1.200
Analog	0.501	1.126

answer available, the large difference between the coefficients of the 2 × 2 and 4 × 4 breakdowns indicates the inadequacy of the coarser network. This problem also illustrates that convergence to the final solution is not always monotonic, as it was in the first problem. In both problems excellent answers are obtained with coarse networks.

As the third problem, consider the square plate of uniform thickness shown in Fig. 3. This cantilevered plate was tested experimentally by Dalley.[2] MacNeal[6] presented the solution of this problem obtained from an analog computer analysis. To compare solutions, the network that MacNeal used (shown in Fig. 3) was utilized in obtaining a stiffness solution. Fig. 3 shows a comparison between the test, analog computer, and stiffness solutions for deflection under a unit load at the lower right-hand corner. A comparison of the frequencies of the natural modes is given in Table 4. Accuracy in the prediction of modes higher than the second is not to be expected, since only nine stations are represented in the matrix iteration for modes. Table 4 shows that the stiffness results are generally better than analog solutions obtained with the same structural refinement.

Plates of Variable Thickness

A limited number of exact solutions for plates of variable thickness are known. The exact solution for the circular plate whose thickness varies as a function of the radial distance has been found.[12] Olsson[2] obtained an exact solution for a rectangular plate of linearly varying thickness in the form of exponential integrals. Reissner's paper[9] presents a simpler derivation of Olsson's results. Fung[4] has presented relaxation solutions for several simple problems, including one of swept planform.

To demonstrate the accuracy of stiffness matrix solutions of variable thickness plate problems, Olsson's problem as particularized in Fig. 4 will be considered. Again the square plate is simply supported on all four edges, but its flexural rigidity varies linearly with the y coordinate from D_0 at the upper edge to $8D_0$ at the lower edge. The distributed loading imposed on the plate varies in the same way as the flexural rigidity.

The networks shown in Fig. 4 were used in obtaining stiffness solutions. For the flexural rigidity of a panel, the average of the rigidities at the four corners of the panel was used. The exact and stiffness solutions for displacements and moments along the centerline are listed in Table 5.

In the solutions I the external work was defined by assuming the deformation shapes to be linear between

TABLE 5

Node	Solution	Deflection, $\pi^5 D_0/4_{q_0}a^4$	φ Moment, $\pi^3/4_{q_0}a^2$	θ Moment, $-\pi^3/4_{q_0}a^2$
1	Exact	0.1996	0.837	0.563
	36 Plate I	0.1891	0.678	0.452
	36 Plate II	0.1966	0.718	0.468
	72 Plate I	0.1938	0.790	0.499
	72 Plate II	0.1964	0.799	0.502
	% Error 72-II	−1.6	−4.5	−10.8
2	Exact	0.3106	1.265	1.212
	36 Plate I	0.2949	1.131	1.013
	36 Plate II	0.3048	1.169	1.039
	72 Plate I	0.3003	1.219	1.091
	72 Plate II	0.3043	1.233	1.099
	% Error 72-II	−2.0	−2.5	−9.3
3	Exact	0.3264	1.483	1.673
	36 Plate I	0.3141	1.338	1.414
	36 Plate II	0.3239	1.363	1.445
	72 Plate I	0.3191	1.425	1.516
	72 Plate II	0.3234	1.442	1.526
	% Error 72-II	−0.9	−2.8	−8.8
4	Exact	0.2724	1.500	1.748
	36 Plate I	0.2597	1.333	1.451
	36 Plate II	0.2681	1.374	1.491
	72 Plate I	0.2639	1.437	1.562
	72 Plate II	0.2676	1.455	1.573
	% Error 72-II	−1.8	−3.0	−10.
5	Exact	0.1653	1.139	1.291
	36 Plate I	0.1474	0.964	0.993
	36 Plate II	0.1526	1.015	1.015
	72 Plate I	0.1502	1.086	1.076
	72 Plate II	0.1525	1.103	1.083
	% Error 72-II	−7.7	−3.2	−16.1

stations, whereas in the solutions II parabolic shapes between stations were assumed. It can be seen that the refined evaluation of the virtual work had little effect on the accuracy of the solutions.

The moments in the plate were calculated in accordance with the expressions

$$M_x = -D(w_{xx} + \nu w_{yy}) \qquad M_y = -D(w_{yy} + \nu w_{xx}) \tag{17a}$$

To obtain the curvatures, the approximate equation

$$w_{xx1} = (w_0 - 2w_1 + w_2)/(\Delta x)^2 \tag{17b}$$

was used. This equation is more convenient than one of the form of Eq. (3), since in the present problem the slope terms were not retained in the final matrix, in order to reduce the numerical work involved in obtaining a solution.

Typical Wing Problem

As an example of the usefulness of the plate bending stiffness matrix, its application to a typical low aspect-ratio wing problem will be given. The structural geometry of this wing is shown in Fig. 5. A plastic model of this wing was tested by Zender[16] and the experimental results were compared with an analog solution performed by MacNeal.[7] In this case the analog circuits were designed so that the wing was treated as a collection of spars, ribs, and skin elements rather than as an equivalent plate.

The wing is biconvex in cross section with a thickness ratio varying from 6 to 10 per cent. It is assumed to be simply supported along the face of the body. Each member of the orthogonal set of spars and ribs is rec-

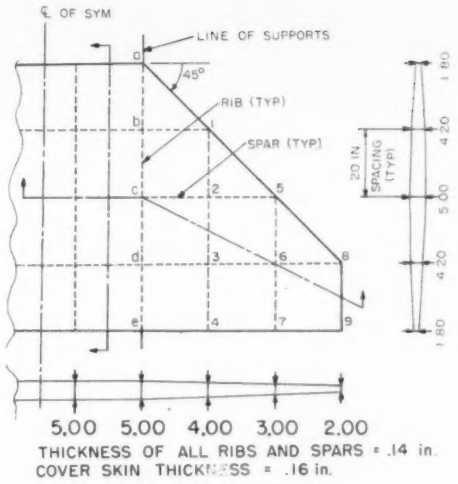

FIG. 5. Delta, Biconvex wing.

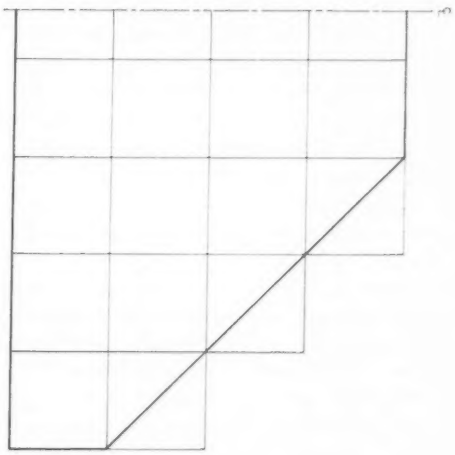

FIG. 6. Coarse nodal network.

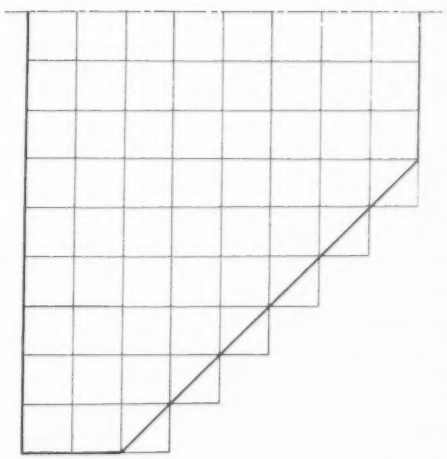

FIG. 7. Fine nodal network.

TABLE 6

Node	w_i 17 Plates	w_i 57 Plates	w_i Exp.	w_i Anal.	Node	σ Exp.	σ Anal.	σ 57 Plate
				Load at Node 8				
9	0.2958	0.3049	0.28	0.2863	*a*	0.75	0.780	0.54
8	0.2897	0.3001	0.30	0.2901	*b*	1.65	1.650	1.673
7	0.1631	0.1670	0.150	0.1574	*c*	1.50	1.500	1.554
6	0.1547	0.1574	0.15	0.1498	*d*	0.85	0.800	0.703
5	0.1316	0.1313	0.130	0.1268	*e*	0.05	0.150	0.077
4	0.0633	0.0637	0.06	0.0596				
3	0.0596	0.0603	0.06	0.0574				
2	0.0505	0.0499	0.05	0.0478				
1	0.0393	0.0373	0.04	0.0354				
				Load at Node 9				
9	0.3879	0.4099	0.39	0.3983	*a*	1.06	1.096	0.874
8	0.2958	0.3049	0.28	0.2863	*b*	1.80	1.792	1.860
7	0.2095	0.2169	0.22	0.2098	*c*	1.44	1.404	1.398
6	0.1646	0.1681	0.16	0.1571	*d*	0.69	0.671	0.549
5	0.1207	0.1202	0.12	0.1142	*e*	0.06	0.087	0.061
4	0.0800	0.0813	0.08	0.0795				
3	0.0645	0.0655	0.07	0.0614				
2	0.0479	0.0474	0.05	0.0443				
1	0.0339	0.0326	0.03	0.0301				

tangular in cross section and the skin thickness is uniform over the entire planform. The depths given in Fig. 5 are the total wing depths, measured from lower to upper outer skin faces.

To analyze this wing as a plate, the equivalent plate was first obtained by computing the flexural rigidity at every node of the network. For simplicity, the rigidity of a given plate panel was taken as the average rigidity of the four corner nodes of the panel. The wing-plate rigidity correspondence was taken as

$$D = EI/(1 - \nu^2)$$

Because the spars and ribs constituted only about three per cent of the bending material of the wing, the inspar network was included by augmenting the plate rigidity by a fixed three per cent. In wing problems where large spars and ribs are present, these can easily be included by using spar and rib bending stiffness matrices (see reference 14). The use of these matrices is not restricted to orthogonal spar and ribs. At the leading edge, flexural rigidities of the triangular panels were taken as the average of the rigidities of the three nodes on the wing. Along the support line, w_i and ϕ_i were required to vanish. A matrix for symmetrical loading about the airplane centerline was obtained by requiring that the θ_i vanish along this line. The solutions obtained permitted vertical loads only. Moments across the support line were calculated by the use of Eqs. (17).

Solutions were obtained with the use of the nodal networks shown in Figs. 6 and 7. In calculating the moments in the finer network, use was made of the deflections at stations closer to the support line than the nodes in the coarser grid.

The reader may note two other differences between the solution of this problem and those of the previous simple problems. In the coarsest-node network a stiffness matrix for a rectangular plate panel was used in conjunction with one for a square panel. In addition, the finer network in the present problem implies a mathematical refinement in the nodal network and a refinement in the structural description. A comparison of experimental and plate and analog solutions is given in Table 6. It should be noted that a full matrix of influence coefficients was not obtained in the test. The comparison represents the major part of the test data available. The excellence of the results is evident. Since the plate equivalence solution neglects shear deformations, the effect of shear must be small in this problem.

Conclusions

(1) The stiffness matrix presented has been shown to exhibit excellent convergence characteristics in the solutions of problems involving plates of uniform thickness.

(2) The success with which this stiffness matrix has been applied to the analysis of a plate of variable thickness confirms its usefulness in this class of problems.

(3) The direct generalization of this matrix to orthotropic panels is justified on the basis of this study.

(4) The accuracy with which the elastic behavior of a thin, low aspect-ratio wing was predicted by the equivalent plate solution verifies the latter as a preliminary design approach.

References

[1] Benscoter, S. U., and MacNeal, R. H., *Equivalent Plate Theory for a Straight Multicell Wing*, C.I.T., NACA TN 2786, September, 1952.

[2] Dalley, J. W., *Experimental Values of Deflection, Stresses, and Influence Coefficients for a Thin Square Plate Fixed Along One Edge*, University of Texas, Defense Research Laboratory Rept. 189, November, 1948.

[3] Duffin, R. J., Gustafson, P. N., and Warner, W. H., *Natural Vibrations of Cantilevered Triangular Plates*, Carnegie Inst. Tech., September, 1952.

[4] Fung, Y. C., *Bending of Thin Elastic Plates of Variable Thickness*, Journal of the Aeronautical Sciences, Vol. 20, No. 7, pp. 455–468, July, 1953.

[5] Lubkin, J. L., and Luke, Y. L., *Modes and Frequencies of Wings of Triangular Planform*, WADC TR 56-335, June, 1956.

(*Continued on page 64*)

On the Approach to Chemical and Vibrational Equilibrium Behind a Strong Normal Shock Wave

WILLIAM H. DORRANCE*

Convair, A Division of General Dynamics Corporation

Summary

The concurrent approach to chemical and vibrational equilibrium of a pure diatomic gas passing through a strong normal shock wave is investigated. It is demonstrated that the equilibrium degree of dissociation behind the shock front, and hence the density, for the case where the vibrational degrees of freedom are frozen out can exceed the degree of dissociation, and hence the density, for the case where all degrees of freedom are in equilibrium. Thus the necessary condition for a maximum of the density between the shock front and the position of full equilibrium flow downstream of the shock front is established. The sufficient condition that such a maximum be observable is shown to be that the approach to equilibrium of the vibrational degrees of freedom (or any other internal degrees of freedom) must lag the approach to dissociation equilibrium by a significant amount; that is, there must be at least an order of magnitude difference in the respective relaxation times before such a maximum might be observed. An example calculation for a Mach 13 strong shock wave in oxygen illustrates the appearance of such a maximum of the density and its dependency upon the relative values of the vibration and dissociation relaxation times.

Symbols

A = chemical symbol for atomic species
A_2 = chemical symbol for diatomic molecules formed with two atoms of A
D = dissociation energy of one molecule A_2
E = internal energy per unit mass of gas
h = Planck constant
k = Boltzmann constant
k_D = forward (dissociation) reaction rate constant
k_R = rearward (recombination) reaction rate constant
K_P = equilibrium constant
M_1 = shock Mach number
m = molecular weight of A
n_A = number of particles of A present in volume V
n_{A_2} = number of particles of A_2 present in volume V
p = pressure
Q = partition function
R = $k/2m$ = gas constant for A_2
T = temperature
T_D = D/k = characteristic temperature for dissociation
T_V = $h\nu/k$ = characteristic temperature for vibration
u = flow speed
V = control volume for chemical reaction
x = distance from shock front
$\bar{x}_d$ = nondimensional distance from shock front, see Eq. (30)
α = fraction of mass of A_2 dissociated
β = see Eq. (13)
ν = frequency of vibration
ρ = density
ρ_D = characteristic density of dissociation
τ_d = dissociation "relaxation time," see Eq. (25)
τ_V = vibration "relaxation time," see Eq. (20)

Subscripts

E = electronic degrees of freedom
d, D = dissociation
R = rotational degrees of freedom
$S.L.$ = sea level value
T = translational degrees of freedom
V = vibrational degrees of freedom
1 = in front of shock wave, free-stream value

Superscripts

$\cdot$ = d/dt
$*$ = equilibrium value

Received October 19, 1959. Revised and received January 2, 1960.

* Senior Staff Scientist, Convair Scientific Research Laboratory, San Diego.

Introduction

BECAUSE of its geometrical simplicity and its obvious relation to the problems of supersonic flight the study of the normal shock wave continues to be pertinent for physicists and fluid dynamicists. As shock Mach numbers become hypersonic the gas passing through the shock front is compressed and heated to higher and higher pressures and temperatures with increasing shock Mach number. As Mach number increases the internal degrees of freedom of the diatomic molecules are activated to an ever increasing extent upon passage through the shock wave and become increasingly important in determining the equilibrium composition of the gas behind the shock wave. Dissociation of the diatomic molecules can take place and must be taken into account. Ionization becomes significant at very high Mach numbers.

Considerable study has already been devoted to the behavior of air and diatomic gases passing through strong normal shock waves. Bethe and Teller[1] determined the equilibrium composition of air behind a strong normal shock wave and discussed the rates of approach to equilibrium of the various internal degrees of freedom of the diatomic molecules and of the dissociation process. More recently, Wood,[2] Evans,[3] and Freeman[4] analyzed the effects of the rates of dissociation and recombination upon the density, velocity, temperature, and pressure profiles behind a strong normal shock wave. Resler and Cary,[5] Byron,[6] and Matthews[7] have experimentally investigated the rate of dissociation of air, or one or more of the components of

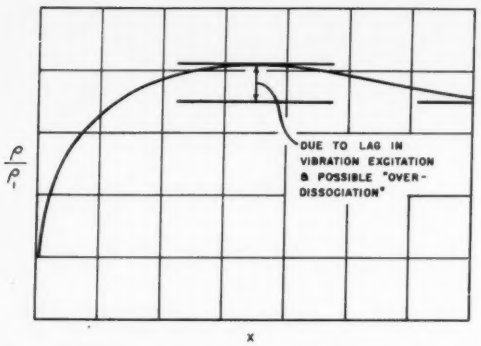

FIG. 1. Schematic of density ratio as a function of distance x from strong normal shock wave in a diatomic gas showing maximum in density ratio at a position between the shock front and equilibrium position downstream which might occur under conditions described in this paper.

air, using a shock tube. Blackman[8] investigated the vibrational relaxation of oxygen and nitrogen and its effect on shock wave structure using the shock tube. In none of the experiments or analyses mentioned was the concurrent approach to chemical and vibrational equilibrium examined. The experimental conditions chosen apparently precluded the possible occurrence of rates of approach to chemical and vibrational equilibrium of the same order of magnitude with the possible exception of those chosen by Resler and Cary.[5] In the other experiments either the shock strength was too low to initiate dissociation[6] (but not too low to excite vibration) or the downstream temperature was low enough that vibrational equilibrium was established at a much higher rate than the rate of approach to dissociation equilibrium.[6, 7]

Interest in the detailed composition of the gas through which a strong normal shock wave has passed has resulted in several computations for strong shock waves passing through air and other gas mixtures. Calculations incorporating some of the features of the calculations reported here were reported by Duff,[9] Hammerling, Teare, and Kivel,[10] and Duff and Davidson.[11] In these calculations the gas through which the strong normal shock wave passed was assumed to reach vibrational equilibrium at a rate faster than the rate of dissociation and ionization ($\tau_V < \tau_d$). It is the purpose of this paper to examine the possibly hypothetical case where the rate of approach to vibrational equilibrium is much slower than the rate of approach to dissociation equilibrium ($\tau_V > \tau_d$) at shock Mach numbers low enough that ionization is not significant but high enough that dissociation occurs. That such a case may not be hypothetical has already been suggested by Heims.[12]

Resler and Cary[5] and Heims[12] suggested that at high temperatures the approach to equilibrium of the various internal degrees of freedom can proceed more or less simultaneously rather than in an ordered sequence as has sometimes conveniently been assumed. If this is the case the rate of approach to chemical equilibrium (dissociation) can depend upon the rate of approach to vibrational equilibrium (or any other internal degree of freedom with comparable rate of approach to equilibrium) and such peculiarities as "overdissociation" can occur. It is the purpose of this paper to present analyses of such cases. In particular, we wish to examine the phenomenon schematically illustrated in Fig. 1 wherein is sketched the variation in density ratio behind a strong normal shock wave in air for the case where vibration excitation lags dissociation by a significant amount.

Method of Analysis

The objective of this analysis is to determine the variables of state, p, ρ, and T, the degree of dissociation, and the gas velocity as a function of distance behind a strong normal shock wave through which a pure diatomic gas is flowing for the cases where the vibrational degree of freedom is excited at a rate equal to or less than the rate at which dissociation of the diatomic gas proceeds. Throughout this analysis the following assumptions will prevail:

(1) The effects of viscosity, thermal conductivity, and diffusion will be neglected.

(2) The internal degrees of freedom of the diatomic molecules which are taken into account include vibration, dissociation, and electronic excitation. Ionization and radiation are neglected as are interactions between degrees of freedom.

(3) The external degrees of freedom of the molecules and atoms are considered here to be the translational and rotational degrees of freedom. These degrees of freedom are assumed to reach equilibrium at rates several orders of magnitude higher than the rates of approach to vibrational and dissociation equilibrium and are assumed to be in equilibrium at all times.

(4) The gases under consideration behave as perfect gases.

These assumptions are generally accepted as reasonable for the gases and their thermodynamic states considered here and will not be discussed further.

Throughout this analysis we will use a coordinate system with the origin fixed at the shock front. To proceed, define for our assumed diatomic gas

$$\alpha = n_A/(n_A + 2n_{A_2}) \tag{1}$$

where α is the fraction by mass of the original molecules dissociated under the reaction

$$A_2 + \begin{Bmatrix} A \\ A_2 \end{Bmatrix} \underset{k_R}{\overset{k_D}{\rightleftharpoons}} A + A + \begin{Bmatrix} A \\ A_2 \end{Bmatrix} \tag{2}$$

and n_A number of atoms present per unit volume

$$n_A = (\rho V/m)\alpha \tag{3a}$$

n_{A_2} = number of molecules present per unit volume

$$n_{A_2} = (\rho V/2m)(1 - \alpha) \tag{3b}$$

At equilibrium the proportions of n_A and n_{A_2} can be determined by the methods of statistical thermodynamics making use of the equation[13, 14]

$$\frac{(n_A^*)^2}{n_{A_2}^*} = \frac{(Q_A)^2}{Q_{A_2}} \exp\left(-\frac{T_D}{T}\right) = K_P \tag{4}$$

where Q_A and Q_{A_2} are the partition functions[15] of A and A_2, respectively, $T_D = D/k$, and the superscripts on n_A and n_{A_2} denote equilibrium values.

It would appear that several reaction rate constants, k_{D_i} and k_{R_i}, would apply to the chemical reaction written as Eq. (2). That is, the rate of dissociation of A_2 would depend upon whether a molecule A_2 or an atom A collided with A_2 and further upon whether A_2 had available energy stored within its vibrational and other internal degrees of freedom or not. However, for the cases considered here we assume the excitation of the vibrational degrees of freedom lags the dissociation process and hence the molecules, A_2, entering into the reaction are for the most part unexcited in their vibrational degrees of freedom. Hence, they enter into the reaction in a state close to that of the vibrationally inert atoms A. We thus assume the reaction rate constants for collisions between A_2 and A and A_2 and A_2 are the same. Thus, two rate constants only, k_D and k_R, represent the chemical kinetics to the order of accuracy of the analysis which follows wherein the effects of any differences in chemical reaction rate constants are overshadowed by the differences between the chemical reaction rates and the rate of excitation of the vibrational degrees of freedom of the molecules.

The relationships between the velocity, the thermodynamic variables of state, and the degree of dissociation behind the shock front and conditions in front of the shock wave can be established by the conservation equations and the equation of state as follows:

equation of state:

$$p = \rho(1 + \alpha)RT \tag{5}$$

where

$$R = k/2m; \qquad m = \text{mass of } A$$

conservation of matter:

$$\rho u = \rho_1 u_1 \tag{6}$$

conservation of momentum:

$$p + \rho u^2 = \rho_1 u_1^2 \tag{7}$$

conservation of energy:

$$E + (p/\rho) + (u^2/2) = u_1^2/2 \tag{8}$$

conservation of species:

$$u(d\alpha/dx) = \dot{\alpha} \tag{9}$$

where $\dot{\alpha}$ is given by the third-order kinetic equation appropriate to the reaction described by Eq. (2). That is, from Eq. (3a),

$$\dot{\alpha} = (m/\rho V)\dot{n}_A \tag{10}$$

and, corresponding to Eq. (2),

$$\dot{n}_A = -(n_A + n_{A_2})k_R[(n_A)^2 - K_P n_{A_2}] \tag{11}$$

where K_P is introduced by making use of the fact that, when $\dot{n}_A = 0$ in Eq. (11),

$$k_D/k_R = (n_A^*)^2/n_{A_2}^* = K_P \tag{12}$$

according to Eq. (4).

The strong shock approximations[1, 12] have been used in writing Eqs. (5), (6), (7), and (8). This implies that we are concerned with Mach numbers high enough that $M_1^2 \gg 2/(\gamma - 1)$, where γ is the ratio of specific heats of the gas in front of the shock front. This approximation makes use of the fact that the kinetic energy far exceeds the internal energy of the gas *in front* of the shock wave at the Mach numbers of interest to us here. For $\gamma = 1.4$, for example, this requires that $M_1^2 \gg 5$, certainly not inappropriate for the case at hand where the shock Mach number has to be higher than about 6 in order that dissociation occur.

We proceed to solve for ρ, p, T, and u as functions of α first, using Eqs. (5), (6), (7), and (8). Introduce the variable β, where

$$\beta = 1 + [E/(1 + \alpha)RT] \tag{13}$$

then it will be found that

$$\rho/\rho_1 = u_1/u = 2\beta - 1 \tag{14}$$

$$\frac{RT}{u_1^2} = \frac{2(\beta - 1)}{(1 + \alpha)(2\beta - 1)^2} = \frac{1}{(1 + \alpha)}\frac{\rho_1}{\rho}\left(1 - \frac{\rho_1}{\rho}\right) \tag{15}$$

and

$$\frac{1}{\gamma M_1^2}\frac{p}{p_1} = \frac{2(\beta - 1)}{2\beta - 1} = 1 - \frac{\rho_1}{\rho} \tag{16}$$

It remains to solve for α and β as a function of distance x behind the normal shock front through differential Eqs. (10) and (11) and approximations yet to be introduced.

In Eq. (13)

$$E = E_T + E_R + E'_V + E_D + E_E \tag{17}$$

where the subscripts T, R, V, D, E refer to translation, rotation, vibration, dissociation, and electronic degrees of freedom, and E is the internal energy per unit mass of the gas. To proceed, we will assume $E_E \equiv 0$, that is, the temperature of the gas is such that negligible energy is stored in the electronic degrees of freedom of A and A_2. (This is not to say, however, that the electronic state partition function will not be used later in determining the equilibrium degree of dissociation.)

$$E_D = (D/2m)\alpha$$

by definition. The remaining components of E are obtained from the partition functions for monatomic and diatomic molecules.[15] That is,

$$E_i = 2\alpha RT^2(d/dT)\{\log [(Q_i)_A]\} + (1 - \alpha)RT^2(d/dT)\{\log[(Q_i)_{A_2}]\} \tag{18}$$

for $i = T$ and R and

$$E'_V = (1 - \alpha)\mathrm{RT}'^2(d/dT')\{\log [(Q_V)_{A_2}]\} \quad (19)$$

In writing Eq. (19) we have assumed the lagging vibrational degrees of freedom are in a quasi-equilibrium state at a representative temperature T' which is less than the temperature T characterizing the other states. Implicit in this relation is the assumption that the vibrational degrees of freedom are initially in equilibrium with a Boltzmann distribution function at a temperature T' equal to the low temperature before the shock front, and that the collision mechanism which raises the vibrational energy after the shock front is such that T' approaches T while the Boltzmann distribution function is maintained at every intermediate temperature T'. The change in distribution of vibrational energy with distance behind the shock front is thus characterized by the variation of T' as it approaches T. The ramifications of this assumption and possible inadequacies of it are discussed in references 16 and 17.

An equation for E'_V in terms of T and T' may be obtained as follows:

$$\frac{dE'_V}{d} = u\frac{dE'_V}{dx} = \frac{\partial E'_V}{\partial T'}\frac{dT'}{dt} + \frac{\partial E'_V}{\partial \alpha}\frac{d\alpha}{dt} \quad (20)$$

where, when α = constant, [1,17,18]

$$\frac{\partial E'_V}{\partial T'}\frac{dT'}{dt} \equiv \frac{dE'_V}{dt} = \frac{1}{\tau_V}(E_V - E'_V) \quad (20a)$$

and, according to our assumptions,

$$E_V = E_V(T); \quad E'_V = E_V(T')$$

Now $T'(x)$ can be related to $T(x)$ through Eqs. (19) and (20). We find[15] for a harmonic oscillator,

$$[Q_V(T')]_{A_2} = \frac{\exp(T_V/T')}{\exp(T_V/T') - 1} \cong 1.58\left(\frac{T'}{T_V}\right)^{1/2} \quad (21)$$

where $T_V = h\nu/k$ and we introduce the approximate vibrational degree of freedom partition function on the right-hand side of Eq. (21) for the following reasons: (1) In the temperature range of interest here it approximates the more exact function and has a much simpler dependency on T', (2) It will allow the derivation of a simple, useful expression for T' as a function of T and x, and (3) When used with Eq. (19) it gives a value for E_V' which is equal to that assumed in references 4 and 13 and thus relates the present qualitative results to earlier investigations.

When Eq. (21) is substituted into Eq. (19) and the proper translational and rotational partition functions for monatomic and diatomic molecules[15] are substituted in Eq. (18) we obtain

$$E_T = (3/2)(1 + \alpha)RT \quad (22a)$$

$$E_R = (1 - \alpha)RT \quad (22b)$$

$$E'_V = (1/2)(1 - \alpha)RT' \quad (22c)$$

and, as was introduced earlier,

$$E_D = (D/2m)\alpha \quad (22d)$$

and

$$E_E \equiv 0 \quad (22e)$$

It will be noted that E_T and E_R reduce to the proper values for monatomic and diatomic molecules when $\alpha = 1$ or 0, respectively, and that $E'_V = (1/2)RT'$, one half the fully excited classical value, when $\alpha = 0$ and that $E'_V = 0$ when $\alpha = 1$.

To obtain $\alpha(x)$, Eqs. (3), (4), the translational, rotational, vibrational, and electronic partition functions for monatomic and diatomic molecules, and Eqs. (10) and (11) must be used. Reference 15 gives partition functions for the translational and rotational degrees of freedom, Eq. (21) gives a convenient approximation for the vibrational degree of freedom which will be used, and the electronic states of any gas considered will be assumed to be either fully excited at the temperatures under consideration or unexcited. For example, for N, N_2, O, and O_2 we assume the ground states only are fully excited with the other states being unexcited at the temperatures under consideration. For O_2 and N_2, the major constituents of air, this gives the values for the electronic degrees of freedom partition functions[19, 20] shown in Table 1.

With these simplifications Eq. (4) becomes

$$\frac{(\alpha^*)^2}{1 - \alpha^*} = \frac{\rho_D}{\rho}\left(\frac{T}{T'}\right)^{1/2}\exp\left(-\frac{T_D}{T}\right) \quad (23)$$

where ρ_D and T_D are characteristic of the gas under consideration. For example, using the appropriate physical constants for oxygen and nitrogen the values shown in Table 2 are obtained.

The local value of α approaches α^* downstream of the shock front at a rate determined by the rate constant k_R and the equilibrium constant K_P as will be shown. Use of Eqs. (3), (9), (10), and (11) yields

$$d\alpha/dx = -(1/u\tau_d)(\alpha - \alpha^*) \quad (24)$$

where

$$\frac{1}{\tau_d} = \frac{k_R}{2}\left(\frac{\rho V}{m}\right)^2(1 + \alpha)\left(\alpha + \frac{\alpha^*}{1 - \alpha^*}\right) \quad (25)$$

Thus τ_d varies with x since k_R, ρ, α, and α^* all vary with distance from the shock front. This completes our system of equations for the variables u, ρ, p, T, T', α, and α^*.

Useful and desirable equations for β and ρ now result from inserting Eqs. (22) into Eqs. (17), (13), and (14). These are

TABLE 1

Gas (A_2)	$(Q_E)_A$	$(Q_E)_{A_2}$
O_2	9	3
N_2	4	1

TABLE 2

Gas	ρ_D (gram/cc.)	T_D (°K.)
O_2	187	59,000 (Ref. 13)
N_2	135	113,300 (Ref. 14)

$$\beta = 3.5 + 0.5\,\frac{T'}{T} - \left(\frac{T_D}{T} - 2 - \frac{T'}{T}\right)\left(\frac{\alpha}{1+\alpha}\right) \tag{26}$$

and

$$\frac{\rho}{\rho_1} = \frac{u_1}{u} = 6.0 + \frac{T'}{T} + 2\left(\frac{T_D}{T} - 2 - \frac{T'}{T}\right)\left(\frac{\alpha}{1+\alpha}\right) \tag{27}$$

where T, T', and α are functions of x to be determined through Eqs. (15), (20), and (24).

Our system of equations can be reduced to four equations to be solved simultaneously for ρ, T, T', and α as functions of the independent variable x. That is.

Eq. (27) gives $\rho(T, T', \alpha)$ and $u(T, T', \alpha)$
Eq. (15) + Eq. (26) gives $T(T', \alpha)$
Eq. (20) + Eq. (22c) gives $T'(T, \alpha, x)$
Eq. (23) + Eq. (24) gives $\alpha(T, T', \rho, x)$
The remaining variable of state, p, can be obtained by using Eq. (5).

The combination of Eqs. (20) and (20a) with Eq. (22c) and Eq. (24) can be integrated to obtain $T'(x)$ and $\alpha(x)$. In order to facilitate the numerical integration these nonlinear differential equations are manipulated in a straightforward fashion to obtain:

$$\frac{dT'}{d\bar{x}_d} + \frac{\tau_d(\bar{x}_d)}{\tau_V(\bar{x}_d)}\,T' - \frac{\tau_d(\bar{x}_d)}{\tau_V(\bar{x}_d)}\,T = 0 \tag{28}$$

with the boundary condition that $T' = T_1$ at $\bar{x}_d = 0$. $\alpha(\bar{x}_d)$ is obtained from Eq. (24) slightly rearranged, viz:

$$(d\alpha/d\bar{x}_d) + \alpha - \alpha^* = 0 \tag{29}$$

with the boundary condition that $\alpha = 0$ at $\bar{x}_d = 0$, and where, in both Eqs. (28) and (29),

$$\bar{x}_d = \int_0^x \frac{dx}{u\tau_d} \tag{30}$$

In Eq. (28) and Eq. (29) α^* and T are both functions of $\bar{x}_d$ determined by Eqs. (23) and (15), respectively.

Thus, Eqs. (28) and (29) can be integrated in combination with Eqs. (5), (15), (26), and (27) to obtain $T'(\bar{x}_d)$, $\alpha(\bar{x}_d)$, $p(\bar{x}_d)$, $T(\bar{x}_d)$, $\rho(\bar{x}_d)$, and $u(\bar{x}_d)$ once appropriate functional relations for $\tau_d(T, T', \rho, \alpha)$ and $\tau_V(T, \rho)$ are known. Because these functional relationships are determined by rate constants at present inexactly determined it was decided to study the problem systematically by assuming various feasible constant ratios of τ_d to τ_V. Eqs. (28) and (29) were integrated numerically, using an IBM 704 Computer, to obtain $T'(\bar{x}_d)$, $T(\bar{x}_d)$, $\rho(\bar{x}_d)$, $\alpha(\bar{x}_d)$, $\alpha^*(\bar{x}_d)$, and $p(\bar{x}_d)$ for constant values of the ratio of τ_d to τ_V. The results are described in the section following.

Once a dependent variable is determined as a function of $\bar{x}_d$, its variation with x, the distance from the shock front, is obtained from a simple inversion and quadrative of Eq. (30)—i.e.,

$$x(\bar{x}_d) = \int_0^{\bar{x}_d} u(\bar{x}_d)\tau_d(\bar{x}_d)d\bar{x}_d \tag{31}$$

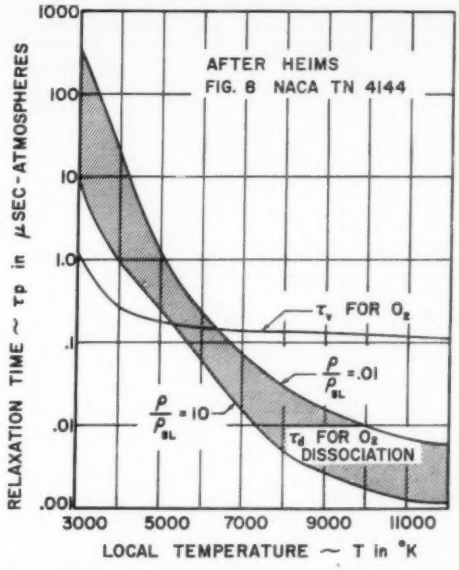

FIG. 2. Calculated values of vibration and dissociation relaxation times according to Eqs. (20a) and (25) with $\alpha = 0$. After Heims.[12]

The example calculations to be described are approximate to the extent that values of τ_d and τ_V constant are assumed for the reasons cited. It should be apparent, upon examining Eqs. (28) and (29), that a simple modification of the integration routine is involved when both τ_d and τ_V are assumed to vary with $\bar{x}_d$ through their dependency upon T, T', ρ, α^*, and α. The resulting curves of $T'(\bar{x}_d)$, $\alpha(\bar{x}_d)$, etc., calculated for τ_d and τ_V varying with $\bar{x}_d$ would then intersect the curves calculated here for constant values of τ_d and τ_V at points of intersection determined by the variation of τ_d and τ_V with $T(\bar{x}_d)$, $T'(\bar{x}_d)$, $\alpha(\bar{x}_d)$, $\alpha^*(\bar{x}_d)$, and $\rho(\bar{x}_d)$. However, the region determined by integrations with τ_d and τ_V constant will cover the region which would result if τ_d and τ_V were allowed to vary. Hence, it was believed that the sought after dependency of state variables behind a strong normal shock front upon reaction and relaxation rates will be illustrated by these calculations.

Example Calculations

It should be apparent that in order for the density "overshoot" phenomenon to occur for the reason described herein the vibrational "relaxation time," τ_V, must exceed the dissociation "relaxation time," τ_d. There has been evidence advanced that vibrational relaxation times for oxygen can exceed dissociation relaxation times for oxygen by an order of magnitude or more at temperatures exceeding 6,000°K. at densities greater than or equal to 0.01 sea level density. Fig. 2, taken from reference 12, illustrates this evidence. The τ_V and τ_d shown on Fig. 2 correspond to the τ_V and τ_d of Eq. (20a) and Eq. (25), respectively, calculated for $\alpha = 0$ which corresponds to $\bar{x}_d = 0$.

Since it is much simpler to deal analytically with a

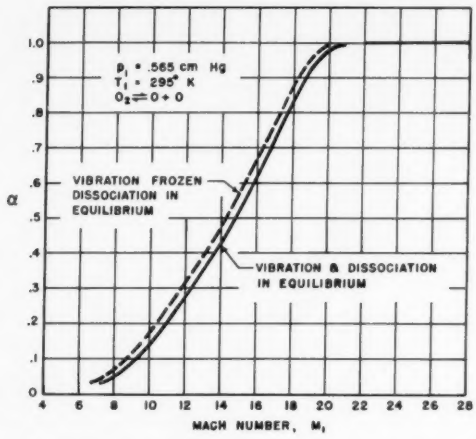

FIG. 3. Equilibrium degree of oxygen dissociated downstream of the shock as a function of shock Mach number for vibration frozen out and in equilibrium. $p_1 = 0.565$ cm. Hg, $T_1 = 295°$K.

pure diatomic gas than a mixture of gases such as air, and since oxygen is a component of air and much data are available for oxygen, this diatomic gas was chosen for example calculations. It would be preferable to treat the case of air as a mixture of monatomic and diatomic gases, chiefly oxygen and nitrogen, and thus deal directly with a clearly practical gas mixture. However, the complexity involved seemed to be an over-refinement to the author, whose objective was to demonstrate the dependency of state variables downstream of the shock front with variations in chemical and vibrational reaction rates. It should be pointed out that the differences in oxygen reaction rates and nitrogen excitation and reaction rates may introduce similar density overshoots for strong shock waves in air as was suggested by Logan.[21] Essentially these are problems in lagging adjustment to equilibrium of one or more internal degrees of freedom similar in principle to the problem dealt with here.

Figs. 3 and 4 show equilibrium degree of dissociation and equilibrium density ratios behind a strong shock wave in oxygen for $T_1 = 295°$K. and $p_1 = 0.565$ cm.Hg. The equilibrium degree of dissociation was calculated using Eqs. (15), (23), (26), and (27) with $T' = T$ when vibration is to be considered in equilibrium and $T' = T_1$ when vibration is frozen out. An iteration is involved in the calculation. As might be expected, the equilibrium degree of dissociation, α, is greater when the vibrational degrees of freedom are frozen out, and, consequently, as Eq. (27) would suggest, the equilibrium density ratio is greater. Thus the necessary condition for a maximum in the density between the shock front and the position where full equilibrium is reached is established. The sufficient condition will be found to be that the rate of vibrational excitation must lag the rate of dissociation by a significant amount.

Note that in Fig. 4 the equilibrium density ratio reaches a maximum with shock Mach number far above the nondissociating, nonvibrating, diatomic strong shock value of six, before ionization becomes significant. Calculations beyond Mach 20 were not undertaken because of the necessity of accounting for ionization which is not related to the objective of this paper.

Data points reported by Byron[6] and by Matthews[7] for pure oxygen at an initial pressure of 1 cm.Hg are shown on Fig. 4 for comparison. Also shown is the curve of equilibrium density ratio calculated for an initial pressure of 1 cm.Hg using the methods of this paper. The agreement between theory and experiment is satisfactory.

Fig. 5 shows the approach to equilibrium of the degree of dissociation behind a normal shock wave with normalized distance behind the shock front at a shock Mach number of 13 for the case of vibration frozen out ($\tau_V = \infty$), vibration in equilibrium ($\tau_V = 0$) and for intermediate cases where vibration is concurrent with or lags dissociation ($\tau_V = \tau_d$, $4\tau_d$, and $20\ \tau_d$). Eqs. (15), (23), (26), (27), (28), and (29) were used to calculate $\alpha(\bar{x}_d)$ for the chosen ratios of τ_d to τ_V. It is seen that when vibration lags dissociation a maximum value of α is realized between the shock front and the position where full equilibrium is achieved.

Fig. 6 shows the density ratio behavior behind the shock front for the cases corresponding to the approaches to equilibrium dissociation shown in Fig. 5. The maximums in density ratio expected are obtained. It can be concluded that a lag of an internal degree of freedom such as vibration behind dissociation can result in a maximum in the density profile behind a strong normal shock providing the relaxation time of the lagging internal degree of freedom is sufficiently greater than the dissociation relaxation time.

The temperature behind the shock front for the Mach 13 shock wave considered in Figs. 5 and 6 varies from about 9,700°K. where the translational and rotational degrees of freedom only are in equilibrium ($\bar{x}_d = 0$) to the downstream equilibrium value of about 3,470°K. ($\bar{x}_d = \infty$). The density varies from 0.046 sea level density at $\bar{x}_d = 0$ to 0.105 sea level density at $\bar{x}_d =$

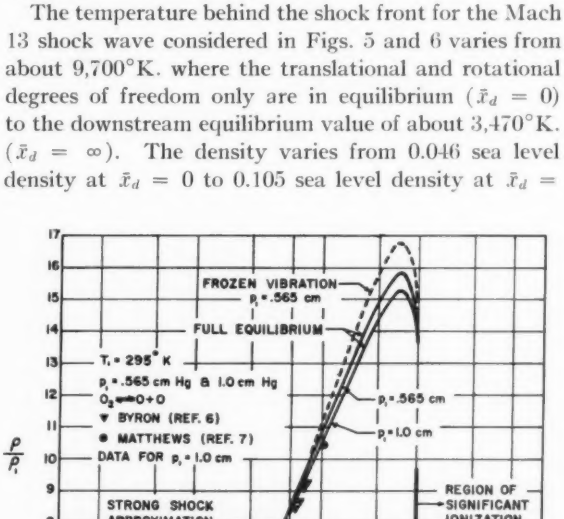

FIG. 4. Equilibrium density ratio downstream of a strong normal shock wave in oxygen for the case of full equilibrium and the case where vibration is frozen out. Data points from reference 6 and reference 7 for $p_1 = 1$ cm. Hg.

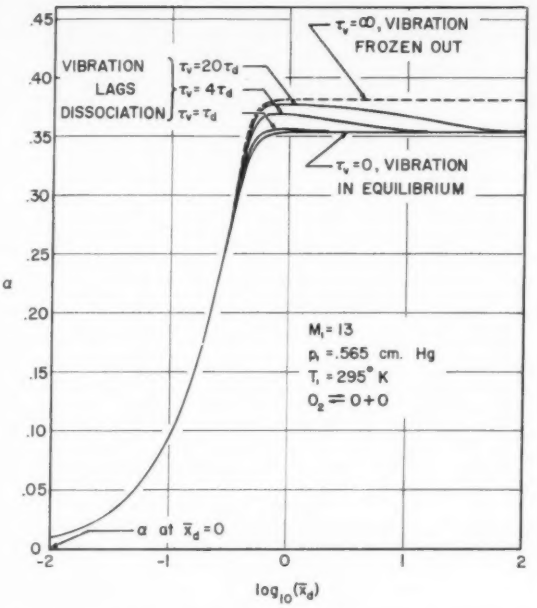

FIG. 5. Variation of degree of oxygen dissociated with normalized distance from the shock front at $M_1 = 13$, $p_1 = 0.565$ cm. Hg, and $T_1 = 295°$K. for the cases of vibration concurrent with or lagging dissociation. Note the appearance of a maximum in α for the latter cases.

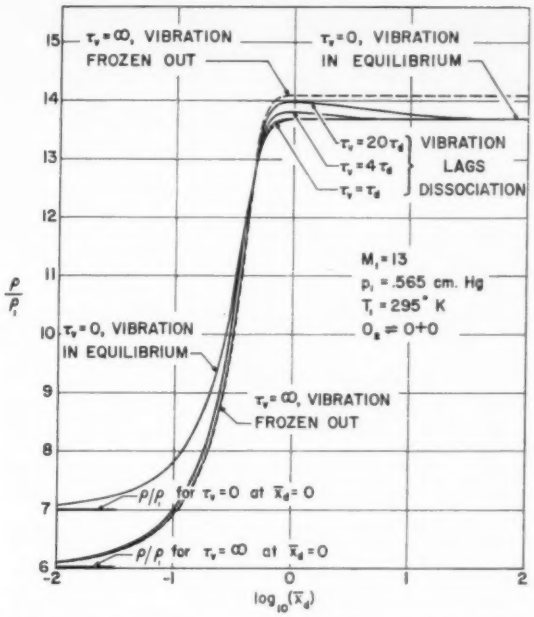

FIG. 6. Variation of density ratio with normalized distance from the shock front at $M_1 = 13$, $p_1 = 0.565$ cm. Hg, and $T_1 = 295°$K. for the cases of vibration frozen out, vibration in equilibrium, and vibration lagging dissociation. Note the maximum in the density ratio for the latter cases.

∞ Thus, according to Fig. 2,

$$\tau_V = 20\tau_d \quad \text{at} \quad \bar{x}_d = 0$$

and

$$\tau_V \to \tau_d/50 \quad \text{as} \quad \bar{x}_d \to \infty$$

At about

$$\bar{x}_d = 0.2 \ (\log_{10} \bar{x}_d = -0.7)$$

the temperature for all cases considered here has dropped to about 6,000°K. at which time, according to Fig. 2, $\tau_d = \tau_V$. When $\bar{x}_d > 0.2$ then $\tau_V < \tau_d$, according to Fig. 2, and based upon Figs. 5 and 6 no maximum in the density ratio or degree of dissociation would occur. However, it should be apparent that when τ_V is larger than τ_d, or when vibrational relaxation lags dissociation, a maximum in the degree of dissociation and hence the density will appear between the shock front and the position of full equilibrium.

Conclusions

The following conclusions are arrived at based upon the findings of this paper:

(1) When a diatomic gas dissociates upon passing through a strong shock wave the degree of dissociation and the density can pass through a maximum with increasing distance from the shock front depending upon the relative rates of dissociation and vibration excitation. However, for the example calculations chosen here it is unlikely that a maximum would occur if the vibration and dissociation relaxation times of Fig. 2 were assumed to apply.

(2) If the vibration and dissociation relaxation times of Fig. 2 are assumed to apply for oxygen then relatively strong shock waves are required to produce the combination of temperature and degree of dissociation downstream of the shock wave necessary for density overshoots to occur. For example, using the shock Hugoniots for oxygen of reference 22, typical shock wave strengths required to produce a temperature of 6,000°K. downstream at equilibrium are tabulated below.

Shock Mach No.	Upstream Pressure	Equilibrium Downstream Temperature	Downstream Equilibrium Degree of Dissociation
17.5	1 atm.	~6,000°K.	~0.50
20.0	0.13 atm.	~6,000°K.	~0.80

(3) The equilibrium values of shock-wave density ratio calculated by the approximate methods of this paper are in good agreement with values reported in reference 22 which were calculated without the simplifying assumptions assumed here. The values of equilibrium density ratio calculated using methods of this paper agree well with measured values reported in references 6 and 7.

References

[1] Bethe, H. A., and Teller, E., *Deviations from Thermal Equilibrium*, Ballistic Research Laboratory, Report X-117, 1941.

[2] Wood, George P., *Calculations of the Rate of Thermal Dissociation of Air Behind Normal Shocks at Mach Numbers of 10, 12, and 14*, NACA TN 3634, 1956.

[3] Evans, John S., *Method for Calculating Effects of Dissociation on Flow Variables in the Relaxation Zone Behind Normal Shock Waves*, NACA TN 3860, 1956.

[4] Freeman, N. C., *Dynamics of a Dissociating Gas—III Non-Equilibrium Theory*, J. Fluid Mech., Vol. 4, p. 407, 1958.

[5] Resler, E. L., and Cary, B. B., *The Threshold of Space*,

"Dissociation of Air Behind Strong Shock Waves," p. 320, Pergamon Press, New York, 1957.

[6] Byron, Stanley Richard, *Interferometric Measurement of the Rate of Dissociation of Oxygen Heated by Strong Shock Waves*, Ph.D. Thesis, Cornell University, Ithaca, New York, 1958.

[7] Matthews, D. L., *Interferometric Measurement in the Shock Tube of the Dissociation Rate of Oxygen*, Physics of Fluids, Vol. 2, No. 2, p. 170, 1959.

[8] Blackman, Vernon, *Vibrational Relaxation in Oxygen and Nitrogen*, J. Fluid Dynamics, Vol. 1, No. 1, p. 61, 1956.

[9] Duff, Russell E., *Calculation of Reaction Profiles Behind Steady State Shock Waves. I Application to Detonation Waves*, J. Chem. Phys., Vol. 28, No. 6, pp. 1193–1197, June, 1958.

[10] Hammerling, P., Teare, J. D., and Kivel, B., *Theory of Radiation From Luminous Shock Waves in Nitrogen*, Physics of Fluids, Vol. 2, No. 4, pp. 422–426, July–August, 1959.

[11] Duff, Russell E., and Davidson, Norman, *Calculation of Reaction Profiles Behind Steady State Shock Waves II. The Dissociation of Air*, J. Chem. Phys., Vol. 31, No. 4, pp. 1018–1027, October, 1959.

[12] Heims, Steve P., *Effect of Oxygen Recombination on One-Dimensional Flow at High Mach Numbers*, NACA TN 4144, 1958.

[13] Lighthill, M. J., *Dynamics of a Dissociating Gas—Part I Equilibrium Flow*, J. Fluid Mechanics, Vol. 2, Part 1, p. 1, 1957.

[14] Heller, Leon, *Equilibrium Statistical Mechanics of Dissociating Diatomic Gases*, Physics of Fluids, Vol. 2, No. 2, p. 147, 1959.

[15] Rossini, Frederick D., "Fundamentals of Thermodynamics," Vol. 1, Princeton Series on "High Speed Aerodynamics and Jet Propulsion," *Thermodynamics and Physics of Matter*, Princeton University Press, Princeton, N. J., 1955.

[16] Rubin, Robert J., and Shuler, Kurt E., *Relaxation of Vibrational Non-Equilibrium Distributions, I. Collisional Relaxation of a System of Harmonic Oscillators*, J. Chem. Phys., Vol. 25, No. 1, p. 59, 1956.

[17] Shuler, Kurt E., *Relaxation Processes in Multistate Systems*, Physics of Fluids, Vol. 2, No. 4, pp. 442–448, July–August, 1959.

[18] Schwartz, R. N., Slawsky, Z. I., and Herzfeld, K. F., *Calculation of Vibrational Relaxation Times in Gases*, J. Chem. Phys., Vol. 20, No. 10, pp. 1591–1599, October, 1952.

[19] Moore, C. E., *Atomic Energy Levels*, Circular Nat. Bur. of Standards 467, 1948.

[20] Herzberg, G., *Molecular Spectra and Molecular Structure I. Spectra of Diatomic Molecules*, D. Van Nostrand Co., 1950.

[21] Logan, Joseph G., Jr., *Relaxation Phenomena in Hypersonic Aerodynamics*, Paper presented at the 25th Annual Meeting, IAS, January 28–31, 1957.

[22] Alpher, R. A., and Greyber, H. D., *Calculation of Shock Hugoniots and Related Quantities for Nitrogen and Oxygen*, Letter to Editor, Physics of Fluids, Vol. 1, No. 2, pp. 160–161, March–April, 1958. See also: Alpher, R. A., and Greyber, H. D., *Calculation of Shock Hugoniots and Related Quantities for Nitrogen and Oxygen*, General Electric Research Laboratory Report No. 58-RL-1915, April, 1958.

✦ ✦ ✦

Stability of Partially Controlled Motions (*Continued from page 26*)

ψ, (A14). Then, the double inequality

$$\int_t^{t+\tau} \Lambda_m(s)ds \leq \psi(t+\tau) - \psi(t) \leq \int_t^{t+\tau} \Lambda_M(s)ds \tag{A16}$$

will be fulfilled at all times. Hence, the sought-for evaluation may be obtained graphically.

A very rough evaluation may be obtained by substituting $\underset{t > t_0}{\text{l.u.b.}}\ \Lambda_M(t)$ in the left-hand side of Eq. (A15):

$$\tau \geq \pi / \underset{t > t_0}{\text{l.u.b.}}\ \Lambda_M(t) \tag{A17}$$

where

$$\Lambda_M(t) = {}^1/_2(-p_{12} + p_{21}) + \sqrt{[{}^1/_4(p_{12} + p_{21})^2 + p_{11}{}^2]}$$

References

[1] Duncan, W. J., *Principles of Control and Stability of Aircraft*, Cambridge University Press, 1952.

[2] Hacker, T., *On the Longitudinal Stability of Aircrafts in the Case of Repeated Disturbances*, Revue de Mécanique Appliquée, Vol. IV, No. 2, 1959.

[3] Hacker, T., *On the Question of Conditional Stability of Aircrafts* (in Russian), Rev. Méc Appl., Vol. II, No. 1, 1957.

[4] Neumark, S., *Problems of Longitudinal Stability Below Minimum Drag Speed, and Theory of Stability Under Constraint*, ARC R&M No. 2983.

[5] Collar, A. R., *On the Stability of Accelerated Motion: Some Thoughts on Linear Differential Equations with Variable Coefficients*, The Aeronautical Quarterly, Vol. VIII, November, 1957.

[6] Liapounoff, A. M., *Problème général de la stabilité du mouvement*, Annals of Math. Studies, No. 17, 1947.

[7] Malkin, I. G., *Theory of Motion Stability* (in Russian), Gos Izd. Tekh.-Teor. Lit., Moscow-Leningrad, 1952.

[8] Massera, J. L., *Contributions to Stability Theory*, Annals of Mathematics (Second Series), Vol. 64, No. 1, July, 1956.

[9] Malkin, I. G., *On the Question of the Reciprocal of Liapounoff's Theorem on Asymptotic Stability* (in Russian), Prikladnaia Matematika i Mekhanika, Vol. 18, No. 2.

[10] Hacker, T., *On the Longitudinal Stability of an Aeroplane in Unsteady, Straight Level Flight*, Revue de Mécanique Appliquée, Vol. I, No. 2, 1956.

[11] Hacker, T., *Contributions to the Study of the Longitudinal Stability of an Aircraft During the Most Unfavorable Evolutions* (in Rumanian), Studii si Cercetări de Mecanică Aplicată, Vol. VI, Nos. 3–4, 1955.

[12] Ostoslavski, I. V., *Aerodynamics of Aircraft* (in Russian), Oborongiz, Moscow, 1957.

[13] Hacker, T., *Influence of Gusts on the Longitudinal Motion of an Aircraft*, Revue de Mécanique Appliquée, Vol. III, No. 1, 1958.

[14] Draper, C. S., *Flight Control*, Journal of the Royal Aeronautical Society, Vol. 59, July, 1955.

✦ ✦ ✦

Experimental Investigation of the Downstream Influence of Stagnation-Point Mass Transfer†

PAUL A. LIBBY* AND ROBERT J. CRESCI**

Polytechnic Institute of Brooklyn

Summary

This report presents the results of an experimental investigation of the downstream influence of localized mass transfer in the stagnation region of a blunt body under hypersonic flow conditions. The coolant is injected through a porous plug coaxial with the centerline of symmetry of the model. The tests were carried out in a wind tunnel with a Mach number of 6.0, stagnation temperatures of approximately 1,600°R., and a stagnation pressure of approximately 600 psia. Four different gases were injected over a range of mass flows. The heat transfer on the impermeable section was measured under isothermal wall conditions; for the higher rates of mass flow, adiabatic surface temperatures were also determined. The theoretical analysis of the boundary-layer flow is investigated in order to establish the similarity parameters for the flow system. These parameters permit the extrapolation of the test results to other flow conditions, provided that laminar flow prevails. Helium is found to be the most efficacious coolant.

Symbols

A = surface area of body
A_P = porous plug area
A_T = total protected surface area
C = $\rho\mu/\rho_e\mu_e$ = density-viscosity ratio
c_p = specific heat at constant pressure
d = shock stand-off distance
f = modified stream function such that $f_\eta = u/u_e$
g = h_s/h_{s_e} = stagnation enthalpy ratio
h = enthalpy
h_i = h_i/h_{s_e} = static enthalpy ratio of species i
K = mass fraction of foreign gas or recovery factor [Eq. (13b)]
k = thermal conductivity
Le = Lewis number
m_c = mass flow of injected gas per unit time
N_{Nu} = $qR_0(c_p)_{s_e}/(h_{s_e} - h_w)k_{s_e}$ = Nusselt number
$\bar{N}_R$ = $(\rho_{s_e}\sqrt{h_{s_e}}R_0/\mu_{s_e})\varphi_{s_e}^{1/2}$ = Reynolds number
N_1 = $(m_c/R_0\mu_{s_e})\bar{N}_R^{-(1/2)}$ = mass-transfer similarity parameter
N_2 = $N_{Nu}\bar{N}_R^{-(1/2)}$ = heat-transfer similarity parameter
p = pressure
Q = effective enthalpy [defined by Eq. (11)]
$\bar{Q}$ = effective enthalpy for isothermal wall
$\tilde{Q}$ = effective enthalpy for adiabatic wall
Q_0 = effective enthalpy on porous plug [$x_T = x_i$ in Eq. (11)]
Q_T = total effective enthalpy of absorption
q = surface heat-transfer rate
R_0 = nondimensionalizing length (hemispherical nose radius)
r_0 = radial coordinate to body surface
$\bar{s}$ = transformed surface coordinate [defined by Eq. (4)]
$\bar{T}$ = T_s/T_{s_e} = temperature ratio
u = velocity component parallel to the surface
v = velocity component normal to the surface
W = $\vartheta_{aw} = T_{aw}/T_{s_e}$ = adiabatic wall-temperature ratio
x = space coordinate along the surface
x_T = maximum length of surface influenced by coolant
$\bar{x}$ = x/R_0 = nondimensionalized space coordinate along the surface
y = space coordinate normal to the surface
α = persistence factor [defined by Eq. (14a)]
β = $(2\bar{s}/u_e)(du_e/d\bar{s})$
η = transformed coordinate normal to the surface [defined by Eq. (5)]
ϑ = T/T_{s_e} = temperature ratio
μ = viscosity coefficient
$\bar{\mu}$ = μ_e/μ_{s_e} = viscosity ratio
ρ = mass density
$\bar{\rho}$ = ρ_e/ρ_{s_e} = density ratio
σ = Prandtl number
φ_{s_e} ≡ $p_{s_e}/\rho_{s_e}h_{s_e}$ = real-gas parameter

Subscripts

aw denotes conditions evaluated at the wall temperature for the case of zero heat transfer
c denotes foreign-gas characteristics prior to injection
e denotes local conditions external to the boundary layer
i denotes the gas under consideration ($i = 1$ for foreign gas; $i = 2$ for primary gas)
s denotes stagnation conditions
s_e denotes conditions external to the boundary layer at the stagnation point
w denotes conditions evaluated at the wall
$(\ )_\eta$ = $\partial/\partial\eta$ partial differentiation with respect to the transformed normal coordinate
$(\ )_{\bar{s}}$ = $\partial/\partial\bar{s}$ partial differentiation with respect to the transformed surface coordinate

Received November 16, 1959. Revised and received May 1, 1960.

† This research was conducted under the sponsorship of Contract No. AF 33(616)-5944 administered under the direction of the Materials Laboratory, Wright Air Development Center, USAF.

* Professor of Aeronautical Engineering and Assistant Director of the Aerodynamics Laboratory.

** Formerly, Research Associate. Now, Research Assistant Professor of Aeronautics.

The authors are pleased to acknowledge the assistance of the staff of the Hypersonic Wind Tunnel of PIBAL and the suggestions of Professor Martin H. Bloom in the research discussed herein.

(1) Introduction

THE PROBLEM of aerodynamic heating in supersonic and hypersonic aircraft and missiles has been the subject of considerable research in recent years. The heating rates encountered in practical flight problems are so severe that a variety of means for alleviation have been proposed and studied. For many years it has been known that significant reductions in heat transfer can be achieved by injecting a fluid into the

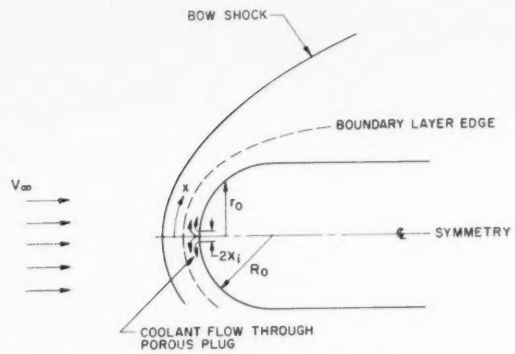

FIG. 1. Schematic diagram of localized mass-transfer system.

boundary layer. Thus a relatively low-energy gas can be interposed between the high-energy stream and the solid surface. Various modes of injection and various cooling fluids have been considered. The selection of the mode of injection and of the coolant from the variety of possibilities depends on the particular application. Indeed, a currently popular heat protection system involves sublimation from the solid surface; thus the mass transfer is continuously distributed along the solid surface and is intimately related to the heat transfer thereto.

Considered here is the mass transfer system shown in Fig. 1. A foreign, chemically inert gas is injected through a porous surface in the nose region of a blunt-nosed, axisymmetric body. The injected mass and momentum are assumed to be so small as not to affect the essentially inviscid flow; thus the influence of the injected fluid can be considered in terms of altered boundary layer behavior. Two regions of the solid surface can be delineated; for values of the surface coordinate measured from the axis of symmetry (denoted as x) such that $0 \leq x \leq x_i$, the injected gas directly influences the boundary layer behavior, while for $x > x_i$ the effect of the injection is to alter the boundary layer behavior because of its downstream influence. If x_i is sufficiently small, the injection region corresponds to stagnation point flow with mass transfer.

Such a mass transfer system corresponds to localized porous cooling wherein the amount of injected gas is more than sufficient to protect the porous region itself but is expected to reduce or to eliminate the heat transfer on the downstream, impermeable region. Localized injection of the type described here may, for example, be of practical utility in connection with radome or infrared seekers wherein the heat protection system must satisfy certain requirements of temperatures, materials, simplicity, and coolant storage volume.

Consider previous research pertaining to the flow treated here. Since the injection is considered to prevail in a stagnation region, the extensive literature on stagnation flows with mass transfer is pertinent. Of particular interest for the injection of chemically inert gases is the work of Hoshizaki and Smith[1, 2] who treated the case of helium injection, and of Hayday,[3] who considered the injection of hydrogen without chemical reaction. The case of homogeneous injection wherein the coolant and the external flow are chemically identical has been studied by Morduchow,[4] Brown and Donoughe,[5] and Reshotko and Cohen.[6] Scala and Sutton[7] have treated the case of air injection into a dissociated air stream in chemical and thermodynamic equilibrium. From these references it may be inferred that considerable work has been devoted to homogeneous flows while relatively little has been devoted to heterogeneous flows.

There appears to have been no analysis of the boundary layer on the impermeable surface ($x \geq x_i$) downstream of the injection region. Hoshizaki and Smith[1] considered the gross downstream influence of helium injection by introducing "a persistence factor" which was "chosen somewhat arbitrarily." Rubesin and Inouye[8] considered a related but simpler problem for a homogeneous gas—namely, the downstream effect of a coolant introduced in a porous region on a flat plate. In passing, it might be mentioned that considerable experimental and theoretical research has been devoted to the related problem of mass transfer through a discrete jet or slot with a liquid and gaseous coolant. The reports by Ferri and Bloom[9] and McMahon[10] provide, *inter alia*, recent reviews of much of the literature pertaining thereto. The problem of the discrete jet differs from that considered here in that the injection may influence significantly the inviscid flow field, at least in the neighborhood of the jet. Thus a boundary layer description of the flow may not be adequate near the jet exit. In reference 9 there was presented an analysis of the turbulent flow on a body of revolution with an upstream air jet; the downstream effect of the jet was represented by an energy sink, in order to derive the correlation parameters of the flow.

In this report an experimental investigation of the laminar heat transfer to the impermeable surface is described. The tests were carried out at a Mach number of 6.0 in the PIBAL Hypersonic Wind Tunnel. Four coolant gases (helium, nitrogen, argon, and krypton) were used; a range of weight flows was covered for the three gases cited first. First the applicable similarity laws are derived from an examination of the boundary layer equations. Then the test conditions and testing techniques are presented. Finally, the experimental results are described and discussed.

(2) The Theoretical Problem and the Similarity Parameters

Consider the problem of treating theoretically the axisymmetric boundary layer under consideration. In order to simplify the discussion the following two assumptions will be made:

(1) $u_e^2/h_{s_e} \ll 1$. Over the nose region of blunt-nosed bodies of practical interest this ratio is on the order of 1/3 to 1/2 and has a small effect on boundary layer behavior.

(2) $Le = 1$. For a Lewis number of unity the

boundary layer equations and the evaluation of heat transfer are greatly simplified.

It will be shown below that these two assumptions are not essential and that the same conclusions and similarity parameters prevail when these assumptions are not applied. Thus the boundary layer in a binary, nonreactive gas mixture can be described when the foreign gas does not exist in the external flow by the equations (cf., for example, reference 11)

$$(Cf_{\eta\eta})_\eta + ff_{\eta\eta} + \beta(\rho_e/\rho - f_\eta^2) = 2\bar{s}(f_\eta f_{\bar{s}} - f f_{\eta\eta}) \quad (1)$$

$$(C\sigma^{-1}K_\eta)_\eta + fK_\eta = 2\bar{s}(f_\eta K_{\bar{s}} - f_{\bar{s}}K_\eta) \quad (2)$$

$$(C\sigma^{-1}g_\eta)_\eta + fg_\eta = 2\bar{s}(f_\eta g_{\bar{s}} - f_{\bar{s}}g_\eta) \quad (3)$$

where the transformed coordinates $\bar{s}$ and η are related to the space coordinates x and y by the transformations

$$\bar{s} = \int_0^x \rho_e \mu_e u_e r_0^2 \, dx \quad (4)$$

$$\eta = \rho_e u_e (2\bar{s})^{-(1/2)} \int_0^y (\rho/\rho_e) r_0 \, dy \quad (5)$$

It should be noted that the analysis of foreign gas injection into a hypersonic airstream with dissociation present is more accurately described in terms of a tertiary system of atoms, molecules, and foreign gas. Hoshizaki and Smith[1, 2] approximate this system by neglecting the diffusion of atoms and molecules while using the equilibrium gas properties of dissociated air. The accuracy of this approximation has apparently not been examined. Here it is assumed either that this approximation is valid, or that the external stream has a negligible degree of dissociation.

Now consider the solution valid in the region $0 \leq \bar{s} \leq \bar{s}_i$, where $\bar{s}_i$ corresponds to the value $x = x_i$. If it is assumed that $\bar{s}_i$ is sufficiently small and the boundary conditions are appropriate so that a stagnation-point solution is valid in this region, then $(\ )_{\bar{s}} \simeq 0$, i.e., f, g, and K are functions of η alone, and $\beta = 1/2$. The boundary conditions which must prevail for this region are:

$$\text{at } \eta = 0\text{:} \quad f = f(0) \quad (6a)$$

$$f_\eta = 0 \quad (6b)$$

$$g = g(0) \quad (6c)$$

$$K = K(0) \quad (6d)$$

$$\text{at } \eta \to \infty\text{:} \quad f_\eta = 1 \quad (6e)$$

$$g = 1 \quad (6f)$$

$$K = 0 \quad (6g)$$

If the coolant is chemically identical with the gas in the external flow, $K \equiv 0$. The values of f, g, and K at $\eta = 0$ are not independent in a practical flow. If it is required that there exist balances of mass and energy at the porous surface ($\eta = 0$)—i.e., that timewise steady conditions prevail—then Eqs. (6c) and (6d) are replaced by

$$f = K_\eta C/(1 - K)\sigma \quad (6h)$$

$$-f(\bar{h}_1 - \bar{h}_e)\sigma = C[g_\eta - (\bar{h}_1 - \bar{h}_2)K_\eta] \quad (6i)$$

where $\bar{h}_i = h_i/h_{i_e}$, $i = 1$ for foreign gas, and $i = 2$ for gas in the external flow; and $\bar{h}_e = h_e/h_{i_e}$, h_e being the enthalpy of the foreign gas prior to injection.

In the region $\bar{s} > \bar{s}_i$ the flow is no longer similar, i.e., $(\ )_{\bar{s}} \not\equiv 0$ in general. The boundary conditions which prevail at $\eta \to \infty$ are those of Eqs. (6e), (6f), and (6g). For $\eta = 0$ the conditions on f and K are clearly

$$f = 0 \quad (6j)$$

$$f_\eta = 0 \quad (6k)$$

$$K_\eta = 0 \quad (6m)$$

while those for g can take on a variety of forms. The most general case involves a relation between g and g_η. However, two limiting cases are of fundamental interest; in the first the surface temperature T_w is constant and thus g and g_η at $\eta = 0$ are to be determined, while in the second g_η at $\eta = 0$ is to be zero; that is, the surface is adiabatic and T_w and g_w are to be determined. (The subscript w denotes wall conditions $\eta = 0$.) The first case corresponds to that prevailing initially in hypersonic wind tunnel tests when a transient technique is applied for the determination of heat transfer; the second can correspond to such tests if continued for long test times. Moreover, the second case may be a good representation of the practical case wherein the stagnation point injection is utilized to keep the surface temperature in steady flight at a tolerable level. Surface radiative heat transfer and streamwise heat conduction within the material can, however, lead to modifications of the adiabatic surface temperature. For clarity, the first limiting case will be discussed here; the same general discussion in modified form can be applied to the second case and to the more general relations between g and g_η at $\eta = 0$. Thus the last boundary condition at $\eta = 0$ is

$$T_w = \text{constant} \quad (6n)$$

It should be noted that the wall temperature in the downstream region is not necessarily equal to that on the porous region.

The nonsimilarity of the flow in the region $\bar{s} > \bar{s}_i$ requires the specification of initial conditions on f, K, and g at $\bar{s} = \bar{s}_i$. This initial point corresponds to a discontinuity in boundary conditions and thus to a point where the boundary layer approximations are not strictly valid. However, it is generally assumed that within a streamwise length corresponding to several boundary layer thicknesses these approximations are again valid; thus the usual procedures for treating discontinuities in finite form are applied. In reference 12, Libby and Pallone treated a similar discontinuity for the homogeneous boundary layer by making the boundary layer thickness, surface temperature, and the fluxes of mass, momentum and energy continuous.*

* Although the matching at the discontinuity was treated properly, the extra parameters so introduced should have been considered functions of x; thus the analysis in reference 12 applies only in the neighborhood of the discontinuity.

Rubesin and Inouye[8] made the boundary layer thickness, the skin friction, and surface temperature continuous.

For the present discussion it is assumed that integral conditions on f, K, and g and the boundary conditions of Eqs. (6e), (6f), (6g), (6j), (6k), (6m), and (6n) are satisfied, and, thus, that at $\bar{s} = \bar{s}_i$, f, K, and g are known functions of η.

Finally, it is necessary to discuss the functional forms for the transport properties of C and σ, mass density ratio ρ_e/ρ, and the component enthalpy ratios $\bar{h}_1$ and $\bar{h}_2$. For a careful description of these quantities it is necessary to specify both pressure and temperature. However, a description which would appear to be quite accurate over wide temperature and pressure ranges can be developed primarily in terms of the temperature ratio $\vartheta \equiv T/T_e$; thus

$$C \simeq \vartheta^{-(1/2)} F_c \tag{7a}$$

$$\sigma \simeq [F_\sigma^{(1)} + F_\sigma^{(2)}\vartheta^{n_1}]/[F_\sigma^{(3)} + F_\sigma^{(4)}\vartheta^{n_2}] \tag{7b}$$

$$\rho_e/\rho \simeq \vartheta F_\rho \tag{7c}$$

$$\bar{h}_1 \simeq a\vartheta^{n_3} \tag{7d}$$

$$\bar{h}_2 \simeq \vartheta^{n_4} \tag{7e}$$

where each F denotes a function of the molecular weights and collision cross sections of the constituent gases, and of the concentration K associated with the transport property denoted by the subscript; a and the parameters n_i are constants selected empirically for the range of temperature and pressure of interest.* The stagnation enthalpy ratio g is related to K and ϑ by the equation

$$g = K(\bar{h}_1 - \bar{h}_2) + \bar{h}_2 = K(a\vartheta^{n_3} - \vartheta^{n_4}) + \vartheta^{n_4} \tag{8}$$

In terms of this description of the gas properties for a given mixture of gases, a solution to the two sets of equations and of boundary conditions for the regions $0 \leq \bar{s} \leq \bar{s}_i$ and $\bar{s} > \bar{s}_i$ is specified, provided that: (1) in the former region f at $\eta = 0$, h_c, and $\bar{s}_i$ (the injection rate, the coolant enthalpy relative to the stagnation enthalpy, and the extent of the injection region) are specified; (2) in the latter region $\vartheta_w = T_w/T_{s_e}$ is specified; and (3) the function $\beta = \beta(\bar{s})$ is known.

The actual solution of the equations applicable to the stagnation region with the approximate description of gas properties given here can be carried out by integration of three ordinary differential equations by either of the two integration techniques usually applied (cf. reference 13). The solution for the impermeable surface ($\bar{s} > \bar{s}_i$), however, involves greater mathematical complexity; simultaneous partial differential equations with split boundary conditions must be solved. In the present formulation only numerical procedures such as those described in reference 41 can be applied.

Although no solutions are available for these equations, the similarity requirements for this flow system can be established from an examination of the equations involved. Consider two geometrically similar bodies; assume that the inviscid flows expressed in terms of stagnation conditions p_{s_e}, h_{s_e}, ρ_{s_e} by means of the variables $\bar{p}$, $\bar{u}$, $\bar{\mu}$ are identical functions of $\bar{x} \equiv x/R_0$, where R_0 is a nondimensionalizing length.† Assume further that the chemical composition of the external and coolant flows are identical; that the boundary conditions in terms of f at $\eta = 0$, $\bar{h}_c$ and ϑ_w are identical in the two systems; and that a, n_1, n_2, etc., are identical. Then the coolant mass flows will be related to one another by the equation

$$\{m_c/R_0\mu_{s_e}\bar{N}_R^{1/2}\}_I = \{m_c/R_0\mu_{s_e}\bar{N}_R^{1/2}\}_{II} \tag{9a}$$

The interesting quantity on the impermeable surface is the heat transfer for the case considered; but this will be related in the two systems by the equation

$$\{N_{Nu}/\bar{N}_R^{1/2}\}_I = \{N_{Nu}/\bar{N}_R^{1/2}\}_{II} = F(\bar{x}) \tag{9b}$$

Thus the similarity parameters are

$$N_1 \equiv (m_c/R_0\mu_{s_e})\bar{N}_R^{-(1/2)} \qquad N_2 \equiv N_{Nu}\bar{N}_R^{-(1/2)}$$

$\bar{h}_c$ and ϑ_w, so that

$$N_2 = N_2(N_1, \bar{h}_c, \vartheta_w, \bar{x})$$

Several comments concerning this result are pertinent:

(1) The assumptions pertaining to u_e^2/h_{s_e} and $Le = 1$ clearly do not alter the discussion; the terms containing the first parameter must be added to Eqs. (2) and (3). For a Lewis number not equal to unity a description similar to Eqs. (7a) and (7b) for the Schmidt number in terms of a function of K must be introduced. On the impermeable section, since $K_\eta = 0$ at $\eta = 0$, the heat transfer at the wall is proportional to g_η and thus is given by the similarity parameter for heat transfer N_2.

(2) The sensitivity of the heat transfer on the impermeable surface in terms of N_2 to the third similarity parameter ϑ_w may not be significant provided ϑ_w is below a certain value. This would be analogous to the insensitivity of the hypersonic heat transfer in terms of N_2 to the wall-to-stagnation temperature ratio, provided this ratio is less than approximately 0.4 (cf. reference 15, for example).

(3) If there is considered the second limiting specification of the boundary condition at $\eta = 0$ for $\bar{s} > \bar{s}_i$, namely, $g_\eta = 0$, the solution of the equations would yield T_w and g_w as functions of $\bar{x}$. In this case the temperature ratio represented by $\vartheta_w = \vartheta_{aw} = W \equiv W(\bar{x})$ would be the interesting similarity parameter, where the subscript aw denotes an adiabatic surface. There results

$$W = W(N_1, \bar{h}_c, \bar{x})$$

* In the constant "a" the stagnation temperature T_{s_e} appears to the power $n_3 - n_4$. Thus it is assumed here that $n_3 - n_4 \ll 1$.

† This requirement is satisfied quite accurately if an effective isentropic exponent $\bar{\gamma}$ can be introduced such that $1.2 < \bar{\gamma} < 1.4$ and if the pressure distribution given by $\bar{p} \equiv p/p_{s_e} = \bar{p}(\bar{x})$ is the same for the two bodies.

The distribution of adiabatic wall temperature is thus seen to depend on N_1 and h_c.

(4) The mass flow similarity parameter $N_1 \equiv m_c \div R_0 \mu_{s_e} \bar{N}_R^{1/2}$ can also be deduced from the representation of the effect of mass transfer on stagnation point heat transfer shown by Lees[16] from the analysis of Reshotko and Cohen.[6] This representation results in the variation of the ratio of heat transfer with mass injection to that without injection (C_H/C_{H_0}) with the quantity

$$B \equiv (\rho v)_w/(\rho_e u_e)C_{H_0} \tag{10a}$$

But by the definition of C_{H_0} for nonreactive mixtures,

$$B \sim (\rho v)_w c_{p_{s_e}} R_0/k_{s_e} \bar{N}_R^{1/2} \tag{10b}$$

or

$$B \sim m_c/R_0 \mu_{s_e} \bar{N}_R^{1/2} \tag{10c}$$

Thus B is proportional to the parameter N_1.

In the experimental research to be described below there were obtained two sets of data corresponding to the two limiting specifications of the boundary conditions at $\eta = 0$. Thus, one set of data is presented in terms of $N_2 = N_2(N_1, \bar{h}_c, \vartheta_w, \bar{x})$ for a given wall temperature, while the second set of data is presented in terms of $W = W(N_1, \bar{h}_c, \bar{x})$. The Reynolds number $\bar{N}_R$, the enthalpy ratio $\bar{h}_c$, and the wall temperature ratio ϑ_w were essentially constant for all data so that a critical examination of the similarity parameters is not possible in terms of these data.

The practical evaluation of a mass transfer system—i.e., a particular mode of injection and a particular cooling fluid—is frequently carried out in terms of an effective enthalpy of the coolant. For the system being considered here, such an effective enthalpy, denoted by Q, can be defined as

$$Q \equiv \frac{1}{m_c} \int_0^{x_T} (q_{m_c=0} - q_{m_c}) dA \tag{11}$$

It is of interest to note that the integrand in Eq. (11) represents the heat reduction due to the injection, and thus can be considered a measure of heat "blockage" and of heat absorption.

The parameter Q can now be evaluated for the two limiting cases, giving the heats of absorption for the isothermal wall and for the adiabatic wall; these are denoted by $\bar{Q}$, and $\tilde{Q}$, respectively.

For consistency, the heat transfer rates with and without mass injection must be evaluated at the same local wall temperature (or enthalpy) if the heat of absorption is to be a measure of coolant efficiency. As a result,

$$\bar{Q} \equiv \frac{1}{m_c} \int_0^{x_T} (q_{m_c=0} - q_{m_c})_{T_w=\text{const.}}\, dA \tag{12a}$$

$$\tilde{Q} \equiv \frac{1}{m_c} \int_0^{x_T} q_{m_c=0} \left[\frac{(h_{aw})_{m_c=0} - (h_{aw})_{m_c}}{(h_{aw} - h_w)_{m_c=0}} \right] dA \tag{12b}$$

since for $\tilde{Q}$, by definition $q_{m_c} = 0$. In Eq. (12b) $q_{m_c=0}$ is taken to be the heat transfer corresponding to the enthalpy difference $(h_{aw} - h_w)_{m_c=0}$; multiplication by the quantity within the brackets in the integrand leads to a rough correction for the heat transfer which would prevail with $N_1 = 0$ and with the surface temperature distribution given by adiabatic conditions with coolant flow.

In terms of the similarity parameters and nondimensionalizing quantities introduced above, $\bar{Q}$ and $\tilde{Q}$ become

$$\bar{Q} = \frac{2\pi h_{s_e}}{N_1 \sigma_{s_e}} (1 - \vartheta_w) \int_0^{\bar{x}_T} [(N_2)_{N_1=0} - N_2] \bar{r} d\bar{x} \tag{13a}$$

$$\tilde{Q} = \frac{2\pi h_{s_e}}{N_1 \sigma_{s_e}} \int_0^{\bar{x}_T} (N_2)_{N_1=0} (W_{m_c=0} - W_{m_c})\, K^{-1} \bar{r} d\bar{x} \tag{13b}$$

where $K \equiv 1 - (1 - \sigma_{s_e}^{1/2})(1 - \bar{T})(1 - \vartheta_w)^{-1}$, ($\bar{T} \equiv T_e/T_{s_e}$). It will be noted that the factor K is introduced to change the enthalpy difference arising in Eq. (12b) to that used in the parameter N_2. Eqs. (13a) and (13b) indicate that $Q \sim h_{s_e} F(N_1, \bar{h}_c)$ and therefore permit extrapolation of test results for Q to other flow conditions, provided that laminar flow prevails.

The persistence factor introduced in reference 1 also provides a measure of coolant effectiveness; it is defined as

$$\alpha \equiv (A_T/A_P)(Q_0/Q_T) \tag{14a}$$

It will be observed that the more persistent the downstream effect of the coolant, the larger Q_T will be and thus the smaller α will be.

The effective enthalpy in the porous region Q_0 and the total effective enthalpy Q_T can correspond to either $\bar{Q}$ or $\tilde{Q}$ defined above; in reference 1 $\tilde{Q}$ was used and, therefore, the experimental data presented here were interpreted in terms of $Q_T = \tilde{Q}$ and of Q_0 given by Eq. (13b) with $\bar{x}_T$ replaced by $\bar{x}_t$. The expression for α in terms of the similarity variables presented here can be simplified if several approximations are employed; over the region $0 \leq \bar{x} \leq \bar{x}_t$ the parameters $(N_2)_{N_1=0}$ and W are assumed constant, and $\bar{r} \simeq \bar{x}$. Then

$$\alpha = \frac{A_T}{2\pi R_0^2} \frac{[(N_2)_{N_1=0}(1 - W)]_{\bar{x} \to 0}}{\displaystyle\int_0^{\bar{x}_T} (N_2)_{N_1=0} (W_{m_c=0} - W_{m_c}) K^{-1} \bar{r} d\bar{x}} \tag{14b}$$

Thus, for a given geometry, $\alpha = \alpha(N_1, \bar{h}_c)$; for N_1 large so that $W_{m_c} \ll W_{m_c=0}$, α should become independent of N_1.

(3) Model Design, Test Procedures, and Test Conditions

A series of tests on the influence of stagnation-point coolant injection was carried out at a Mach number of 6.0 in the PIBAL hypersonic wind tunnel, which is described in reference 17. The model used in the tests is shown schematically in Fig. 1. Details of the model construction and instrumentation are shown in Fig. 2. The injection region, made from porous stainless steel with a porosity of 50 per cent, subtended at the surface a total angle of 19.1°; thus $\bar{x}_t = 0.167$. Considerable

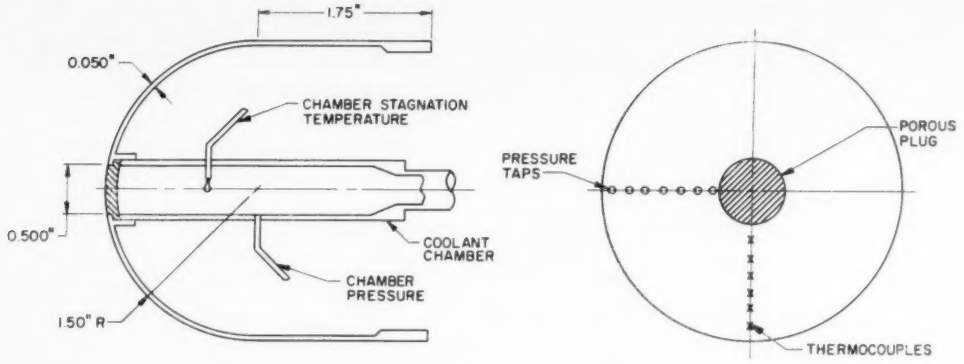

$\bar{x}$	0.333	0.500	0.667	0.833	1.000	1.167	1.333	1.500	1.667	2.000	2.333
THERMOCOUPLE #	1	2	3	4	5	6	7	8	9	10	11
PRESSURE TAP #	1	2	3	–	4	5	6	7	8	9	10

FIG. 2. Details of model design and instrumentation.

care was devoted to minimizing any step in the surface at the junction of the porous plug and the impermeable surface. The coolant gas was introduced into a stagnation chamber inside the model. A pressure tap on the coolant chamber and a thermocouple within the chamber permitted measurement of the coolant pressure and temperature. The model was constructed of stainless steel with a wall thickness of 0.050 in. and was instrumented with surface pressure taps and thermocouples located as shown in Fig. 2.

The pressures were measured during the test on transducers and recorded on single-channel recording potentiometers. The pitot pressure and stagnation temperatures were measured on probes mounted on the model support and similarly recorded. The model thermocouples were also recorded on single-channel recording potentiometers.

A transient technique was used to determine the heat transfer with an essentially uniform model temperature. The test procedure involved setting a coolant flow, activating all recording potentiometers and then establishing the hypersonic flow by withdrawing the valve in the throat of the nozzle. The initial rate of temperature rise can be directly interpreted in terms of the local rate of heat transfer (cf., for example, reference 18). Since the initial temperature is uniform, no corrections for surface conduction are required and the heat transfer corresponds to isothermal conditions.

For the larger rates of coolant flow, the adiabatic surface temperatures were sufficiently low to be tolerable to the model. Therefore, the tests at these larger rates were continued until essentially timewise-steady surface temperatures were recorded.

The coolant mass flow was determined from the initial temperature of the injected gas within the coolant chamber and from the pressure drop across the porous plug. The plug was calibrated over the entire range of coolant flows outside the wind tunnel by a flow meter.* For even the smallest rates of injection the mass flow is so large relative to that required for reducing the heat transfer to the porous plate itself, that the temperature rise of the porous plate during testing is negligible. Thus calibration external to the tunnel is considered satisfactory.

An attempt was made to measure the temperature of the exposed surface of the porous plug by means of a bare-wire thermocouple inserted through the impermeable sections of the model and spot-welded to the

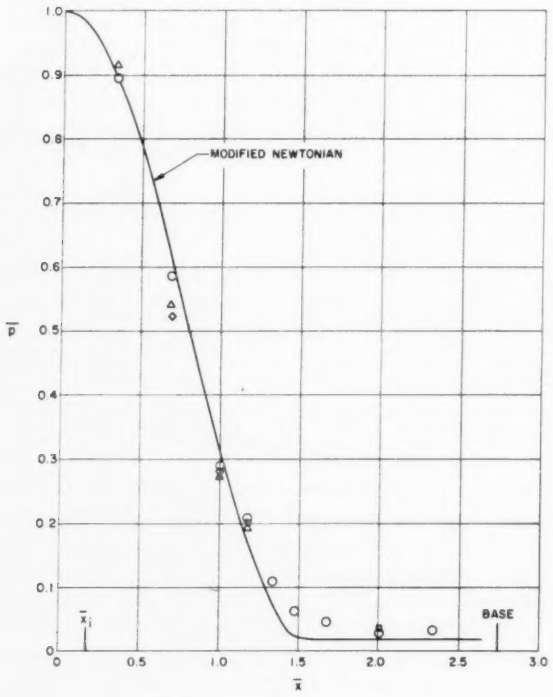

FIG. 3. Pressure distribution.

* It was found that the mass flow (lbs./sec.) could be correlated by the relation $m_c = 0.205 \times 10^{-4} m^{0.526} [p_c^2 - p_e^2]^{0.526}$, where m = the coolant molecular weight, p_c = chamber pressure (psia), and p_e = model stagnation pressure (more generally the pressure on the low-pressure side of porous material).

porous material. This thermocouple was located off the centerline and at an azimuthal position so as not to disturb the flow over the pressure taps or thermocouples. This attempt proved to be unsuccessful since conduction along the thermocouple wires was excessive and the thermocouple reading, therefore, was erroneous.

All tests were carried out at stagnation conditions of approximately 600 psia and from 1,500 to 1,700°R. The gas temperature in the coolant chamber was approximately 530°R. for all coolants; thus, the range of values of $\bar{h}_c$ for each gas was as follows:

Helium	$1.58 \leq \bar{h}_c \leq 1.70$
Nitrogen	$0.32 \leq \bar{h}_c \leq 0.35$
Argon	$0.16 \leq \bar{h}_c \leq 0.18$
Krypton	$\bar{h}_c \simeq 0.08$

With the reference length of the model taken to be the hemispherical radius $R_0 = 1.5$ in., the tests were performed in the Reynolds number range $0.22 < \tilde{N}_R(10^{-6}) < 0.29$. The initial model temperature was approximately 550 to 600°R., so that the heat transfer data with isothermal surface temperature correspond to $0.33 < \vartheta_w < 0.4$.

The roughness on the impermeable surface of the model was initially uniform and equal to approximately 5 to 10 microinches r.m.s., as measured on a Brush Surface Indicator. At the completion of the test program of over twenty tests, the roughness was approximately 175 microinches in the stagnation region and 100 microinches near the junction of the hemisphere-cylinder. Thus, there was a progressive degradation of surface finish as the test program proceeded.

The accuracy of the measurements is estimated to be as follows: for pressures in the neighborhood of the stagnation value (approximately 18 psia), the error in overall pressure measurement is estimated to be $\Delta p = \pm 0.10$ psia; the coolant mass flow is estimated to be accurate within ± 5 per cent. The temperatures read by thermocouples and recorded on strip-chart potentiometers are estimated to be in error by ± 5°R. Because of the large number of parameters contributing to the heat transfer rate, it is possible to make on the basis of consistency and reproducibility only a rough estimate of the overall accuracy of the Nusselt number, N_{Nu}; this is believed to be ± 10 per cent.

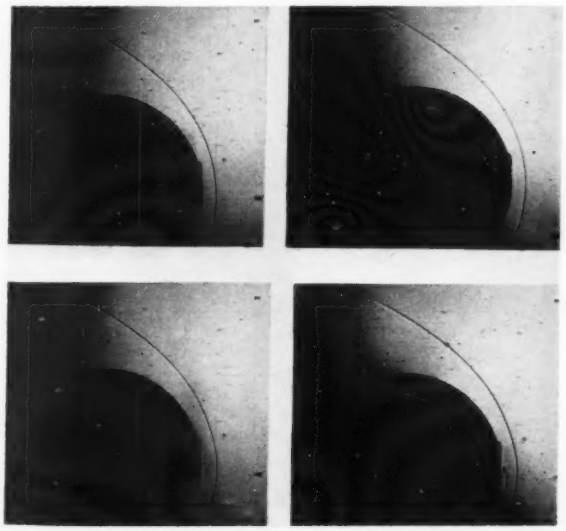

FIG. 4. Shadowgraphs for various injection rates: (*top left*) $N_1 = 0$; (*top right*) helium, $N_1 = 1.64$; (*bottom left*) nitrogen, $N_1 = 9.53$; (*bottom right*) argon, $N_1 = 11.73$.

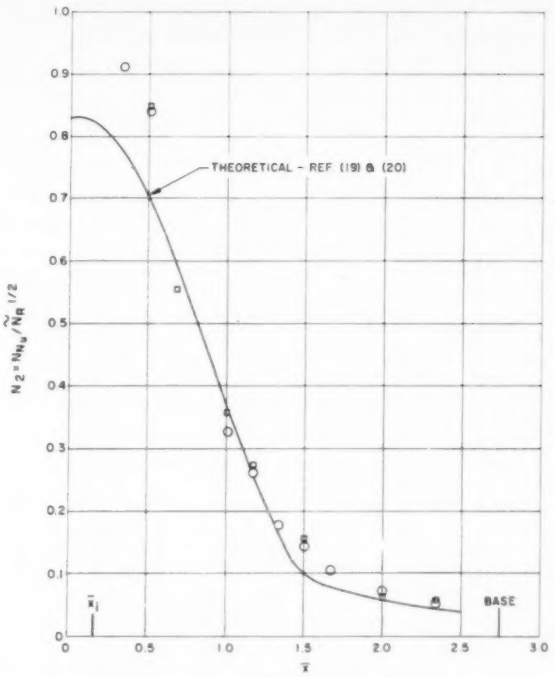

FIG. 5. Comparison of theoretical and experimental heat transfer with zero injection.

(4) Presentation and Discussion of Experimental Results

The experimental pressure distribution is shown in Fig. 3 along with the modified Newtonian pressure distribution usually used for comparison purposes. Within the experimental error the pressure distribution was unaltered by the coolant flow even for the highest rates of injection. However, for the highest injection rates of nitrogen ($N_1 = 9.53$) and argon ($N_1 = 11.73$), the shadowgraph pictures indicated that the shock stand-off distance was slightly increased; d/R_0, the ratio of stand-off distance to the radius of the hemisphere, was found to be $\simeq 0.14$ for all coolant flows except those cited above; for these $d/R \simeq 0.16$. In Fig. 4 are presented four typical shadowgraph pictures,*

* The protuberance from the model above its centerline, seen in these pictures, is the external thermocouple with which an attempt was made to determine the surface temperature of the porous plug. Attention is also invited to the line which may be faintly seen in the flow ahead of the porous region; subsequent analysis of the stagnation-point boundary layer with large rates of injection has indicated that such a boundary layer consists of an isothermal layer close to the wall and a region of rapidly changing temperature and therefore of density at the outer edge of the boundary layer. It is this outer region which appears in the shadowgraphs.

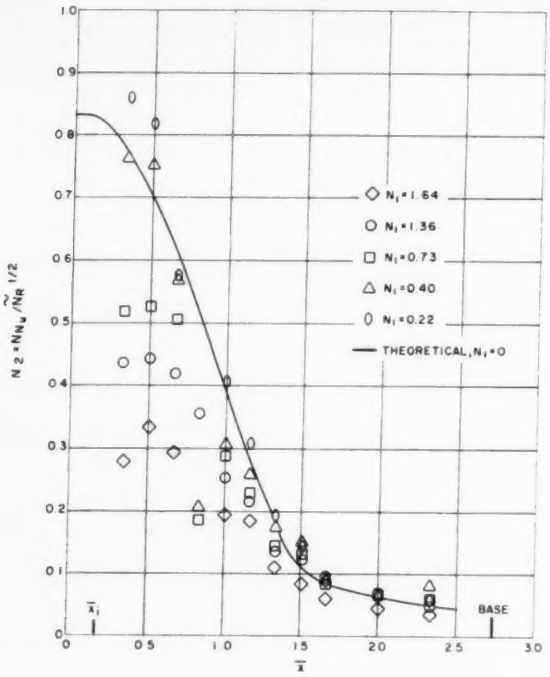

(a) Helium

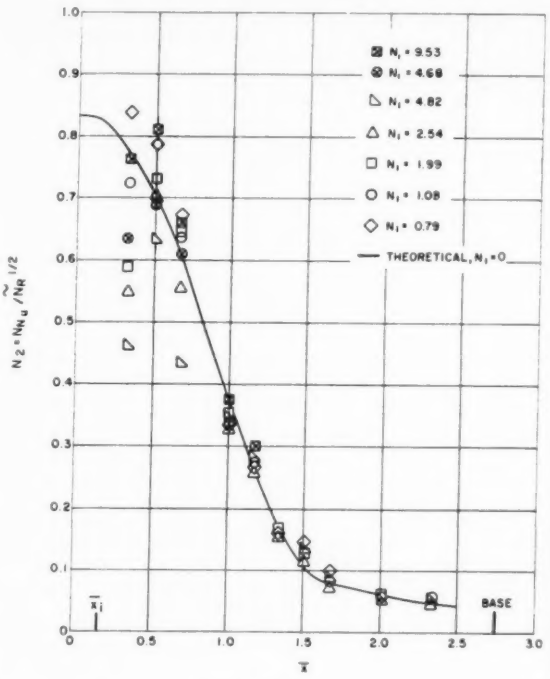

(b) Nitrogen

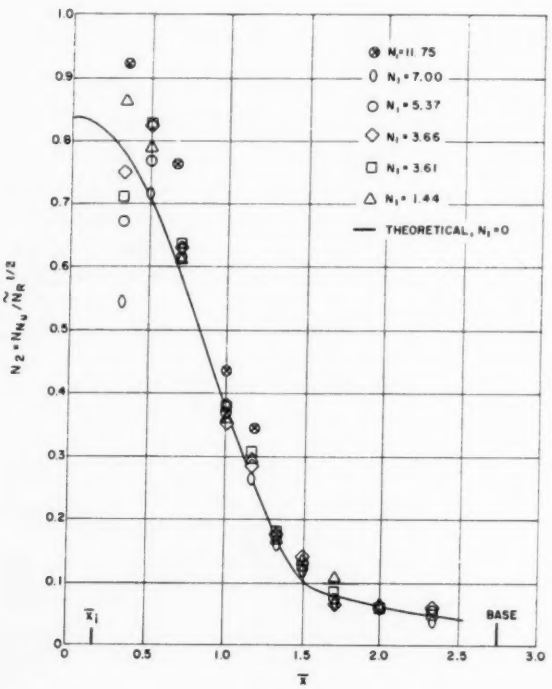

(c) Argon

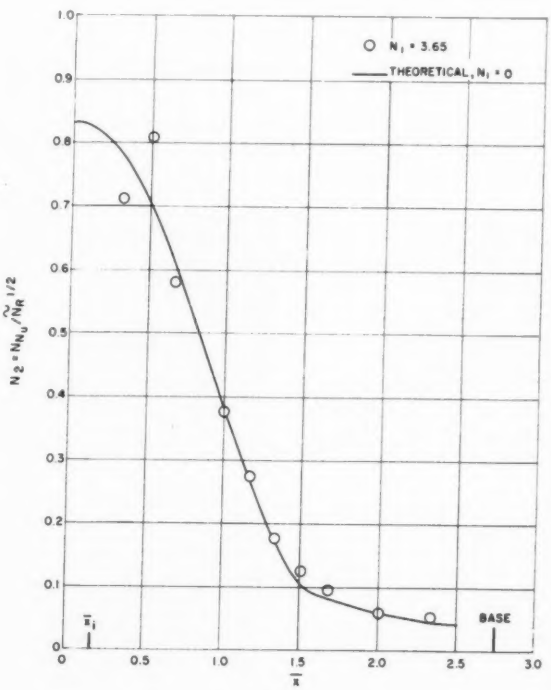

(d) Krypton

FIG. 6. Distribution of heat transfer for various values of the injection-rate parameter.

one with zero injection and the other three with the highest rates of helium, nitrogen, and argon injection. Careful examination of the last two are required to indicate the change in the position of the bow shock. It is concluded from these results that the experimental conditions correspond closely to the flow model discussed in connection with Fig. 1.

The heat transfer without coolant injection ($N_1 = 0$) is compared with laminar theory in Fig. 5. The theoretical prediction is based on the heat transfer distribution of Lees[19] and the stagnation-point value of Fay and Riddell.[20] In evaluating the external flow properties, an effective isentropic exponent equal to 1.32 was assumed along with the experimentally determined pressure distribution. It will be noted that the agreement between theory and experiment is good except in the stagnation region ($x < 0.6$) where the experimental values are approximately 15 per cent above the theoretical prediction. This may be associated with the roughness of the porous surface or with the discontinuity between the porous plug and the impermeable surface.

In Figs. 6a–6d the distributions of $N_2 \equiv N_{Nu}\tilde{N}_R^{-(1/2)}$ with x for various values of the injection parameter N_1 are presented for helium, nitrogen, argon, and krypton. Also shown on each graph for orientation is the theoretical, zero-injection curve. All coolants exhibit the same general behavior; at low rates of injection the heat transfer is essentially that without injection except in the immediate region of the porous plug ($\bar{x} - \bar{x}_1$); as the injection rate increases, the region of influence in

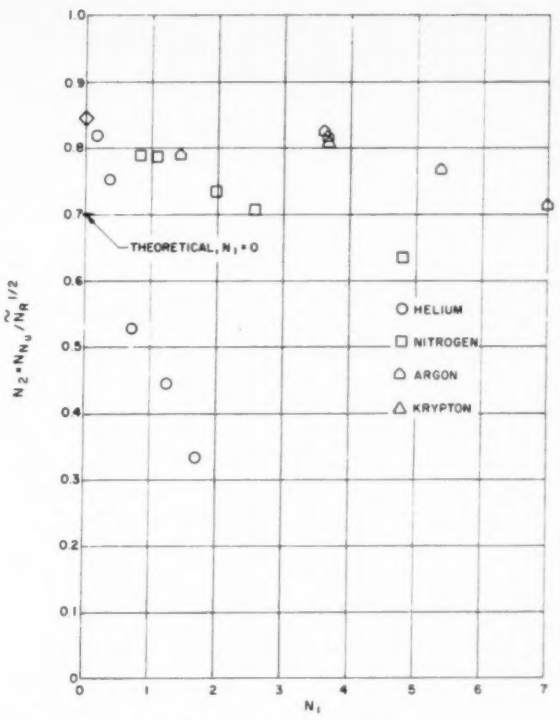

FIG. 7 (b). Variation of heat transfer with injection-rate parameter. $\bar{x} = 2.333$.

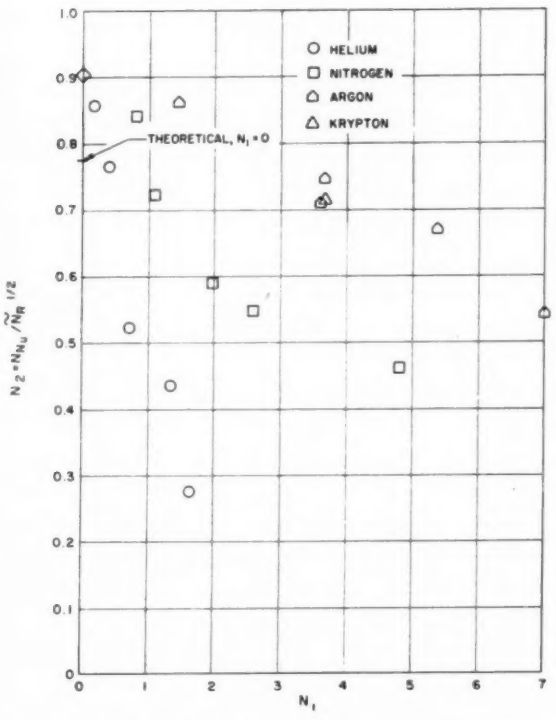

FIG. 7 (a). Variation of heat transfer with injection-rate parameter. $\bar{x} = 0.500$.

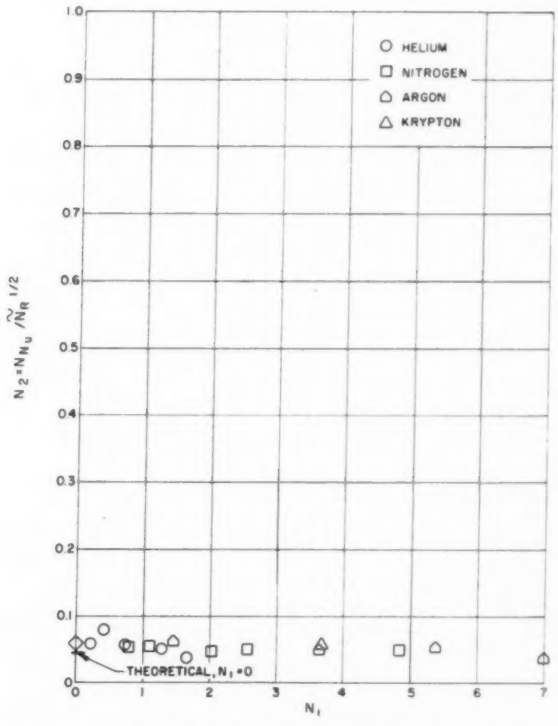

FIG. 7 (c). Variation of heat transfer with injection-rate parameter. $\bar{x} = 0.333$.

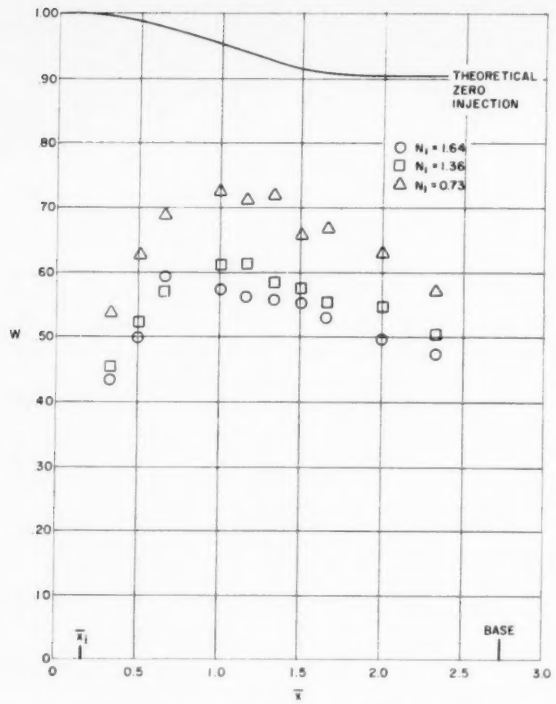

FIG. 8 (a). Distribution of adiabatic surface temperature ratio for various values of the injection-rate parameter. Helium.

the downstream direction progressively increases, except for three tests at high injection rates (nitrogen at $N_1 = 4.68$ and 9.53, and argon at $N_1 = 11.73$). The heat transfer in all cases appears to correspond to laminar flow, inasmuch as the laminar values with no injection are approached for large $\bar{x}(\bar{x} > 2)$.

The three tests for which the region of influence did not increase monotonically as the coolant flow increased were the last three of the test series; thus they correspond to maximum surface roughness as well as large weight flow. It appears that this combination results in an increase in heat transfer without producing transition, and thus that these data should be disregarded in terms of boundary layer behavior on smooth surfaces. Therefore these data are not considered in the subsequent analysis.

From Fig. 6a it will be seen that helium injection at a rate corresponding to $N_1 = 1.64$ reduces the peak heating rate by a factor of roughly 2.7. Similarly, from Fig. 6b nitrogen injection corresponding to $N_1 = 4.82$ is seen to reduce the peak heating rate by a factor of two. The highest injection rates of argon and krypton are seen to be less effective in reducing peak heating values.

The data of Fig. 6a–6d can be cross-plotted to yield the variation of $N_2 \equiv \bar{N}_{Nu}\bar{N}_R^{-(1/2)}$ with N_1 at the thermocouple stations. This has been done for representative values of $\bar{x}$ and shown in Figs. 7a–7c. For small values of $\bar{x}$ ($\bar{x} = 0.333$, 0.500) the variation of N_2 with N_1 for the various gases is in accordance with the

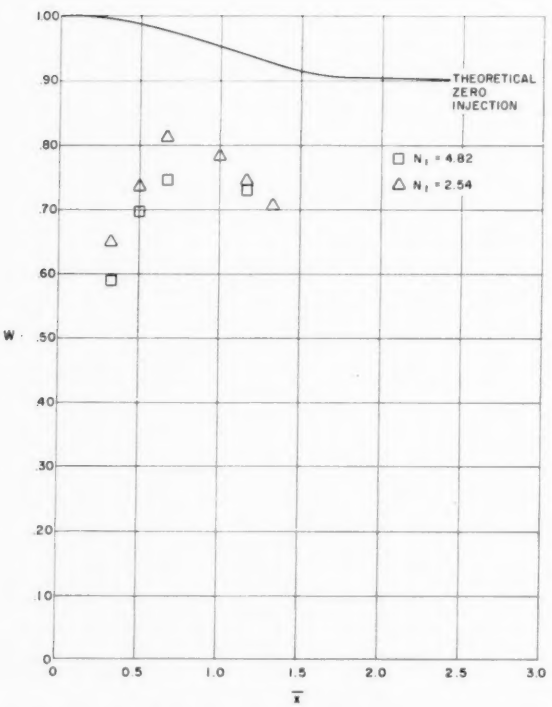

FIG. 8 (b). Distribution of adiabatic surface temperature ratio for various values of the injection-rate parameter. Nitrogen.

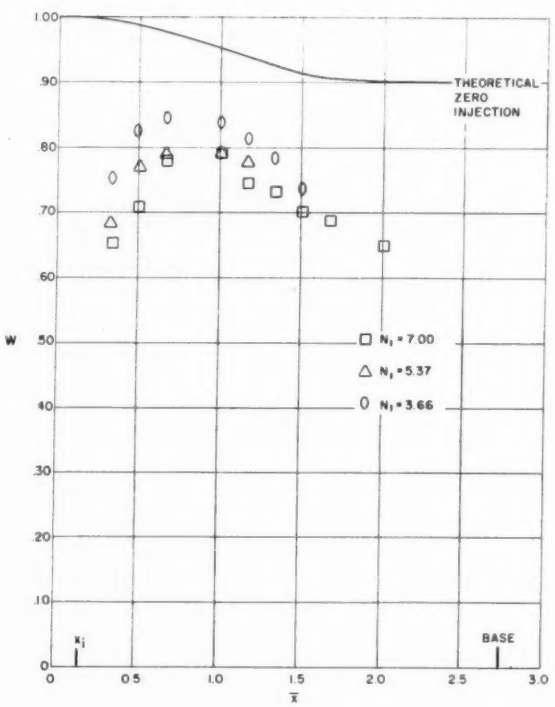

FIG. 8 (c). Distribution of adiabatic surface temperature ratio for various values of the injection-rate parameter. Argon.

theoretical analysis of the stagnation point heat transfer with injection; the heat transfer decreases as the injection rate increases, the rate of decrease being more rapid as the molecular weight of the injected gas decreases. Thus, for a given mass flow, corresponding, for example, to $N_1 = 1.5$, helium is roughly twice as efficient as nitrogen in reducing heat transfer. At the more downstream stations corresponding to larger values of $\bar{x}$, the variation of heat transfer with rate of injection decreases until for $\bar{x} > 1.500$, it is constant within the experimental accuracy. The influence of helium is seen to persist to larger values of $\bar{x}$ than that of the gases of greater molecular weight.

In Figs. 8a–8c there are given the experimentally determined distributions of W (the adiabatic wall temperature divided by the stagnation temperature) for various values of N_1 with helium, nitrogen, and argon. To give an indication of the effect of mass transfer, there is shown in these figures the distribution of W without mass transfer; this has been estimated according to the relation

$$(W)_{N_1=0} \simeq 1 - (1 - \sigma_{s_e}^{1/2})(1 - \bar{T}) \qquad (15)$$

where $\bar{T}$ is the ratio of static temperature external to the boundary layer to the stagnation temperature. In evaluating $\bar{T}$ an effective isentropic exponent of 1.32 was used in connection with the experimentally determined pressure distribution. Eq. (15) applies for the flow with a recovery factor of $\sigma_{s_e}^{1/2}$ and with constant specific heats.

Examination of Figs. 8a–8c indicates that the effect of mass transfer on the adiabatic wall temperature persists further downstream than the effect on heat transfer with an isothermal wall. The adiabatic temperature increases from the end of injection ($\bar{x} = \bar{x}_l$) to a maximum in the neighborhood of the sonic point and then decreases slightly over the remainder of the model. It should be noted that surface conduction and radiation from the model can alter somewhat the measured adiabatic surface temperatures. However, the greater influence of mass transfer on adiabatic surface temperatures is in accord with the results of references 9 and 10. Indeed, the influence of localized mass transfer in the region far from the region of injection has been analyzed in reference 9 by assuming that a heat transfer coefficient without mass transfer applies to a temperature potential representing the difference between the adiabatic surface temperature with mass transfer and the desired surface temperature.

From Fig. 8a it will be noted that helium injection at a rate corresponding to $N_1 = 1.64$ results in a peak adiabatic surface temperature equal to 57 per cent of stagnation temperature. From Figs. 8b and 8c it will be seen that considerably larger rates of nitrogen and argon injection are required to obtain peak adiabatic temperatures of 75 to 80 per cent of stagnation. The insensitivity of these peak temperatures for nitrogen and argon to increasing injection rates indicates

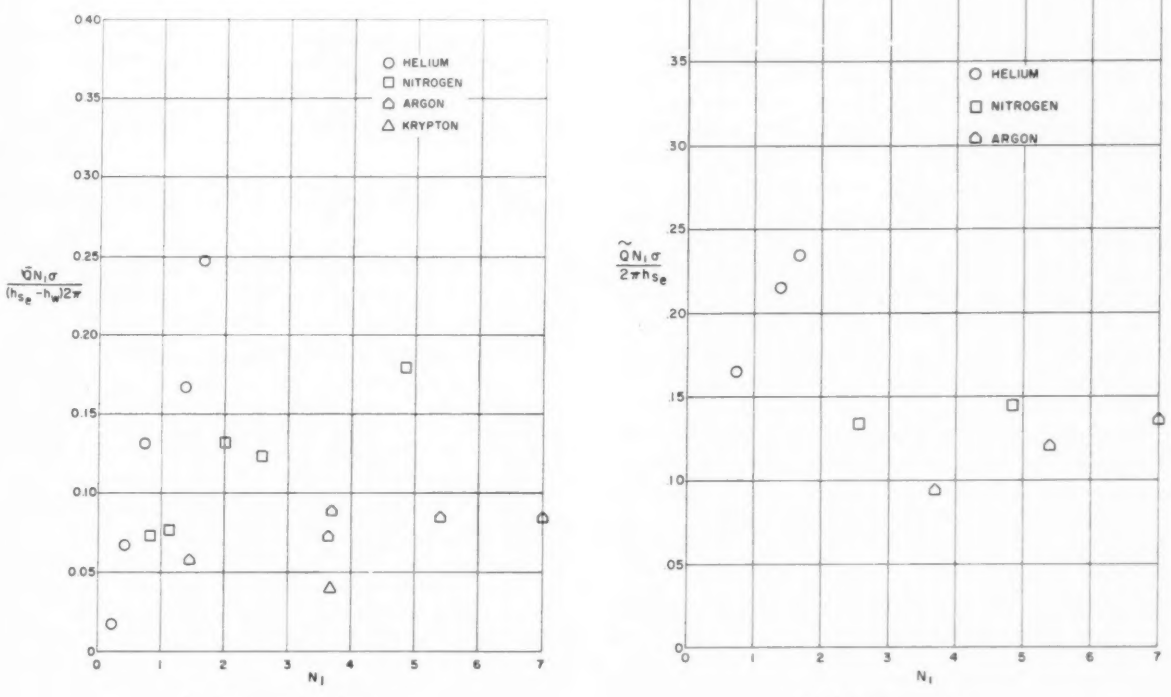

(a) Isothermal surface (b) Adiabatic surface

FIG. 9. Variation of effective enthalpy parameter with injection-rate parameter.

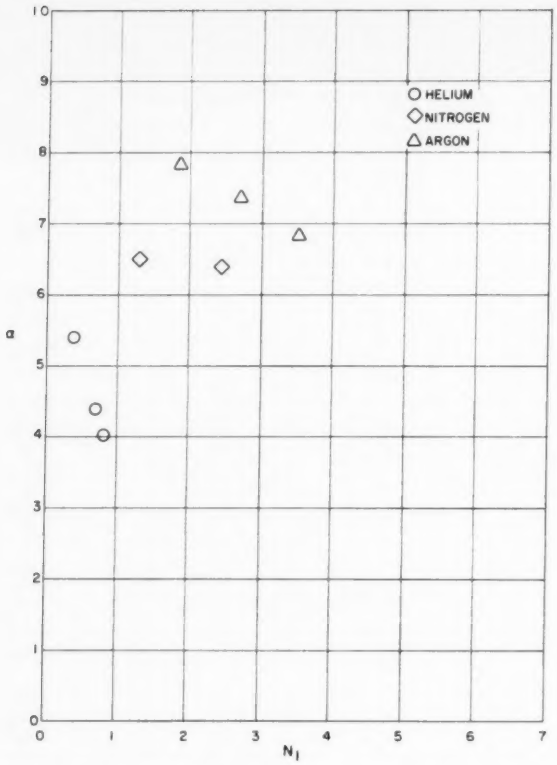

FIG. 10. Variation of persistence factor with injection rate parameter.

that larger porous regions (larger values of $\bar{x}_t$) should probably be considered for these coolant gases.

In Figs. 9a–9b the effective enthalpies of the coolants in terms of $\bar{Q}$ and $\tilde{Q}$ in nondimensionalized form are presented as functions of N_1. The same general behavior is exhibited by both sets of curves; the product QN_1 appears to increase initially with N_1 in such a way that Q varies only slightly with N_1. The results for argon indicate, however, that at some value of N_1, the product QN_1 becomes almost constant with N_1, implying that $Q \sim N_1^{-1}$. Comparison of the effective enthalpies for the various gases clearly indicates the superiority of helium in terms of mass flow.

In Fig. 10, the persistence factor α given by Eq. (14b) is presented for helium, nitrogen and argon as a function of the injection rate parameter N_1.* The results for helium and argon clearly indicate a decrease in α (increasing effectiveness) with increasing N_1; the results for nitrogen indicate an almost constant value. It is not possible from these data to confirm the value of $\alpha = 10$ used in reference 1 for helium; the value of N_1 used there is less than the lowest value for which data on α were obtained.

The experimental data presented here have verified the generally accepted superiority of helium as a coolant to the other gases employed in this test series. The relative efficacy of coolant is usually evaluated on the basis of mass flow. However, there may be applications of mass transfer systems in which volume requirements on coolant storage are more stringent than mass requirements.† It is, therefore, of interest to compare the efficacy of the gases considered here in terms of volume time rate of coolant flow.

Neither the temperature of the exposed surface of the porous plug nor the concentration of foreign gas there were obtained in the tests. Thus, a direct determination of volumetric flow rate, independent of the particular porous plug used in these tests, cannot be made. However, an indication thereof can be obtained from an estimate of the injection velocity (v_w) at the exposed surface of the porous plug. To permit a comparison of the relative efficacy of the coolants, there is formed the ratio of the injection velocity to that of nitrogen for the same heat transfer rate in terms of N_2. Thus, Figs. 7a–7c can be used to find the values of N_1 for each coolant yielding the same values for N_2. In computing the ratio $v_w/(v_w)_{N_2}$ the injection rates are assumed sufficiently high that the concentration of foreign gas at the surface of the porous plug is 100 per cent‡ and the exposed temperatures

* In evaluating $(W)_{\bar{x}\to 0}$ in Eq. (14b) it was considered sufficiently accurate to use the experimentally determined values of surface temperature on the porous plug. Although these were known to be high by 50 to 100°R., little error is involved in the calculation of $(1 - W)_{\bar{x}\to 0}$.

† This consideration was suggested to the authors by Professor Antonio Ferri.

‡ The smallest value of N_1 used in these tests corresponds to a value of $-f(0)$ in reference 1 greater than unity; clearly, $K_w \simeq 1$.

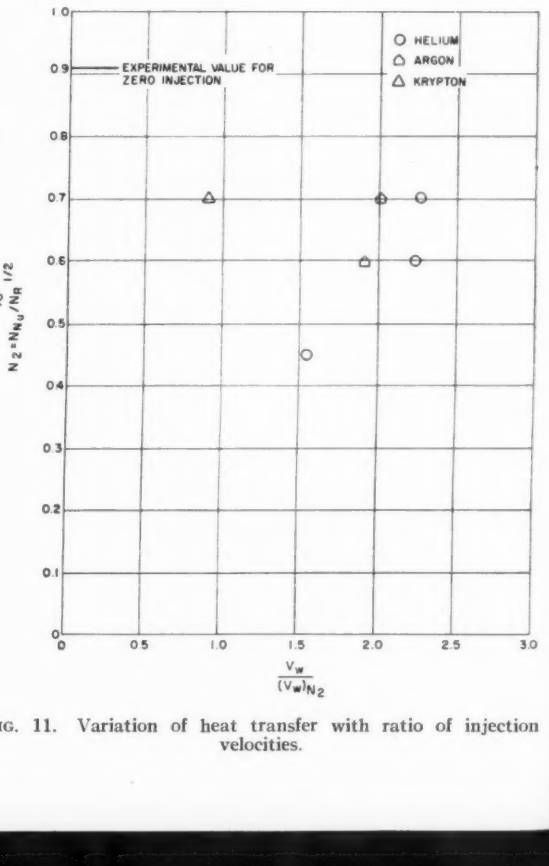

FIG. 11. Variation of heat transfer with ratio of injection velocities.

are assumed the same for all coolants. The results so obtained for $\bar{x} = 0.333$ are shown in Fig. 11. It may be seen that the volumetric injection rate for helium is greater than that for nitrogen for relatively small reductions in heat transfer from the zero injection value. However, for larger rates of cooling the volumetric helium flow approaches that of nitrogen. The same general behavior would be expected at all values of $\bar{x}$. It appears from these data that in terms of volumetric injection rate and under some conditions, gases other than helium may be the most efficient.

In closing this discussion of experimental results, several limitations of the data are emphasized. First, the data and similarity parameters presented here should be applied only when laminar flow exists. To establish the influence of mass transfer on boundary layer transition, tests at higher Reynolds numbers and larger rates of injection (larger values of N_1) are required. Until such data are obtained, application of these data to Reynolds numbers greater than 0.3×10^6 should be provisional. Second, additional experimental data with $\bar{h}_e$ varied are required to evaluate the influence of this parameter on the heat transfer in terms of N_2 and on the adiabatic surface temperature in terms of W.*

(5) Conclusions

An investigation of the influence of stagnation-point mass transfer on the boundary layer on a blunt-nosed body in hypersonic flow has been carried out. In the experimental research the injected gases (helium, nitrogen, argon, and krypton) were introduced through a porous plug in the stagnation region. The body was a hemisphere-cylinder combination and was tested in a Mach number 6.0 stream. The distributions of heat transfer with an isothermal surface and of the adiabatic surface temperature were measured at various rates of injection.

On the assumption that the mass transfer does not alter the inviscid flow, the influence of the coolant can be considered in terms of an alteration of the boundary layer over the downstream, impermeable section. For laminar flow the describing differential equations are considered in order to obtain the similarity parameters for use in data correlation and in the evaluation of coolant efficiency.

The experimental data indicated that the mass transfer did not alter significantly the inviscid flow. At the highest rates of coolant injection the pressure distribution was unaltered within experimental accuracy, but the shock stand-off distance was increased by approximately 15 per cent. The heat transfer with an isothermal surface was found to decrease with increasing coolant flow. Near the aft end of the model no significant alteration in heat transfer was obtained for even the highest rates of coolant flow. The experimental heat transfer rates at the aft end were found to be in good agreement with theoretical predictions of laminar heat transfer; as a result it is concluded that the boundary layer was completely laminar and that no transition occurred. With a relatively small rate of helium injection peak heating was reduced by a factor of roughly 2.7.

The downstream influence of the mass transfer on the adiabatic wall temperature was found to be greater than that on the heat transfer with an isothermal surface. With helium, for example, the adiabatic surface temperature was reduced to 57 per cent of the stagnation temperature, the peak value occurring in the neighborhood of the sonic point.

A comparison of the efficacy of the four coolants in terms of mass rate of coolant flow indicates that helium is superior to the other gases. At a given coolant mass flow the effective enthalpy of helium is twice as large as that of nitrogen and a greater multiple of that of argon and krypton. However, the data indicate that on the basis of volumetric flow rates, a gas of greater molecular weight may, under some circumstances, be superior to helium.

* In the course of the review of this paper prior to publication an anonymous reviewer suggested that there be formed the ratio of the heat reduction represented by $\bar{Q}$ to the coolant mass flow times the difference in enthalpy of the coolant at the free-stream stagnation temperature and at the coolant temperature prior to injection. The reviewer stated: "If this ratio is nearly unity, the coolant is acting as a pure heat sink. If this ratio is significantly larger than unity, the coolant is also altering the temperature distribution across the boundary layer." Following this suggestion, the authors evaluated this ratio, denoted by Q', for all four gases over the available range of N_1. It was found that for nitrogen, argon, and krypton, Q' could be represented by a relatively smooth curve varying from approximately 0.75 at $N_1 \simeq 1$ to 0.2 at $N_1 \simeq 7$; the values of Q' for helium were approximately 0.23 ± 0.07 for all N_1. This result seems to imply that over the relatively extended, impermeable surface, the coolant does behave as a heat sink; the distribution of adiabatic surface temperature shown in Figs. 8a–8c also implies this behavior. It would be interesting to determine by additional measurements the influence of $\bar{h}_e$ and ϑ_w on this ratio Q'; if it were found that Q' is insensitive thereto, a convenient correlation parameter resulting in $Q' \simeq Q'(N_1)$ would be available.

References

[1] Hoshizaki, H., and Smith, H. J., *Axisymmetric Stagnation Point Mass-Transfer Cooling*, Lockheed Missiles and Space Division LMSD-48379, December 17, 1958.

[2] Hoshizaki, H., and Smith, H. J., *The Effect of Helium Injection at an Axially Symmetric Stagnation Point*, Journal of the Aero/Space Sciences, Vol. 26, No. 6, pp. 399–400, June, 1959

[3] Hayday, A. A., *Mass Transfer Cooling in a Laminar Boundary Layer in Steady Two-Dimensional Stagnation Flow*, University of Minnesota, Technical Note 19, AFOSR TN 58-337, AD 154 241, April, 1958.

[4] Morduchow, M., *On Heat Transfer Over a Sweat-Cooled Surface in Laminar Compressible Flow with a Pressure Gradient*, Journal of the Aeronautical Sciences, Vol. 19, No. 10, pp. 705–712, October, 1952.

[5] Brown, W. B., and Donoughe, P. L., *Tables of Exact Laminar-Boundary-Layer Solutions When the Wall is Porous and Fluid Properties are Variable*, NACA TN 2479, September, 1951.

[6] Reshotko, E., and Cohen, C. B., *Heat Transfer at the Forward Stagnation Point of Blunt Bodies*, NACA TN 3513, July, 1955.

[7] Scala, S. M., and Sutton, G. W., *Vectored Injection with a Hypersonic Laminar Boundary Layer*, Jet Propulsion, Vol. 27, No. 8, pp. 895–896, August, 1957.

[8] Rubesin, M. W., and Inouye, M., *A Theoretical Study of the Effect of Upstream Transpiration-Cooling on the Heat-Transfer and Skin-Friction Characteristics of a Compressible, Laminar Boundary Layer*, NACA TN 3969, May, 1957.

[9] Ferri, A., and Bloom, M. H., *Cooling by Jets Directed Upstream in Hypersonic Flow*, Polytechnic Institute of Brooklyn, WADC TN 56-382, AD 97232, (PIBAL Report No. 382), September, 1957.

[10] McMahon, H. M., *An Experimental Study of the Effect of Mass Injection at the Stagnation Point of a Blunt Body*, GALCIT Memorandum 42, May 1, 1958.

[11] Hayes, W. D., and Probstein, R. F., *Hypersonic Flow Theory*, pp. 288–291; Academic Press, 1959.

[12] Libby, P. A., and Pallone, A., *A Method for Analyzing the Insulating Properties of the Laminar Compressible Boundary Layer*, Journal of the Aeronautical Sciences, Vol. 21, No. 12, pp. 825–834, December, 1954.

[13] Cohen, C. B., and Reshotko, E., *Similar Solutions for the Compressible Laminar Boundary Layer with Heat Transfer and Pressure Gradient*, NACA TR 1293, 1956.

[14] Kramer, R. F., and Lieberstein, H. M., *Numerical Solution of the Boundary-Layer Equations without Similarity Assumptions*, Journal of the Aero/Space Sciences, Vol. 26, No. 8, pp. 508–514, August, 1959.

[15] Ferri, A., *A Review of Some Recent Developments in Hypersonic Flow*, Polytechnic Institute of Brooklyn, WADC TN 58-230, AD 155 822, (PIBAL Report No. 426), September, 1958.

[16] Lees, L., *Convective Heat Transfer with Mass Addition and Chemical Reactions*, Presented at the Third AGARD Colloquium on Combustion and Propulsion, Palermo, Sicily, March 17–21, 1958.

[17] Ferri, A., and Libby, P. A., *The Hypersonic Facility of the Polytechnic Institute of Brooklyn and its Application to Problems of Hypersonic Flight*, Polytechnic Institute of Brooklyn, WADC TN 57-369, AD 130 809, (PIBAL Report No. 392), August, 1957.

[18] Zakkay, V., *Pressure and Laminar Heat Transfer Results in Three-Dimensional Hypersonic Flow*, Polytechnic Institute of Brooklyn, WADC TN 58-182, AD 155 679, (PIBAL Report No. 447), September, 1958.

[19] Lees, L., *Laminar Heat Transfer Over Blunt-Nosed Bodies at Hypersonic Flow Speeds*, Jet Propulsion, Vol. 26, No. 4, April, 1956.

[20] Fay, J. A., and Riddell, F. R., *Theory of Stagnation Point Heat Transfer in Dissociated Air*, Journal of the Aeronautical Sciences, Vol. 25, No. 2, pp. 73–85, February, 1958.

✦ ✦ ✦

A Stiffness Matrix (*Continued from page 42*)

[6] MacNeal, R. H., *The Solution of Elastic Plate Problems by Electrical Analogies*, J. Appl. Mech., pp. 59–67, March, 1951.

[7] MacNeal, R. H., and Benscoter, S. U., *Analysis of Multicell Delta Wings on Cal-Tech Analog Computer*, NACA TN 3114, December, 1953.

[8] Olsson, R. G., *Biegung der Rechteckplatte bei linear veränderlicher Biegungssteifigkeit*, Ingenieur-Archiv, Vol. 5, p. 363, 1934.

[9] Reissner, M. E., *Remark on the Theory of Bending of Plates of Variable Thickness*, J. Math. and Phys., Vol. 16, 1937.

[10] Reissner, E., and Stein, M., *Torsion and Transverse Bending of Cantilever Plates*, NACA TR 2369, June, 1951.

[11] Stein, M., and Sanders, L., *A Method for Deflection Analysis of Thin Low-Aspect-Ratio Wings*, NACA TN 3640, June, 1956.

[12] Timoshenko, S., *Theory of Plates and Shells*, McGraw-Hill Book Company, Inc., New York, 1940.

[13] Turing, A. M., *Rounding-Off Errors in Matrix Processes*, Quart. J. Mech. and Phys., September, 1948.

[14] Turner, M. J., Clough, R. W., Martin, H. C., and Topp, L. J., *Stiffness and Deflection Analysis of Complex Structures*, Journal of the Aeronautical Sciences, Vol. 23, No. 9, pp. 805–823, September, 1956.

[15] Williams, D., *A General Method (Depending on the Aid of a Digital Computer) for Deriving the Structural Influence Coefficients of Aeroplane Wings*, RAE Rept. Structures 168, November, 1954.

[16] Zender, G. W., *Comparison of Theoretical Stresses and Deflections of Multicell Wings with Experimental Results Obtained from Plastic Models*, NACA TN 3813, November, 1956.

[17] Levy, S., *Structural Analysis and Influence Coefficients for Delta Wings*, Journal of the Aeronautical Sciences, Vol. 20, No. 7, pp. 449–454, July, 1953.

INTERNATIONAL AEROSPACE ABSTRACTS

New IAS Periodical—First Issue January, 1961

This new monthly combines, in improved format, the abstracts and books sections formerly printed in *Aerospace Engineering*. For uninterrupted abstract service, enter your subscription now.

See Inside Back Cover of December, 1960, Issue for Further Details.

Readers' Forum

BRIEF REPORTS of investigations in the aerospace sciences and discussions of papers published in the JOURNAL are presented in this special department. Entries must be restricted to a maximum of 1,300 words or the equivalent of one JOURNAL page including formulas and illustrations. Publication is completed as soon as possible after receipt of the material. The Editorial Committee does not hold itself responsible for the opinions expressed by the correspondents.

Contents

On Vibration and Flutter Analysis With Free-Free Boundary Conditions ..... WILLIAM P. RODDEN 65

Comment on "Application of Adaptive Control Techniques to Aerospace Vehicles" ..... EUGENE A. O'HERN 66

Authors' Reply ..... W. F. O'NEIL AND M. T. ABZUG 67

Some Additional Plasticity Coefficients for the Plastic Buckling of Plates and Shells ..... ALEXANDER KRIVETSKY 67

Addendum—"Minor-Circle Flight at Large Angles of Inclination" ..... W. H. T. LOH 68

Comment on "Beam-Columns With Elastically Restrained Ends" ..... BEN A. NEFFSON 68

Heat-Flux Distribution Over Hemispherical-Nosed Bodies in Hypersonic Flight ..... CRAIG G. SMITH 69

An Approximate Solution for the Symmetrical End Problem of Conical Shells ..... WILLEM STUIVER 71

A Note on the Minimum-Weight Design of Spherical and Cylindrical Pressure Surfaces ..... B. SAELMAN 72

Laminar Mixing in the Presence of Axial Pressure Gradients ..... L. G. NAPOLITANO AND A. POZZI 73

Some Comments on Standing Detonation Waves in a Combustion Tunnel ..... A. A. KOVITZ 75

Hypervelocity Gasdynamic Charts for Equilibrium Air ..... RICHARD W. ZIEMER 76

A Note on the Impact Pressure Loading of a Rigid Plastic Spherical Shell ..... R. SANKARANARAYANAN 77

Simple Graphical Method for Temperature Distribution in Bodies With Linear Change in Environment Temperature ..... WALTER UNTERBERG 78

On the Use of Quaternions to Describe the Angular Orientation of Space Vehicles ..... T. E. SURBER 79

On Vibration and Flutter Analysis With Free-Free Boundary Conditions

William P. Rodden

Senior Technical Specialist, Dynamics and Loads Branch, Norair Div., Northrop Corporation, Hawthorne, Calif.

July 5, 1960

A COLLOCATION FORMULATION of the vibration and flutter problems is presented in reference 1, which also gives the specific forms of the collocation equation in the cases of free-free symmetric and free-free antisymmetric boundary conditions. The purpose of the present note is to generalize the previous analysis for any combination of rigid-body degrees of freedom. The free-free collocation formulation begins with the deflection equation

$$\{h_1 - h_0\} = [a]\{F\} \tag{1}$$

where $\{h_1\}$ is the set of absolute control-point deflections, $\{h_0\}$ is the set of control-point deflections due to the rigid-body motion of some reference point, $[a]$ is the set of structural influence coefficients for the system *cantilevered* from the reference point, and $\{F\}$ is the set of control-point forces. If we assume harmonic motion of frequency ω, then the control-point forces (the sum of the inertial and aerodynamic forces) may be written in terms of the mass matrix $[M]$, and the (complex) matrix of oscillatory aerodynamic influence coefficients $[C_h]$.

$$\{F\} = \omega^2[M]\{h_1\} + \rho\omega^2 b_r^2 s[C_h]\{h_1\} \tag{2a}$$

$$= \omega^2[\bar{M}]\{h_1\} \tag{2b}$$

where ρ is the atmospheric density, and b_r and s are the reference semichord and reference span, respectively. (In a vibration

Contributors Please Note

Readers' Forum items must be confined to the equivalent of one page in the *Journal*. Contributions that exceed this limit will be returned to the authors for condensation and rewrite. To avoid inconvenience and delay, please adhere to the following specifications:

(1) Five, double-spaced, typewritten, manuscript pages (8½ by 11 in.), including wide margins, formulas, and headings, equal one printed page.

(2) For every illustration, deduct at least one-half or as much as one manuscript page, depending on the size of the illustration.

analysis, the aerodynamic term is deleted.) Substituting Eq. (2b) into Eq. (1) and adding the structural-damping factor $(1 + ig)$ necessary to sustain the assumed harmonic motion of the flutter system, we obtain

$$\lambda\{h_1 - h_0\} = [a][\bar{M}]\{h_1\} \quad (3a)$$

$$= [U]\{h_1\} \quad (3b)$$

where the eigenvalue λ denotes $(1 + ig)/\omega^2$.

It is now necessary to eliminate the rigid-body degrees of freedom from Eq. (3b). To do so, we define a rigid-body modal matrix $[h_R]$ from which

$$\{h_0\} = [h_R]\{a_R\} \quad (4)$$

where $\{a_R\}$ is the set of amplitudes of the rigid-body motion of the reference point. As an example, if we consider symmetrical motion, $[h_R]$ is composed of two columns: the first is a unit column corresponding to the plunging mode, the second consists of the x-coordinate of each control point corresponding to the pitching mode. The rigid-body modal matrix provides the basis for a general statement of the boundary conditions

$$[h_R]^*[\bar{M}]\{h_1\} + [\Delta\bar{m}]\{a_R\} = 0 \quad (5)$$

where the asterisk denotes transposition, and $[\Delta\bar{m}]$ is an incremental generalized mass matrix, including aerodynamic effects, of any rigid component of the system attached to the reference point (e.g., a fuselage), and not considered in the formation of the basic mass and aerodynamic matrices.

Substituting Eq. (4) into Eq. (3b), premultiplying Eq. (3b) by $[h_R]^*[\bar{M}]$, and subtracting Eq. (5), permits solution for the amplitudes of the rigid-body motion:

$$\lambda\{a_R\} = -[\bar{m}]^{-1}[h_R]^*[\bar{M}][U]\{h_1\} \quad (6)$$

where

$$[\bar{m}] = [h_R]^*[\bar{M}][h_R] + [\Delta\bar{m}] \quad (7)$$

Eliminating the rigid-body degrees of freedom from Eq. (3b) yields the generalized free-free collocation equation

$$\lambda\{h_1\} = ([I] - [h_R][\bar{m}]^{-1}[h_R]^*[\bar{M}])[U]\{h_1\} \quad (8)$$

where $[I]$ is the unit matrix. The solution of Eq. (8) (by iteration or determinant expansion and root extraction) for the complex eigenvalues, $\lambda = \lambda_R + i\,\lambda_I$, yields the free-free frequency

$$\omega = 1/\sqrt{\lambda_R} \quad (9)$$

the required structural damping

$$g = \lambda_I/\lambda_R \quad (10)$$

and, since the matrix of aerodynamic influence coefficients requires the assumption of a reduced frequency, $k = \omega b_r/V$, for its formulation, the velocity

$$V = \omega b_r/k \quad (11)$$

Eq. (8) is seen to be completely general being applicable from the cantilever case (in which we let $[h_R]$ vanish) to the case of six rigid-body degrees of freedom. In the antisymmetrical case (a single rigid degree of freedom in roll), Eq. (8) reduces to Eq. (65) of reference 1. In the symmetrical case (two rigid degrees of freedom in plunge and pitch), Eq. (8) reduces to Eq. (69) of reference 1. We also observe that Eq. (8) is a matrix formulation of the algebraic procedures for free-free vibration analysis described by Bisplinghoff, Ashley, and Halfman (reference 2, §4–6), and by Scanlan and Rosenbaum (reference 3, §11.2).

References

[1] Rodden, William P., *A Matrix Approach to Flutter Analysis*, Institute of the Aeronautical Sciences, Sherman M. Fairchild Publication Fund Paper No. FF-23, May, 1959.

[2] Bisplinghoff, Raymond L., Ashley, Holt, and Halfman, Robert L., *Aeroelasticity*, Addison-Wesley Publishing Co., Inc., Cambridge, Mass., 1955.

[3] Scanlan, Robert H., and Rosenbaum, Robert, *Introduction to the Study of Aircraft Vibration and Flutter*, The MacMillan Co., New York, 1951.

Comment on "Application of Adaptive Control Techniques to Aerospace Vehicles"

Eugene A. O'Hern

Chief, Preliminary Engineering, Flight Control, Autonetics Div., North American Aviation, Downey, Calif.

July 5, 1960

THE SUBJECT PAPER,[1] presented at the National Specialists Meeting on Guidance of Aerospace Vehicles, discussed two distinct areas of adaptive control techniques. The first section was concerned with the development of performance-oriented definitions and classifications of adaptive systems. In the second section, the difficulty of meeting reliability requirements imposed by extremely long mission times typical of interplanetary travel, even utilizing redundant systems, was emphasized. A means of improving redundant-system performance by optimizing utilization of majority circuitry was developed. The portion of the second section of the paper dealing with the relative reliability of single- and redundant-channel systems forms the basis of the discussion to follow.

The authors point out that reliability gains to be realized from the employment of redundant channels are substantially diminished as mission times approach and exceed the mean time to failure of a single channel. This fact is certainly important to remember. Quantitatively, however, it appears that a fault in the derivation of the redundant-channel failure-probability expression has resulted in the erroneous indication that additional redundant channels, even for the case of the perfect-monitor circuitry as assumed here, actually *reduce* the probability of successful system operation for high mission times. It is hoped that the following discussion will clarify this matter.

For a system of m channels, each having failure-probability p_s (approximated in the paper as $n\,\dot{p}\,t$, where $n\,\dot{p}$ = the total failure rate per channel and t = time), the general expression for overall system failure (defined in the paper as continuing operation of less than two channels) can be derived as the probability of all channels having failed, plus the m probabilities of each of the channels being operative alone, that is

$$P_s = p_s^m + m p_s^{m-1}(1 - p_s); \qquad m \geq 2, \quad \ldots \quad (1)$$

This expression differs from its counterpart Eq. (5) of the paper, repeated here:

$$P_s = m!\,(n\,\dot{p}\,t)^{m-1}; \qquad m > 2$$

The derivation of this latter equation is invalid because of dependency of the ordered failure events. It can be seen that [from Eq. (1)]

$$P_s > p_s \text{ for } m = 2, \qquad 0 < p_s < 1$$

since

$$P_s(2) = p_s^2 + 2p_s(1 - p_s)$$
$$= 2p_s - p_s^2$$
$$= p_s(2 - p_s) > p_s. \ldots \quad (2)$$

However, for $m \geq 2$, it can be shown that

$$P_s(m) > P_s(m + 1), \ldots \quad (3)$$

that is, failure probability decreases monotonically with increasing numbers of redundant channels. This can be shown from Eq. (1)

$$P_s(m) = m\,p_s^{m-1} - (m - 1)\,p_s^m. \ldots \quad (4)$$

$$\therefore P_s(m + 1) = (m + 1)\,p_s^m - m\,p_s^{m+1}. \ldots \quad (5)$$

So

$$P_s(m) - P_s(m + 1) = m\,p_s^{m-1} - 2m\,p_s^m + m\,p_s^{m+1}$$
$$= m\,p_s^{m-1}(1 - 2p_s + p_s^2)$$
$$= m\,p_s^{m-1}(1 - p_s)^2 > 0, \ldots \quad (6)$$

since $0 < p_s < 1$.

Further, it is felt that the case for the redundant system was also presented pessimistically in that overall system failure was assumed to occur when either one of the last two channels failed. It would appear that no significant additional sophistication of the monitoring circuitry would be required to cause a

final arbitrary selection of one of the last two operable channels, thereby increasing somewhat the probability of continuing system operation after the next to the last channel has failed. Using this more realistic philosophy, the overall system probability becomes

$$P_s' = p_s^m + {}^1/_2\, m\, p_s^{m-1}(1 - p_s) \ldots \quad (7)$$

Now, for $m = 2$

$$P_s' = p_s^2 + p_s(1 - p_s) = p_s \quad (8)$$

which is logical, inasmuch as one of the two channels is arbitrarily selected for system operation. However, as before, it can again be shown that

$$P_s'(m) > P_s'(m + 1) \text{ for } m \geq 2 \quad (9)$$

From Eq. (7)

$$P_s'(m) = [1 - (m/2)]p_s^m + (m/2)p_s^{m-1} \quad (10)$$

from which

$$P_s'(m) - P_s'(m + 1) = {}^1/_2\, m\, p_s^{m-1} + ({}^1/_2 - m)\, p_s^m - [1 - (m + 1)/2]\, p_s^{m+1} \quad (11)$$

$$= (p_s^{m-1}/2)\,[m - (2m - 1)\, p_s + (m - 1)\, p_s^2]$$

$$= (p_s^{m-1}/2)\,[m - (m - 1)\, p_s][1 - p_s] > 0 \quad (12)$$

since $0 < p_s < 1$, thus clearly establishing the fact that, for any $0 < p_s < 1$, P_s' is monotone nonincreasing for increasing numbers of channels m.

The curve of Fig. 7 in the paper can then be replotted from Eq. (1) above, or preferably, Eq. (7). Also, since the values of mission time may be large relative to the single-channel mean-time-to-failure, the more generally applicable expression for single-channel failure probability should be employed, i.e.,

$$p_s = 1 - e^{-n\dot{p}t} \quad (13)$$

It must be recognized that, because of the basic errors herein discussed, many of the relations developed in the succeeding paragraphs of the paper are accordingly invalid. These must be reviewed in light of the true analytical expressions for failure probability.

REFERENCE

[1] O'Neil, W. F., and Abzug, M. J., *Application of Adaptive Control Techniques to Aero/Space Vehicles*, Proceedings of the National Specialists Meeting on Guidance of Aerospace Vehicles, pp. 197–208, May 25–27, 1960.

Authors' Reply

W. F. O'Neil and M. T. Abzug
Douglas Aircraft Company, Inc., El Segundo Division, El Segundo, Calif.

August 18, 1960

REFERENCE 1 notes that the redundant-system failure-probability Eq. (5) in the writers' paper "Application of Adaptive Control Techniques to Aerospace Vehicles" is in error as a result of assuming events are ordered. The writers thank E. A. O'Hern for bringing this error to their attention. However, it should be noted that for high-failure probability of a single channel, the redundant-system failure probability derived from the correct expression, Eq. (1) of reference 1, does exceed the single-channel failure probability, as originally stated.

Referring to Eq. (13) of reference 1, for times less than $1/n\dot{p}$, the simpler expression $p_s = n\dot{p}t$, given in the writers' paper, is evidently a satisfactory approximation.

In addition to the foregoing comments, a review of the writers' paper in the light of reference 1 discloses that the implications of Eq. (10), leading to the analysis of the Random Adaptive Fault Locator, are qualitatively correct.

REFERENCE

[1] O'Hern, E. A., *Comment on "Application of Adaptive Control Techniques to Aerospace Vehicles,"* Journal of the Aerospace Sciences, Readers' Forum, Vol. 28, No. 1, pp. 66–67, January, 1961.

Some Additional Plasticity Coefficients for the Plastic Buckling of Plates and Shells

Alexander Krivetsky
Staff Engineer, Structures, Aero Space Dept., Bell Aircraft Corporation, Buffalo, N.Y.

June 27, 1960

IN A PREVIOUS PAPER,[1] plasticity coefficients for several plate and shell configurations were presented. Since that time, additional cases have been evaluated and are presented in the subject paper. The results are based on the original work of Bijlaard and are again presented in carpet plots for engineering use.

A Long Plate Under Compression Where one of the Unloaded Edges is Fixed and the Other is Free

From Table 5 of reference 2, the equation for η is given as

$$\eta = 0.473(\sqrt{AD} + 2.97F - 0.405B) \quad (1)$$

The functions A, B, D, and F, which are defined in references 5 and 6, are based on $\beta = 0$. Eq. (1) is depicted graphically in Fig. 1 in terms of the tangent and secant modulus ratios.

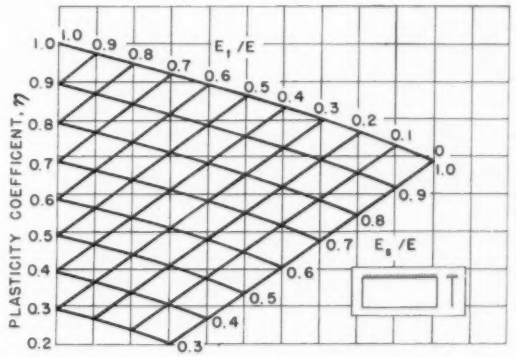

FIG. 1. Plasticity coefficient, η, for a long plate under compression where one of the unloaded edges is fixed and the other is free.

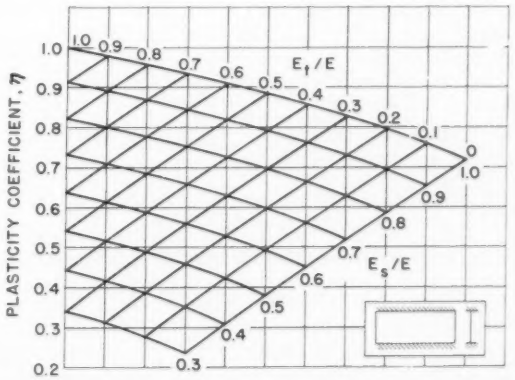

FIG. 2. Plasticity coefficient, η, for a long plate under compression where both of the unloaded edges are fixed.

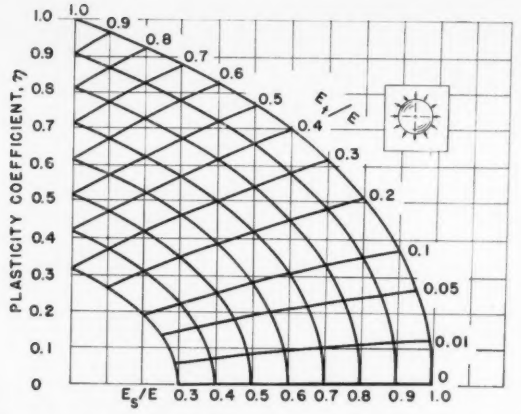

FIG. 3. Plasticity coefficient, η, for a spherical shell under external pressure.

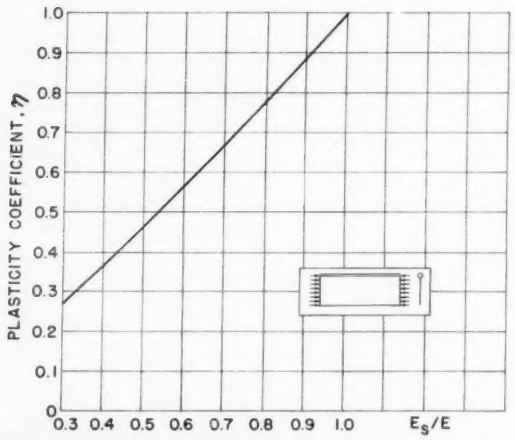

FIG. 4. Plasticity coefficient, η, for a long plate under compression with one of the unloaded edges simply supported and the other free.

A Long Plate Under Compression Where Both of the Unloaded Edges are Fixed

The plasticity coefficient η for this configuration is given by

$$\eta = 0.598\sqrt{AD} + 0.312(B + 2F) \tag{2}$$

Again the reference source is Table 5 of reference 2. With $\beta = 0$, the curves in Fig. 2 are obtained for the plasticity coefficient.

Spherical Shell Under External Pressure

From reference 2, the plasticity coefficient for a spherical shell under external pressure is given as

$$\eta = \sqrt{0.91(A^2 - B^2)} \tag{3}$$

The A and B plasticity functions are based on a value of $\beta = 1$. A plot of Eq. (3) is shown in Fig. 3.

A Long Plate Under Compression Where one of the Unloaded Edges is Simply Supported and the Other is Free

The expression for the plasticity coefficient η is given by

$$\eta = 2.6F \tag{4}$$

This expression is given in Table 5 of reference 2 and can also be obtained from Eq. (35) of reference 3. Since the plate is under a compressive stress only, the value of $\beta = 0$ must be employed in the above-mentioned references. Fig. 4 represents the value of the plasticity coefficient for this plate configuration and loading.

A Long Simply Supported Plate Subjected to Pure Bending in its Plane

Investigations for the case of a long simply supported plate subjected to pure bending in its plane has disclosed that η can be represented by (see reference 4)

$$\eta = E_s/E \tag{5}$$

REFERENCES

[1] Krivetsky, A., *Plasticity Coefficients for the Plastic Buckling of Plates and Shells*, Journal of the Aeronautical Sciences, Vol. 22, No. 6, pp. 432–435, June, 1955.

[2] Bijlaard, P. P., *Theory and Tests on the Plastic Stability of Plates and Shells*, Journal of the Aeronautical Sciences, Vol. 16, No. 9, pp. 529–541, September, 1949.

[3] Bijlaard, P. P., *Some Contributions to the Theory of Elastic and Plastic Stability*, Publication of the International Assn. Bridge and Structural Engineering, Vol. 8, pp. 17–80, Zurich, 1947.

[4] Bijlaard, P. P., *Theory of Plastic Buckling of Plates and Applications to Simply Supported Plates Subjected to Bending or Eccentric Compression in Their Plane*, J. Appl. Mech., Vol. 23, No. 1, pp. 27–34, March, 1956.

[5] Krivetsky, A., *Plasticity Parameters and Coefficients for Plates and Shells*, Bell Aircraft Corporation Rept. 02-984-019, November, 1954.

[6] Krivetsky, A., *Buckling Stresses of Various Plate and Shell Configurations Including Effects of Plasticity*, Bell Aircraft Corporation, Rept. 9041-18-001, July, 1957.

Addendum—"Minor-Circle Flight at Large Angles of Inclination"

W. H. T. Loh*
Senior Post Doctoral Fellow, National Science Foundation, Imperial College and Cambridge University, England
July 7, 1960

THE COMPARISONS shown in Fig. 1, reference 1, are only for order of magnitude comparisons at L/D nearly zero, where such small values of L/D, whether positive or negative, do not materially alter the trajectory itself too much. When the angle of re-entry is not small, a large negative L/D must be used in order to enforce the descent at large angles of inclination which is the case of primary interest of reference 1.

REFERENCE

[1] Loh, W. H. T., *Minor Circle Flight At Large Angles of Inclination*, Journal of the Aero/Space Sciences, Vol. 27, No. 5, pp. 397–398, May, 1960.

* On one year's leave of absence (1959–1960) from Chance Vought Aircraft, Dallas, Tex.

Comments on "Beam-Columns With Elastically Restrained Ends"

Ben A. Neffson
Design Specialist, North America Aviation, Inc., Los Angeles, Calif.
June 24, 1960

RECENTLY,[1] Professor Niles took exception to a Readers' Forum note by the writer[2] saying that it was needlessly complex and tedious as to its computational procedure. At first glance, the criticism appears justified in that none of the plots mentioned in reference 2 were included in that paper. Actually, however, the method is no more complicated than that advocated by Professor Niles, once the necessary curves have been made available. Such a set is shown in Figs. 1, 2, and 3 for the case of a concentrated load W, where a is the distance of the load from the left support. With all the necessary data plotted as a function of the single nondimensional parameter λl, the solution of Eqs. (5a) and (5b) of reference 2 is certainly

a simple and rapid matter. It should be noted that the end moments M_A and M_B are given explicitly, and do not require the solution of a set of simultaneous equations as in reference 1.

Curves, similar to Figs. 2 and 3, may be plotted for distributed uniform and triangular lateral loads and, by superposition, a limited number of plots may thus be used for a great variety of lateral load distributions. For the random, single, concentrated load W, the lateral load function $f_A(W)$ is given by

$$f_A(W) = (W/P)[W(\lambda l)]$$

where $W(\lambda l)$ is obtained from Fig. 2. A similar relation exists for other lateral loads. As indicated in reference 2, $f_n(\lambda l)$ is independent of the lateral loading and, hence, a single presentation suffices.

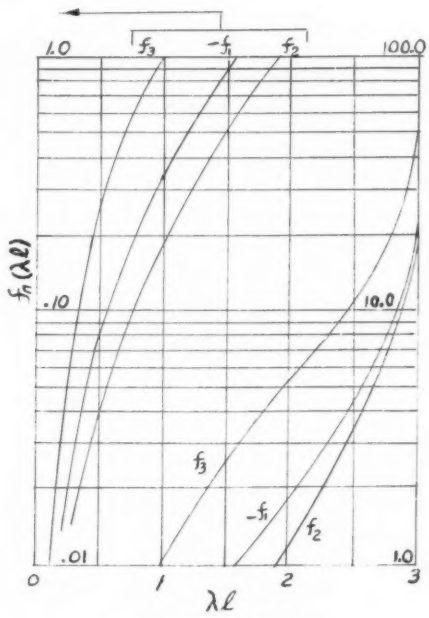

FIG. 1. Variation of $f_n(\lambda l)$.

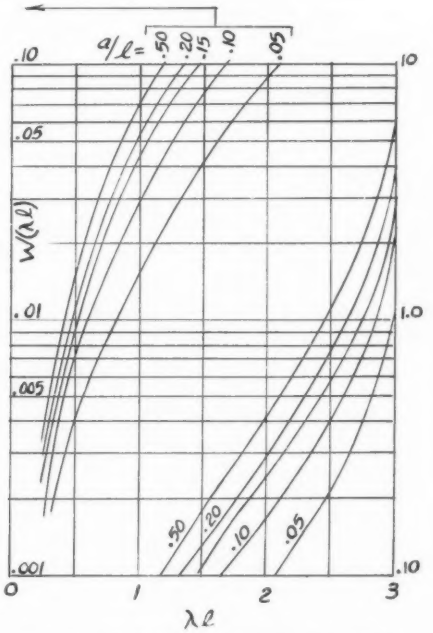

FIG. 2. W(λl) for single, concentrated load.

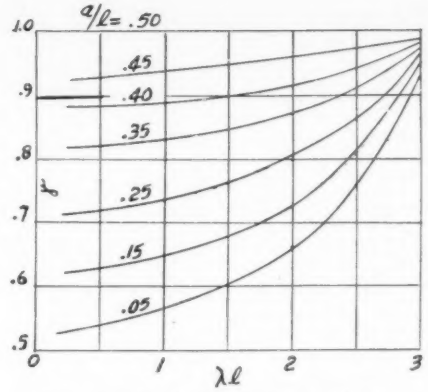

FIG. 3. γ for single, concentrated load.

It is readily seen that expressions (1a), (1b), and (4a), (4b) of reference 1 are but specialized cases of the general formulation (1) given in reference 2. If the relations for a uniform or concentrated load given by Professor Niles are divided through by $6EI$, it will be found that the factors multiplying M_A and M_B are precisely the k_1 and k_2 of reference 2. While the writer may have been remiss in not recalling that the tabulated functions of Professor Niles could also have been adapted to the solution of the problem, there was certainly no intention of slighting his work.

REFERENCES

[1] Niles, A. S., *Beam Columns with Elastically Restrained Ends*, Journal of the Aero/Space Sciences, Readers' Forum, Vol. 27, No. 4, pp. 316–317, April, 1960.

[2] Neffson, B. A., *Beam Columns on Elastic Supports*, Journal of the Aero/Space Sciences, Readers' Forum, Vol. 26, No. 4, pp. 255–256, April, 1959.

[3] Niles, A. S., and Newell, J. S., *Airplane Structures*, 3rd Ed., Vol. 2 John Wiley and Sons, Inc., New York, 1943.

Heat-Flux Distribution Over Hemispherical-Nosed Bodies in Hypersonic Flight*

Craig G. Smith
Research Engineer, American Machine and Foundry Co., Mechanics Research Div., Niles, Ill.
April 25, 1960

THE EXTENSION of stagnation-point heat transfer to regions away from the stagnation point on axisymmetric bodies at zero incidence has recently been developed by Kemp, Rose, and Detra,[1] who obtained local-similarity solutions of the laminar-boundary-layer equations including the effects of pressure gradient, variable properties and dissociation. The purpose of this note is to extend the generalized results of reference 1 in closed forms for the case of a hemisphere-cylinder and clarify the nature of the Mach-number dependence.

The laminar heat-flux distribution away from the stagnation point for axisymmetric bodies is given by Eq. (27) of reference 1; viz.,

$$q/q_s = (r\rho_w\mu_w u_e/\sqrt{2\xi})\{2\rho_{ws}\mu_{ws}(du_e/dx)_s\}^{-(1/2)} g_{\eta w}/g_{\eta ws} \quad (1)$$

where

$$\xi(x) = \int_0^x \rho_{ws}\mu_w u_e r^2 dx \quad (2)$$

* This work was supported in part by the United States Air Force under Contract AF 33(616)-6673, monitored by the Nonmetallic Materials Laboratory, Materials Central, Directorate Advanced Systems Technology, Wright Air Development Division, Wright Patterson Air Force Base Ohio.,

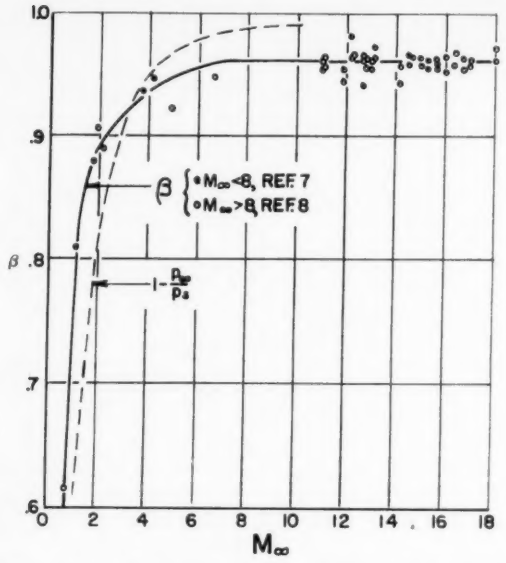

FIG. 1. Relation between β and free-stream Mach number.

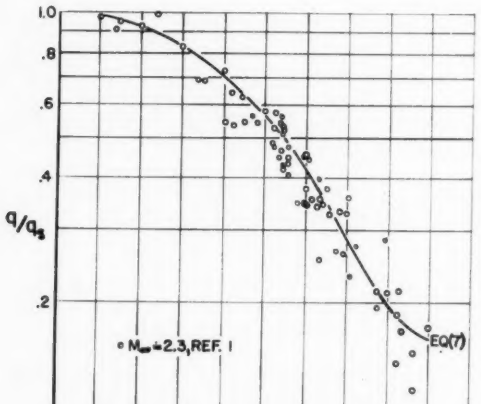

FIG. 2. Comparison of theoretical and experimental heat-flux distributions.

The notation of reference 1 is employed in this note, and the stagnation-point heat transfer, q_s, is to be determined by the method of Fay and Riddell.[2]

For the nose of a hemisphere-cylinder the following relationships are valid. First, the most convenient independent variable is the polar angle with respect to the axis of symmetry, θ, obtained from the transformation

$$\theta = x/R, \qquad r = R \sin \theta \tag{3}$$

The pressure impressed upon the boundary layer may be represented as

$$p_s/p_s = 1 - \sin^2 \theta\,(p_s - p')/p_s \tag{4}$$

where p' is the pressure at the shoulder ($\theta = \pi/2$). In modified Newtonian theory, $p' = p_\infty$, so that the functional form of the theory is here employed but with the boundary (stagnation and shoulder) values being obtained from experimental observations. This additional modification is important since at high Mach number the ratio p'/p_∞ departs appreciably from unity, at $M_\infty = 20$ the ratio being 18. Further, as demonstrated by Li and Geiger,[3] the flow velocity at the edge of the boundary layer is a linear function of x; i.e.,

$$u_s = (du_s/dx)_s R\theta \tag{5}$$

The ratio $g_{\eta w}/g_{\eta w s}$, as noted in reference 1, is approximately constant over the hemisphere and may be taken as unity.

The integration of Eq. (2) may be considerably simplified by noting that for a constant wall temperature the product $\rho_w \mu_w$ is independent of temperature. Taking this to be the case for a variable wall temperature is tantamount to making the assumption of a $\mu \propto T$ viscosity law of all constant-$\rho\mu$ solutions with the one exception that here the assumption is made along the wall instead of the more severe case of across the boundary layer. Combining this assumption with the perfect-gas law

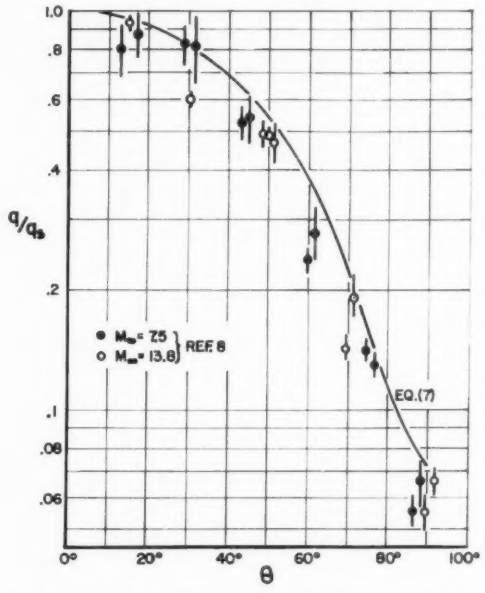

FIG. 3. Comparison of theoretical and experimental heat-flux distributions.

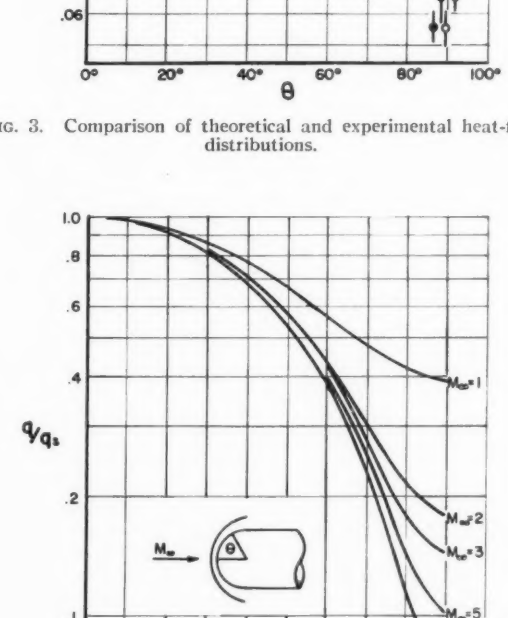

FIG. 4. Laminar heat transfer over a hemispherical-nosed body for selected values of free-stream Mach number.

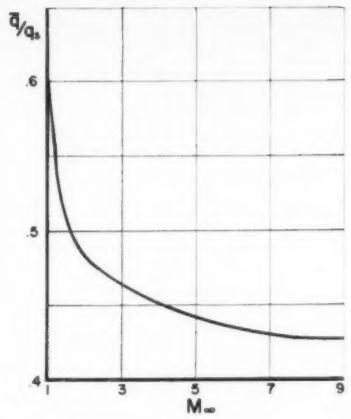

FIG. 5. Area-weighted mean laminar heat transfer to a hemispherical-nosed body.

and the standard notion of impressed pressure across the boundary layer, one has

$$\rho_w \mu_w = \rho_{ws} \mu_{ws} (p_e/p_s) \tag{6}$$

Substituting the pressure distribution, Eq. (4), into Eq. (6), and performing the integration of Eq. (2) leads to the following relationship for the heat-flux distribution:

$$q/q_s = [(1 - \beta \sin^2\theta)\theta \sin\theta]/[F_1(\theta) + \beta F_2(\theta)] \tag{7}$$

where

$$\beta = 1 - p'/p_s \tag{8}$$

$$F_1(\theta) = \theta^2 - \theta \sin 2\theta + \sin^2\theta \tag{9}$$

$$F_2(\theta) = -1/2[3/2\theta^2 - \theta \sin 2\theta(3/2 + \sin^2\theta) + 3/2 \sin^2\theta + 1/2 \sin^4\theta] \tag{10}$$

The dependence of β upon M_∞ is indicated in Fig. 1. The solid curve is a mean β drawn for the indicated experimental points. The low-Mach-number data were calculated from a report by Katz[4] on the observations of five investigators. The high-Mach-number data from Boison,[5] measured at nominal stagnation temperatures of 4,000, 6,000, and 8,000 K., well establish the hypersonic β limit. It is seen in Fig. 1 that a radical dependence of β (and hence q/q_s) occurs only at $M_\infty < 3$. The dotted curve in Fig. 1 represents β as determined by the modified Newtonian theory and points to the importance of matching the functional form of the theory with the actual shoulder pressure.

Eq. (7) is compared to experimental observations at three Mach numbers in Figs 2 and 3, with β being determined from Fig. 1. It is seen in Fig. 3 that the distributions for Mach numbers equal to 7.5 and 13.8 are essentially the same, and thus the hypersonic limit extends somewhat below $M_\infty = 8$. Eq. (7) is plotted in Fig. 4 for selected values of free-stream Mach number. The area-weighted mean heat flux was numerically calculated for the distribution of Eq. (7), the results of which are presented in Fig. 5.

REFERENCES

[1] Kemp, N. H., Rose, P. H., and Detra, R. W., *Laminar Heat Transfer Around Blunt Bodies in Dissociated Air*, Journal of the Aero/Space Sciences, Vol. 26, No. 7, pp. 421–430, July, 1959.

[2] Fay, J. A., and Riddell, F. R., *Theory of Stagnation Point Heat Transfer in Dissociated Air*, Journal of the Aeronautical Sciences, Vol. 25, No. 2, pp. 73–85, February, 1958.

[3] Li, Ting-Yi, and Geiger, R. E., *Stagnation Point of a Blunt Body in Hypersonic Flow*, Journal of the Aeronautical Sciences, Vol. 24, No. 1, pp. 25–32, January, 1957.

[4] Katz, J. R., *Pressure and Wave Drag Coefficients for Hemispheres, Hemisphere-Cones, and Hemisphere-Ogives*, NAVORD Report 5849, March, 1958.

[5] Boison, J. C., *Experimental Investigation of the Hemisphere-Cylinder at Hypervelocities in Air*, AEDC-TR-58-20, November, 1958.

An Approximate Solution for the Symmetrical End Problem of Conical Shells

Willem Stuiver*
Research Assistant, Stanford University, Stanford, Calif.

July 5, 1960

SYMMETRICAL PROBLEMS for conical shells have been studied extensively and exact solutions have been presented in the literature. It seems appropriate, however, to point out that an extremely simple approximation to the solution of the end problem can be construed. This approximation is based on the solution of the corresponding problem for the circular cylindrical shell. It is sufficiently accurate, for a wide range of apex angles, to be of practical interest.

The differential equation for the *radial* displacements u (Fig. 1) of the cylindrical shell is[1]

$$u'''' + 4\mu^4 u = 0 \tag{1}$$

with

$$\mu^4 = 3(1 - \nu^2)/(r^2 t^2) \tag{2}$$

and primes indicating differentiation with respect to z. Considering here only the case $u(0) = u_0$, $u'(0) = 0$, with corresponding edge loads, we find for the displacements $u(z)$ the expression

$$u = u_0 e^{-\mu z}(\cos \mu z + \sin \mu z) \tag{3}$$

A plot of this relation shows (Fig. 2) that the displacements die out rapidly, and that they amount to less than 5 per cent of the value u_0 for distances z larger than 3μ.

The differential equation for the *normal* displacements u (Fig. 3) of the conical shell is considerably more involved. This equation can be written in the form[2]

$$LL[du/dy] + n^2(du/dy) = 0 \tag{4}$$

The operator L is defined as $L = y\, tg\theta(d^2/dy^2) - (tg\theta/y)$ and the parameter n by the relation

$$n^2 = 12(1 - \nu^2)/t^2 \tag{5}$$

For sufficiently small values of the apex angle θ, it can be shown that the resulting displacements $u(y)$ are closely approximated by the values $\bar{u}(z)$ calculated from the "equivalent-cylinder equation"

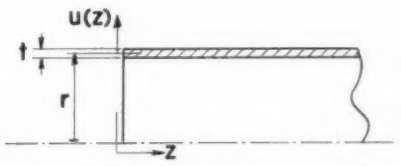

FIG. 1. Cylinder geometry and coordinates.

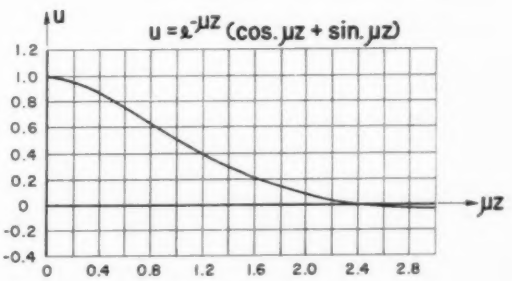

FIG. 2. The cylinder displacement function.

* At present with IBM Research Laboratory, San Jose, Calif.

Acknowledgments are due to the National Aeronautical Research Institute, Amsterdam, the Netherlands, for permission to publish this note, the contents of which originally formed part of the stress analysis pertaining to the Institute's transonic wind tunnel.[4]

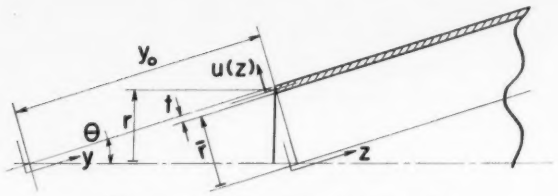

FIG. 3. Cone geometry and coordinates.

$$\bar{u}'''' + 4\bar{\mu}^4\,\bar{u} = 0 \tag{6}$$

with $y = y_0 + z$ (Fig. 3) and $\bar{\mu}$ given by

$$\bar{\mu}^4 = 3(1 - \nu^2)\cos^2\theta/(r^2t^2) \tag{7}$$

For the case $\bar{u}(0) = u_0$, $\bar{u}'(0) = 0$, we thus find displacements

$$\bar{u} = u_0 e^{-\bar{\mu}z}(\cos\bar{\mu}z + \sin\bar{\mu}z) \tag{8}$$

analogous to Eq. (3) for the solution of Eq. (1). It follows that these displacements are negligibly small for distances z larger than $3\bar{\mu}$.

Application of the operator L and substitution of the parameter n in Eq. (4) yields

$$y^2\frac{d^6u}{dy^6} + 2y\frac{d^4u}{dy^4} - 2\frac{d^3u}{dy^3} + \frac{2}{y}\frac{d^2u}{dy^2} - \frac{1}{y^2}\frac{du}{dy} + \frac{12(1-\nu^2)}{t^2tg^2\theta}\frac{du}{dy} = 0 \tag{9}$$

for the displacements $u(y)$. With $r = y_0 \sin\theta$ and $y = y_0 + z$ (Fig. 3), this equation can be written in the form

$$u''''' + 2u''''/(y_0 + z) - 2u'''/(y_0 + z)^2 + 2u''/(y_0 + z)^3 + \{-1 + 4\bar{\mu}^4y_0^4[1 + (z/y_0)]^2\}u'/(y_0 + z)^4 = 0 \tag{10}$$

For small values of the factor $3\bar{\mu}/y_0$, this equation is approximately satisfied in the region $0 \le z \le 3\bar{\mu}$ by the function

$$u' = [1 + (z/y_0)]^a$$

if the exponent a is a root of the quartic

$$a^4 - 4a^3 + 3a^2 + 2a + 4N^4 = 0$$

with

$$4N^4 = -1 + 4\bar{\mu}^4y_0^4[1 + (3\bar{\mu}/y_0)]^2 \tag{11}$$

The roots of this quartic can be found most easily from the procedure proposed by Lanczos.[3] They are

$$a = 1 \mp (1 \pm i)N$$

and it follows, after some obvious manipulations, that for the case $u(0) = u_0$, $u'(0) = 0$ considered here, Eq. (10) leads to the solution

$$u = u_0[1 + (z/y_0)]^{2-N}[\cos\{N\ln[1 + (z/y_0)]\} + [1 - (2/N)]\sin\{N\ln[1 + (z/y_0)]\}] \tag{12}$$

It is easily verified that this solution reduces to the approximation (8) for large values of N.

We compare here only the bending stresses at the edge $z = 0$, given, respectively, by Eqs. (8) and (12). These stresses depend on the value of the second derivative $u''(0)$. From expression (8) for the solution $\bar{u}(z)$, we find

$$\bar{u}''(0) = -2\bar{\mu}^2u_0 \tag{13}$$

The solution (12) yields

$$u''(0) = [-2(N^2 - 2N + 2)/y_0^2]\,u_0 \tag{14}$$

hence, with $\bar{\mu}y_0 \gg 1$, $N = \bar{\mu}y_0$,

$$u''(0) = -2\bar{\mu}^2u_0[1 - (2/\bar{\mu}y_0) + (2/\bar{\mu}^2y_0^2)] \tag{15}$$

Writing $u''(0) = \lambda\bar{u}''(0)$, we have

$$\lambda = 1 - 2[(\sin\theta/\bar{\mu}r)] + 2[(\sin\theta/\bar{\mu}r)]^2 \tag{16}$$

with, directly from Eq. (7)

$$\bar{\mu}r = \{3(1 - \nu^2)\}^{1/4}[(r\cos\theta)/t]^{1/2} \tag{17}$$

The factor λ is a measure of the relative accuracy of the two solutions (8) and (12). Numerical values of this factor are given in Table 1 for some specific cases.

TABLE 1

Numerical Values of the Correction Factor λ

r	t	$tg\,\theta$	$\bar{\mu}$	λ
338	2.5	1.00238	0.0373	0.894
210	2.5	0.70040	0.0510	0.898
451	2.5	0.46980	0.0365	0.950
148	1.0	0.12221	0.1056	0.985
148	1.0	0.04549	0.1059	0.994
233	1.2	0.04559	0.0771	0.995
210	2.1	−0.10518	0.0613	1.016

REFERENCES

[1] Biezeno, C. B., and Grammel, R., *Engineering Dynamics*, Chapt. VI, Section 19, Eq. 9, Blackie & Son Ltd., Glasgow, 1954.
[2] Loc. cit., Chapt. VI, Section 24, Eq. 16.
[3] Lanczos, C., *Applied Analysis*, Chapts. I, II, Prentice Hall, Inc. Englewood Cliffs, 1956.
[4] Report NLL-I, ST-4 (in Dutch).

A Note on the Minimum-Weight Design of Spherical and Cylindrical Pressure Surfaces

B. Saelman
Design-Weight Engineer, Lockheed Aircraft Corporation, Burbank, Calif.
June 14, 1960

SYMBOLS

σ_c	=	applied hoop-compression stress, psi
σ_t	=	hoop-tension stress, psi
σ_r	=	buckling stress in hoop compression, psi
ρ	=	material density, lbs./in.^{3}
W	=	weight, lbs.
L	=	length, in.
r	=	radius of shell (fixed), in.
R	=	radius of spherical or cylindrical surface, in.
d	=	chord of cylinder (fixed), in.
p	=	applied pressure, psi
p_r	=	critical buckling pressure, psi
t	=	thickness of shell, in.
σ_{tu}	=	allowable tensile stress, psi
I_R	=	moment of inertia of bulkhead-ring section, in.^{4}
q_r	=	buckling load on bulkhead ring, lbs./in.
b	=	width of bulkhead-ring section, in.
h	=	depth of bulkhead-ring section, in.
W_T	=	sum of weight of bulkhead plus ring, lbs.

PORTIONS of spherical and cylindrical surfaces are used extensively in pressurized aircraft structures—e.g., spherical surfaces are used for the boundary bulkheads of pressurized cabins and for the end surfaces of cylindrical tanks; cylindrical surfaces are used for portions of fuselage bodies, missile housings, etc. In most of these instances, a fixed dimension such as the fuselage radius at the station is given, then, as the radius of the spherical surface increases, the area and required thickness of the surface decreases and increases, respectively. Hence, it is suspected that a unique value of the radius for minimum weight will exist.

SPHERICAL PRESSURE SURFACES

For hoop-tension loadings

$$\sigma_t = (pr)/(2t\sin\theta) \tag{1}$$

Solving for t, substituting into the weight equation,

$$w = \rho\,t\,A \tag{2}$$

we have

$$w = [(\pi r^2p\rho)/\sigma_{tu}][(1 - \cos\theta)/(\sin^3\theta)] \tag{3}$$

Differentiating W with respect to θ, equating to zero, and solving

for θ, we have

$$\theta_{opt.} = 60°, \qquad R_{opt.} = (2/\sqrt{3})r \tag{4}$$

It is easy to show that Eqs. (4) correspond to minimum weight.

For the case of loadings in hoop compression, we have

$$\sigma_r = KE(t/R) \tag{5}$$

where the classical value of $K = 0.606$ and for which values as low as $K = 0.156$ have been derived under the assumption that surface imperfections exist. However, it will be seen that the optimum value of R is independent of K. Equating σ_r from Eq. (5) to the applied hoop-compression stress

$$\sigma_c = pR/2t \tag{6}$$

solving for t, and substituting into Eq. (2), we have

$$W = [(\sqrt{2}\,\pi\rho)/\sqrt{K}\sqrt{E}]\sqrt{p}\,r^2[(1 - \cos\theta)/\sin^3\theta] \tag{7}$$

Since the function of θ in Eq. (7) is identical to that in Eq. (3), the optimum value of R in this case is also given by Eq. (4).

In the case of tension loading on the bulkhead, the bulkhead ring will be designed by a compression loading on its periphery and given by

$$q_r = (3E\,I_R)/r^3 = q_{app.} = (pr\cot\theta)/2$$

Then the weight of the bulkhead and the bulkhead ring can be expressed by

$$W_T = W_B + W_R = [\alpha(1 - \cos\theta)/(\sin^3\theta)] + (\beta\cos\theta)/(\sin\theta)$$

where

$$\alpha = \pi r^3 p\rho/\sigma_{tu}$$

$$\beta = [4\pi p r^3(2b + h)\rho]/[E(6bh^2 + h^3)]$$

Differentiating W_t with respect to θ, setting equal to zero, we have the quadratic in

$$(2\alpha + \beta)\cos^2\theta - 3\alpha\cos\theta + \alpha - \beta = 0$$

which yields the criterion for minimum weight. Crippling of the ring flange is a possible mode of failure and should be checked.

Cylindrical Pressure Surfaces

For hoop-tension loadings

$$\sigma_t = pR/t \tag{8}$$

Solving for t and substituting into the weight equation, we have

$$W = \rho\,A\,t = [(2\rho\,d^2\,L)/\sigma_{tu}]p[\theta/\sin^2\theta] \tag{9}$$

Differentiating W with respect to θ, equating to zero, and solving, we find

$$\theta_{opt.} = 67°, \qquad R_{opt.} = d/(\sin 67°) \tag{10}$$

For hoop-compression loadings on long thin cylinders

$$pr = E/[4(1 - \mu^2)](t/R)^3 = KE(t/R)^3 = p \tag{11}$$

Solving for t and substituting into the weight equation

$$W = \rho tsl = (2\rho l d^2)/(\sqrt[3]{K}\sqrt[3]{E})\sqrt[3]{p}[\theta/(\sin^2\theta)] \tag{12}$$

Since the function of θ in Eq. (11) is identical to that in Eq. (9), Eq. (10) also gives the optimum value of R in this case.

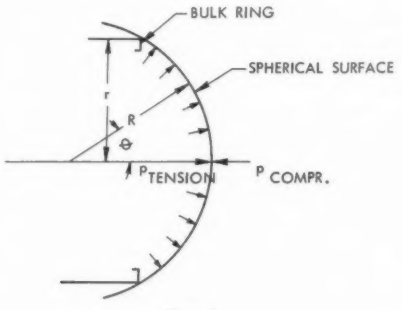

Fig. 1.

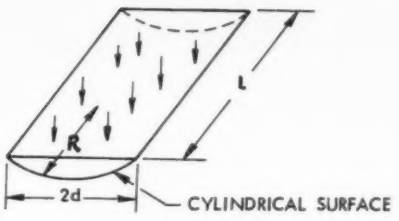

Fig. 2.

When the cylinder is short or when the length is less than the critical length, the governing equation is

$$pr = \frac{8\sqrt{6}\,\pi}{27}\,\frac{E}{(1 - \mu^2)^{3/4}}\,\frac{(t/D)^{5/2}}{L/D} = K\,\frac{(t/D)^{5/2}}{L/D} \tag{13}$$

Solving for t, substituting into the weight equation, we find

$$W = 2(2)^{3/5}\rho(p/K)^{2/5}L^{7/5}d^{8/5}[\theta/(\sin\theta)^{8/5}] \tag{14}$$

Differentiating W with respect to θ, equating to zero, and solving, we find the optimum value to be

$$\theta_{opt.} \sim 60°$$

Laminar Mixing in the Presence of Axial Pressure Gradients†

L. G. Napolitano and A. Pozzi
Associate Professor of Aerodynamics and Research Associate, Respectively, University of Naples, Italy
June 27, 1960

Studies of dissipative flows in the absence of solid boundaries have been mostly concerned with the isobaric case,[1, 2] the only exception being, to the authors knowledge, the work of reference (3). Yet, situations in which the mixing process occurs in the presence of a streamwise pressure gradient are far from being rare. A thorough investigation of the role played by pressure gradients in mixing phenomena appears to be necessary to the understanding of such situations and will certainly prove useful in many practical instances in which it may be desirable to control the mixing rates. Such an investigation is being carried out at the University of Naples and some preliminary results for plane, laminar, incompressible mixing in the presence of axial pressure gradients are reported here.

The basic Prandtl equations[4] can be reduced by means of the von Mises transformation[4] to the following partial differential equations:

$$\zeta_\xi = [1 - (\zeta/a)]^{1/2}\,\zeta_{\eta\eta} \tag{1}$$

with the boundary and initial conditions

$$\zeta(\xi, +\infty) = 0, \qquad \zeta(\xi, -\infty) = 1 - (U_{20}^2/U_{10}^2) \tag{1a}$$

$$\zeta(0, \eta) = 0 \quad \eta > 0, \qquad \zeta(0, \eta) = \zeta(\xi, -\infty) \quad (\eta < 0)$$

† The work presented in this paper was carried out under the sponsorship and the support of Contract AF(052)-160, administered by the European Office of the ARDC.

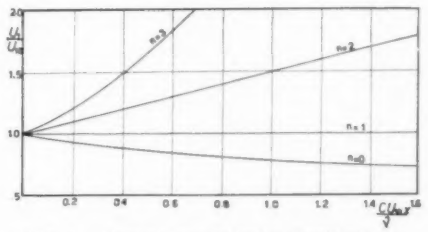

Fig. 1. Free-stream velocity distributions.

where

$$\left.\begin{aligned} \zeta &= [U_1^2(x) - U^2]/U_{10}^2, \qquad a(x) = U_1^2/U_{10}^2 \\ \xi &= \int_0^x \frac{U_1(x)}{U_{10}}\frac{dx}{L}, \qquad \eta = \frac{\psi}{U_{10}L}\left(\frac{U_{10}L}{\nu}\right)^{1/2} \end{aligned}\right\} \tag{2}$$

Here ψ is the stream function, $U_1(x)$ and $U_2(x)$ are the velocities of the two free streams, $U_{io} = (U_i)_{x=0}$, and all other symbols have conventional meanings.

Series solutions for Eq. (1) have been found in terms of the parameter $A = 1 - (U_{20}/U_{10})$. Each term of this series can be expressed by means of single quadrature and can be given, for particular classes of pressure gradients, a closed form in terms of the complementary error function and of its repeated integrals.

The essential quantities describing a mixing process are the rate of change of velocity along the x-axis; the spreading of the dissipative region, and the rate of entrainment of mass along the outer boundaries of the dissipative region. The influence of axial pressure gradients on the first of the above three quantities is discussed here. A full account of the method and a more detailed analysis of the flow field will be presented in a forthcoming paper.

The solution of Eq. (1) to within terms of order A^2 gives, at $y = \eta = 0$

$$\zeta(\xi, 0) = A + A^2\left\{\frac{1}{2\pi a} - \frac{1}{2} + \frac{1}{2\pi\xi}\int_0^\xi \frac{\sqrt{x(2\xi - x)}}{a}\frac{da}{dx}\,dx\right\}$$

The integral in this equation can be evaluated in closed form when the axial pressure gradient is taken to be of the type

$$\frac{2p_x}{\rho U_{10}^2} = \begin{cases} (1 - n)(C/L)\{1 + [(3 - n)/2](Cx/L)\}^{(2n-5)/(3-n)} & n \neq 3 \\ (2C/L)\exp(2Cx/L) & n = 3 \end{cases}$$

with n integer and C an arbitrary constant. For n equals to 0, 1, 2, and 3, respectively, one has

$$\left.\begin{aligned} &\zeta(\xi, 0) = A + A^2\{(2\pi a)^{-1} - (1/2) - (C\xi/8)\} \quad (n = 0) \\ &\zeta(\xi, 0) = A + A^2\{(2\pi)^{-1} - 1/2\} \quad (n = 1) \\ &\zeta(\xi, 0) = A + A^2\{(2\pi a)^{-1} - 1/2 + 1/(2\pi C\xi)[(2 + 2C\xi)/(1 + 2C\xi)^{1/2}\tan^{-1}(1 + 2C\xi)^{1/2} - \pi/2 - 8C\xi/(1 + C\xi)]\} \quad (n = 2) \\ &\zeta(\xi, 0) = A + A^2\left\{(2\pi a)^{-1} - 1/2 + \frac{2C\xi}{2\pi(1 + 2C\xi)}\left[\frac{\tan^{-1}(1 + 2C\xi)^{1/2}}{(1 + 2C\xi)^{1/2}} + \frac{2C\xi}{2 + 2C\xi}\right]\right\} \quad (n = 3) \end{aligned}\right\} \tag{3}$$

The case ($n = 1$) corresponds to zero pressure gradient and can therefore be used to check on the accuracy of the method since exact numerical solutions are available.[6] The comparison is shown in Table 1 for three indicative values of the ratio U_{20}/U_{10}, and it is seen that the accuracy is exceedingly good.

The nature of the pressure gradients considered is shown in Fig. 1. Therein, the velocity ratio $U_1(x)/U_{10}$ is plotted against $(CU_{10}x/\nu)$; $n = 0$ corresponds to a comparatively weak adverse pressure gradient; $n = 2$ corresponds to a moderate favorable pressure gradient, and $n = 3$ to a very strong favorable pressure gradient.

The values of $U(O, x)/U_1(x)$ as derived from Eqs. (3) are plotted against $(CU_{10}x/\nu)$ in Fig. 2 for the values of n considered and for indicative values of (U_{20}/U_{10}). The foreseeable qualitative trends are apparent. The ratio $U(O, x)/U_1(x)$, constant for an isobaric mixing with uniform initial conditions, is now a function of x which depends both on the pressure gradient and on the initial velocity ratio. For favorable gradients, $U(O, x)/U_1(x)$ tends to reach the value one more rapidly the stronger the pressure gradients, and for given p_x, the initial rate of growth increases as the ratio U_{20}/U_{10} decreases. The opposite occurs for adverse pressure gradients, the ratio $U(O, x)/U_1(x)$ decreases with x until conditions, for which the boundary-layer approach is no longer valid, are reached.

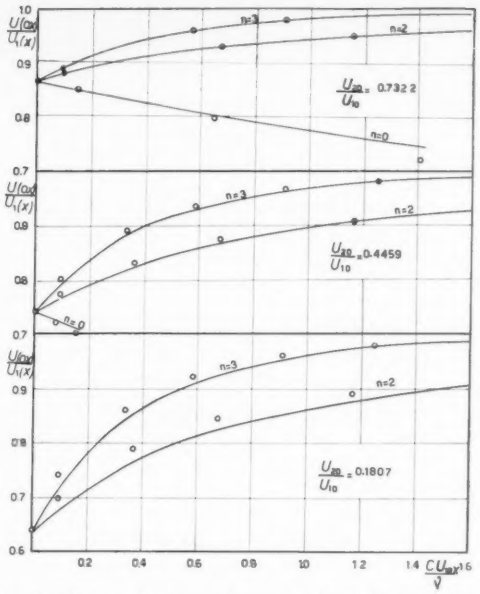

FIG. 2. Variation of the velocity ratio along the x-axis, taken to coincide with the streamline through the origin

A further insight into the nature of the phenomenon is gained by analyzing the results in terms of the values of the local free-stream velocity ratio $U_2(x)/U_1(x)$. This ratio is plotted in Fig. 3 for two indicative values of U_{20}/U_{10}. The slower stream, having a smaller "inertia" per unit volume is accelerated ($p_x < 0$) or decelerated ($p_x > 0$) more rapidly than the faster stream, the difference between the momentum fluxes of the two streams remaining constant. Thus, the free-stream velocity ratio shows roughly the same qualitative and quantitative behavior as the ratio $U(O, x)/U_1(x)$. This suggests that the noticed variation of the ratio $U(O)/U_1(x)$ might be essentially due to the analogous variation of the "local" values of the free-stream velocity ratio. To assess this point, we have computed the values of $U(O, x)/U_1(x)$ at each station as though the mixing were originated by two uniform streams with a velocity ratio equal to the one prevailing at the considered station. These new values are shown in Fig. 2 as circled points, and they are obviously not too different

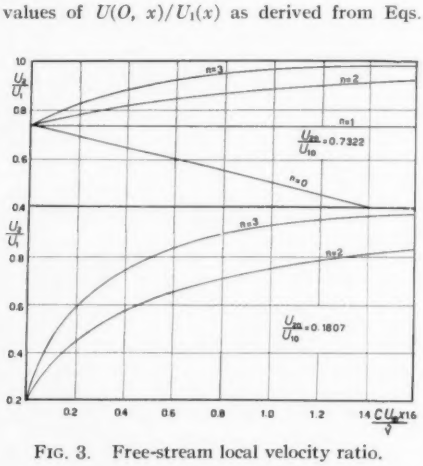

FIG. 3. Free-stream local velocity ratio.

TABLE 1

U_{20}/U_{10}	$U_0(O)/U_{10}$ Exact	$U_0(O)/U_{10}$ Present Method	Error (%)
0.7322	0.8698	0.8698	0
0.4459	0.7421	0.7420	0.01
0.1807	0.6407	0.6399	0.13

from the former ones, especially for large values of the initial velocity ratio U_{20}/U_{10}. This means that at any given station the velocity ratio on the x-axis, taken to coincide with the streamline through the origin, is roughly independent of the previous history of the interaction from 0 to $x(°)$.* The previous history will affect the actual position and shape of the streamline through the origin, the mass entrained, and the spread of the mixing region.

REFERENCES

[1] Fai, S. I., *Fluid Dynamics of Jets*, D. Van Nostrand Co. Inc., N. Y., 1954.

[2] Napolitano, L. G., Ferri, A., and Libby, P. A., *Recent Work on Mixing*, Combustion and Propulsion Third AGARD Colloquium, Pergamon Press, 1958.

[3] Napolitano, L. G., *On an Exact Solution of Laminar Mixing of Two Different Gases*, Journal of the Aero/Space Sciences, Readers' Forum. Vol. 27, No. 2, pp. 144–145, February, 1960.

[4] Schlichting, H., *Boundary Layer Theory*, Pergamon Press, 1955.

[5] Napolitano, L. G., *The Blasius Equation With Three-Point Boundary Conditions*, Quart. Appl. Math., Vol. 16, No. 4, April, 1959.

* (°) This consideration has conceivable practical importance from the computational point of view, since the ratio U(O)/U$_i$ for uniform free streams can be determined with accuracy in an almost immediate way.[2]

Some Comments on Standing Detonation Waves in a Combustion Tunnel

A. A. Kovitz
Assistant Professor, Gas Dynamics Laboratory,
Dept. of Mechanical Engineering,
Northwestern University, Evanston, Ill.

June 27, 1960

GROSS AND CHINITZ[1] reported an interesting series of experiments using a supersonic flow of combustible gas in a wind tunnel. One experiment concerned the production of a plane steady-state detonation wave—i.e., "... a wave in which an exothermal chemical reaction takes place and which moves with supersonic velocity with respect to the undetonated gas." (This definition is quoted from Hirschfelder and Curtiss[2].)

A curious result was the observation that the location in the tunnel of these plane steady-state detonation waves was a function of the energy released. Specifically, it was found that as Q/c_pT_1, Damköhler's second parameter, was increased, the position of the detonation shifted upstream to a new steady position and the wave area increased. This occurred without any observed changes in other upstream flow properties. In this note, an attempt is made to explain this change in wave position and area with change in Q/c_pT_1.*

Fig. 1 is a schematic drawing of the flow conditions ahead of the detonation wave and the wave configuration based upon observations in reference (1). The curves labeled "Q increasing" represent the distribution of fuel just upstream of the detonation. Increasing Q implies increasing the rate of fuel injection upstream of the nozzle throat (not shown in the figure). One of the unexpected results of the experiments was the appearance of a *flat* wave front in spite of the nonuniform fuel distribution. Gross[3] believes that the main reason for this is the fact that the waves are of a kind where the ratio of downstream to upstream density is greater than unity. This conforms to existing analyses of plane shock-wave formation and stability in a shock tube.

Let H be the heat of reaction and q_i be the rate of fuel injection into the tunnel. If m_t is the air-mass flow rate through the tunnel, then $Q = q_i H/(m_t + q_i)$ is the thermal energy added per unit of *total* mass flow. But if $q_i \ll m_t$ and $m_t = \rho_1 V_1 A_t$ (A_t is tunnel area upstream of oblique shocks), then this becomes

$$Q \cong q_i H/\rho_1 V_1 A_t \tag{1}$$

Now consider the portion of the flow intercepted by the detonation wave. Let $Q_{eff.}$ be the thermal energy added per unit mass of flow passing through the detonation. This may be formulated as

$$Q_{eff.} \cong q_{iD} H/\rho_1 V_1 A_D \tag{2}$$

where q_{iD} is the mass-flow rate of fuel through the detonation. In terms of a one-dimensional approximation to the actual flow, it is $Q_{eff.}$ that must be inserted into the Rankine-Hugoniot equations to obtain flow properties across the detonation—i.e., wave speed, pressure ratio, etc.

An estimate of q_i and q_{iD} could yield

$$q_i = \bar{\rho}_f V_1 A_t, \quad q_{iD} = \bar{\rho}_{fD} V_1 A_D \tag{3}$$

where $\bar{\rho}_f$ and $\bar{\rho}_{fD}$ are the average fuel densities at A_t and A_D, respectively. Then the ratio

$$Q/Q_{eff.} \cong \bar{\rho}_f/\bar{\rho}_{fD} \tag{4}$$

by use of Eqs. (1), (2), and (3). If the fuel distribution were uniform $\bar{\rho}_f = \bar{\rho}_{fD}$, implying $Q = Q_{eff.}$

An estimate of $\bar{\rho}_f/\bar{\rho}_{fD}$ may be obtained by noting that

$$\bar{\rho}_f \equiv \int_{A_t} \rho_f dA/A_t \quad \text{and} \quad \bar{\rho}_{fD} \equiv \int_{A_D} \rho_f dA/A_D$$

But

$$\int_{A_t} \rho_f dA \cong \int_{A_t - A_D} \rho_f dA + \int_{A_D} \rho_f dA$$

where $A_t - A_D$ is the difference between the detonation area and the tunnel area upstream of the oblique shocks. Therefore,

$$\bar{\rho}_f/\bar{\rho}_{fD} \cong (A_D/A_t)\left(1 + \int_{A_t - A_D} \rho_f dA \Big/ \int_{A_D} \rho_f dA\right) \tag{5}$$

It may be reasonable to neglect the ratio of the two integrals under the assumption that most of the fuel is flowing through the detonation. Then combining Eqs. (5) and (4) yields

$$Q_{eff.} \cong A_t Q/A_D \tag{6}$$

The *effective* Damköhler parameter is then

$$\bar{Q}_{eff.} = Q_{eff.}/c_pT_1 = A_t\bar{Q}/A_D \tag{7}$$

where $\bar{Q} = Q/c_pT_1$ is the quantity measured and reported by Gross and Chinitz.[1]

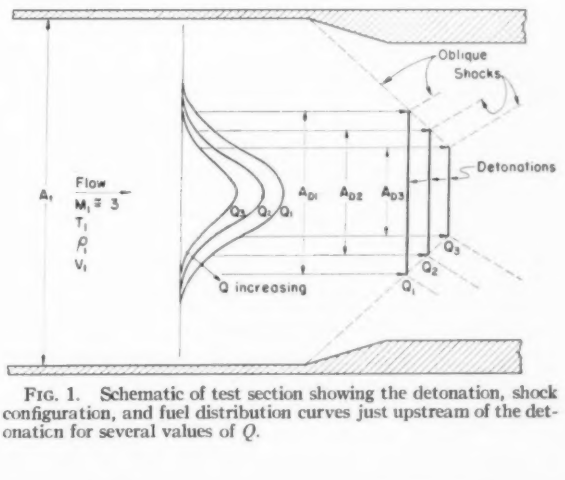

FIG. 1. Schematic of test section showing the detonation, shock configuration, and fuel distribution curves just upstream of the detonation for several values of Q.

* Recent experiments by Smith at ARO Inc., Tullahoma, Tenn., indicated some combustion occurred at the fuel injector. If it was moderate compared to that occurring in the wave then the discussion in this note is relevant.

TABLE 1
Values of $\bar{Q}/A_D$ Based on Data Taken From Reference (1)

$\bar{Q}$	A_D	$\bar{Q}/A_D$	$\bar{Q}$	A_D	$\bar{Q}/A_D$
1.53	1.7	0.90	3.18	4.0	0.79
2.6	2.2	1.2	3.2	5.0	0.64
2.68	2.9	0.92	3.4	5.5	0.62
3.0	4.0	0.75	5.0	5.9	0.85

Now, if one applies the classical Rankine-Hugoniot formulation to the flow passing through the steady, plane detonation, $\bar{Q}_{eff.}$ should remain constant if all other flow properties are not varied. Gross and Chinitz[1] indicate that they can vary $\bar{Q}$ and still obtain a steady, plane detonation with upstream Mach number unchanged. Essentially, only the position and area of the detonation changes. All other upstream properties remain fixed. One might also note that the downstream pressure does not change much because the oblique shock configuration is quite unaltered. Put in terms of one-dimensional flow, this means that $\bar{Q}_{eff.}$ should remain constant. From Eq. (7), with A_t constant, this criterion leads one to expect

$$\bar{Q}/A_D \cong \text{constant} \tag{8}$$

This very approximate result may be checked using the data given in reference (1). The numerical results are presented in Table 1. Actually, all are for the same value of T_1 with H_2 burning in air. The units of A_D are arbitrary for these purposes.

In view of the approximations made in obtaining Eq. (8), it seems reasonable to say that the numerical result at least does not contradict the explanation. It could be expected to be better if the ratio of integrals in Eq. (5) were not neglected. In other words, when Q or $\bar{Q}$ (for lean fuel-air ratios) is increased, the wave speed may be expected to increase when downstream pressure remains constant. This causes the wave to move forward, and increase in area until it is intercepting flow with the same $\bar{Q}_{eff.}$ as it did in its initial position.

Finally, one might mention the ignition hysteresis effect observed by Gross and Chinitz[1]—i.e., that once the combustion is initiated at a minimum ignition temperature, it will persist even though the static temperature T_1 ahead of the wave is then decreased below the necessary initial starting temperature. With this decrease in T_1 the wave again moves forward in much the same manner as for increase in Q. It is tempting to explain this in terms of keeping $\bar{Q}_{eff.}$ constant just as was done previously in explaining the wave growth with increase in Q.

REFERENCES

[1] Gross, R. A., and Chinitz, W., *A Study of Supersonic Combustion*, Journal of the Aero/Space Sciences, Vol. 27, No. 7, pp. 517–524, July, 1960.

[2] Hirschfelder, J. O., and Curtiss, C. F., *Theory of Detonations, I. Irreversible Unimolecular Reaction*, J. Chem. Phys., Vol. 28, No. 6, pp. 1130–1147, June, 1958.

[3] Private communication.

Hypervelocity Gasdynamic Charts for Equilibrium Air†

Richard W. Ziemer*
Physical Research Laboratory, Space Technology Laboratories, Inc., Los Angeles, Calif.
June 27, 1960

THIS NOTE describes a set of hypervelocity gasdynamic charts for air that recently has been prepared. The gasdynamic properties associated with a traveling normal shock, stationary normal shock, stagnation point, and reflected normal shock have been computed and graphed for incident-shock Mach numbers of up to 50.[1] The computational method and accuracy, and the extent of the data are given. The availability of the report containing the series of charts is indicated.

† This work was performed under sponsorship of the USAF Ballistic Missile Division, Contract AF 04(647)-309.

* Now Senior Scientists, Astro Systems and Research Labs., Norair.

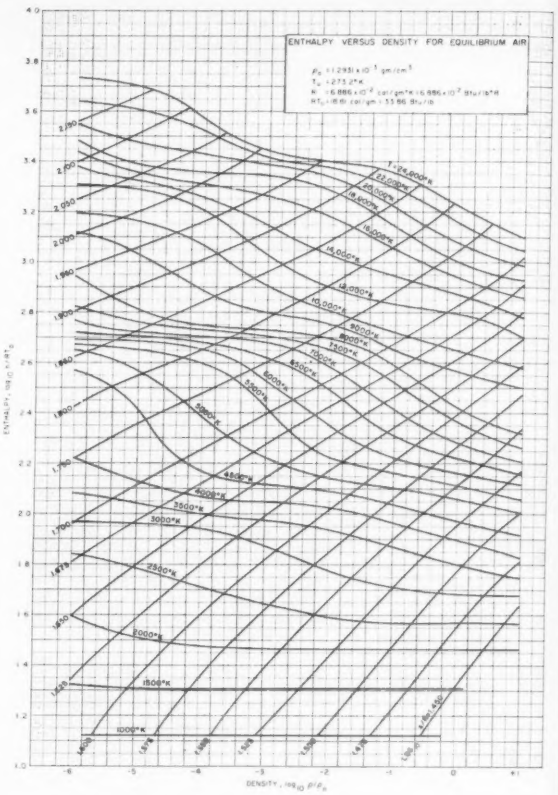

FIG. 1. Thermodynamic state properties of equilibrium air; enthalpy versus density with curves of constant temperature and constant entropy. (From Gilmore's data.[2])

INTRODUCTION

For theoretical or experimental research in areas of re-entry heating, magnetoaerodynamics and other phenomena of hypersonic aerodynamics, the thermodynamic properties of the high-temperature shocked gas must be known. To the present time, real-gas equilibrium composition and thermodynamic properties of air to 24,000°K. and the Hugoniot curves for single normal shocks at speeds up to Mach 50 have been computed by Gilmore.[2] Using the data of Hilsenrath and Beckett,[3] Feldman[4] computed and charted a rather extensive set of curves including the various gasdynamic properties associated with traveling, reflected, and stationary shock fronts as functions of shock speed and initial density for a range of shock speeds up to about Mach 22. These charts are extremely convenient for use in shock-tube research.

Although this range is sufficient for studies with pressure-driven and combustion-driven shock tubes, it is far below the shock speeds obtainable and normally used in electromagnetic shock tubes. Moreover, advances in space technology have brought into consideration vehicles with speeds exceeding satellite velocity. Hence, there arose a need for an extension of the gasdynamic charts to higher shock speeds. For this reason, several of the more important shock relations were computed up to the limit of the available thermodynamic data, extending some of the previous charts to shock speeds of about Mach 50. These extended gasdynamic charts are reported in reference 1.

COMPUTATIONAL METHOD AND RESULTS

The computation of the gasdynamic properties, unlike the electronic-computer method of Feldman, was a successive-

approximation hand computation utilizing normal-shock equations and graphical thermodynamic-state data. The accuracy of the method is dependent on the assumed curvature between data points in plotting the tabular data of Gilmore and the error in logarithmic interpolation between curves. It was estimated that these errors are between 1 and 10 per cent, with the error of the major portion of the data less than 5 per cent. The charts, in general, are not as accurate as could be obtained with an electronic computer, but the method is justified on the basis of the relatively low cost in time and effort. The charts should, nonetheless, prove useful to those working in hypervelocity gasdynamics until more refined calculations are available.

The series of gasdynamic charts of reference 1 include the following properties: flow velocity, density, pressure, temperature, internal energy and enthalpy associated with a traveling normal shock, stationary normal shock (bow wave), stagnation point, and reflected normal shock. Curves are plotted versus incident-shock velocity for initial air densities of 10^{-1} to 10^{-5} times atmospheric density and an initial temperature of 273.2°K. The range of incident-shock speeds is from Mach 10 to Mach 50 or to the limit of the thermodynamic data, 24,000°K. Included is a plot of Gilmore's data in the form of a Mollier diagram. The thermodynamic-state data were plotted as enthalpy versus density with lines of constant entropy and temperature because the curves become more orthogonal and, therefore, greater accuracy in reading is obtainable. This general plot is presented in Fig. 1.

It is felt that the gasdynamic charts are of general usefulness to many scientists and engineers and may satisfy a current need. However, the volume of the charts precludes publishing in a technical journal. The report is available to those interested and copies may be obtained by request to the author.

Reference

[1] Ziemer, R. W., *Extended Hypervelocity Gas Dynamic Charts for Equilibrium Air*, Rept. STL/TR-60-0000-09093, Space Tech. Laboratories, April 14, 1960.

[2] Gilmore, F. R., *Equilibrium Composition and Thermodynamic Properties of Air to 24,000°K.*, Rept. RM-1543, RAND Corporation, August 24, 1955.

[3] Hilsenrath, J., and Beckett, C. W., *Table of Thermodynamic Properties of Argon-Free Air to 15,000°K.*, ARO Rept. AEDC-TN-56-12, September, 1956.

[4] Feldman, S., *Hypersonic Gas Dynamic Charts for Equilibrium Air*, Res. Rept. 40, AVCO Research Laboratory, January, 1957.

A Note on the Impact Pressure Loading of a Rigid Plastic Spherical Shell*

R. Sankaranarayanan**

Research Assistant Professor, Dept. of Aerospace Engineering and Applied Mechanics, Polytechnic Institute of Brooklyn, N.Y.

June 29, 1960

Introduction

According to conventional elastic analysis, the maximum load which a given structure can carry is the smallest load that produces plastic behavior at the most highly stressed portion of the structure. However, such an estimate neglects the reserve plastic strength which most redundant structures possess, even after some stresses have exceeded the yield stress. If the load is increased above that predicted by the elastic analysis, there will exist a more or less sharply defined point at which small-load increments rapidly produce large deformation. The load at which this takes place is called the "collapse load."

When an ideal rigid plastic structure is subjected to a load greater than the collapse load, no equilibrium configuration of the stresses can exist and the structure will accelerate. Obviously, if such a load is applied for any appreciable time, the resulting deformations will become very large and the structure will no longer be serviceable. However, if the load is applied for an extremely short time, the inertial resistance of the structure may be sufficient to prevent excessive motion.

In this paper, the behavior of a complete spherical shell under stepwise-impulsive loading by uniform external pressure is discussed. The material of the shell is assumed to be rigid perfectly-plastic and to obey Tresca's yield condition and the associated-flow rule. The load is assumed to be greater than the static collapse load and to act for a short period of time.

Basic Equations

The state of stress in a rotationally symmetric shell is described by four generalized stresses: the circumferential and meridional bending moments M_ϑ and M_φ and the circumferential and meridional membrane N_ϑ and N_φ. Similarly, the state of strain is described by four generalized strains which may, in turn, be expressed in terms of the meridional and normal components of the displacement V and W.

The plastic yield condition for a rotationally symmetric shell based on the Tresca criterion has been described by Onat and Prager.[1] The yield surface is a closed convex hypersurface in the four-dimensional stress space, with the rectangular Cartesian coordinates M_ϑ, M_φ, N_ϑ, and N_φ.

If the load is applied impulsively, the generalized stresses must satisfy three equations of motion, which may be written

$$\left.\begin{aligned} &(n_\varphi \sin\varphi)' - n_\vartheta \cos\varphi = \sin\varphi(s + \gamma\ddot{v}) \\ &(s \sin\varphi)' + \sin\varphi(p_r + n_\vartheta + n_\varphi) = \gamma\ddot{w}\sin\varphi \\ &k[(m_\varphi \sin\varphi)' - m_\vartheta \cos\varphi] = s \sin\varphi \end{aligned}\right\} \quad (1)$$

where we have defined

$$n = N/N_0 = N/2\sigma_0 H, \quad m = M/M_0 = M/\sigma_0 H^2, \quad s = S/N_0,$$
$$p_r = R\,P_r/N_0, \quad k = M_0/R\,N_0, \quad v = V/R, \quad w = W/R,$$
$$\tau = t/T_0, \quad \gamma = \rho R^2/N_0 T_0^2$$

σ_0 is the tensile yield stress of the material and ρ is the surface density. The shell is of uniform thickness $2H$, and radius R, and is subjected to a uniform radial pressure P_r. Primes and dots denote differentiation with respect to φ and τ, respectively. The generalized strain rates and the velocities are related by

$$\epsilon_\vartheta = \dot{v}\cot\varphi - \dot{w}, \qquad \epsilon_\varphi = \dot{v}' - \dot{w}$$
$$\kappa_\vartheta = -k\cot\varphi(\dot{v} + \dot{w}'), \quad \kappa_\varphi = -k[\dot{v} + \dot{w}']' \quad (2)$$

Onat and Prager[1] have defined the yield surface for a rotationally symmetric shell in terms of the parameters p, q, and r which are related to the strain rates by

$$p = -\epsilon_\vartheta/h\kappa_\varphi, \quad q = -(\epsilon_\vartheta + \epsilon_\varphi)/h(\kappa_\vartheta + \kappa_\varphi), \quad r = -\epsilon_\varphi/h\kappa_\varphi.$$

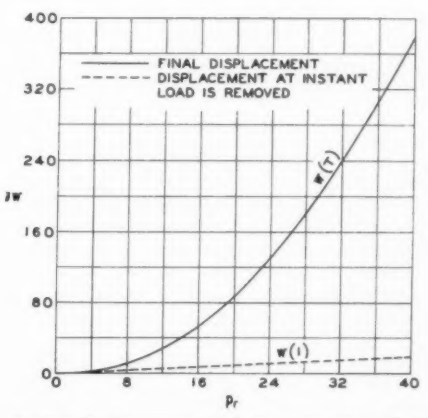

Fig. 1. Radial displacement of shell as function of the load.

* This research was supported by the USAF through the Air Force Office of Scientific Research of the Air Research and Development Command, under Contract Number AF 49(638)-302. Reproduction in whole or in part is permitted for any purpose of the United States Government.

** On leave of absence at the Polish Academy of Sciences, Warsaw, Poland.

The yield surface consists of several regions which are distinguished by the relative magnitudes of p, q, and r.

Solution

The first problem is to determine the static collapse load. For this consider the velocity field given by

$$\dot{w} = \dot{w}_0, \quad \dot{v} = 0 \tag{3}$$

The corresponding strain rates are

$$\epsilon_\vartheta = \epsilon_\varphi = -\dot{w}_0, \quad \kappa_\vartheta = \kappa_\varphi = 0 \tag{4}$$

Consequently, the parameters p, q and r tend to infinity. It follows[1] that

$$n_\vartheta = n_\varphi = -1, \quad m_\vartheta = m_\varphi = 0 \tag{5}$$

In the case of static loading, the equations of equilibrium are obtained by deleting the inertia terms in Eqs. (1). Substitution of Eqs. (5) into the equations of equilibrium yields

$$p_{r_{\text{static}}} = 2 \tag{6}$$

The solution given by Eqs. (3), (5), and (6) is statically and kinematically admissible.

If the load is slightly greater than the static collapse load, it is reasonable to expect that the same plastic regime is applicable for dynamic loading. This hypothesis is tested by solving Eqs. (1) and (5). The resulting radial acceleration is given by

$$\gamma\ddot{w} = p_r - 2 \tag{7}$$

where $p_r \geq p_{r_{\text{static}}}$ for $0 \leq \tau \leq 1$.

Since there is no deformation prior to the application of the load

$$w(\varphi, 0) = \dot{w}(\varphi, 0) = 0 \tag{8}$$

Integration of Eq. (7) subject to the initial conditions (8) leads to

$$\gamma\dot{w} = (p_r - 2)\tau, \quad \gamma w = (p_r - 2)(\tau^2/2)$$
$$0 \leq \tau \leq 1, \quad p_{r_{\text{static}}} \leq p_r \tag{9}$$

The inequality $\dot{w} \geq 0$ is obviously satisfied for $p_{r_{\text{static}}} \leq p_r$.

At $\tau = 1$ the external load is removed. However, since the shell is already in motion, it continues to move until all of the kinetic energy has been dissipated into plastic work. Assuming that the same plastic regime continues to apply during this second phase of motion, the same equations are now to be solved with $p_r = 0$. The radial acceleration is now given by

$$\gamma\ddot{w} = -2 \tag{10}$$

Integration of Eq. (10) subject to the continuity conditions that at $\tau = 1$, $\dot{w}$ and w must be continuous, leads to

$$\gamma\dot{w} = (p_r - 2\tau); \quad \gamma w = -\tau^2 + p_r\tau - (p_r/2)$$
$$1 < \tau \leq T, \quad p_{r_{\text{static}}} \leq p_r \tag{11}$$

The inequality $\dot{w} \geq 0$ leads to the requirement that τ be less than T where

$$T = p_r/2 \tag{12}$$

Discussion

Fig. 1 shows the displacement at the instant of the removal of the load and the final displacement as a function of the load. As the magnitude of the load is increased, the displacement during application varies linearly, in accordance with Eq. (9). However, the length of time for which the deformation continues and the corresponding total displacement increase rapidly with increasing load. For a load $p = 40$, about 95 per cent of the final displacement occurs after the load is removed.

Reference

[1] Onat, E. T., and Prager, W., *Limit Analysis of Shells of Revolution*, Royal Netherlands Acad. Sc. Proc., Ser. B Vol 57, No. 5, pp. 534–548, 1954.

Simple Graphical Method for Temperature Distribution in Bodies With Linear Change in Environment Temperature

Walter Unterberg
Senior Technical Specialist, Rocketdyne, Canoga Park, Calif.
June 27, 1960

Symbols

- a = thermal diffusivity of body
- l = pX^2/a, linear proportionality constant in $T_e = lt^+$
- n = number of steps in approximation
- p = linear proportionality constant in $T_e = pt$
- $2r$ = duration of each step, in t^+ units
- t = time
- t^+ = $t(a/X^2)$, nondimensional (Fourier) time—abscissa on Gurney-Lurie chart
- T = temperature
- T^+ = $(T - T_e)/(T_i - T_e)$, nondimensional body temperature—ordinate on Gurney-Lurie chart
- X = half-thickness of body
- τ^+ = $2nr$, value of t^+ at end of linear T_e change

Subscripts

- e = environment
- i = initial (time zero)
- s = simple-step T_e change—Gurney-Lurie chart condition

When the environment temperature of a body is subjected to a combination of stepwise changes with time, it has been shown[1] that the charts of Gurney-Lurie[2] and others for a simple-step change in environment temperature may be applied, due to the linearity of the solutions. Here the case of a linear environment-temperature change with time is treated, based on the same principle.

An approximation to the linear variation by a series of finite steps is first considered. It is then shown that when the steps are allowed to degenerate into the straight line, the body-temperature response is simply found from the area under the applicable Gurney-Lurie simple-step curve, so that it is possible for this case to construct a set of generalized charts.

The entire temperature field was assumed to be zero at time zero, but what follows is equally applicable to finite values of T_i. Further, all times are expressed in nondimensional Fourier time t^+. Fig. 1 is a plot of T_e vs. t^+, showing the linear variation

$$T_e = pt = lt^+ \; (0 < t^+ < \tau^+)$$

circumscribed by n steps, each of duration $2r$ and height $2rl$ (except for first-step height rl).

Noting that here $T = T_e(1 - T^+)$, and applying the superposition of simple-step solutions for all individual steps yields

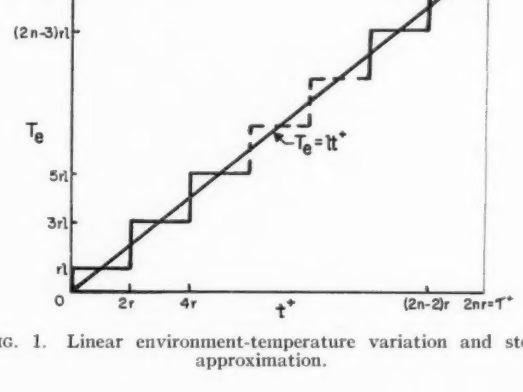

FIG. 1. Linear environment-temperature variation and step approximation.

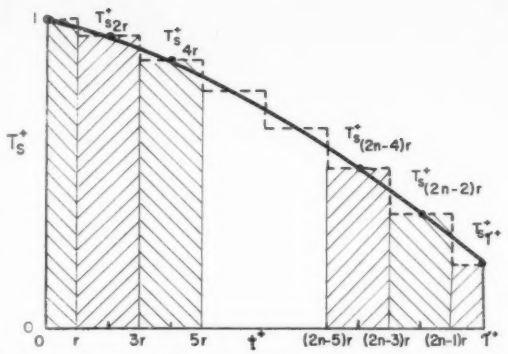

FIG. 2. Typical simple-step Gurney-Lurie curve for fixed resistance and body coordinate.

$r(1 + 2\sum_{k=1}^{n-1} T_{s_{2kr}}{}^+ + T_{s_{\tau^+}}{}^+)$ = sum of shaded areas → area under curve as $n \to \infty$ and $r \to 0$.

$$T_{\tau^+} = rl(2n - 1 - 2\sum_{k=1}^{n-1} T^+_{s_{2kr}} - T^+_{s_{\tau^+}}) \ldots \quad (1)$$

This may be nondimensionalized and written in the form

$$\tau^+ T^+_{\tau^+} = r(1 + 2\sum_{k=1}^{n-1} T^+_{s_{2kr}} + T^+_{s_{\tau^+}}) \ldots \quad (2)$$

Thus, a solution for the body temperature at terminal time $\tau^+ = 2nr$ may be obtained in terms of n, r, and corresponding $T_s{}^+$ values. $T_s{}^+$ is the ordinate of the Gurney-Lurie charts[3] for simple-step T_s changes, and t^+ the abscissa. The chart for the proper resistance and body coordinate must be used. As n is increased and r reduced accordingly, the accuracy of the answer increases. In the limit, as n tends to infinity and r to zero, the steps will vanish into the straight line.

To pursue this further, Fig. 2 was drawn, showing a typical $T_s{}^+$ vs. t^+ Gurney-Lurie curve for fixed dimensionless body coordinate and dimensionless resistance over the time interval $0 < t^+ < \tau^+$, divided into n steps of duration $2r$. It is seen that the right-hand side of Eq. (2) is equivalent to the sum of the shaded areas on Fig. 2, and further, that in the limit the sum of the shaded arcas becomes the area under the curve. Then Eq. (2) becomes simply

$$T^+_{\tau^+} = \text{area under curve } (0 < t^+ < \tau^+)/\tau^+ = \text{average } T_s{}^+ \text{ over } (0 < t^+ < \tau^+) \ldots \quad (3)$$

Thus, a graphical or planimeter integration of the area under the applicable simple-step Gurney-Lurie curve (on linear axes) gives the body-temperature variation resulting from a linear change with time of environment temperature. The result is general and may be used to solve for a succession of points along a linear change, be it an increase or decrease. A set of generalized charts for linear change may be constructed, therefore, from integration of the simple step charts.

A numerical check for one case (midplane of slab and zero resistance) revealed perfect agreement between the present integration method and an exact analytical solution.[4] Further, the finite-step solution was within 1 per cent of the exact solution when either n exceeded 10 or r was less than 1/10.

REFERENCES

[1] Landis, F., Tearnen, J. O., *Graphical Methods for the Temperature Response of Bodies in a Varying Temperature Medium*, ASME Paper No. 55-A-141, November, 1955.

[3] Gurney, H. P., and Lurie, J., *Charts for Estimating Temperature Distribution in Heating or Cooling Solid Shapes*, Industrial Engineering Chemistry, Vol. 15, No. 11, pp. 1170–1172, November, 1923.

[3] McAdams, W. H., *Heat Transmission*, 3rd Ed., p. 35, et seq., McGraw Hill, Inc., New York, 1954.

[4] Anthony, M. L., *Temperature Distribution in Slabs with Linear Temperature Rise at One Surface (Part 1 - Distributions in a Single Slab)*, General Discussion on Heat Transfer IME-ASME, pp. 250-253, September, 1951.

On the Use of Quaternions to Describe the Angular Orientation of Space Vehicles

T. E. Surber
North American Aviation, Inc., Los Angeles Division, Los Angeles, Calif.
June 31, 1960

SYMBOLS

- Λ = conjugate of quaternion λ
- η = pure quaternion
- $(\ )\sigma$ = conjugate of $(\ )$
- $D(\ )$ = operator $d(\ )/dt$
- Ω = skew-symmetric tensor (see Eq. 13)

LOH[1] presented a set of dynamical equations generalized to analyze the dynamics of ballistic configurations as well as conventional aircraft. Consistent with standard aerodynamic practice, Loh has used the Euler-angle technique to specify the angular orientation of the vehicle relative to a set of inertial axes. Consequently, the resulting set of equations contain numerous trigonometric terms. Because of the trigonometric form of the angular displacements, the use of Eulerian angles to specify the vehicle angular orientation results in a relatively large amount of computing time. A more serious drawback is the presence of a discontinuity in the differential equations which express the Euler-angle rates in terms of vehicle angular rates. The only way of avoiding this discontinuity is by the introduction of a cumbersome change of variables in the middle of the integration.

It is the purpose of this note to present an alternative angular-orientation scheme based on quaternions. The proposed method specifies the angular orientation of the vehicle in terms of non-trigonometric variables, hence, the inherent difficulties of the Euler technique are avoided. The quaternion method, because of its generality, can be incorporated into any dynamic investigation where it is necessary to specify angular orientation.

Courant and Hilbert[2] describe quaternions as "hypercomplex" numbers with three imaginary units i, j, k which satisfy the relations

$$(i)^2 = (j)^2 = (k)^2 = -1$$
$$ij = k, \quad jk = i, \quad ki = j$$
$$ij + ji = 0, \quad ik + ki = 0, \quad jk + kj = 0$$

The general quaternion is

$$\lambda = \lambda_0 + i\lambda_1 + j\lambda_2 + k\lambda_3 \quad (1)$$

where $\lambda_0, \lambda_1, \lambda_2$ and λ_3 are real numbers.

In general, we can write the general form of a quaternion in terms of a rotation angle ω and the norm (length) of the quaternion (see Whittaker[3])

$$\lambda = \lambda_0 + i\lambda_1 + j\lambda_2 + k\lambda_3 = \sqrt{N(\lambda)}\ [\cos(\omega/2) + \sin(\omega/2) \times (i\cos\alpha + j\cos\beta + k\cos\gamma)] \quad (2)$$

where α, β, and γ are the direction cosines, and ω is the angle of rotation about the line defined by α, β, and γ. From this relation we obtain the relationship of the quaternion components to the rotation angle and direction cosines:

$$\lambda_0 = \cos(\omega/2), \qquad \lambda_1 = \cos\alpha \sin(\omega/2)$$
$$\lambda_2 = \cos\beta \sin(\omega/2), \qquad \lambda_3 = \cos\gamma \sin(\omega/2)$$

The problem now is to express the components of the quaternion in the form of a rotation matrix similar to the familiar Euler transformation matrix which relates a vector in one axis system to another axis system. The desired transformation is

$$\begin{bmatrix} X_E \\ Y_E \\ Z_E \end{bmatrix} = \begin{bmatrix} \lambda_0^2 + \lambda_1^2 - \lambda_2 - \lambda_3 & 2(\lambda_1\lambda_2 - \lambda_3\lambda_0) & 2(\lambda_1\lambda_3 + \lambda_2\lambda_0) \\ 2(\lambda_1\lambda_2 + \lambda_3\lambda_0) & \lambda_0^2 + \lambda_2^2 - \lambda_1^2 - \lambda_3^2 & 2(\lambda_2\lambda_3 - \lambda_1\lambda_0) \\ 2(\lambda_1\lambda_3 - \lambda_2\lambda_0) & 2(\lambda_2\lambda_3 + \lambda_1\lambda_0) & \lambda_0^2 + \lambda_3^2 - \lambda_1^2 - \lambda_2^2 \end{bmatrix} \begin{bmatrix} X_B \\ Y_B \\ Z_B \end{bmatrix} \tag{3}$$

The matrix (3) expresses the relationship between the vehicle body axes and the earth axes in terms of quaternion components. The Euler transformation matrix (4) is identical to (3):

$$\begin{bmatrix} X_E \\ Y_E \\ Z_E \end{bmatrix} = \begin{bmatrix} \cos\theta\cos\psi & \sin\phi\sin\theta\cos\psi - \cos\phi\sin\psi & \cos\phi\sin\theta\cos\psi + \sin\phi\sin\psi \\ \cos\theta\sin\psi & \sin\phi\sin\theta\sin\psi + \cos\psi\cos\phi & \cos\phi\sin\theta\sin\psi - \sin\phi\cos\psi \\ -\sin\theta & \sin\phi\cos\theta & \cos\phi\cos\theta \end{bmatrix} \begin{bmatrix} X_B \\ Y_B \\ Z_B \end{bmatrix} \tag{4}$$

This fact allows us to define the initial quaternion components in terms of the familiar Euler angles:

$$\lambda_0^2 = (1/4)[1 + \cos\theta\cos\psi + \sin\theta\sin\psi\sin\phi + \cos\psi\cos\phi + \cos\theta\cos\phi] \tag{5}$$

$$\lambda_1^2 = (1/4)[1 + \cos\theta\cos\psi - \sin\theta\sin\psi\sin\phi - \cos\psi\cos\phi - \cos\theta\cos\phi] \tag{6}$$

$$\lambda_2^2 = (1/4)[1 + \sin\theta\sin\psi\sin\phi + \cos\psi\cos\phi - \cos\theta\cos\phi - \cos\theta\cos\psi] \tag{7}$$

$$\lambda_3^2 = (1/4)[1 - \cos\theta\cos\psi - \sin\theta\sin\psi\sin\phi - \cos\psi\cos\phi + \cos\vartheta\cos\phi] \tag{8}$$

One relation remains to be determined: the differential equations describing the rate of change of the quaternion components in terms of the vehicle angular velocities.

Define a fixed reference frame by the symbol F and the moving reference frame by M. The formula that expresses a rotation is (3)

$$\boldsymbol{\zeta}_F = \lambda\eta_M\Lambda \tag{9}$$

Now, for an arbitrary λ, $\boldsymbol{\zeta}$ (the pure or vector part of the quaternion) is fixed in a moving frame M, and suppose that the moving frame M coincides with the fixed frame F when $\lambda = 1$. Thus, from Eq. (9)

$$\boldsymbol{\zeta}_M = \Lambda\boldsymbol{\zeta}_F\lambda \tag{10}$$

which gives the components of the vector $\boldsymbol{\zeta}$ in the two frames M and F.

Differentiating both sides of Eq. (10)

$$D(\boldsymbol{\zeta}_M) = [D(\Lambda)\mathfrak{L} - (D(\Lambda)\mathfrak{L})\sigma]\boldsymbol{\zeta}_M \tag{11}$$

Both $D(\Lambda)\mathfrak{L}$ and $\boldsymbol{\zeta}_M$ may be shown to be pure quaternions, therefore Eq. (11) may be placed in the following equivalent cross product form:

$$D(\boldsymbol{\zeta}_M) = 2[D(\Lambda)\mathfrak{L} \times \boldsymbol{\zeta}_M]$$

From basic mechanics, the following comparison is obvious

$$D(\boldsymbol{\zeta}_M) = \boldsymbol{\omega}_M \times \boldsymbol{\zeta}_M$$

where $\boldsymbol{\omega}_M$ is the angular velocity vector of the moving frame presented in terms of the moving frame angular velocities

$$\boldsymbol{\omega}_M = \mathbf{i}p + \mathbf{j}q + \mathbf{k}r \text{ (angular velocity components),}$$

hence

$$D(\lambda) = -(1/2)\lambda\omega_M \tag{12}$$

The right side of Eq. (12) may be expanded by multiplying λ by ω_M

$$\begin{bmatrix} D(\lambda_0) \\ D(\lambda_1) \\ D(\lambda_2) \\ D(\lambda_3) \end{bmatrix} = -\frac{1}{2}\begin{bmatrix} 0 & -p & -q & -r \\ p & 0 & -r & q \\ q & r & 0 & -p \\ r & -q & p & 0 \end{bmatrix}\begin{bmatrix} \lambda_0 \\ \lambda_1 \\ \lambda_2 \\ \lambda_3 \end{bmatrix} = -\frac{1}{2}\Omega\lambda \tag{13}$$

where $\lambda_0^2 + \lambda_1^2 + \lambda_2^2 + \lambda_3^2 = 1$

Eq. (13) gives the differential equation for the rate of change of the quaternions in terms of the vehicle angular rates.

The general equations of motion for any vehicle become in vector notation

$$D(m\mathbf{v}_B) = \mathbf{F} - \boldsymbol{\omega}_M \times (m\mathbf{v}_B) + mg\lambda$$

$$D(I\boldsymbol{\omega}_M) = M - \boldsymbol{\omega}_M \times (I\boldsymbol{\omega}_M)$$

$$[V_E] = [\text{Eq. (3)}][V_B]$$

$$D(\lambda) = -(1/2)\Omega\lambda$$

Initial values of λ are obtained from Eqs. (5), (6), (7), and (8). Hence, the dynamical and kinematical relations are given completely by the above equations.

References

[1] Loh, W. H. T., *Spinning Ballistic Missiles*, Journal of the Aero/Space Sciences, Readers' Forum, Vol. 26, No. 12, p. 844–846, December, 1959.

[2] Courant-Hilbert, *Methods of Mathematical Physics*, Vol. 1, Interscience Publishers, Inc., New York, 1953.

[3] Whittaker, E. T., *Treatise on the Analytical Dynamics of Particles and Rigid Bodies*, Cambridge University Press, 1959.

Notice to Contributors

To expedite review, an additional copy of both the manuscript and figures should be submitted. The manuscript submitted for publication *must* be a double- or triple-spaced original. There should be wide margins on all sides of the sheets and triple spacing around formulas to allow for the marking of directions to the printer.

Original drawings (jet black India ink on white paper or tracing cloth) should accompany the manuscript. *(Blueprints are not acceptable.)* Photographs *must* be on glossy white paper. The smallest lettering on 8- by 10-in. figures should be no less than $^1/_4$ in. high.

Formulas should be typewritten or carefully written in pen and ink. The difference between capital and lower-case letters and Greek symbols should be clearly distinguished.

Turn to Inside Back Cover for Further Details.

(3)

(4)

(5)
(6)
(7)
(8)

(12)
ying λ

(13)

hange

me in

nd (8).
com-

/Space
9.
science

les and

REQUIREMENTS *for* CONTRIBUTIONS

to the publications of the

INSTITUTE *of the* AEROSPACE SCIENCES

The Institute of the Aerospace Sciences invites both members and nonmembers from any country to submit papers for publication in the JOURNAL OF THE AEROSPACE SCIENCES and AEROSPACE ENGINEERING. The Institute, following the practice of other societies, does not pay for contributions.

The following directions for the preparation of papers, if followed by authors, will save correspondence, avoid the return of papers for changes, minimize the work of preparation for the printer, and save the expense due to the charges made for "author's corrections."

MANUSCRIPTS: The original typewritten copy of the paper is desired. **To expedite review, an additional copy of both the manuscript and figures should be submitted.** The manuscript must be double or triple spaced on one side of white paper sheets, consecutively numbered. There should be wide margins to allow for the marking of directions to the printer. Correcting, changing, or adding to papers after they are in type is costly. It is, therefore, imperative that papers submitted be in final form. Typographical errors may be corrected on proofs, but if authors wish to add material, they may do so at their own expense. In mailing, drawings may be rolled, but manuscripts should be sent flat. Send by first-class mail (register if you wish for your own protection) to the Editorial Office, Institute of the Aerospace Sciences, 2 East 64th Street, New York 21, N.Y. All manuscripts will be examined by the Editorial Committee and by the Editor. Authors will be advised as promptly as possible whether the paper is acceptable for publication.

TITLES: The title of the paper should be brief. The name and initials of the author should be written as he prefers. The use of the full name of an author is advocated because of the frequent duplication of initials and surnames which sometimes makes it difficult to establish the identity of the author. This is particularly important for large annual indexing and abstracting services. All titles and degrees or honors are omitted. The name of the organization with which the author is associated should be placed after his name on a separate line. The date on which the paper is received will be inserted by the Editor. The author's title or position should be indicated in a footnote.

SUMMARIES OR ABSTRACTS: An abstract to be printed at the beginning should accompany each article. It should be adequate as an *index* and as a *summary*. It should contain a statement of major conclusions reached, since summaries in many cases constitute the only source of information used in compiling scientific reference indexes. Abstracts printed in other journals, especially foreign, in most cases consist of summaries from printed papers. The summary should explain as adequately as possible the major conclusions to a nonspecialist in the subject and should contain from 100 to 300 words, depending on the length of the paper.

SUBHEADINGS: Subheadings should be inserted by the author at frequent intervals. The work of editorial preparation will be simplified by the author's provision of many subheadings.

MATTER USUALLY DELETED: Photographs or illustrations of little technical interest and not showing advances in general practice. Too detailed tabular matter (general results of such tables may be included in the text). Lengthy descriptions of materials or processes or of preliminary experiments or theories that preceded final results; salient features only are of interest.

REFERENCES: References should be numbered consecutively and grouped together at the end of the manuscript, with only the corresponding number being mentioned in the text. The arrangement should be as follows. For books: [1]Durand, W. F., *Aerodynamic Theory*, 1st Ed., Vol. 1, p. 23; Julius Springer, Berlin, 1934. For magazines: [1]England, C. R., Crawford, A. B., and Mumford, W. W., *Some Results of a Study of Ultra-Short-Wave Transmission Phenomenon*, Proc. IRE, Vol. 20, No. 12, pp. 481–482, March, 1933. Please give author, title edition, volume, number, page, publisher, and place and date of publication as indicated. Omission of one required fact causes much extra editorial work and possible inaccuracies.

ILLUSTRATIONS: Illustrations should accompany manuscripts, and each should always be referred to in the text by number. Drawings or graphs should not be larger than 12 × 16 inches, and must be made with jet black India ink on white paper or tracing cloth, the latter being preferred. *Do not use typewriter for lettering.* The smallest lettering on 8 × 10 inch figures should be no less than $1/4$ inch high. Cross-section paper (white with black lines) may be used, but it should not have more than 4 lines per inch. If finer ruled paper is used, the major division lines should be drawn in with black ink, omitting the finer divisions. In the case of finely ruled paper, only blue-lined paper can be accepted. *Tracing paper and blueprints* are not acceptable. Lettering and all markings must be large enough to be readable after reduction to single-column width ($3^3/_{16}$ in.) Mail rolled or flat; never fold. Drawings that cannot be reproduced (including pencil drawings) will be returned to the author for redrawing, thus delaying publication of the paper. Photographs should be distinct and show clear black and white contrasts. They must be on glossy white paper. Avoid round or oval photographs.

CAPTIONS AND LEGENDS: Legends or captions must accompany each drawing or photograph submitted. If written on the drawing or photograph they should be placed below and well outside the part to be reproduced. Each table should have a caption such as Table 1, Table 2, Table 3, etc. Captions should be complete in themselves so as to make the data intelligible to the reader without reference to the text. A duplicate list of captions for figures should be included as the last page of the manuscript. Use "Fig. 1" (not Figure 1), "Figs. 3 and 4," etc., in both the text and the numbering of illustrations. In the text, "Eq. (1)" or "Eqs. (1) and (2)" is used, not "Equation (1)." In captions, legends, and in table headings, write all words in full; do not abbreviate, except for "Fig." and "Eq."

MATHEMATICAL WORK: Formulas may be typewritten or carefully written in pen and ink, the writing to be large enough so that it can be marked for the printer. Considerable space for marking should be allowed above and below all equations. All complicated equations should be repeated on separate sheets with adequate space left for marking. The solidus should be used for simple fractions appearing within the text. Make all expressions clear to the typesetter. Greek letters used in formulas should be clearly designated by name in the margin of the manuscript. The difference between capital and lower-case letters should be clearly distinguished and care taken to avoid confusion between zero (0) and the letter (o), between the numerical (one) and the letter (ell) and the prime (′), between alpha and a, kappa and k, u and mu, v and nu, n and eta. All subscripts and exponents should be clearly distinguished. Avoid complicated exponents and subscripts. Dots and bars over letters or mathematical expressions should also be avoided. When it is necessary to repeat a complicated expression, it should be represented by some convenient symbol.

SYMBOLS AND ABBREVIATIONS: The symbols recommended in the American Standard Association "Letter Symbols for Aeronautical Sciences," ASA Y10.7—1954, should be used wherever practicable. All symbols should be clearly written and carefully checked. Standard abbreviations should be used, and it should be noted that most abbreviations are lower case.

CORPORATE MEMBERS

OF THE

INSTITUTE OF THE AEROSPACE SCIENCES

AC SPARK PLUG DIVISION, GENERAL MOTORS CORPORATION

ACADEMY OF AERONAUTICS

AEROJET-GENERAL CORPORATION

AERONCA MANUFACTURING CORPORATION

AERONUTRONIC, DIVISION OF FORD MOTOR COMPANY

AGAWAM AIRCRAFT PRODUCTS, INC.

ALLIED RESEARCH ASSOCIATES, INC.

ALLISON DIVISION, GENERAL MOTORS CORPORATION

ALUMINUM COMPANY OF AMERICA

AMERICAN AIRLINES, INC.

AMERICAN BOSCH ARMA CORPORATION

AMERICAN STEEL & WIRE DIVISION, UNITED STATES STEEL CORPORATION

AMOCO CHEMICALS CORPORATION

AMPHENOL-BORG ELECTRONICS CORPORATION

ARDE ASSOCIATES

ASTRO-ELECTRONIC PRODUCTS DIVISION, RADIO CORPORATION OF AMERICA

AUTOMATION INDUSTRIES, INCORPORATED

AVCO-EVERETT RESEARCH LABORATORY

AVIEN, INC.

BEECH AIRCRAFT CORPORATION

BELL AEROSPACE CORPORATION

THE BENDIX CORPORATION

BOEING AIRPLANE COMPANY

BOOZ, ALLEN APPLIED RESEARCH, INC.

BULOVA RESEARCH AND DEVELOPMENT LABORATORIES, INC.

CANADAIR, LTD.

CHANCE VOUGHT AIRCRAFT, INCORPORATED

THE CHASE MANHATTAN BANK

CHICAGO AERIAL INDUSTRIES, INC.

THE CLEVELAND PNEUMATIC INDUSTRIES, INC.

CLIFFORD MANUFACTURING DIVISION, STANDARD-THOMSON CORPORATION

CONTINENTAL MOTORS CORPORATION

CORNELL AERONAUTICAL LABORATORY, INC.

COX & COMPANY, INC.

CURTISS-WRIGHT CORPORATION

DANIEL, MANN, JOHNSON, & MENDENHALL

THE DECKER CORPORATION

DEFENSE ELECTRONIC PRODUCTS DIVISION, RADIO CORPORATION OF AMERICA

DEFENSE SYSTEMS DIVISION, GENERAL MOTORS CORPORATION

DEL MAR ENGINEERING LABORATORIES

DELCO-RADIO DIVISION, GENERAL MOTORS CORPORATION

DELCO-REMY DIVISION, GENERAL MOTORS CORPORATION

DOAK AIRCRAFT COMPANY, INC.

DOUGLAS AIRCRAFT COMPANY, INC.

DZUS FASTENER COMPANY, INC.

EASTERN AIRLINES, INC.

EATON MANUFACTURING COMPANY

EDO CORPORATION

ELASTIC STOP NUT CORPORATION OF AMERICA

ENGINEERING SUPERVISION COMPANY

FAIRCHILD CAMERA AND INSTRUMENT CORPORATION

FAIRCHILD ENGINE AND AIRPLANE CORPORATION

THE GARRETT CORPORATION

GENERAL APPLIED SCIENCE LABORATORIES, INC.

GENERAL DYNAMICS CORPORATION

GENERAL ELECTRIC COMPANY

GENERAL PRECISION, INC.

GIANNINI CONTROLS CORPORATION

THE B. F. GOODRICH COMPANY

GOODYEAR AIRCRAFT CORPORATION

GRUMMAN AIRCRAFT ENGINEERING CORPORATION

HOFFMANN AIRCRAFT COMPANY

HUGHES AIRCRAFT COMPANY

INSURANCE COMPANY OF NORTH AMERICA COMPANIES

INTERNATIONAL BUSINESS MACHINES CORPORATION FEDERAL SYSTEMS DIVISION

THE INTERNATIONAL NICKEL COMPANY, INC.

ITT LABORATORIES, DIVISION OF INTERNATIONAL TELEPHONE AND TELEGRAPH CORPORATION

JANITROL AIRCRAFT DIVISION, MIDLAND-ROSS CORPORATION

JOHNS-MANVILLE SALES CORPORATION

KOLLSMAN INSTRUMENT CORPORATION

LAVELLE AIRCRAFT CORPORATION

LEAR, INCORPORATED

C. W. LEMMERMAN, INC.

THE LIQUIDOMETER CORPORATION

ARTHUR D. LITTLE, INC.

LOCKHEED AIRCRAFT CORPORATION

THE MARQUARDT CORPORATION

THE MARTIN CORPORATION

McDONNELL AIRCRAFT CORPORATION

MELETRON CORPORATION

MINNEAPOLIS-HONEYWELL REGULATOR COMPANY

MOBIL OIL COMPANY

NATIONAL CREDIT OFFICE, INC.

NORTH AMERICAN AVIATION, INC.

NORTHROP CORPORATION

NUCLEAR DEVELOPMENT CORPORATION OF AMERICA

PAN AMERICAN WORLD AIRWAYS, INC.

THE RALPH M. PARSONS COMPANY

PESCO PRODUCT DIVISION, BORG-WARNER CORPORATION

PIASECKI AIRCRAFT CORPORATION

POLY INDUSTRIES, INC.

REPUBLIC AVIATION CORPORATION

ROHR AIRCRAFT CORPORATION

PAUL ROSENBERG ASSOCIATES

RYAN AERONAUTICAL COMPANY

SANDBERG-SERRELL CORPORATION

SHELL OIL COMPANY

SIMMONDS PRECISION PRODUCTS, INC.

SOLAR AIRCRAFT COMPANY

SOUTHWEST PRODUCTS COMPANY

SPACE TECHNOLOGY LABORATORIES, INC.

R. DIXON SPEAS ASSOCIATES

SPERRY GYROSCOPE COMPANY, DIVISION OF SPERRY RAND CORPORATION

STANDARD OIL COMPANY (INDIANA)

STANLEY AVIATION CORPORATION

THERM, INCORPORATED

THIOKOL CHEMICAL CORPORATION

THOMPSON RAMO WOOLDRIDGE INC.

TRANS WORLD AIRLINES, INC.

UNION CARBIDE METALS COMPANY, DIVISION OF UNION CARBIDE CORPORATION

UNITED AIR LINES, INC.

UNITED AIRCRAFT CORPORATION

UNITED STATES AVIATION UNDERWRITERS, INC.

VEHICLE RESEARCH CORPORATION

VITRO CORPORATION OF AMERICA

WESTERN GEAR CORPORATION

WESTINGHOUSE ELECTRIC CORPORATION

WYMAN-GORDON COMPANY

YOUNG RADIATOR COMPANY